Fakultät Wissenschaftszentrum Weihenstephan für Ernährung, Landnutzung und Umwelt
Lehrstuhl für Phytopathologie

Investigations on the Physiological Role of the Powdery Mildew Susceptibility Factor HvRACB in Barley

Björn Scheler

Vollständiger Abdruck der von der Fakultät Wissenschaftszentrum Weihenstephan für Ernährung, Landnutzung und Umwelt der Technischen Universität München zur Erlangung des akademischen Grades
eines Doktor der Naturwissenschaften (Dr.rer.nat)
genehmigten Dissertation.

Vorsitzender: Prof. Dr. Erwin Grill
Prüfer der Dissertation:
1. Prof. Dr. Ralph Hückelhoven
2. Prof. Dr. Kay H. Schneitz

Die Dissertation wurde am 24.11.2016 bei der Technischen Universität München eingereicht und durch die Fakultät Wissenschaftszentrum Weihenstephan für Ernährung, Landnutzung und Umwelt am 12.02.2017 angenommen.

Contents

Contents

Publication

Parts of this thesis have been already published in a peer reviewed Journal:

Scheler B, Schnepf V, Galgenmüller C, Ranf S, Hückelhoven R. 2016. Barley disease susceptibility factor RACB acts in epidermal cell polarity and positioning of the nucleus. Journal of Experimental Botany **67**, 3263–3275.

List of figures

List of figures

List of tables

Abbreviations

%	percent
aa	amino acids
AF	actin filaments
AGT	appressorial germ tube
AMF	arbuscular mycorrhizal fungi
AMP	antimicrobial peptide
APP	appressorium
At	*Arabidopsis thaliana*
Auto	autofluorescence
Bgh	*Blumeria graminis f. sp. hordei*
BSA	bovine serum albumine
chi^2	chi-squared test
CI	confidence interval
cm	centimeter
CP	conidiophore
CPD	critical point drying
cv	cultivar
CW	cell wall
CWDE	cell wall degrading enzyme
CWI	cell wall integrity
DAB	3,3-diaminobenzidine
DAMP	Damage-Associated Molecular Pattern
ddH_2O	double distilled water
DN	dominant negative
DP	digitate processes
dpi	days post inoculation
DPI	diphenyleneiodonium chloride
ECM	extracellular material
ETI	effector-triggered immunity
EtOH	ethanol
ETS	effector-triggered susceptibility
ff.	following pages
FPA	formalin, propionic acid, alcohol
FUC	α-Fucosidase
FUT	α-Fucosyltransferase
GAP	GTPase-activating protein
GDI	ROP-GDP dissociation inhibitor
gDNA	genomic DNA
GEF	ROP-Guanine Exchange Factor
GFP	green fluorescent protein
GC	guard cell
GMC	guard mother cell
HA	haustorium
HI	haustorial initial

HPF	3'-(p-hydroxyphenyl) fluorescein
hoi	hours of incubation
HPAEC-PAD	High-Performance Anion-Exchange Chromatography with Pulsed Amperometric Detection
hpi	hours post inoculation
Hsp	heat shock protein
JA	jasmonic acid
JIP	jasmonate induced protein
LB	lysogeny broth
MAMP	Microbe-Associated Molecular Pattern
MeOH	methanol
MLG	mixed linkage glucans
mm	millimeter
mm^2	square millimeter
mPS-PI	modified pseudo Schiff – propidium iodide
MES	2-(N-Morpholino) ethansulfonsäure
MS	Murashige-Skoog
MT	microtubules
NaAc	sodium acetate
NaCl	sodium chloride
NADP	nicotinamide adenine dinucleotide phosphate
NAI	nucleus attraction index
NaN_3	sodium azide
NaOH	sodium hydroxide
NB-LRR	nucleotide-binding leucine-rich repeat protein
NBT	nitroblue tetrazolium
NHR	non-host resistance
OECA	over expressing, constitutively activated
OH•	hydroxyl radical
$O_2^{\bullet -}$	superoxide anion
PAMP	Pathogen-Associated Molecular Pattern
PBS	phosphate-buffered saline
PC	pavement cell
PCR	polymerase chain reaction
PCW	primary cell wall
PEG	polyethylene glycol
PFA	paraformaldehyde
PGT	primary germ tube
PE	penetration efficiency
PI	propidium iodide
PP	penetration peg
PRR	pattern recognition receptor
PM	plasma membrane
PMR	powdery mildew resistant
PMSC	primary stomatal mother cell
PR	pathogenesis-related
PTI	PAMP-triggered immunity
qPCR	quantitative RT PCR
r123	rhodamine 123
RIC	ROP-interactive CRIB motif-containing protein

RIP	ROP Interactive Partner
RLCK	receptor-like cytoplasmic kinase
RLK	receptor-like kinase
RLP	receptor-like protein
RNAi	RNA interference
ROI	region of interest
ROP	rho of plants
ROS	reactive oxygen species
R-protein	resistance protein
RT	reverse transcription
SA	salicylic acid
SC	subsidiary cell
sqPCR	semi quantitative PCR
SDS	sodium dodecyl sulfate
SEM	scanning electron microscopy
SH	secondary hyphae
SHAM	salicylhydroxamic acid
SMC	subsidiary mother cell
sqPCR	semiquantitative reverse transcription PCR
STD	standard deviation
TF	transcription factor
TFA	trifluoroacetic acid
TIGS	transient induced gene silencing
TM	transmembrane
u	unit
UBC2	ubiquitin-conjugating enzyme E2
µm	micrometer
µm²	square micrometer
WGA	wheat germ agglutinin
WT	wildtype

Summary

Plant small monomeric RHO GTPases, also called ROP proteins, are molecular switches transmitting extracellular signals to intracellular pathways. ROP proteins in plants are essential regulators for manifold cellular processes such as the single cell polarization. This process is among others necessary for the formation of root hairs, pollen tubes, stomata, and the anisotropic diffuse growth of leaf cells. However, it also takes place during the plant-microbe interactions.

The ROP protein *Hv*RACB is a susceptibility factor in the compatible interaction of barley (*Hordeum vulgare*) and the obligate biotrophic barley powdery mildew fungus *Blumeria graminis hordei* (*Bgh*). *Hv*RACB does not negatively regulate defense responses of the plant. Instead it supports the fungal penetration of the plant cell wall as well as post-penetrational establishment of the haustorium. However, its function as susceptibility factor is incompletely understood. Stable transgenic barley plants, overexpressing a constitutively activated version of *Hv*RACB (*HvRACB* OECA), or suppressing *HvRACB* expression (*HvRACB* RNAi) were generated. These exhibited defects in growth and development as well as differential expression of genes related to the cell wall. Therefore, the participation of *Hv*RACB in the formation of root hairs and stomata as well as expansion of cells was suggested, which include the remodeling and synthesis of the cell wall.

To gain further insights into the physiological role of *Hv*RACB in barley and therefore its function as susceptibility factor, stable *HvRACB* RNAi plants were examined here in detail. Hereby, growth and development of the plants, the cell polarization after fungal attack as well as alterations of the cell wall were analyzed. This revealed, when compared to the control, a defective formation of stomata and a reduced expansion of the leaf cells. Additionally, generation of the root hairs was impaired whereas the number of cells determined to initiate root hairs was unaltered. The migration of the nucleus, as indicator for cell polarization, towards the site of attempted penetration of *Bgh* was reduced. Examination of the *HvRACB* RNAi cell wall exhibited an enhanced lytic resistance against fungal cell wall degrading enzymes. Furthermore, the composition of the cell wall was altered, which was traced back to the hemicellulose xyloglucan. Altogether, the data confirmed the physiological role of *Hv*RACB as regulator of the cell polarization and accompanying modifications of the cell wall. This physiological function may be co-opted by *Bgh* to support its own penetration and subsequent haustorial development.

Zusammenfassung

Kleine monomerische RHO GTPasen der Pflanzen, auch ROP Proteine genannt, sind molekulare Schalter, welche extrazelluläre Signale an intrazelluläre Signalwege weiterleiten. In Pflanzen regulieren sie vielfältige zelluläre Prozesse, darunter die Polarisierung einzelner Zellen, welche für die Wurzelhaarbildung, Pollenschlauchwachstum, Stomataenwicklung und anistropisches diffuses Wachstum von Blattzellen notwendig ist. Auch während der Interaktion der Pflanzenzelle mit Mikroben kommt es zur Polarisierung.

Das ROP Protein *Hv*RACB wurde dabei als Anfälligkeitsfaktor in der kompatiblen Interaktion zwischen Gerste (*Hordeum vulgare*) und dem obligat biotrophen Gerstenmehltaupilz *Blumeria graminis hordei* (*Bgh*) identifiziert. Hierbei hat *Hv*RACB keinen negativ regulatorischen Einfluss auf die pflanzliche Pathogenabwehr, sondern unterstützt die Penetration der pflanzlichen Zellwand durch *Bgh*, sowie die nachfolgende Etablierung des pilzlichen Haustoriums. Das Verständnis über die Funktionsweise von *Hv*RACB als Anfälligkeitsfaktor ist jedoch noch unvollständig. Es wurden stabil transgenen Gerstepflanzen, welche eine konstitutiv aktivierte Version von *Hv*RACB (*HvRACB* OECA) überexpremieren, bzw. die Expression des *HvRACB* Gens supprimieren (*HvRACB* RNAi) erzeugt. Diese entwickelten Wachstums- und Entwicklungsphänotypen. Zudem konnte eine differenzielle Expression zellwandmodifizierender Enzyme beobachtet werden. Daher wurde eine Teilnahme von *Hv*RACB an der Wurzelhaar- und Stomatabildung, sowie der Expansion von Blattzellen vorgeschlagen. Diese Prozesse beinhalten Umbildungen und Neusynthesen der pflanzlichen Zellwand.

Um weitere Erkenntnisse über die physiologische Rolle von *Hv*RACB in Gerste und damit über seine Funktion als Anfälligkeitsfaktor zu erlangen, wurden jetzt stabile *HvRACB* RNAi Pflanzen bezüglich Wachstum, Entwicklung, Polarisierung in der Interaktion mit *Bgh*, sowie Veränderung der Zellwand untersucht und mit Kontrollpflanzen verglichen. Die Analysen offenbarten eine fehlerhafte Stomataentwicklung, und reduzierte Zellexpansion. Auch die Wurzelhaarbildung war gestört, jedoch nicht die Entwicklung wurzelhaarbildender Zellen. Die Kernwanderung zur möglichen Penetrationsstelle, als Indikator für die Polarisierung der Pflanzenzelle, war reduziert. Untersuchungen der Zellwand der *HvRACB* RNAi Gerste zeigten eine höhere lytische Resistenz gegen zellwandverdauende Pilzenzyme, sowie eine veränderte Zusammensetzung, welche auf die Hemizellulose Xyloglucan zurückgeführt werden konnte. Insgesamt bestätigten die Daten, die physiologische Rolle von *Hv*RACB als Regulator der Zellpolarisierung und einhergehender Zellwandmodifikationen. *Bgh* könnte sich der physiologischen Funktion HvRACBs bemächtigen um seine Penetration und nachfolgende Haustorienentwicklung zu unterstützen.

1 Introduction

This dissertation considers itself as a small piece of the basic research in the field of phytopathology. Fundamental biological studies are primarily dedicated to basic knowledge acquisition comprehending the functionality of the living beings on this planet. An assessment based on political and economic criteria as well as on possible implementations should be rejected (NFS, 1953).

However, the human population will grow from approximately 7.3 billion people to more than 9.1 billion in the year 2050 (Jaggard *et al.*, 2010). To ensure an adequate supply with nutrients and calories the average yield of the most important grains would have to increase 2.4 % per year (Ray *et al.*, 2013). Studies which deal with predictions on the future grain yield raise serious doubts that this goal will be achieved by the global community (Jaggard *et al.*, 2010; Parry and Hawkesford, 2010; Ray *et al.*, 2013). Further complications in this direction are the increasing scarcity of phosphorus as important fertilizer contribution and the predicted climate change which probably results in changes of the global mean of temperature and rainfall (Jaggard *et al.*, 2010; Schröder *et al.*, 2011; Baker *et al.*, 2015). High pressure of phytopathogens and weeds on the plant cultures become more difficult to counteract because more and more common pesticides lose their efficacy due to evolving resistant pests and pathogens (Jaggard *et al.*, 2010; Sammons and Gaines, 2014; Bardin *et al.*, 2015). Hereby, pathogens account for more than 15 % of the global crop yield loss (Oerke and Dehne, 2004)

Insufficient food supply in the Third-World countries is not only an imminent problem of the directly affected populations. Also, the First-World countries can be affected if starving populations lead to collapsing economies and state structures, which may result in destabilizations of world regions and mass migration towards the industrialized countries. The principal understanding of the plant-pathogen interaction could help breeding resistant crop plants which could withstand pests and pathogens also in suboptimal cultivation conditions and would reduce the amount of applied pesticides (Jaggard *et al.*, 2010).

The above described scenario shows why fundamental research in phytopathology has always a political and an economical point of view and why this topic should go beyond the interest of basic researchers. Hence, this work was funded by the collaborative research project SFB 924 “Molecular mechanisms regulating yield and yield stability in plants”. The aim was to throw some light on the simple asked but difficult to answer question how the barley powdery mildew fungus *Blumeria graminis f. sp. hordei* (*Bgh*) overcomes the barley pathogen defense.

1.1 The barley plant

The crop barley (*Hordeum vulgare L)* represents in the basic plant research a plant model organism of the tribe Triticeae which includes important other important crop species such as rye and wheat. It combines the relevance as important agricultural crop on the field with a large genetic and molecular dataset available in the lab.

1.1.1 Origin, domestication and relevance of *Hordeum vulgare L.*

Barley is next to maize, rice, and wheat one of the most important crops in the world and comprises about 5 % of the world crop production. Except Antarctica it is grown on all continents. The potential yield loss to pest contains about 50 % of the attainable yield. Thereof, about 15 % can be assigned to fungal pathogens. Even under practices of crop protection the losses are estimated to 27 % of the attainable yield (Oerke & Dehne, 2004, FAOSTAT Gateway 2014).

The barley grain is used to produce human food, brewing malts, and for animal feed. Barley (*Hordeum vulgare L.*) is likely the first crop plant species domesticated by mankind, approximately 10,000 years ago from the wild barley *Hordeum spontaneum* (Harlan and Zohary, 1966; Weiss *et al.*, 2004). It belongs to the family of *Poaceae* (grasses), together with other quite important crops such as rice (*Oryza sativa L.*), maize (Zea mays), and oat (*Avena sativa L.*). Furthermore, the agricultural species wheat (*Triticum aestivum L.*) and rye (*Secale cereale L.*) even belong to the same tribe *Triticeae* such as barley (Harlan and Zohary, 1966; Allard, 1999). All mentioned species play an essential role in world nutrition.

Barley is a diploid (n = 7), self-fertile, and inbreeding plant with a haploid genome size of about 5.1 billion base pairs (Bennett and Leitch, 1995; Mayer *et al.*, 2012). Because of the genetic relationship to the above mentioned essential crop plants and rich genetic and genomic resources such as a physical, genetic, and functional sequence assembly of the barley genome, a large dataset of public microarray and RNAseq experiments and a structured mutant population for forward and reverse genetics, barley can be considered as model organism for genetic and molecular biological research (Caldwell *et al.*, 2004; Hruz *et al.*, 2008; Dash *et al.*, 2012; Mayer *et al.*, 2012)

1.1.2 The barley leaf cell morphology and nomenclature

As usual for grasses the barley leaf consists of the leaf sheath which embraces the culm, and the free hanging leaf blade. Sheaths and blades are growing through the cell division activity of different

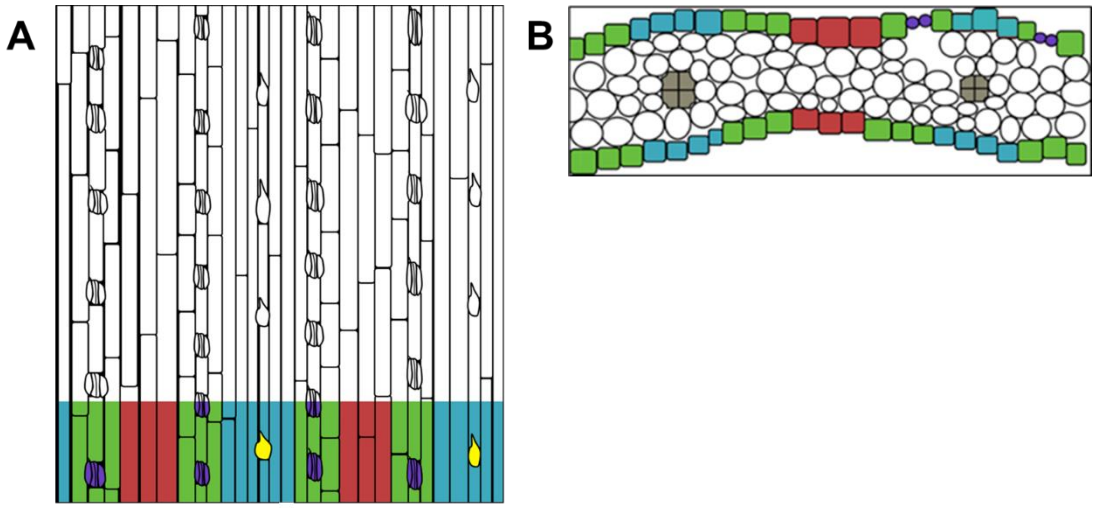

Figure 1: Schematic top view and cross-section of the barley leaf (based on Stebbins & Jain 1960; Koga *et al.* 1990; Sylvester *et al.* 1996).
(A) Top view of the adaxial (culm facing) epidermis of the leaf blade. Orientation: acropetal, tip at the top. Cell types *are* differently colored. Blue: C-cells. Green: A-cells. Purple: Stomata. Red: B-cells. Yellow: Trichomes (B) cross-section of the leaf blade. Adaxial epidermis points up. Color scheme according (A). Additional colors: Grey: Vessels. White: Mesophyll cells. Intercellular space: Area between the mesophyll cells.

and independent intercalary meristems located at their bases. Hence, growth and development is limited to these basal growth zones (Sylvester *et al.*, 1996; Kavanova *et al.*, 2006; Anderson *et al.*, 2013). The nomenclature of Koga and colleagues (Koga *et al.*, 1990) comprises six different cell classes on the barley epidermis based on their differentiation and location (Figure 1A, B). The long cells over the vascular bundles are called C-cells which can be interrupted by trichomes. Two subsidiary cells and two guard cells form together a stomatal complex. Epidermal cells which flank and alternate with the stomatal complexes are called A-cells. The cells which do not touch the stomatal complexes and do not lie over a vascular bundle, are the B-cells (Stebbins and Jain, 1960; Koga *et al.*, 1990). The inner of the barley leaf consists of vascular bundles surrounded by mesophyll cells and intercellular space which is filled with air (Figure 1E, Stebbins and Jain, 1960).

1.1.3 Formation of the barley stomatal complexes

In barley and other grasses stomata complexes are arranged in rows. They run parallel to the vascular bundles along the leaf axis and are usually flanked by a row of A-cells (chapter 1.1.2; Figure 1). Hence, before onset of the formation of a stomatal complex, the definition of the

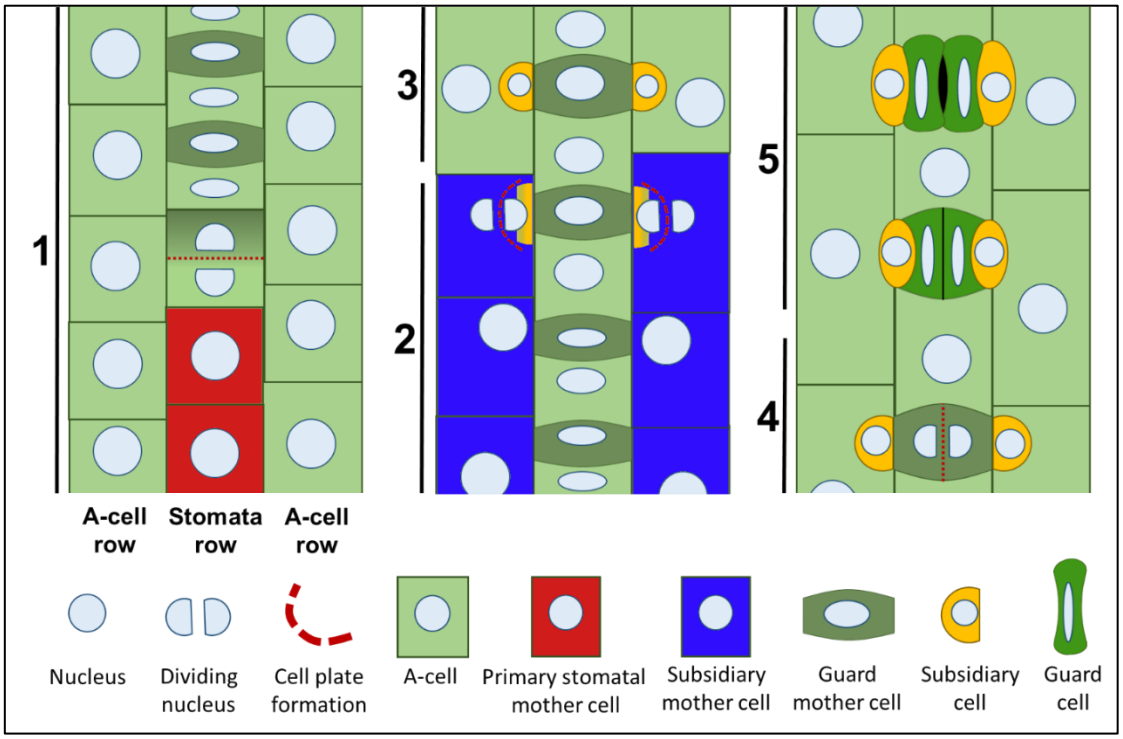

Figure 2: Schematic formation of the stomata complex in barley (based on Stebbins and Jain, 1960; Facette and Smith, 2012).
Top view on an evolving stomata row on the adaxial barley epidermis. Orientation: acropetal, tip at the top. The stomata development in barley can be divided in five morphological stages (1 – 5). (1) Differentiation of the guard mother cell and an A-cell by an asymmetric cell division of the primary stomatal mother cell. (2) Formation of the two subsidiary cells and A-cells by asymmetric cell divisions of the subsidiary mother cell. (3) Triad stage. The subsidiary cells are completely formed. The stomatal complex comprises three cells. (4) A symmetric division of the guard mother cell generates two guard cells. (5) Final maturation of the stomatal complex.

prospective stomatal rows and the A-cell rows is accomplished. This takes place in young primordia of the leaf. Defined rows of stomata are already detected on the cotyledon of the embryo, even before seed germination (Stebbins and Jain, 1960; Koga *et al.*, 1990). Stebbins and Jain (Stebbins and Jain, 1960) divided the formation of the barley stomatal complexes in five morphological stages (Figure 2). In the first stage the primary stomatal mother cell (PSMC) undergoes an asymmetric cell division transverse to the leaf axis. The distal cell shows denser cytoplasm and less vacuolization than the proximal cell. It becomes the guard mother cell (GMC). The proximal cell becomes an undifferentiated A-cell. Both daughter cells are similar in their cell size. From now on, A-cells and GMCs alternate in the stomata row. After slight enlargement the GMC exhibits a characteristic convex outline to the A-cells in the stomatal row but remains flat to the parallel A-cell rows (Stebbins and Jain, 1960). In stage 2 the adjacent A-cells act as subsidiary mother cells (SMCs). Probably, extrinsic signals from the GMC lead to premitotic polarization of the subsidiary mother cell towards

the GMC. This polarization includes a directed migration of the nucleus to the future site of cell division. The following asymmetric cell division leads to a small subsidiary cell (SC) and a large A-cell (Stebbins and Jain, 1960; Facette and Smith, 2012). Stage 3 (Triad Stage) is characterized by a stomatal complex which comprises three cells (one GMC and two SCs). A symmetric division of the GMC along the leaf axis generates two guard cells (GC) and defines stage 4. In the fifth and last stage the stomatal complex matures. The GCs gain their characteristic dumbbell-like shape and the SCs their ellipsoid shape (Stebbins and Jain, 1960).

1.1.4 The barley root epidermis patterning

In the plant root four different growth zones are distinguished (Verbelen *et al.*, 2006, Figure 3A). These are, ordered from the root tip to the shoot, the meristematic zone, transition zone, elongation zone, and growth terminating zone. The cells in these zones show, among others, specific properties concerning the rate of cell division, cell expansion, nucleus localization, cytoskeleton organization, and the status of cell differentiation. The transition from one growth zone into another occurs as gradual process (Verbelen *et al.*, 2006; Baluška and Mancuso, 2013).

The meristem lies at the tip of the root apex and characterized by active cell division. More proximal it turns into the transition zone where the cells are almost isodiametric with small vacuoles and a centered nucleus. This enables a microscopic recognition of this area. The expansion of the cells is slow and the ability for cell division drops from the distal to the proximal end of the transition zone. However, at the proximal end the cells gain the competence for instant and rapid expansion. In the following elongation zone the cells rapidly elongate without considerable growth in width. The nucleus is pushed out of the center to the side due to fast vacuole expansion. Onset of rapid elongation of the cell is accompanied by initiation of visible outgrowths of the root hairs. At its proximal end the elongation zone turns into the growth terminating zone. Cells slow down their rate of elongation until a complete growth stop defines their final size. In this zone a very active tip growth of root hairs can be observed (Verbelen *et al.*, 2006; Baluška and Mancuso, 2013).

Not all epidermal cells in the plant root are capable to produce root hairs. Non - root hair forming cells are called atrichoblasts, root hair forming cells are called trichoblasts (Bibikova and Gilroy, 2003). To form both cell types in barley, an undifferentiated epidermal mother cell divides symmetrically in its shootward-last cell division, which results in morphological identical daughter cells (Marzec *et al.*, 2013, 2014; Figure 3B). Differences between the daughter cells become visible during differentiation. Thus, trichoblasts and atrichoblasts expand asymmetrically. Trichoblasts remain shorter than the atrichoblasts.

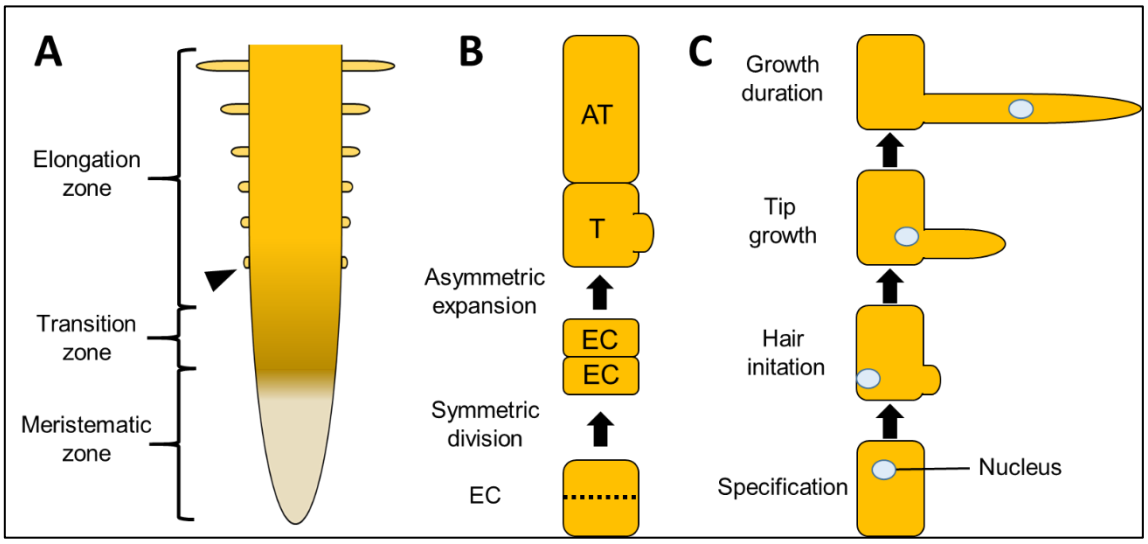

Figure 3: Patterning of the root epidermis in plants (based on Gilroy and Jones, 2000; Verbelen et al., 2006; Marzec et al., 2014).
(A) Four zones of the root apex can be distinguished (growth terminating zone not shown). The arrowhead points to the visible beginning of bulge formation. The color scheme depicts the gradual transition from one zone to another. (B) Illustrated differentiation of trichoblasts 'T' and atrichoblasts 'A' as proposed for barley. An epidermal mother cell 'EC' divides symmetrically to morphological identical daughter cells. Differences, like their cell size, occur during differentiation. Only the shorter trichoblasts form root hairs. (C) Root hair formation comprises four subsequent phases, including a nucleus specific localization pattern.

Additionally, trichoblasts exhibit cellular characteristics such as denser cytoplasm, less vacuolization, and more mitochondria than the atrichoblasts (Marzec *et al.*, 2013).

The root hair development comprises four subsequent phases which includes a phase specific localization pattern of the nucleus (Gilroy and Jones, 2000; Ketelaar *et al.*, 2002; Čiamporová *et al.*, 2003; Figure 3C). After specification as trichoblast, the cell initiates formation of a root hair. First visible evidence for the initiation is a spatial restricted bulging of the cell which is localized at its distal pole. Even before visible bulging, the nucleus takes the place at the periclinal cell wall, opposite to the following outgrowth. The subsequent tip growth of the bulging leads to an elongated hair-like morphology. The nucleus starts to move towards the basis of the root hair. During duration of growth the nucleus is located at a fixed distance to the apex of the root hair and therefore must enter the tube of the root hair. After termination of growth the nucleus obtains a random position in the root hair (Gilroy and Jones, 2000; Ketelaar *et al.*, 2002; Čiamporová *et al.*, 2003).

1.1.5 The barley plant cell wall

The cell wall provides structural support, a barrier between the plant and abiotic and biotic stresses, and regulates the flow of materials through the plant. The primary cell walls (PCWs) of plants are mainly composed of polysaccharides, aromatic substances as well as structural and nonstructural proteins. The polysaccharides are further divided in cellulose, hemicelluloses, and pectins (Carpita and Gibeaut, 1993).

Cellulose chains consist of several thousand β (1→4) linked units of the monosugar D-glucose. About three dozen of these unbranched chains form a para-crystalline cellulose microfibril. These microfibrils represent the skeleton of the PCW. The hemicelluloses and pectins form a matrix embedding these microfibrils (Carpita and Gibeaut, 1993; Fry, 2004). Important hemicelluloses are heteroxylans, (1→3; 1→4) - β- Glucans (also described as mixed linkage glucans or MLGs), xyloglucans, and glucomannans. Based on differences in the composition and content of hemicellulose and pectin, PCWs are divided in two main types. Type I is mostly found in dicots, gymnosperms, and noncommelinoid monocots. The latter includes for example orchids and lilies. Type II is restricted to commelinoid monocots such as grasses, including barley (Carpita and Gibeaut, 1993; Carpita, 1996). When compared to the Type I PCWs, Type II cell walls possess less pectin. Xyloglucans and glucomannans are available only in traces. However, the amount of heteroxylans is enhanced, when compared to Type I cell walls, and MLGs are even unique for Type II PCWs and absent in Type I. A further feature of Type II PCWs is their enrichment of aromatic substances (Carpita, 1996; Vogel, 2008). However, composition of the walls which belong to the same PCW Type can still considerably differ among different species and even within the same species, dependent on tissue type and tissue age (Gibeaut *et al.*, 2005; Fincher, 2009). In barley (Table 1) the relative amount of xyloglucan ranges from 'not detected' in the stem and 'traces' in young leaves to 10 % in four days old coleoptiles. Similar results are obtained for pectins. The barley coleoptile cell walls also exhibit significant changes in the relative composition of the polysaccharides according to the tissue age (1 to 8 days old). The relative amount of pectins decreases from about 29 mol % (day 0) to about 11 mol % (day 8).

Table 1: Polysaccharide composition of the cell wall in aerial organs of barley (Fincher, 2009, modified).
"ND": Not Detected

Barley tissue	Cellulose	MLG	Heteroxylan	Xyloglucan	Pectin
Coleoptile (4 d)	35%	10%	32%	10%	12%
Young leaf	63%	16%	11%	Trace	5%
Stem	65%	5%	28%	ND	ND

1.2 The plant pathogen *Blumeria graminis*

In 2012 fungi-interested authors, reviewers, editorial board members, and senior editors of the journal "Molecular Plant Pathology" were asked to estimate the scientifically and economically most important fungal plant pathogens (Dean *et al.*, 2012). Based on this survey a top ten list was created with the plant pathogen *Blumeria graminis* on the sixth place.

1.2.1 Taxonomy, caused disease and relevance of *Blumeria graminis*

The pathogenic ascomycete *Blumeria graminis* causes the plant disease powdery mildew which occurs on aerial organs of grasses such as wheat, rye, and barley. Symptoms of an advanced infection with the fungus are powdery spots on leaves, culms, and stems. These spots served as eponym for the powdery mildew disease (Glawe, 2008; Dean *et al.*, 2012). As an obligate biotrophic fungus, it closely associates with its living host for further development and reproduction and cannot be cultivated in culture. The genome size of the haploid *Blumeria graminis* is about 120 Mb and therefore about four times the size of other ascomycetes. For specific pathways such as the anaerobic fermentation, the incorporation of inorganic nitrate and sulfate, the production of selected primary and secondary metabolites, and transporter proteins, no genes were found. It is supposed that the lack of these genes directly correlates with the unability for cultivation away from the plant (Glawe, 2008; Spanu *et al.*, 2010; Dean *et al.*, 2012).

Blumeria graminis is the only species in the genus *Blumeria* of the tribe *Blumerieae*. However, special forms or *formae speciales* (f. spp.) of *Blumeria graminis* are distinguished according their host specificity for a single genus of grasses. For example, wheat is infected by *B. graminis* f.sp. *tritici* and barley by *B. graminis f. sp. hordei* (*Bgh*) (Glawe, 2008; Dean *et al.*, 2012). *Bgh* can further differentiated in races concerning their virulence frequency on individual barley cultivars (Tratwal and Weber, 2006).

The average yield loss caused by *Bgh* reach about 10 % to 20 %, but can exceed 50 % under favorable conditions for the pathogen. Yield loss and quality is affected by reduction of photosynthetic active leaf area, smaller size and number of kernels per ear, and less tillers per plant (Tratwal and Weber, 2006).

1.2.2 The asexual life cycle of Blumeria graminis

The asexual fungal spores of *Bgh*, also called 'conidia', land on the barley epidermis via wind-dispersion (Figure 4A). After about one minute, extracellular material (ECM) which contains

esterases and cutinases, is released and bonds the spore to the leaf (Wright *et al.*, 2002). Approximately one hour later the primary germ tube (PGT) of the conidium emerges (Figure 4B). The PGT is thought to play a pivotal role in water uptake, receive signals derived from the plant, and attachment to the epidermal surface via ECM, different from the spore ECM (Nielsen *et al.*, 2000; Wright *et al.*, 2002).

Furthermore, the PGT forms a small cuticular peg which penetrates the cuticle but not the wall of the plant cell (Edwards, 2002). About 8 to 10 hours later the appressorial germ tube (AGT) is formed (Figure 4C), elongates and develops a swollen, hooked appressorium (APP) at its end. Again the adhesion is achieved by released ECM (Wright *et al.*, 2002). Under the appressorium the penetration peg (PP) evolves at about 12 hours (Figure 4D). In an event of successful penetration the PP penetrates the cuticle, the preformed plant cell wall, and the papillae. The latter is an apposition to reinforce the cell wall. It is formed by the plant as an answer to the penetration attempt of the fungus (Hückelhoven, 2014). To break through the border of the plant cell, *Bgh* uses mechanical force as well as cuticle and cell wall lytic enzymes (Pryce-Jones *et al.*, 1999). After penetration, the PP grows

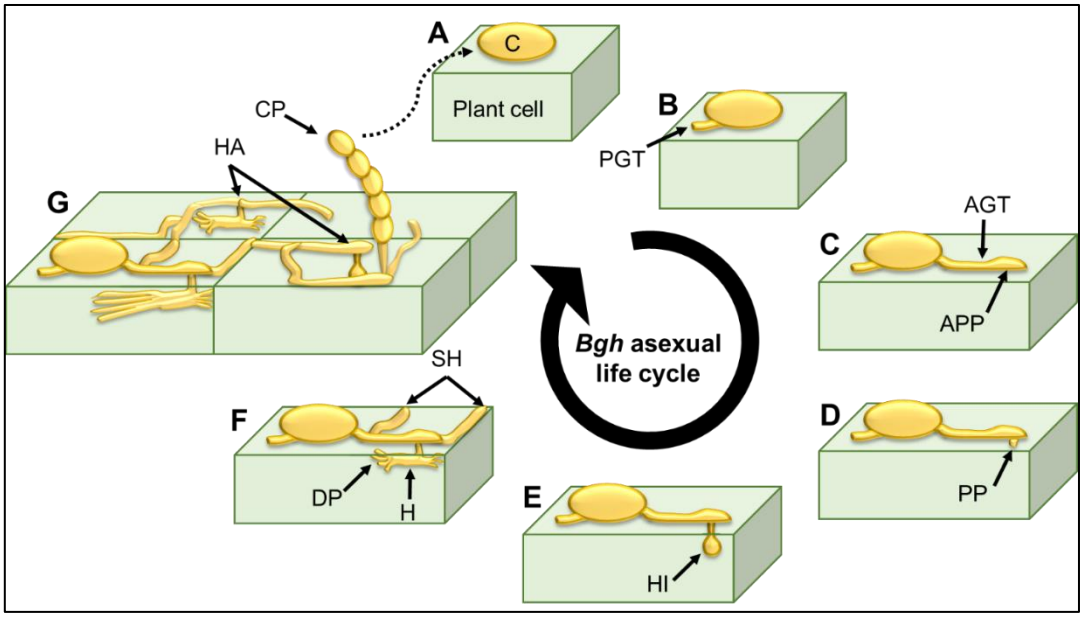

Figure 4: The asexual life cycle of *Blumeria graminis* (based on Zhang et al., 2005).
(A – G) Asexual life cycle of *Bgh*. (A) A single conidium 'C' on a barley epidermal cell. (B) The primary germ tube 'PGT' emerges. (C) The appressorial germ tube 'AGT' emerges and forms an appressorium 'APP' at its end. (D) The penetration peg 'PP' occurs, breaking plant cuticle and cell wall. (E) After breakthrough, the PP forms a haustorial initial 'HI' at its end. (F) During maturation the haustorium 'H' develops digitate protrusions 'DP'. Secondary hyphae grow out from the AGT. (G) Hyphal appressoria 'HA' are formed and function like the APP of the AGT. Finally, conidiophores 'CP' are formed, producing new conidia.

as penetration hypha into the plant cell. At its tip the hypha expands club-like and forms the haustorial initial (HI) as an early developmental stage of the fungal feeding organ (Figure 1E). During this processes the fungus does not puncture the membrane of the plant cell but is enclosed by an extrahaustorial matrix. It separates the haustorium from the surrounding and plant derived extrahaustorial membrane. (Zhang *et al.*, 2005; O'Connell and Panstruga, 2006). As part of maturation, the haustorium further expands and forms about ten digitate protrusions (DP) at both haustorial poles to increase the surface for the nutrient uptake (Figure 4F). Meanwhile, about 24 hours after arrival of the spore and successful establishment of the haustorium, secondary hyphae (SH) emerge which originate from the AGT (Zhang *et al.*, 2005). The SH further branche and evolve about one day later hyphal appressoria (HA). The HA start to parasite adjacent epidermal plant cells via PP and the establishment of haustoria (Figure 4G). Approximately five days after onset of infection the *Bgh* colony starts sporulation. Conidia are developed in chains from reproductive structures which are called conidiophores (CP). The conidia advance in maturation toward the CP apex. Except the haustoria, *Bgh* growths epiphytically on the epidermal surface of barley. Concerning its biotrophic life-style the parasitized plant cells stay intact (Gjetting *et al.*, 2004). A colony which derives from a single spore and under favorable conditions can establish up to 5000 haustoria and conidiophores which can produce as many as 200.000 spores during the life-time of a colony (Gjetting *et al.*, 2004; Zhang *et al.*, 2005).

1.3 The plant immunity

In contrast to animals, plants are sessile organisms unable to escape abiotic and biotic stresses by relocation of their place of residence. Additionally, they lack immunoglobulin molecules, circulating immune cells, and phagocytic processes. Hence, plants do not possess an adaptive immune system comparable to the animals. The innate immunity is therefore the only defense system of the plants. It is germline encoded and therefore already pre-existent before pathogen challenge (Iriti and Faoro, 2007). However, the diseased plant is an exception in nature which illustrates the efficacy of the plant immunity (Thordal-Christensen, 2003).

1.3.1 Basic concepts and terminology of plant immunity

In the clear majority of interactions, phytopathogens do not cause a disease on the attacked plant. In such interactions, the microbe is called heterologous or non-adapted, the plant is a non-host and the

interaction is referred to as incompatible or heterologous. If a plant species is susceptible to a plant pathogen and colonized, this plant-microbe interaction is called compatible or homologous, the pathogen is an adapted or homologous pathogen and the plant is referred to as host (Gabriel and Rolfe, 1990; Prell and Day, 2001). Plant species which lose in a current evolutionary process their status as host or non-host are neither completely resistant nor completely susceptible to a specific pathogen. This means that compatible interactions between plant and pathogen occur occasionally on limited genotypes of the plant species. This intermediate status between host and non-host is termed marginal host (Heath *et al.*, 1997; Atienza *et al.*, 2004; Niks and Marcel, 2009).

Often, all genotypes of a plant species are resistant to all genotypes of a phytopathogen species. This broad-spectrum resistance is called non-host resistance (NHR) and is achieved through a plant immune system of multiple layers. The immune system can be divided in a constitutive defense and an induced defense (Thordal-Christensen, 2003; Mysore and Ryu, 2004; Ham *et al.*, 2007). First one includes preformed physical and chemical barriers such as the cuticle, the plant cell wall, and many deposited secondary metabolites and defense proteins. The latter comprises directed reinforcement of the cell wall, defense associated cell polarization, production of secondary metabolites, and transcription of genes related to defense (Nuernberger and Lipka, 2005; da Cunha *et al.*, 2006; Iriti and Faoro, 2007). It is supposed that the constitutive defense mainly contributes to NHR if host and non-host are distantly related plant species. The induced defense is thought to contribute mainly to NHR if host and non-host plants are closely related (Niks and Marcel, 2009).

The entirety of plant defense, mounted against unadapted pathogens, is collectively referred to as basic defense or basic resistance. In the case of complete and effective defeat of the heterologous pathogen the defense results in NHR. The complement of the basic resistance is the basic compatibility of adapted pathogens which overcome host defense in homologous interactions (Heath, 1997; Niks and Marcel, 2009).

In general, susceptible genotypes of a host plant differ in their susceptibility to an adapted and virulent pathogen, due to the ‘basal resistance’. This basal resistance which reduces the spread of adapted pathogens after successful infection, is supposed to be polygenetic and to rely on similar, if not the same principles as the basic resistance (Parlevliet, 1978; Dangl and Jones, 2001; Atienza *et al.*, 2004; Niks and Marcel, 2009).

Additional, plants can recognize particular races or strains of the pathogen by their specific secreted proteins such as effector molecules. These proteins induce further plant defense reactions. This race specific resistance is also called quantitative resistance or effector triggered immunity (ETI), according the perceived effector molecules. It fulfills a role similar to that of the adaptive immune

systems in animals and will be discussed later (chapter 1.3.5; chapter 1.3.7; Jones and Dangl, 2006; Iriti and Faoro, 2007)

Concerning fungal pathogens which form haustoria such as *Bgh*, resistance is also distinguished in pre-haustorial or penetration resistance and post-penetration resistance. The penetration resistance is achieved by plant defense which inhibits the fungus to break through the cuticle and the cell wall to establish its feeding organ. Post-penetration resistance describes the prevention of further proliferation of the fungus after successful penetration (O'Connell and Panstruga, 2006; Hückelhoven, 2007).

In the barley-*Bgh* pathosystem the host plant barley can restrict infection success of adapted *Bgh* in an inductive basal defense pre-haustorial and post-penetrational. The degree of successful infections of *Bgh* depends on the quantitative resistance of the particular cultivar. Furthermore, whether *Bgh* can establish a haustorium and further proliferates, remains a host phenomenon of each autonomous cell. This means that the outcome of the interaction of barley and *Bgh* varies not only between different cell types of the epidermis but also between cells of the same cell type (Lin and Edwards, 1974; Schultheiss *et al.*, 2002; Pathuri *et al.*, 2008; Hückelhoven, 2014).

1.3.2 Preformed barriers of the constitutive basal defense

All plants possess preformed physical and biochemical barriers as part of their system of constitutive basal defense to avoid invasion of a pathogen (Nuernberger and Lipka, 2005). As first physical barrier, the pathogen hast to overcome the plant cuticle, a layer of the polyester cutin, impregnated with intracuticular and covered with epicuticular waxes. The cuticle coats the aerial organs of vascular plants and the precise composition can be quite diverse between different species. The main function of the cuticle is the protection against dehydration as well as abiotic and biotic stresses (Serrano *et al.*, 2014). The penetration of the cuticle layer is thought to be achieved by cutinases and lipases which are secreted by the fungal appressorium. These enzymes are known to hydrolyze cutin, respectively lipids (fats) and were shown to be secreted by the PGT as well as the AGT of *Bgh* (chapter 1.2.2; Nielsen *et al.*, 2000; Wright *et al.*, 2002). It is assumed that *Bgh* AGT and PP turgor pressure have a supportive effect on breaching of the cuticle, as it was shown for the hemibiotrophic rice blast fungus *Magnaporthe grisea* (Edwards and Allen, 1970; Zhang *et al.*, 2005).

After penetration of the cuticle, the fungus must penetrate the plant cell wall. It is constitutively enriched with antimicrobial peptides (AMPs) and toxic secondary metabolites which form a preformed biochemical barrier (Hückelhoven, 2007; Takken and Tameling, 2009; Nawrot *et al.*, 2014). To the AMPs belong for example defensins and thionins. The latter is a family of peptides

with a molecular weight of about 5 kDa and a common peptide structure. Former studies revealed an antimicrobial effect of several leaf thionins of barley to *Bgh* and other pathogenic fungi and their importance to the plant defense machinery. However, the precise antifungal activity of thionins remains unclear (Bohlmann *et al.*, 1988; Andresen *et al.*, 1992; Ma *et al.*, 2010; Nawrot *et al.*, 2014). To break through the cell wall, plant pathogens produce a whole set of degrading enzymes. Fungal cellulases degrade the main component of the cell wall, the cellulose fibrils (Vogel, 2008; Bellincampi *et al.*, 2014). Pectinases are active on the pectin, whereas xylanases loose the polysaccharide xylan as one of the major hemicelluloses (Walton, 1994; Bellincampi *et al.*, 2014). For *Bgh* it was shown that conidia, which germinate on cellulose membranes, secrete cellulases (Suzuki *et al.*, 1998). Additionally, cellobiohydrolase activity at the tip of PGT and AGT was proven (Pryce-Jones *et al.*, 1999). Also here a supportive turgor pressure of the AGT and PP is assumed for effective penetration of the cell wall (Edwards and Allen, 1970; Zhang *et al.*, 2005).

The chemical composition of the preformed cell wall of the plant determines its lytic and mechanical resistance and hence, the success of fungal penetration. It was shown that the *Arabidopsis thaliana* double mutants *pmr5/pmr6* which encode an O-acetyltransferase and a pectate-lyase, possess an altered amount and composition of pectin. Furthermore, they were resistant to the *Arabidopsis* powdery mildew fungus (Vogel *et al.*, 2002, 2004). *Arabidopsis* lines, mutated in the cellulose-synthase gene *CESA3*, such as *eli1* and *cev1* show differences in the composition of their cell wall. Additionally, these lines are more resistant to powdery mildew (Ellis and Turner, 2001; Cano-Delgado *et al.*, 2003).

However, in both *CESA3* mutants an increase in jasmonate signaling was shown. This makes it difficult to distinguish between effects derived directly by the altered mechanic or lytic features of the cell wall and indirect effects via cell wall integrity sensing or altered cell wall degradation products (Vorwerk *et al.*, 2004; Hématy *et al.*, 2009).

1.3.3 The elicitor-triggered basal defense

The above mentioned preformed physical and biochemical barriers of the constitutive defense can stop the attempts of invasion of many non-adapted pathogens (Underwood and Somerville, 2008). However, for efficient resistance against a pathogen the preformed barriers are complemented by a layer of inductive defense. This was illustrated by Jones and Dangl (Jones and Dangl, 2006) via their ‘zig-zag’ model (chapter 1.3.5; Figure 6). The presence of a non-self, a wrong-self or a damaged-self can be detected by perceiving molecular elicitors via surface and intracellular receptors. The

perception results in an induction of a plant defense response (Nuernberger and Lipka, 2005; Heil, 2012; Henry *et al.*, 2012).

An elicitor which induces basal defense in a broad range of cultivars of the same species is called a general elicitor (Montesano *et al.*, 2003). General elicitors are subdivided according their origin from non-pathogenic microbes, phytopathogens or the plant itself. Microbe-associated molecular pattern (MAMPs) and pathogen-associated molecular pattern (PAMPs) are general molecules of a broad range of microbes. They are indispensable for the organisms and include motifs which cannot be modified without considerable disadvantages for the fitness of the pathogen. Examples for elicitors, recognized by a wide spectrum of plants, are bacterial lipopolysaccharides and flagellin as well as chitin, an elicitor from the fungal cell wall (Zipfel *et al.*, 2004, 2006; Zipfel, 2009). Furthermore, when the pathogen breaks through the preformed physical plant barriers, the hydrolysis unavoidably releases products of degradation of the macromolecules. It is supposed that these endogenous molecules of the plant are perceived by the plant as damage-associated-molecular-patterns (DAMPs) (Henry *et al.*, 2012). One example of a putative DAMP are the pectin-derived oligogalacturonides of the plant cell wall which are released through hydrolytic activity of the pathogen (Reymond *et al.*, 1995; D'Ovidio *et al.*, 2004).

The general elicitors are perceived by the plant via surface pattern recognition receptors (PRRs). Most PRRs can be assigned to one of two different groups, distinguishable by their protein domains. Receptor-like kinases (RLKs) possess an extracellular domain, a transmembrane domain (TM), and an intracellular kinase domain. They perceive signals through their extracellular domain and transmit signals through their intracellular signaling molecules via their kinase domain. The other group comprises receptor-like proteins (RLPs) which lack the kinase domain (Shiu *et al.*, 2004; Monaghan and Zipfel, 2012). Recent data indicates that Receptor-like cytoplasmic kinases (RLCKs) which possess only a cytoplasmic kinase domain, are directly activated by PRRs bound to elicitors. Thus, they could function as intracellular signaling kinases to link PRRs and MAPK cascades in pattern triggered plant immunity (Yamaguchi *et al.*, 2013).

Several PRRs were already discovered, especially in the plant model organism *Arabidopsis thaliana*. Thus, bacterial flagellin is perceived by FLAGELLIN SENSING2 (FLS2). Oligogalacturonides, derived from the cell wall of the plant, are perceived via the WALL-ASSOCIATED KINASE 1 (WAK1) (Gómez-Gómez and Boller, 2000; Miya *et al.*, 2007; Brutus *et al.*, 2010). For instance, after flagellin is recognized, FLS2 activates a downstream MAP kinase pathway which triggers the inductive layer of the plant defense (Gómez-Gómez and Boller, 2002). In rice, chitin as a component of the fungal cell wall is recognized by a receptor complex. This complex consists of the RLP OsCEBiP (CHITIN ELICITOR BINDING PROTEIN) which binds chitin and the RLK OsCERK1

(CHITIN ELICITOR RECEPTOR KINASE), necessary for downstream signaling (Kaku *et al.*, 2006; Shimizu *et al.*, 2010). Defense responses, induced by M/P/DAMPs, are called Pattern-Triggered Immunity (PTI) and represent the primary layer of the inductive defense (Shiu and Bleecker, 2001; Nicaise *et al.*, 2009; Henry *et al.*, 2012).

1.3.4 Cell wall associated basal defense

First counteractions as primary layer of the inductive defense of the plant take place at the cell wall (Figure 5). As part of their inductive immunity, plants can distinguish between self and non-self. Furthermore, they are also monitoring their cell wall integrity (CWI), differentiating between intact self and damaged self (Hématy *et al.*, 2009). The latter can be sensed by the cell via DAMPs, perturbations in the synthesis, and assembly of the cell wall as well as deformations of the plasma membrane in consequence of a weakened cell wall (Hématy *et al.*, 2009; Henry *et al.*, 2012; Pogorelko *et al.*, 2013). To sense and process these endogenous and exogenous signals the plants rely on a high variety of receptors and signal transductors (Hématy *et al.*, 2009).

Receptor like kinases (RLKs), the mitogen-activated protein kinase (MAPK) pathway, and arabinogalactan proteins are thought to be involved in the survey of the plant CWI and the following signal integration (Humphrey *et al.*, 2007; Cheung and Wu, 2011; Wolf *et al.*, 2012). After perception of a non-self, a wrong-self or a damaged-self, the cytoplasm , the endomembrane system, and the cytoskeleton of the plant cell are drastically rearranged and polarized towards the site of perception (Nuernberger and Lipka, 2005; Hückelhoven, 2007; Hématy *et al.*, 2009). These mechanisms for cell polarization are pivotal for an effective counteraction against an imminent collapse of CWI and pathogenic threat. They ensure the transport and secretion of defense compounds and components which are necessary for strengthening the cell wall towards the attempted site of penetration. The speed and the spatial accuracy of these actions are thought to be crucial for a successful plant defense. If the reorganization of the actin cytoskeleton is inhibited, for example by the drug cytochalasin E, the defense associated to the cell wall is disturbed. A consequence the penetration success of compatible and nonhost pathogens is enhanced (Kobayashi *et al.*, 1997; Opalski *et al.*, 2005; Hückelhoven, 2007).

Additional to the polarization of the cell, the synthesis and transport of defense compounds is initiated. These comprise inhibitors of pathogenic enzymes which are capable to degrade the cell wall of the plant. Also antimicrobial molecules of low mass such as phytoalexins and antimicrobial peptides such as thionins and defensins are targeted to the site of fungal attack (Ahuja *et al.*, 2012; Nawrot *et al.*, 2014). Material for strengthening of the cell wall, in form of a papillae is synthesized

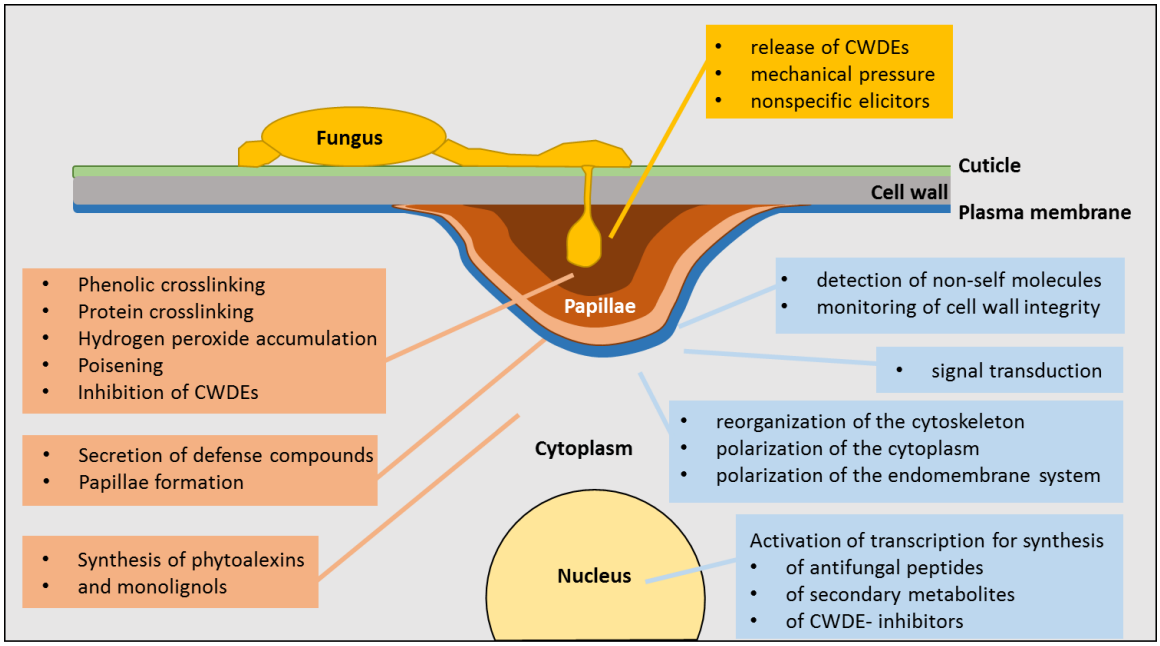

Figure 5: Plant defense associated to the cell wall (Hückelhoven 2007b, 2014, modified). The picture should be considered clock-wise. Fungal actions at the cell wall (yellow box) can lead to penetration of cuticle and cell wall. This enables the initial formation of the haustorium. Perception of the pathogen and signal transduction result in polarization of the cell towards the site of attack. Transcription of defense compounds is activated (blue boxes). These compounds are synthesized and transported to the site of attack, directly harming the fungus or inhibiting fungal activity after their secretion. Additionally, a papilla is formed, strengthened by diverse crosslinking reactions (red boxes). The papillae consist of several layers. A phenolic enriched inner layer (dark brown), a callose and arabinoxylans enriched middle layer (light brown) and a cellulose and arabinoxylans enriched outer layer (salmon). A non-penetrated (effective) papillae is shown. CWDE: cell wall degrading enzymes.

and transported to the site of attempted penetration. The papilla is a cell wall apposition which consists of several layers, different in their enrichments in phenolics (lignin derived from oxidative monolignol polymerization and phenolic conjugates), callose, cellulose, and arabinoxylan (Boerjan *et al.*, 2003; Chowdhury *et al.*, 2014). Accumulation of hydrogen peroxide (H_2O_2), dependent on the activity of peroxidases, is detected via DAB staining. It is thought to play an important role in the crosslinking of the components of the cell wall, comparable to crosslinking by phenolic bridges. Papillae of barley, formed after attack of *Bgh*, can be distinguished in effective (non-penetrated) and non-effective (penetrated) papillae. Recently it was shown that effective papillae are richer in callose, cellulose, arabinoxylans, and H_2O_2, when compared to penetrated appositions (Hückelhoven, 2007, 2014; Chowdhury *et al.*, 2014).

1.3.5 Effector-triggered susceptibility

Most pathogens are stopped by the preformed defense barriers or PTI. However, some adapted pathogens can overcome the basal defense by delivering host interacting proteins, so called effectors, to the attacked cell. The resulting susceptibility of the host is therefore called effector-triggered susceptibility (ETS). These effectors interact with their targets of the host cell to inhibit signaling pathways, suppress the production of compounds which participate in the basal defense or manipulate the host cell to cooperate in disease (chapter 1.3.3; Jones and Dangl, 2006; Koeck *et al.*, 2011).

Hence, pathogens can address two kinds of effector targets (Pavan *et al.*, 2010). Host resistance factors (RFs) with a positive role in plant defense are suppressed or inhibited by the effector to induce susceptibility of the plant. However, absence (in this context, also including loss of function) of this effector targets can also result in susceptibility, because of the absent positive effect of the host factor on plant defense. The second group of effector targets are susceptibility factors (SFs), required by the pathogen for full virulence. They can be separated in negative defense regulators and factors necessary for accommodation of the pathogen according its metabolism and development (Hückelhoven, 2005; Pavan *et al.*, 2010; Hückelhoven *et al.*, 2013). Latter are of especial necessity for pathogens which form feeding structures and are dependent on metabolic pathways of the host. Like in the obligate biotrophic *Bgh*, these metabolic pathways were lost during evolution. In such cases the host cell is forced by manipulation of the SFs to accommodate its cell architecture and metabolism. Thus, the plant is effected to support haustorial formation and subsequent establishment of nutrient supply of the fungus (Zhang *et al.*, 2005; Spanu *et al.*, 2010; Chen *et al.*, 2010; Koeck *et al.*, 2011). The pathogen must promote or activate this group of effector targets to achieve susceptibility. Hence, absence of SFs as effector targets results in resistance to the particular pathogen. However, it can also result in an enhanced susceptibility to other pathogens, or in pleiotropic effects on development and metabolism of the plant (Pavan *et al.*, 2010; Hückelhoven *et al.*, 2013).

Inhibited or retarded development of the fungus due to poor accommodation of the host cell can lead to an enhanced plant defense. However, vice versa enhanced plant defense can result in poor infection success or development of the fungus (Hückelhoven *et al.*, 2013). Hence, the reason of altered fungal success is phenotypically often indistinguishable. Therefore, the molecular characterization of the effector target and its role in the interaction of the plant and the pathogen is an imperative.

1.3.6 *Bgh* effectors and their potential targets in barley

In the *Bgh* genome 784 effector candidates (BECs) are found so far which represents about 13.5 % of all annotated genes. All effector candidates have in common that their quantitative proliferation is putatively due to the association with transposable elements based on retro-transposon driven *Bgh* genome expansion. Furthermore, no homologs of the BECs are found outside the powdery mildew fungi (Pedersen *et al.*, 2012; Amselem *et al.*, 2015). Many BECs are expressed in the *Bgh* haustorium which underlines its additional function as delivery system for the effectors (Pennington *et al.*, 2016).

491 putative effector genes are associated to the Candidates for Secreted Effector Proteins (CSEPs) superfamily which possess a signal peptide but no transmembrane domain. It is supposed that many CSEPs originated from a secreted fungal ribonuclease by gene duplication (Pedersen *et al.*, 2012). 293 effector candidates are assigned to the Effectors homologous to *Avrk1* and *Avra10* (EKA) gene family. It is supposed that the EKA members originated from the truncated ORF1 of Class I-LINE retrotransposons. They lack an N-terminal signal sequence or a signature for uptake by host cells and the mechanism of their secretion remains unknown (Amselem *et al.*, 2015).

The BEC characterization is still restricted to a small number of putative effectors and the molecular mechanisms of manipulation in barley are rarely understood (Whigham *et al.*, 2015). It was shown that the BEC CSEP0055 interacts with pathogen-related protein *Hv*PR17c which was confirmed in its role in penetration resistance to *Bgh* (Zhang *et al.*, 2012*b*). The heat shock proteins (Hsps) *Hv*Hsp16.9 and *Hv*Hsp17.5 were identified as putative effector targets of CSEP0105. Hsps are known to provide thermotolerance to the cell. However, for some Hsps also contribution to the plant defense was shown, for example via stabilization of R-proteins (Maimbo *et al.*, 2007; Van Ooijen *et al.*, 2010; Ahmed *et al.*, 2015). The effectors BEC3 and BEC4 exhibited interactions with a thiopurine methyltransferase, an ubiquitin-conjugating enzyme, and an ADP ribosylation factor-GTPase-activating protein (ARF-GAP). For the latter the authors supposed that BEC4 may manipulate defense-associated vesicle trafficking of the host to suppress pre-haustorial resistance (Schmidt *et al.*, 2014).

ARF-GAPs are regulators of ARF-GTPases which are necessary for the induction of vesicle budding. The ARF-GTPase *Hv*ARFA1b/1c was identified as RF in the interaction of barley and *Bgh*. Additionally, it was suggested that ARFA1b/1c is functionally linked to the *Hv*ROR2 syntaxin in pathogen defense regulation. *Hv*ROR2 is an orthologue of *At*Pen1 and supposed to be involved in defense-associated vesicle trafficking. *Hv*ROR2 was also found to interact with the SNARE protein *Hv*SNAP34, another RF essential for penetration resistance. *Hv*SNAP34 is likely

participating in vesicle-docking to the target membrane (Collins *et al.*, 2003; Assaad *et al.*, 2004; Douchkov *et al.*, 2005; Böhlenius *et al.*, 2010).

The functional *Hv*ROR2 syntaxin and the *Hv*SNAP34 SNARE protein are also required for the broad-spectrum resistance of barley against all races of *Bgh*. The resistance is mediated through absence of *Hv*MLO, a seven-transmembrane domain containing protein. It is the most prominent SF in the barley-*Bgh* pathosystem and was shown to be located in the plasma membrane and to interact calcium dependently with calmodulin. However, its exact biochemical function is still unknown (Jorgensen, 1994; Buschges *et al.*, 1997; Kim *et al.*, 2002*b*; Douchkov *et al.*, 2005; O'Connell and Panstruga, 2006; Eichmann and Hückelhoven, 2008). *Hv*MLO is the hub of an *Hv*MLO-dependent regulon and probably a negative regulator of the cell wall-related defense of barley against *Bgh*, associated with vesicles and mediated by SNARE (Douchkov *et al.*, 2005; Humphry *et al.*, 2010; Hückelhoven *et al.*, 2013). A possible member of the regulon, dependent on *Hv*MLO, is the putative SF *Hv*CRK1, an ER localized cysteine-rich receptor-like kinase. It is *Hv*MLO-dependently induced and exhibits also an negative impact on barley penetration resistance to *Bgh* (Rayapuram *et al.*, 2012). Additionally, barley BAX INHIBITOR-1 (*Hv*BI-1) is ER localized and likely a negative regulator of penetration resistance associated with the cell wall. Thus, it represents a putative SF to *Bgh* during infection. However, the expression of *Hv*BI-1 seems not as strictly dependent on *Hv*MLO like *Hv*CRK1 (Eichmann *et al.*, 2010).

Other effector targets could be SFs with a rather supportive effect on *Bgh* accommodation and development. Due to the obligate biotrophic lifestyle of *Bgh*, these SFs would be promoted by the pathogen. Barley alcohol dehydrogenase 1 (*Hv*ADH1) may be such an SF. Its expression and its activity was shown to be induced during attack of *Bgh*. It was assumed that *Hv*ADH1 possess a role in the glycolytic/fermentative pathway of the plant cell. This *Hv*ADH1 could be crucial for the hexose supply and thus nutrition of *Bgh* (Pathuri *et al.*, 2011; Proels *et al.*, 2011). Also, the small GTPase *Hv*RACB, object of study in this work, is required by *Bgh* for the host cell invasion and subsequent haustorial expansion. The role of *Hv*RACB as SF is likely due to its activity in the modulation of the cytoskeleton (Schultheiss *et al.*, 2002; Hoefle *et al.*, 2011). *Hv*RACB and its acting in the interaction of barley and *Bgh* will be introduced later in more detail.

1.3.7 Effector-triggered immunity

To overcome ETS the plants evolved a second layer of inductive defense, named effector-triggered immunity (ETI) (chapter 1.3.3; Figure 6; Jones and Dangl, 2006). It is based on the evolutionary gained ability of the plant immunity to recognize pathogen effectors. When compared to the race-unspecific defense via preformed barriers and PTI, ETI leads to a race-specific resistance. It refers to similar responses of defense like the basal defense. However, ETI is executed faster and more intensively. It can even induce hypersensitive reaction (HR) which results in cell death and functions as a physical block to further proliferation of the pathogen (Hadwiger and Culley, 1993; Greenberg, 1997; Jones and Dangl, 2006). ETI is induced by the perception of pathogen effectors via specific disease resistance proteins (R-proteins) which are encoded by *R*-genes. R-proteins are mostly intracellular nucleotide-binding leucine-rich repeat proteins (NB-LRRs) or extracellular leucine-rich repeat proteins connected to a short transmembrane domain (eLRRs-TM, receptor-like proteins). The perceived effectors are called specific elicitors or avirulence proteins (AVRs). They occur in

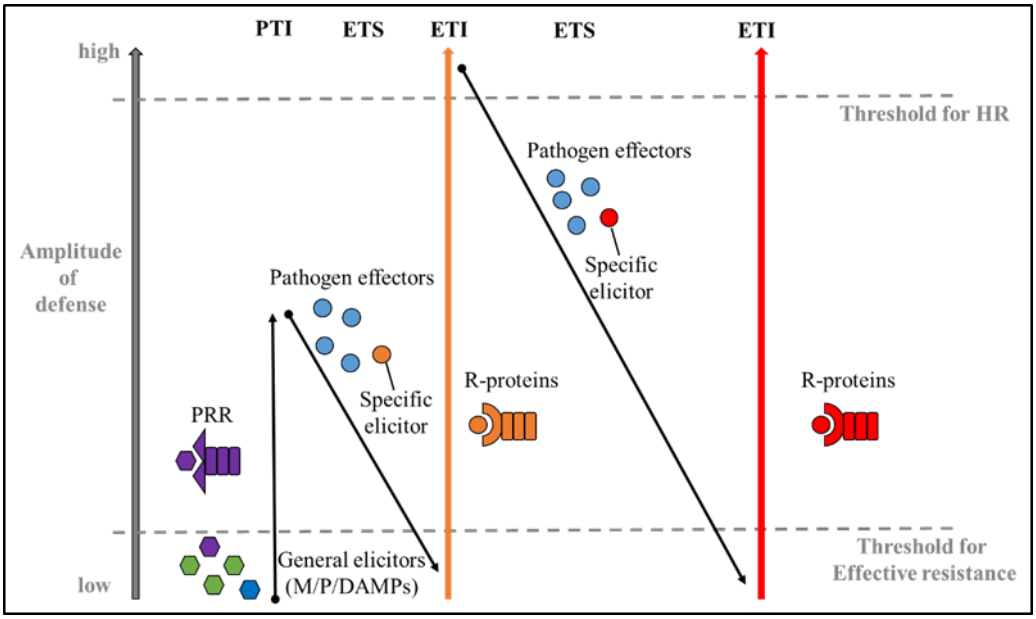

Figure 6: The 'zig-zag'-model of the inductive plant immunity (Jones & Dangl 2006, modified).
General elicitors (purple hexagon) are perceived by pattern recognition receptors (PRRs) and PAMP-triggered immunity (PTI) is induced. PTI can be overcome by pathogen-derived effectors, forcing an effector-triggered susceptibility (ETS). Some effectors (orange circle) function as specific elicitors, recognized by a plant resistance protein (R-protein). The induced effector-triggered immunity (ETI) is similar to PTI but faster and stronger and can lead to hypersensitive cell death (HR). Natural selection can force the loss of the specific elicitor and evolvement of new or modified effectors, which do not function as elicitors and hence cause ETS again. The newly gained ETS can lead to an evolvement of an R-protein. This new R-protein detects the ETS causing effector (red circle), which therefore turns to a specific elicitor effecting ETI.

specific races or strains of the pathogen and can only be detected by plants with the respective *R*-gene as counterpart (Montesano *et al.*, 2003; Jones and Dangl, 2006; Stergiopoulos and de Wit, 2009).

The perception of the effector proteins can take place via a direct physical interaction between the R-protein and the effector (receptor-ligand model) or indirectly by sensing effector mediated modifications of the effector target (guard-model) (Jones and Dangl, 2006; Stergiopoulos and de Wit, 2009). The guard-model was extended by the decoy-model. It suggests that plants evolved decoy molecules to mimic effector targets. Such decoys trap effector proteins but would not lead to an enhanced fitness of the pathogen, regardless if an appropriate R-protein is expressed in the plant or not. However, if the decoy is guarded by an R-protein the manipulation of the decoy will be detected and ETI induced. (van der Hoorn and Kamoun, 2008).

AVRK1 and AVRA10 are two putative effectors of *Bgh* and eponyms of the EKA gene family (Ridout *et al.*, 2006). Both induce ETI in barley cultivars which carry the respective R-proteins MLK1 and MLA10. It was shown that MLA10 interacts with the two WRKY transcription factors (TFs) *Hv*WRKY1 and *Hv*WRKY2 of barley in an AVRA10-dependent manner. It is thought that these immediate downstream targets of the activated MLA10 mediate ETI which include HR dependent cell death (Shen *et al.*, 2007; Stergiopoulos and de Wit, 2009). Next to MLA10, further genes (MLA1, MLA6, MLA7, MLA12, AND MLA13) which are located at the *MLA* locus of barley were shown to code for R-genes. They perceive race specific effectors of *Bgh.* Recently, further WRKY TFs were found (*Hv*WRKY10, *Hv*WRKY19, *Hv*WRKY28) which participate in MLA triggered ETI and basal defense (Halterman *et al.*, 2001; Shen, 2003; Halterman and Wise, 2004; Stergiopoulos and de Wit, 2009; Meng and Wise, 2012).

Natural selection which is driven by ETI can cause the loss of effectors if they function as specific elicitors. Furthermore, it causes the development of new or modified pathogen effector proteins. These cannot be detected by the plants because no appropriate R-proteins are existent which could perceive the new or modified effectors directly or the manipulations of their operative targets. The resulting ETS will drive again a natural selection in the plant to develop new R-genes as counterparts which will induce ETI. Both processes can be assumed to boost each other in a never ending evolutionary arms race (Jones and Dangl, 2006; Stergiopoulos and de Wit, 2009).

1.4 Rho-related GTPase from plants

The above described stomata formation, root hair development, and plant defense responses depend on complex signaling pathways which are triggered by extracellular signaling cues. Hence, cellular key molecules are needed to perceive and integrate these complex signaling pathways. For all mentioned and further processes the regulatory participation of small GTPases was shown (Agrawal *et al.*, 2003; Berken, 2006; Humphries *et al.*, 2011).

1.4.1 Nomenclature, phylogenetic and basic functionality of ROPs

Small GTPases, also known as small G-Proteins, exist in all eukaryotes. They belong to the Ras superfamily of small GTPases, named after their founding member 'Ras'. The Ras superfamily is further divided in the 'Ras', 'Rho', 'Arf', 'Ran' and 'Rab' families (Macara *et al.*, 1996; Takai *et al.*, 2001). Arf, Rab and Ran are conserved in all eukaryotes and known to control processes of vesicular or nuclear trafficking. On the other hand, Ras and Rho G-Proteins were shown to transmit extracellular signals (Takai *et al.*, 2001; Yang, 2002). However, unlike animals and yeast, in plants no true Ras proteins were found. This makes Rho the exclusive family of G-Proteins in plants for transmission of extracellular signals. Furthermore, in animals the Rho family is further divided in the Rac, Rho and Cdc42 subfamilies, whereas in plants a unique subfamily of Rho exists. This Rho subfamily is called ROP (Rho-related GTPase from plants) or RAC, according to the protein sequence similarities to the human Rac subfamily (Winge *et al.*, 1997; Takai *et al.*, 2001; Vernoud *et al.*, 2003). To avoid confusion, in this work exclusively the term 'ROP' will be used for the Rho subfamily of small GTPases, unique for plants. In all examined plant species the ROP subfamily represents a multigenic family. It contains closely related members with redundant, overlapping, distinct or multiple functions in the cell. In *Arabidopsis thaliana* 11 ROPs were found, in rice 7 and in barley 6 (Christensen *et al.*, 2003; Schultheiss *et al.*, 2003; Nibau *et al.*, 2006; Craddock *et al.*, 2012; Fehér and Lajkó, 2015).

Like the other members of the Ras superfamily, all ROPs share the conserved G-domain. This domain is necessary for the basic function of ROPs to bind GTP with high affinity and inefficiently hydrolyze it to GDP (Macara *et al.*, 1996; Takai *et al.*, 2001). The alternation between an active GTP-bound status and an inactive GDP-bound status let them serve as molecular switches. The third possible status, namely the GTP/GDP unbound status, is only quite short-living (Vetter and Wittinghofer, 2001; Berken and Wittinghofer, 2008). Shuttling between the ON and the OFF status and subcellular localization is regulated by three major upstream regulators. They directly interact

with ROPs, partly dependent on diverse posttranslational modifications (Kost, 2008; Craddock *et al.*, 2012). The guanine nucleotide exchange factors (GEFs) promote the release of GDP from the ROP G-domain. GTP effectively occupies the G-domain due to higher cellular concentrations than GDP (Berken *et al.*, 2005; Gu *et al.*, 2006). The OFF-status is promoted by GTPase activating proteins (GAPs). They increase GTP hydrolysis activity of the G-domain which leads to an accelerated inactivation of the ROP (Wu *et al.*, 2000). It is supposed that transmembrane RLKs regulate the activation of ROPs via GEFs. This corresponds to the association of most ROPs to the plasma membrane (Miyawaki and Yang, 2014; Fehér and Lajkó, 2015). Hence, the RLK-GEF-ROP complex is suggested as early signaling complex. Furthermore, the membrane association is thought to be pivotal for activity regulation and dependent on post-translational modifications. Based on the their variable region at the C-terminus, type I and type II ROPs can be distinguished (Winge *et al.*, 1997; Nibau *et al.*, 2006). Members of both groups are thought to be post-translationally modified at the C-terminus for attachment to the membrane. Hereby, type I ROPs are putatively prenylated and type II proteins palmitoylated (S-acetylated) (Lavy *et al.*, 2002; Lavy and Yalovsky, 2006; Sorek *et al.*, 2007). Palmitoylation inhibits interaction with guanine nucleotide dissociation inhibitors (GDIs). These upstream regulators extract inactivated prenylated G-Proteins from the membrane, sequesters them in the cytosol, and inhibits the exchange of GDP for GTP (Pozo *et al.*, 2002; Lin *et al.*, 2003; DerMardirossian and Bokoch, 2005; Kost, 2008). Consequently, GDIs are negative regulators, likely involved in a mechanism for ROP recycling to stabilize a polarized and spatially restricted activity of type I ROPs. However, recycling of ROPs seems not to be necessary for ROP type II regulation (Nibau *et al.*, 2006; Kost, 2008). Further possible post-translational modifications exist which effect ROP activity. The phosphorylation of a conserved serine residue is essential for the ROP-GEF interaction. The S-acylation of conserved G-domain cysteines is important for association with lipid rafts and thus for subcellular localization (Sorek *et al.*, 2010; Fodor-Dunai *et al.*, 2011).

Only the GTP-bound ROPs are active and interact with downstream effectors. These effectors then interact with further cellular components to relay and integrate the extracellular signals for responses via intracellular pathways (Wu *et al.*, 2011). Plants possess two unique families of ROP effectors. They are called ROP-interactive CRIB motif-containing proteins (RICs) and ROP Interactive Partners (RIPs). RICs and RIPs were shown to participate in regulation of fundamental processes in the cell such as polar growth, cell morphogenesis, and plant defense (Wu *et al.*, 2001; Li *et al.*, 2008; Schultheiss *et al.*, 2008). Furthermore, these processes are based on the establishment of cell polarity which is tightly linked to the cytoskeleton and vesicular trafficking (Hall, 1998; Molendijk *et al.*, 2004; Hückelhoven, 2005; Lavy *et al.*, 2007; Fu *et al.*, 2009). Hence, F-actin, microtubules, and

vesicle trafficking are universal targets of G-Protein signaling in animals and plants (Brembu *et al.*, 2006).

1.4.2 ROP-regulated polar tip growth

The tip growth is characterized by a sustained unidirectional growth and is the basis for the tubular elongated cells of root hairs and pollen tubes. It needs massive and polar secretion of cell wall material to the spatial restricted site of growth (Carol and Dolan, 2002; Gu and Nielsen, 2013). The polarization of the cell is regulated by a self-organizing system. It is based on the asymmetrical distribution of organelles, vesicles, cytoskeletal elements, and signaling molecules such as ROPs and its associated regulators and effectors towards and at the future cell apex (Grebe *et al.*, 2001; Cole and Fowler, 2006; Kost, 2008).

In *Arabidopsis thaliana, At*ROP1 accumulates at the future apex of the pollen tube before any visible bulging of the pollen (Fu *et al.*, 2001). *At*ROP1 organizes its own activity at the apex and therefore at the tip growth domain of the pollen tube via counteracting downstream pathways which balance each other (Figure 7; Gu *et al.*, 2005). The molecular mechanisms of these pathways are not known in detail. However, it was shown that *At*RIC4, an effector of *At*ROP1, is dependent for the assembly of F-actin at the tip of the pollen tube (Gu *et al.*, 2005; Yang and Lavagi, 2012). It is supposed that this assembly of F-actin supports the accumulation of vesicles, directed to the tip. The vesicles putatively contain positive regulators of *At*ROP1 such as *At*RopGEF1 or the RLK *At*PRK2. These regulators propagate further activation of *At*ROP1 at the apex of the pollen tube and hence a positive feedback loop (Gu *et al.*, 2006; Zhang and McCormick, 2007; Chang *et al.*, 2013). *At*RIP1 (*At*ICR1), another effector of *At*ROP1, participates in polar exocytosis and activation of *At*ROP1 via interaction with the *At*SEC3 exocyst subunit which is necessary to tether the vesicles to the PM (Lavy *et al.*, 2007; Craddock *et al.*, 2012). The exocytosis of the vesicles is facilitated through the *At*ROP1-dependent activation of *At*RIC3 which promotes Ca^{2+} influx at the tip. The increase of calcium could lead to disassembly of F-actin and hence to a promoted exocytosis of the accumulated and tethered vesicles (Gu *et al.*, 2005; Yan *et al.*, 2009). On the other side, it was shown that these vesicles also contain the GAP *At*REN1. It spatially restricts together with the GDI *At*RhoGDI2a the *At*ROP1 activity and hence the domain of the tip growth of the pollen tube apex (Hwang *et al.*, 2008, 2010). It was further suggested that Ca^{2+} influx negatively regulates *At*ROP1 via an activation of *At*REN1 at the PM at higher calcium concentrations (Craddock *et al.*, 2012).

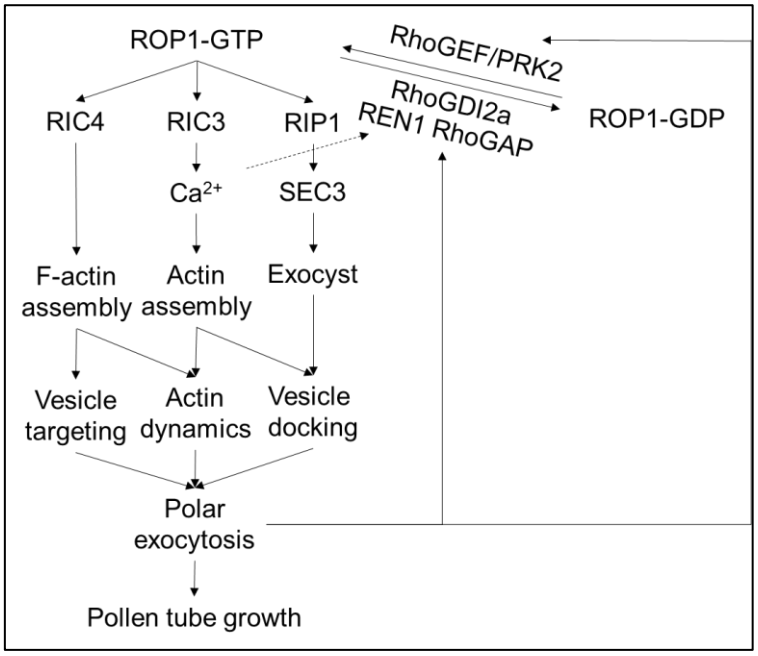

Figure 7: The *At*ROP1 self-regulating network of *At*ROP1 in the tip growth of pollen tubes (Based on Qin and Dong, 2015, modified).
***At*ROP1 promotes polar exocytosis of vesicles at the apex of the pollen tube through regulation of the F-actin dynamics. The vesicles contain cell wall and membrane material, necessary for pollen tube growth, but also positive and negative upstream regulators of *At*ROP1. Furthermore, activity of *At*ROP1 is reduced via *At*RhoGDI2a and the negative regulator *At*REN1, putatively dependent on Ca^{2+}.**

Also in the root, ROPs regulate the initiation of root hairs and their tip growth via actin dynamics, polar exocytosis, and Ca^{2+} gradient establishment. Hence, their role is similar to the role of ROPs in the above described tip growth of the pollen tube (Pei *et al.*, 2012). *At*ROP2 accumulates in the trichoblast at the future apex of the root hair even before any visible bulging of the trichoblast. This suggests a role in the initiation of root hairs whereas *At*ROP4 and *At*ROP6 may regulate their elongation (Molendijk *et al.*, 2001; Jones *et al.*, 2002; Grierson *et al.*, 2014). The RLK FERONIA (*At*FER) was shown to interact with the ROP positive regulators *At*RopGEF10 and *At*RopGEF4. The first one is assumed to be involved in the initiation and the latter in the elongation of root hairs. Both were proven to directly bind different ROPs such as *At*ROP2 and *At*ROP6. This suggests a function as possible RLK-GEF-ROP complex which recruits the ROPs to the growth site (Yu *et al.*, 2012; Huang *et al.*, 2013; Grierson *et al.*, 2014). The GDI *At*RhoGDI1 (*At*SCN1) is probably involved in determining and restricting the area of ROP activity. Furthermore, recent data confirmed a direct interaction of *At*RopGDI1 and *At*ROP2 *in vivo* (Carol *et al.*, 2005; Chai *et al.*, 2016). Minutes after accumulation of *At*ROP2, a drop of pH can be observed and the cell wall bulges out. This is possibly due to the loosening activity of pH-dependent expansins on the cell wall (Bibikova *et al.*,

1998; Baluska *et al.*, 2000). Additionally, *At*ROP2 initiates the production of ROS by the NAD(P)H oxidase *At*RHD2. This leads to the activation of calcium channels at the site of ROP accumulation. The Ca^{2+} influx establishes a Ca^{2+} gradient with the highest concentration at the apex of the root hair. The Ca^{2+} gradient probably promotes polar exocytosis as described above for the pollen tube and drives further activation of *At*RHD2 in an Ca^{2+} dependent positive feedback loop (Foreman *et al.*, 2003; Jones *et al.*, 2007; Grierson *et al.*, 2014). Furthermore, it is proposed that activation of ROPs in the trichoblast and hence, spatial determination of root hair initiation occurs in an auxin dependent manner. Payne and Grierson (Payne and Grierson, 2009) published an computational model which assumes auxin dependent activation of ROPs in the cell. Interestingly, the model could account root hair initiations in trichoblasts of WT and various mutant plants.

1.4.3 ROP-regulated interdigitated diffuse growth

In the unicellular pollen system, the tight regulation of cell polarity, necessary for polar tip growth of the pollen tube, is organized without any external cue. In contrast, the interdigitation of pavement cells (PCs) in *Arabidopsis thaliana* needs multiple polarities and complex cell-to-cell signaling (Hwang *et al.*, 2010; Craddock *et al.*, 2012). To establish the jigsaw puzzled shape of the cells, adjacent PCs locally expand into each other. Hereby they form alternatively outgrowing lobes and invaginated indents (Craddock *et al.*, 2012).

It was shown that ROPs orchestrate the multiple polarities which are essential for interdigitation of the PCs via the regulation of F-actin and MTs (Figure 8). The self-organization is ROP-dependent and based on a RLK signaling complex which activates the counteracting ROPs *At*ROP2 and *At*ROP6. *At*ROP2 is interacting with the ROP downstream effector *At*RIC4. Hereby, it promotes the local cell expansion which generates the lobe via propagation of the assembly of fine F-actin. This is similar to *At*ROP1-mediated polar tip growth in the pollen tube (Gu *et al.*, 2005; Fu *et al.*, 2005; Xu *et al.*, 2010; Qin and Dong, 2015). Opposite of *At*ROP2 activity, in the indenting region of the adjacent PC, *At*ROP6 interacts with the downstream effector *At*RIC1. Thus, *At*ROP6 regulates the spatially restricted indentation accordingly to the expanding lobe via promotion of cortical MTs (Fu *et al.*, 2005, 2009).

Furthermore, it was shown that this process is supported by the *At*RIC1 binding protein Katanin (*At*KTN1). It severs branched MTs for local arrangement of well-ordered MTs (Lin *et al.*, 2013). Similar to the *At*ROP1 regulated growth of the pollen tube, both pathways antagonistically coordinate each other to stabilize the alternating expanding and invagination of the cell boundary

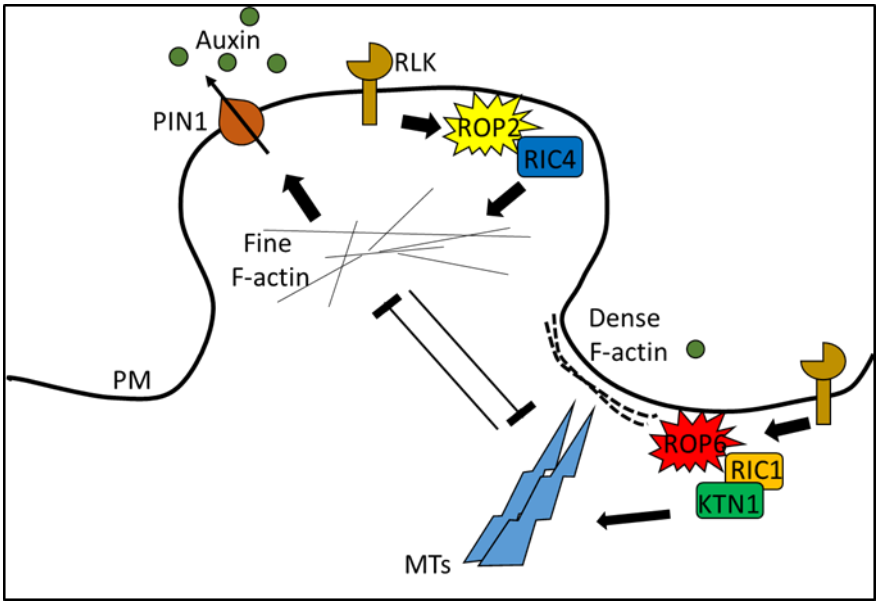

Figure 8: Model of the ROP regulated interdigitation of pavement cells in *A. thaliana* (based on Craddock *et al.*, 2012; Qin and Dong, 2015, modified).
For clarity, only one PC is shown. Both pathways are activated via auxin and a RLK, acting as ROP upstream regulator. *At*ROP2 mediates F-actin dynamics and *At*PIN1 mediates auxin efflux. Both processes are connected in a positive feedback loop. *At*ROP6 promotes suppression of outgrowth and therefore PC indentation through propagation of well-ordered MTs. *At*ROP2 promotes lobe expansion via positive regulation of fine F-actin. Both pathways suppress each other to establish an alternating indentation and lobe formation

(Craddock *et al.*, 2012). Hence, active *At*ROP2/*At*RIC4, localized at the lobe, inactivates *At*RIC1 to suppress the establishment of well-ordered cortical MTs in this area. Accordingly, well-ordered MTs which are localized at the indentation are promoted by AtROP6/AtRIC1 activity. Furthermore, their activity suppresses *At*ROP2 and consequently the lobe forming processes (Fu *et al.*, 2005, 2009).
A crosstalk between ROP- and PIN protein regulated cell polarization pathways is likely (Nagawa *et al.*, 2012; Qin and Dong, 2015). The auxin efflux carrier *At*PIN1 enriches in the PC lobes parallelly to *At*ROP2 activity. This is further supported through enhanced *At*PIN1 derived auxin efflux. *At*ROP2 promotes again accumulation of *At*PIN1 via F-actin dependent reduction of *At*PIN1 endocytosis. Thus, a positive feedback loop between *At*PIN1 and *At*ROP2 activity in the lobe is established (Xu *et al.*, 2010; Nagawa *et al.*, 2012; Qin and Dong, 2015).

1.4.4 ROP-regulated stomatal asymmetric cell division

Daughter cells which can follow different developmental fates are generated via asymmetric cell divisions. This includes often but not necessarily physiological cell asymmetries such as size and

shape. These asymmetries are achieved by premitotic polarizations of the mother cell. Polarization of the cell is visible through obligatory nucleus migration which defines the future localization of the division plane (Facette and Smith, 2012). In the stomata formation of maize the ROPs are essential participants in SMC polarization before asymmetric cell division which generates the SC and an undifferentiated epidermal cell (Humphries *et al.*, 2011; Facette and Smith, 2012).

Polarization of the SMC occurs towards the adjacent GMC, putatively due to extracellular signals deriving from the GMC (chapter 1.1.3; Stebbins and Shah, 1960; Facette and Smith, 2012). As the first known SMC polarization marker the receptor like proteins (RLPs) *Zm*PAN2 and *Zm*PAN1 accumulate at the SMC/GMC contact site. Hereby, *Zm*PAN2 is required for *Zm*PAN1 localization. It is assumed that *Zm*PAN2 and *Zm*PAN1 perceive the cues for GMC polarization and promote upstream of ROPs further SMC polarization events. Subsequent signaling events remain unclear because both RLPs possess catalytically inactive kinase domains and no direct interaction partners have been identified so far (Cartwright *et al.*, 2009; Zhang *et al.*, 2012*a*). However, ROPs can be co-immunoprecipitated together with ZmPAN1 (Humphries *et al.*, 2011). It was shown that the maize type I ROPs, *Zm*ROP2, and *Zm*ROP9 are obligatory for further SMC polarization and subsequently co-localize with *Zm*PAN1 at SMC/GMC contact site. Furthermore, it is suggested that *Zm*ROP2 and *Zm*ROP9 are activated and localized via a not further characterized pathway which is dependent on *Zm*PAN1 (Humphries *et al.*, 2011; Facette and Smith, 2012). An actin patch forms at the contact site of SMC and GMC. This occurs likely after polar localization of PANs and ROPs and is putatively ROP regulated (Cartwright *et al.*, 2009; Humphries *et al.*, 2011). The last observed step represents the migration of the SMC nucleus towards the GMC contact site. It was shown that previous patch formation of F-actin is mandatory for correct nucleus positioning. Hence, F-actin is possibly responsible for migration or anchoring of the nucleus, or both (Panteris *et al.*, 2006, 2007).

1.4.5 ROP-regulated pathogen defense

In several plant organisms ROPs positively and negatively influence plant-pathogen interactions (Schultheiss *et al.*, 2002; Chen *et al.*, 2010; Poraty-Gavra *et al.*, 2013). In rice (*Oryza sativa, Os*) *Os*RAC1 was shown to participate in chitin induced PTI. Chitin is bound by the OsCEBiP-OsCERK1 chitin-receptor complex which activates *Os*RacGEF1, an *Os*RAC1 upstream positive regulator (Akamatsu *et al.*, 2013). Active *Os*RAC1 is subsequently regulating defense-relevant ROS production and HR dependent cell death. Therefore, it enhances the activity of the NAD(P)H oxidase *Os*RbohB via a direct interaction (Kawasaki *et al.*, 1999; Ono *et al.*, 2001; Kosami *et al.*, 2014). On the other hand, *Os*RAC1 was shown, similar to rice-blast pathogen derived effectors, to down-

regulate the expression of the gene metallothionein-like protein 2b (*OsMT2b*) which encodes for a ROS scavenger protein (Wong *et al.*, 2004). Furthermore, recent data indicates that *Os*RAC1 activates the transcription factors *Os*RAI1 and *Os*RAP2.6 via MAPK signaling. These transcription factors are known to regulate phytoalexin biosynthesis and PR-gene expression (Wamaitha *et al.*, 2012; Kim *et al.*, 2012; Kawano *et al.*, 2014). Additionally, the defense relevant production of lignin is supported by *Os*RAC1. It was shown that *Os*CCR1, an enzyme involved in lignin production, is bound by active *Os*RAC1 and enzymatically activated in vitro. This makes *Os*CCR1 a quite likely *Os*RAC1 downstream effector (Kawasaki *et al.*, 2006).

Next to PTI, *Os*RAC1 is involved in ETI. The ROP directly interacts with the R-protein *Os*Pit which is activated via an effector of the hemibiotrophic rice blast fungus *Magnaporthe oryzae* (*Mo*). Thus, the effector functions as a specific elicitor and mediates disease resistance in rice. *Os*Pit activates *Os*RAC1 at the plasma membrane which subsequently induces production of ROS and HR-mediated cell death (Kawano *et al.*, 2010). *Mo*AVRPIA is another specific elicitor of the rice blast fungus. It is recognized by the hetero-complex of the two R-proteins *Os*RGA4 and *Os*RGA5. Both R-proteins are necessary for activation of *Os*RAC1 and disease resistance mediated by *Mo*AVRPIA (Okuyama *et al.*, 2011; Cesari *et al.*, 2013; Césari *et al.*, 2014).

It is supposed that *Os*RAC1 functions downstream of additional R-proteins not yet identified. This underlines the high number of diverse functions which can be performed by a single ROP (Kawano *et al.*, 2014).

1.5 The barley ROP protein *Hv*RACB

*Hv*RACB represents the most intensive characterized ROP in barley and stands together with *Hv*RACD for the type I ROPs in *Hordeum vulgare*. The ROP *Os*RAC6 (also known as *Os*RACB) is its putative ortholog in rice and shows 98 % identity to *Hv*RACB (Schultheiss *et al.*, 2002; Miki *et al.*, 2005).

*Os*RAC6 was shown to play a role as negative regulator of the plant defense in the interaction of rice and *Magnaporthe oryzae*. Additionally, *Hv*RACB participates as susceptibility factor in the barley-*Bgh* interaction (Figure 9; Schultheiss *et al.*, 2002, 2003; Jung *et al.*, 2006; Chen *et al.*, 2010). Transient knockdown of *HvRACB* (*HvRACB* RNAi) in barley results in a reduced penetration efficiency (PE) of *Bgh*. On the other hand, transient overexpression of a constitutive activated form of *Hv*RACB (*HvRACB* OECA) enhances the penetration success. However, transient overexpression of the *HvRACB* wildtype form and of a dominant negative form showed no

significant effects (Schultheiss *et al.*, 2002, 2003). Furthermore, *HvRACB* OECA and *HvRACB* RNAi did not affect the super-susceptibility of *MLO ror1* mutant barley plants or the partial susceptibility of *mlo ror1* plants. This strongly suggested a functional link to the SF *Hv*MLO and the RF *Hv*ROR1 (Kim *et al.*, 2002*a*; Schultheiss *et al.*, 2002). Stable transgenic *HvRACB* RNAi and *HvRACB* OECA lines confirmed the results of the transient assays and revealed further developmental defects of the mutant lines (Schultheiss *et al.*, 2005; Pathuri *et al.*, 2008; Hoefle *et al.*, 2011). In stable *HvRACB* OECA plants depolarized growth of root hairs, increased B-cell length, a reduced number of stomata, and enhanced number of abnormal developed stomata were reported. In stable *HvRACB* RNAi plants a severe failure of root hair outgrowth was detected. This supported the idea of *Hv*RACB as SF. It was suggested that *Hv*RACB could function in polarization events of the cell such as polar growth processes of the membrane, necessary for accommodation of the haustorium of *Bgh* (Schultheiss *et al.*, 2005; Pathuri *et al.*, 2008, 2009; Hoefle *et al.*, 2011). In the homologous interaction of *Bgh* and barley the attacked epidermal cells show a cell polarization towards the attempted site of penetration. This includes reorganization of the actin cytoskeleton which is crucial for successful penetration resistance. Furthermore, it is regulated by the SFs *Hv*MLO and *Hv*RACB (chapter 1.3.4; Kobayashi *et al.*, 1997; Opalski *et al.*, 2005). Accordingly, it was shown that polarization of F-actin is reduced by *HvRACB* OECA but increased by *HvRACB* RNAi. The same is observed for polarized F-actin and the presence and absence of functional *Hv*MLO (Opalski *et al.*, 2005).

Activated *Hv*RACB interacts with its putative downstream effector *Hv*RIC171 which accumulates at the attempted site of penetration. The cellular function of *Hv*RIC171 is unknown. However, overexpression of the putative ROP effector exhibits similar effects on the penetration efficiency of *Bgh* like *HvRACB* OECA (Schultheiss *et al.*, 2008). Like F-actin also MTs exhibit a stronger polarization towards the site of fungal attack if the penetration attempt was unsuccessful, compared to successful penetrations. Furthermore, MTs even loosen at the sites of successful penetration events (Hoefle *et al.*, 2011). *Hv*RACB directly interacts with the MICROTUBULE-ASSOCIATED ROP-GTPASE ACTIVATING PROTEIN1 (*Hv*MAGAP1). *Hv*MAGAP1 is associated with MTs but released after *Hv*RACB activation and recruited by the ROP to the cell periphery. The RhoGAP functions as negative regulator of *Hv*RACB and as RF since abundance of *Hv*MAGAP1 was shown to reduce penetration efficiency of *Bgh* (Hoefle *et al.*, 2011). The influence of *Hv*MAGAP1 on the interaction of barley and *Bgh* could be uncoupled from the association to the MTs. Hence, the authors proposed that the association is due to a sequestration mechanism which is dependent on MTs instead of a direct impact of the RhoGAP on the organization of MTs (Hoefle *et al.*, 2011). Recently, the barley Engulfment and Motility (ELMO) Domain Containing Protein, *Hv*ELMOD_C

was identified as *Hv*MAGAP1 interactor in a Y2H screen. It was observed to co-localize with the RhoGAP on the MTs *in planta* (Hoefle and Hückelhoven, 2014). Co-expression of *Hv*ELMOD_C and *Hv*MAGAP1 eliminates the limiting effect of the GAP on the penetration efficiency of *Bgh*.

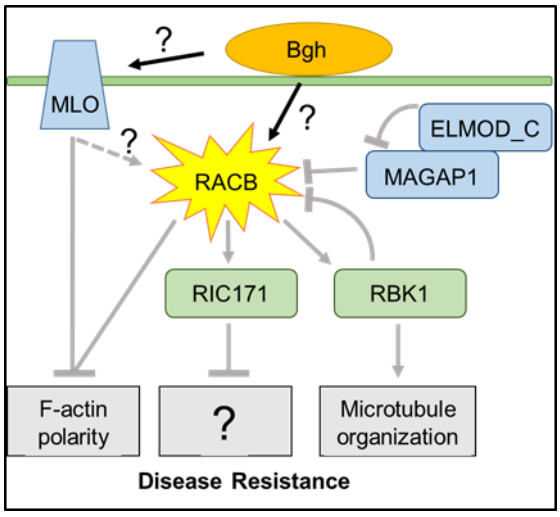

Figure 9: *Hv*RACB and its role in the interaction of barley and *Bgh* (based on Kawano et al., 2014).
The susceptibility factors *Hv*MLO and *Hv*RACB regulate cytoskeleton dynamics. Hereby, they negatively affect polarization of F-actin stability of MTs. Both are crucial for penetration resistance against *Bgh*. The activation via *Bgh* is unknown, but *Hv*MAGAP1 represents a negative upstream regulator. It is itself negatively regulated by *Hv*ELMOD_C. *Hv*RIC171, as *Hv*RACB downstream effector, negatively effects disease resistance through an unknown pathway. *Hv*RBK1 exhibits a positive effect on the stability of cortical MTs and hence a putative negative feedback loop on the activity of *Hv*RACB.

Therefore, it was suggested that the ELMO protein functions as negative regulator of *Hv*MAGAP1 and hence as positive regulator of *Hv*RACB activity (Hoefle and Hückelhoven, 2014).
However, interaction of *Hv*RACB OECA with the protein kinase *Hv*RBK1 suggests that *Hv*RACB signaling could also promote basal resistance (Huesmann *et al.*, 2012). *Hv*RBK1 is bound by *Hv*RACB OECA in planta and is recruited to the cell periphery. An increased kinase activity of *Hv*RBK1, when bound to *Hv*RACB OECA, was measured in vitro. *Hv*RBK1 was shown to restrict the penetration efficiency of *Bgh*. This probably works through stabilization of cortical MTs which could also include a negative feedback on *Hv*RACB (Huesmann *et al.*, 2012)

1.6 Objectives

*Hv*RACB has been known to participate in the interaction of barley and *Bgh* for some time (chapter 1.5; Schultheiss *et al.*, 2002). It was suggested quite early that this ROP belongs to the category of SFs, co-opted by the fungus to support penetration of the cell wall and establishment of the haustorium (chapter 1.3.5; Schultheiss *et al.*, 2003). However, the precise mechanism how *Bgh* could take advantage of *Hv*RACB remained incomplete. Based on this situation, the aim of the work was to obtain further data at the interface of plant development and phytopathology to elucidate the functional principle of *Hv*RACB in the susceptibility to the barley powdery mildew fungus.

One potential approach is the further investigation of the actual *Hv*RACB functionality in barley development. Hence, the first part of this work was the search for developmental phenotypes in stable *HvRACB* RNAi mutant plants. Subsequently, these phenotypes were qualitatively and quantitatively characterized. Fortunately, the search could be set up in a targeted manner due to already published data. The studies described phenotypes of root hair formation, stomata development, and epidermal cell expansion in stable *HvRACB* OECA and *HvRACB* RNAi plants, as well as other plant species such as Arabidopsis thaliana and maize (Schultheiss *et al.*, 2005; Fu *et al.*, 2005; Pathuri *et al.*, 2008, 2009; Humphries *et al.*, 2011; Hoefle *et al.*, 2011).

Furthermore, the data of several independent microarray experiments were used. The transcriptomic data comprised *HvRACB* OECA and *HvRACB* RNAi without and with *Bgh* challenging and enabled a second targeted approach (Ralph Hückelhoven and Vera Schnepf; both TU München, unpublished data). The microarrays revealed a high quantity of genes which are altered at their transcriptional level, when compared to the wildtype. A considerable number of these genes were assigned to processes related to the cell wall. This appeared to be in accordance with already published ROP relevant data (Schultheiss *et al.*, 2005; Pathuri *et al.*, 2008; Hoefle *et al.*, 2011). Hence, in parallel to the analysis of the phenotypes of the *HvRACB* RNAi plants the expression of cell wall modifier genes and the biochemical features of the cell wall were examined in detail.

Together, this should allow for a better understanding of *Hv*RACB function in healthy plants. Furthermore, it should enrich our knowledge about ROP functions in grasses and help building or supporting hypotheses about functions of *Hv*RACB in compatibility with *Bgh*.

2 Material and methods

2.1 Plant material, growth conditions and pathogens

2.1.1 Plant material

Barley (*Hordeum vulgare L.*) cv. Golden Promise was used as wildtype (WT) and represents also the genetic background of the *HvRACB* RNAi line 16/2-4B (*HvRACB* RNAi). This line expresses a RNAi construct under control of the ectopic and constitutive maize *ZmUBIQUITIN1* gene promotor which reduces available *HvRACB* transcript amount (Hoefle *et al.*, 2011). The *HvRACB* RNAi line does not produce homozygous offspring. Offspring of transgenic T3 donor plants were genotyped to separate transgenic offspring carrying the *HvRACB* RNAi construct from azygous offspring that lost the knockdown construct due to segregation (chapter 2.4.1). Azygous sister plants are similar to the wild type (Hoefle *et al.*, 2011) and thus served as ideal controls (azygous control). Kernels were stored at 4 °C in darkness.

2.1.2 Pre-germination and growth conditions

Kernels were surface-sterilized for 3 min, in 70 % (v/v) EtOH and afterwards in sterilization solution (4 % NaOCl, Tween-20), shaking for 1.5 h. After replacing the solution three times with H_2O, kernels were washed in H_2O, shaking for 30 min. Husks were carefully removed with a tweezer without damaging the embryo. Seeds were pre-germinated on H_2O wetted filter paper for 2 d, in the dark, at RT. Seedlings, showing coleoptile and roots, were sown into and slightly covered with soil (Typ ED73, Einheitserde- und Humuswerke, Gebr. Patzer GmbH & Co KG, Sinntal-Jossa, Germany). Plants were transferred in an environmental chamber (Conviron, Winnipeg, Canada), adjusted to 18 °C, a relative humidity of 65% and a photoperiod of 16 h with h 150 $\mu mol/s \times m^2$ photon flux density.

2.1.3 *Blumeria graminis* cultivation and plant inoculation

As phytopathogen the barley powdery mildew fungus *Blumeria graminis f.sp. hordei* (*Bgh*) race A6 was used. The fungus was propagated on the barley cultivar Golden Promise in an environmental chamber (Sanyo, München, Germany) at the above described conditions (chapter 2.1.2). For inoculation the pots with the barley plants were laid in the inoculation chamber together with a

hemocytometer. Spores were blown from infected plants into the inoculation chamber and swirled for homogenous dispersion. After a five-minutes waiting period for conidia settlement the hemocytometer was used to evaluate for conidia density per mm^2, using a binocular. If necessary, the inoculation procedure was repeated to reach the desired density. The control plants were treated equally but without spore inoculation. After inoculation, the plants were put back into the environmental chamber under the above described conditions (chapter 2.1.2).

2.1.4 Inoculation of barley with *Rhizophagus irregularis*

For barley experiments, concerning the root colonization, the arbuscular mycorrhizal fungus *Rhizophagus irregularis* was used. AM inoculation was performed in the lab of Dr. Carolin Gutjahr, LMU München according the published lab protocol (Gutjahr *et al.*, 2008). The inoculum (spores and carrier) was ordered from a commercially supplier (SYMPLANTA, München, Germany).
The bottoms of the plant pots were covered with cotton wool and afterwards filled to the half with a gravel-vermiculite mix (1:1) (v/v). In the middle of each pot about 1000 *Rhizophagus irregularis* spores mixed with carrier material (attapulgit clay based dry powder) were placed and covered with the gravel-vermiculite mix. Barley seedlings, treated as described above (chapter 2.1.2), were planted in the sand-vermiculite mix. They were put directly above the placed inoculum to ensure the contact between the roots and the spores after elongation of the root. Plants were transferred in an environmental chamber under conditions as described above (chapter 2.1.2). In the first week, each pot was watered three times with 20 ml distilled H_2O. The following weeks, they were watered twice per week with 20 ml 0.5x Hoagland's nutrient solution (100 µM potassium chloride and 100µM potassium dihydrogen phosphate in ddH_2O) and once with distilled water. After six weeks, the roots were cleaned from the gravel-vermiculite with tab water and put in 70 % (v/v) EtOH for preservation and storage at RT, in darkness. The control plants were treated equally with a control inoculum, containing carrier material but no spores.

2.2 Staining procedures and microscopic evaluation

2.2.1 Trypan blue staining and quantification of mycorrhizal *Rhizophagus irregularis* root colonization

Fresh or in 70 % (v/v) EtOH preserved AM colonized barley root tissue (chapter 2.1.4) was incubated for 30 minutes, at 96 °C, in 10 % (w/v) KOH. Afterwards, the tissue was shortly washed

three times in ddH_2O before incubation for 30 minutes, at RT, in 0.3 M HCl. The HCl was discarded and the samples were put in the staining solution, consisting of a 4:2:1:1 (v/v/v/v) mixture of an aqueous 0.1 % (w/v) trypan blue solution (Sigma-Aldrich, St Louis, MO, USA), ddH_2O, glycerol and 0.3 M HCl, for five minutes, at 96 °C. The samples were subsequently transferred to a 1:1 (v/v) mix of glycerol and 0.3 M HCl, and stored there at RT, in darkness until microscopic evaluation. Control plants were treated equally. Mycorrhizal colonization was quantified with a binocular and a modified grid-line intersect procedure as described previously (Paszkowski *et al.*, 2006). A line was drawn on the ocular, using an 'Edding 3000' (Edding AG, Ahrensburg, Germany) which was now latently visible during sample evaluation. Random root pieces of about 2 cm length were placed on a microscope slide and examined at several points along the root axis. The AM structures 'arbuscle', 'hyphopodium' and 'vesicle', in contact with the Edding line, were counted.

2.2.2 Modified pseudo Schiff propidium iodide staining (mPS-PI) of the barley leaf epidermis

To visualize the shapes of epidermal cells, sample fixation and modified pseudo-Schiff propidium iodide (mPS-PI) staining was performed (Truernit *et al.*, 2008; Pathuri *et al.*, 2008). Leaves were cut in fixation solution in about 1 cm^2 pieces at 4 °C and stayed there at least for several hours. As fixative a 4 % (w/v) PFA in 1 x PBS, pH 7.4 was used. Washing, decoloring, dewaxing and rehydration was performed according to Sauer and Friml, 2010. Fixed leaf material was washed three times in 1 x PBS, pH 7.4, for 10 min, at RT, followed by at least three washing steps in pure MeOH for 10 min, at 37 °C. Thereafter, leaves were dewaxed three times in EtOH/xylene 1:1 (v/v) at 37 °C, for 10 min, followed by three washing steps in pure xylene at the same conditions. Subsequently, the material was washed twice in EtOH/xylene 1:1 (v/v) for 10 min, at RT and twice in pure EtOH, at the same conditions. Rehydration was performed in a decreasing ethanol series of 75 % (v/v), 50 % (v/v), and 25 % (v/v) in ddH_2O and pure water for at least 5 min, followed by two washing steps in ddH_2O, at RT, for five minutes. Next, tissue was incubated in 1% (w/v) aqueous periodic acid solution at RT, for 40 min, rinsed again with water and incubated in Schiff reagent with propidium iodide (100 mM sodium metabisulphite and 0.15 N HCl in ddH_2O; propidium iodide to a final concentration of 100 µg/mL was freshly added) for 1-2 h or until plants were visibly stained. Afterwards, the samples were transferred onto microscope slides and covered with a chloral hydrate solution (4 g chloral hydrate, 1 mL glycerol, and 2 mL water). Slides were kept overnight at RT, in a closed environment to prevent drying out. Next, excess chloral hydrate was removed and

several drops of Hoyer's solution, as a mix of gum arabic, chloral hydrate, glycerol and water in a ratio of 1.5:10:1:2.5 (w/w/w/v), were placed over the tissue and a cover slip was placed on top. Epidermal cells were examined by using a confocal laser scanning microscope (Leica SP5 running the LAS AF Microscope Application Suite, Mannheim, Germany). Samples were excited with a 488 nm laser lane. Emission was detected between 560 and 675 nm.

2.2.3 Scanning electron microscopy

For scanning electron microscopy (SEM), root and leaf material was harvested and fixed as described above (chapter 2.2.2). Fixed material was washed three times in 1 x PBS, pH 7.4, for 10 min, followed by three washing steps in ddH_2O, for 10 min. Dehydration occurred in an increasing ethanol series of 25 % (v/v), 50 % (v/v), and 75 % (v/v) in ddH_2O and absolute EtOH three times, each for at least 10 min. For critical point drying, the EM CPD300 Automated Critical Point Dryer (Leica, Vienna, Austria) was used. The system settings for drying were configured, following the 'Rice Root' protocol for root tissue and the 'Tobacco Leaf' protocol for barley leaf material as described in the manufacturer´s manual. The imaging was done using the TM300 Tabletop Microscope (Hitachi, Tokyo, Japan). The image editing program GIMP 2.8 was used to merge single root pictures to generate root overviews and to color subsidiary cells in the leaf images.

2.2.4 Microtome Sectioning and toluidine blue staining

Microtome sectioning, staining and microscopic evaluation were performed in the lab of Prof. Dr. Dieter Treutter, TUM München under supervision of Ina Tittel. The barley leaves were harvested and tissue blocks were cut, using a scalpel and a 4 mm^2 stencil. The tissue squares were immediately transferred to 70 % FPA fixative, consisting of 63 % parts by volume absolute EtOH, 27 % ddH_2O, 5 % propionic acid and 5 % formaldehyde, incubating for two days, at RT. Dehydration occurred in an increasing ethanol series of 70 % (v/v), 80 % (v/v), 90 % (v/v) in ddH_2O and twice in absolute EtOH, at RT, each time over night or at least several hours. Afterwards, the dehydrated tissues were put in prepenetration solution (50 % activated LEICA HISTORESIN (v/v) in absolute EtOH; Leica Microsystems, Heidelberg, Germany) for one day, continuously shaking, at RT, followed by incubation in penetration solution (activated LEICA HISTORESIN), for two days under the same conditions. The samples were subsequently embedded in embedding solution which consisted of activated LEICA HISTORESIN and LEICA HIISTORESIN Hardener (Leica Microsystems, Heidelberg, Germany) in a ratio of 4: 0,267 (v/v), in plastic casting molds and covered with plastic

film. The embedded tissue was incubated at 60 °C until complete hardening of the embedding solution. The hardened plastic blocks, containing the plant samples, were liberated from the molds and stuck to a small wooden block. Cutting of 8 µm thick sections was performed using a slide based microtome (SM 1400, Jung, Heidelberg). The first 50 sections were discarded to minimize morphological impacts due to sample preparation before fixation. The following sections were laid onto a drop of ddH_2O on a microscope slide. Next, the slides were first incubated at RT until complete evaporation of the ddH_2O and afterwards at 60 °C, for 30 min. For staining, the heat- treated slides were incubated in 0.05 % (w/v) aqueous toluidine blue (Applichem, Darmstadt, Germany) staining solution, at RT, for five minutes. Afterwards, the slides were washed in ddH_2O and incubated in xylene, for ten minutes, at RT. The samples were finally sealed by a drop of quick-hardening mounting medium (Eukitt®, Sigma-Aldrich, St Louis, MO, USA) and a cover glass. Subsequently, samples were incubated in the fume hood, at RT until complete hardening of the mounting medium and stored at RT, in darkness. Observation was done using a brightfield microscope (Axioplan 2, Carl Zeiss AG, Jena, Deutschland) with a connected CCD camera (AxioCam MRC5, Carl Zeiss AG, Jena, Germany) and the AxioVision Software (Axio VS40, Carl Zeiss AG, Jena, Germany). Cell size measurement was performed using the software ImageJ (Schneider *et al.*, 2012).

2.2.5 Propidium iodide (PI) staining

In this work two kinds of PI staining protocols were used: A short protocol and an improved one with additional clearing steps.

In the short protocol, detached barley seedling roots were washed in 1 x PBS, pH 7.4 for five minutes, at RT and subsequently incubated in the aqueous 2.5 % PI (w/v) (Applichem, Darmstadt, Germany) staining solution for ten minutes, at RT, in darkness. Afterwards, the roots were washed in 1 x PBS, pH 7.4 for five minutes, at RT and immediately microscopically examined via a scanning fluorescence microscope (Leica TCS SP5 running the LAS AF Microscope Application Suite, Mannheim, Germany). Samples were excited with a 488 nm laser lane. Emission was detected between 560 and 675 nm.

In the improved PI staining protocol, seedling roots were harvested, fixed, and washed as described above (chapter 2.2.2). For staining of *HvRACB* RNAi root material, an aqueous 10 % (w/v) PI solution was used and an aqueous 2.5 % (w/v) PI solution for the azygous control plants. Roots were incubated in the staining solution for one hour, in the dark, at RT and subsequently transferred to a clearing solution, prepared by mixing chloral hydrate, glycerol, and water in the ratio 4:1:2 (w/v/v)

and kept there for 15 hours at RT in darkness. After clearing, the roots were directly mounted in Hoyer's solution and immediately microscopically examined, as described above (chapter 2.2.2).

2.2.6 Hydroxyl radical (OH•) detection in barley germling roots

For detection of hydroxyl radicals in barley seedling roots, hydroxyphenyl fluorescein (HPF) was used, based on protocols described elsewhere with minor modifications (Hückelhoven and Kogel, 1998; Kwasniewski *et al.*, 2013). 2 days old barley plants, pre-germinated as described above (chapter 2.1.2), were incubated in 20 mM potassium phosphate buffer, pH 6.1, for 30 min, at RT. For staining a 5 mM HPF (Sigma-Aldrich, St Louis, MO, USA) stock solution in DMSO was diluted in 20 mM potassium phosphate buffer, pH 6.1 to a 5 µM HPF working solution. If necessary, salicylhydroxamic acid (SHAM), diphenyleneidonium chloride (DPI) or sodium azide (NaN_3) were added to the working solution to final concentrations of 5 mM (SHAM), 50 µM (DPI) and 10 mM (NaN_3), directly before seedling incubation, to inhibit the activity of different ROS generating enzymes. DPI is hereby diluted from a prior mixed 50 mM stock solution in DMSO. The seedlings were incubated in the working solution for 10 min, in darkness, at RT and afterwards washed in 20 mM potassium phosphate buffer, pH 6.1 for 5 min, at RT, in darkness. Microscopic evaluation of the root transition zones was done directly after washing, using a confocal laser scanning microscope (Leica SP5 running the LAS AF Microscope Application Suite, Mannheim, Germany), with following settings: HyD2 detector (100%), 488nm excitation (10%), 20x water immersion objective, 1,0X Zoom, emission between 510- 580nm. The control plants were treated equally without HPF but with the corresponding DMSO concentration in the staining solution. For quantification of the HPF derived fluorescence signal, the mean pixel intensity of the pictured root transition zones was measured using the software ImageJ (Schneider *et al.*, 2012) and the settings: pixel intensity: 0 ("black") and 255 ("white").

2.2.7 Super Oxide Anion ($O_2^{\bullet-}$) detection in barley germling roots

For detection of super oxide anions ($O_2^{\bullet-}$) in barley, seedling roots nitro blue tetrazolium chloride (NBT, Applichem, Darmstadt, Germany) was used, according to the protocols described elsewhere with minor modifications (Hückelhoven and Kogel, 1998; Kwasniewski *et al.*, 2013). 2 days old barley plants, pre-germinated as described above (chapter 2.1.2), were incubated in 20 mM potassium phosphate buffer, pH 6.1 for 30 min, at RT. For staining, NBT was solved in 20 mM potassium phosphate buffer, pH 6.1 to a 2 mM NBT working solution. If necessary,

diphenyleneidonium chloride (DPI) was added to the working solution, directly before seedling incubation, to inhibit the activity of NAD(P)H oxidases (NOX). DPI was hereby diluted from a prior mixed 50 mM stock solution in DMSO to a final concentration of 50 µM. Intact barley seedlings were incubated in the working solution for 10 min, at RT, in darkness and afterwards washed in 20 mM potassium phosphate buffer, pH 6.1 for 5 min, at the same conditions. The control plants were treated equally without HPF but with the corresponding DMSO in the staining solution. Microscopic picturing of the root transition zones followed directly after washing, using a brightfield microscope (Axioplan 2, Carl Zeiss AG, Jena, Deutschland) with a connected CCD camera (AxioCam MRC5, Carl Zeiss AG, Jena, Germany) and the AxioVision Software (Axio VS40, Carl Zeiss AG, Jena, Germany).

2.2.8 Rhodamine 123 staining of root epidermal cells

Rhodamine 123 (R123) selectively stains mitochondria in living cells (Wu, 1987). A stock solution was prepared by dissolving R123 (Sigma-Aldrich, St Louis, MO, USA) in DMSO to a final concentration of 10 mg/ml. For staining, the stock solution was diluted in 0.5× Murashige and Skoog medium with modified vitamins (0.5× MS; Duchefa Biochemie, Harleem, Netherlands) mixed with sucrose to 1% (w/v) and 2-(N-morpholino) ethanesulphonic acid (MES; Carl Roth, Karlsruhe, Germany) to 0.05% (w/v) final concentration, pH 5.6 to 1 µg/ml. Intact seedlings were incubated in the staining solution for 10 min, in darkness. After staining, seedlings were briefly rinsed in an excess of 0.5 x MS, pH 5.6 and immediately visualized by confocal microscopy as described above. R123 was excited by a 488 nm laser line and the emission was detected from 515 nm to 575 nm. In an early developmental state, trichoblasts were counted before root hair initiation, each in an area of 0.024 mm^2.

2.2.9 Metabolic click labeling of barley roots with a fucose analog

Click labeling of barley roots was performed based on the published *Arabidopsis thaliana* protocol of Anderson and colleagues (Anderson *et al.*, 2012). Barley seedlings, pre-germinated as described above (chapter 2.1.2), were incubated in 10 µM tetraacetylfucose alkyne (Click-It® fucose alkyne; FucAl Thermo Fisher Scientific, St. Leon-Rot, Germany) in 0.5 x MS medium, for five hours, at the growth conditions described above (chapter 2.1.2). As control DMSO instead of the fucose analog was used. After incorporation, the plants were washed three times in 0.5 x MS without FucAl and transferred to labeling solution, containing 1 mM $CuSO_4$, 1 mM ascorbic acid and 0.1 µM Alexa488

azide (Alexa Flour ® 488 azide; Thermo Fisher Scientific, St. Leon-Rot, Germany) in 0.5 x MS, at RT, in darkness, for 1 h. Afterwards, seedlings were washed three times with 0.5 x MS before confocal imaging was performed via a scanning fluorescence microscope (Leica TCS SP5 running the LAS AF Microscope Application Suite, Mannheim, Germany). Samples were excited with a 488 nm laser lane. Emission was detected between 500 and 600 nm.

2.2.10 Staining of fungal structures with wheat germ agglutinin-tetramethylrhodamin (WGA-TMR)

Fungal chitin, intracellular and extracellular of barley epidermal cells, was stained with wheat germ agglutinin-tetramethylrhodamin (WGA-TMR; Invitrogen, Karlsruhe, Germany). Inoculation of the barley leaves with *Bgh* and subsequent harvest and fixation in 4 % (w/v) PFA in 1 x PBS, pH 7.4 occurred as already described above (chapter 2.1.3 and chapter 2.2.2) and according Sauer and Friml, 2010. For decoloring and dehydration, the fixed leaf material was washed once in 1 x PBS, pH 7.4, for 10 min, at RT, followed by an increasing ethanol series of 25 % (v/v), 50 % (v/v) and 75 % (v/v) in 1 x PBS, for 10 min, at RT, each. Afterwards, the samples were transferred to absolute EtOH and stayed there at 4 °C until complete decoloring. Rehydration was performed in a decreasing ethanol series of 75 % (v/v), 50 % (v/v), and 25 % (v/v) in 1 x PBS and pure 1 x PBS, for 10 min, at RT, each. For the staining solution WGA-TMR and bovine serum albumin (BSA) were solved in 1 x PBS buffer to 0.01 µg/µl final concentration, each. The leaves were transferred to the staining solution and vacuum infiltration (26 mm Hg) was applied several times until all leaf pieces sank to the ground. Incubation of the samples lasted at least 24 hours at 4°C in darkness. Visualization occurred under a confocal laser scanning microscope (Leica SP5 running the LAS AF Microscope Application Suite, Mannheim, Germany). Samples were excited with a 561 nm laser lane. Emission was detected between 580 and 650 nm. Transmitted light pictures were obtained using the brightfield settings of the microscope and merged with the according fluorescence pictures using the software ImageJ (Schneider *et al.*, 2012).

2.2.11 Measurement of the Nucleus Attraction Index (NAI) and the penetration efficiency

The first leaves of barley plants were inoculated, harvested and halved along the transversal axis using a razor blade. The lower half was subsequently split in half again, but along the longitudinal

axis. One half was used for the determination of the *HvRACB* transcription level (chapter 2.4 and chapter 2.5), whereby the other half was fixed, de-waxed, and decolored according Sauer and Friml, 2010 and as described above (chapter 2.2.2 and chapter 2.2.10) and finally used for quantification of the nucleus attraction or the penetration efficiency. For the last rehydration step, 1× PBS, pH 7.4 was used. To remove RNA from the tissue, RNase A (DNase free, Applichem, Darmstadt, Germany) was dissolved in 10 mM Tris–HCl, pH 7.5 to a final concentration of 10 mg/ml. The stock solution was subsequently diluted in 1 x PBS, pH 7.4 to 100 µg/ml to achieve the RNase A solution in which leaf material was incubated for 1 h, at RT. Subsequently, the leaves were placed in the staining solution (100 µg/ml PI in ddH_2O) for at least 5 min, at RT. To determine the nucleus attraction index (NAI), epidermal B cells (Koga *et al.*, 1990) which were attacked by a single fungal appressorium, were imaged by using a confocal laser scanning microscope (Leica SP5 running the LAS AF Microscope Application Suite, Mannheim, Germany). Samples were excited with a 488 nm laser lane. Emission was detected between 560 and 675 nm. A z-stack was recorded starting from the brightest fluorescence of the fungal appressorium to the brightest fluorescence of the plant nucleus. The picture number and increments were adjusted for each cell and z-stack, depending on the vertical distance between the appressorium and plant nucleus. The NAI was calculated as follows: $NAI = \sqrt{a^2 + b^2}/d$ where 'a' reflects the depth of the z-stack and 'b' the planar distance between the appressorium and the nucleus. Both represent the legs of a right-angled triangle. The diagonal of the B cell is represented by 'd'. Cell size measurement was performed using the software ImageJ (Schneider *et al.*, 2012).

For quantification of the penetration efficiency, the leave halves were prepared as described above (chapter 2.2.10) and epidermal B cells (Koga *et al.*, 1990), which were attacked by a single fungal appressorium, were visualized as depicted in this chapter. *Bgh*-barley interactions showing a clear haustorial initial were regarded as 'penetrated', whereby interactions, exhibition no such structure were counted as 'non-penetrated'.

2.3 Evaluation of the primary cell wall composition

2.3.1 The protoplast release assay

Leaves were cut in pieces of about 25 mm^2, using stencil and scalpel. Four leaf explants were put in and completely covered with freshly prepared plant cell wall digestion solution, containing 0.45 M mannitol, 1 % (w/v) Macerozyme R-10 (Duchefa Biochemie, Harleem, Netherlands), 1 % (w/v) Cellulase Onozuka R-10 (Duchefa Biochemie, Harleem, Netherlands), 1 % (w/v) Driselage (Sigma-

Aldrich, St Louis, MO, USA) in aqueous 3.16 % (w/v) Gamborg's B5 medium (Duchefa Biochemie, Harleem, Netherlands). The leaf pieces were incubated in the cell wall degrading solution at RT, in darkness, without shaking. For quantification of released protoplasts, the solution is gently shaken, before a small volume is taken and dropped on a hemocytometer.

2.3.2 Determination of cell wall monosugar composition

Monosaccharide composition was determined by High-Performance Anion-Exchange Chromatography with Pulsed Amperometric Detection (HPAEC-PAD) in the lab of Dr. Lars Voll; University Erlangen under supervision of Timo Engelsdorf. About 30 mg fresh barley leaf material was harvested, put in micro tubes and quick-frozen in liquid nitrogen. The samples were incubated two times in 1 ml 80 % (v/v) EtOH, at 80 °C, for 20 min and once in 1 ml acetone, at RT, for 5 min, before complete drying at 60 °C under a fume hood. 0.5 ml aqueous, 2 M trifluoroacetic acid (TFA) was added to each sample and the insoluble material was resuspended via a rotating pestle which was rinsed in 0.5 ml aqueous, 2 M TFA, added to the sample afterwards. The micro tubes were sealed with Mµlti®-Verschlussclips (Carl Roth GmbH + Co. KG, Karlsruhe, Germany) and the plant material was hydrolyzed at 120 °C, for 1 h. After centrifugation 500 µl supernatant were transferred to a new micro tube and dried under vacuum, before resolving the monosaccharides in 500 µl ddH_2O. For measurement, the extract was mixed 1:10 (v/v) with 1 mM aqueous fructose solution as internal/technical standard and applied to an ion chromatography system (ICS-3000, Thermo Fisher Scientific, St. Leon-Rot, Germany) with a CarboPac® PA20 column (Thermo Fisher Scientific, St. Leon-Rot, Germany). As external standard, a fructose dilution series was used (600 µM; 400 µM; 300 µM; 200 µM; 100 µM; 50 µM; 25 µM; 5 µM). To obtain complete fractionation of xylose and mannose, elution was started isocratically with 100 % buffer C (2 mM NaOH; Sigma-Aldrich, St Louis, MO, USA) for 21 min. In 2nd min the eluent was changed to 5 % buffer A (20 mM NaOH, 1 M NaAc), 50 % buffer B (200 mM NaOH) and 45 % buffer C, in the following 19 min to 30 % buffer A, 50 buffer B and 20 % buffer C and then in 5th min to 50 % buffer A and 50 % buffer B. After 2 min of isocratic elution, the eluent was changed to 100 % buffer B in the 2nd min and kept isocratic for 3 min to wash the column. The eluent was then changed to 100 % buffer C in the 3rd min, followed by 13 min of recalibration. To obtain complete fractionation of rhamnose and arabinose, elution was started isocratically with 4 % buffer B and 96 % buffer C for 14 min. In the 2nd min the eluent was changed to 2 % buffer A, 48 % buffer B and 50 % buffer C, in the following 16 min to 30 % buffer A, 50 % buffer B and 20 % buffer C and then in the 4th min to 50 % buffer A and 50 % buffer B. Washing and recalibration was performed as described above.

2.4 DNA/RNA extraction and cDNA synthesis

2.4.1 DNA extraction and genotyping of *HvRACB* RNAi barley plant offspring

Leaf material was harvested, put in a micro tube and directly quick-frozen in liquid nitrogen. Samples were grinded in a ball mill (Retsch MM300, Qiagen, Hilden, Germany) and 500 µl DNA extraction buffer, containing 200 mM TRIS- HCl pH 7.5; 250 mM NaCl; 25 mM EDTA, pH 8; 0.5 % SDS (w/v) solved in ddH_2O, were added. Samples were vortexed and incubated at RT, for 5 min. Afterwards, 500 µl chloroform were added and the tubes were vigorously shaken by hand. After centrifugation, the supernatant was transferred to a new micro tube and the same volume isopropanol was added. The samples were gently inverted until the fluids were completely mixed and incubated at RT, for 2 min. After centrifugation the supernatant above the pellet was discarded and the pellet was washed in 70 % (v/v) EtOH and centrifuged. The supernatant was discarded and after evaporation of the residual alcohol, the DNA pellet was resolved in ddH_2O. DNA concentration was photometrically measured (NanoDrop 1000, VWR Life Science, Erlangen, Germany).

Genotyping was carried out by a standard PCR. Reaction were performed with 0.5 µl DNA template, 400 nM forward, reverse primer, respectively, 8 mM dNTP mix, 0.025 u Taq DNA Polymerase (SupraTherm, Ares Bioscience GmbH, Köln, Germany) and Taq Polymerase buffer (10x) in a final volume of 25 µl. The PCR cycler program consisted of an initial step at 95 °C for 5 min, followed by 36 cycles with 95 °C for 30 s, 60 °C for 30 s and at 72 °C for 30 sec and a final elongation step at 72 °C for 10 min. For genotyping two PCRs were carried out for each plant, addressing the *HvUBC2* gene, to evaluate proper DNA extraction and PCR, and the actual *HvRACB* RNAi construct (Supp table 1). The PCRs were evaluated via agarose gel electrophoresis for *HvUBC2* and *HvRACB* RNAi amplification products on a UV transilluminator.

2.4.2 RNA extraction and RNA quality evaluation

Plant material was harvested and grinded as described above (chapter 2.4.1). 1 ml RiboZol® (Amresco, Solon, OH, USA) was added to 50 – 100 mg deep-frozen tissue powder, vigorously vortexed and incubated for 1 min, at RT, before vortexed again. After centrifugation at 4 °C, the clear supernatant was transferred to a new micro tube and incubated for 5 min, at RT. For each ml RiboZol® used in the beginning, 200 µl chloroform is added and each tube is vigorously shaken by hand and subsequently incubated at RT, for 2 min. After centrifugation at 4 °C, the clear supernatant

was transferred to a new micro tube and an equal volume of isopropanol was added. The tubes were gently inverted until complete mixing of the fluids and afterwards incubated for 10 min, at RT. After centrifugation at 4 °C, the supernatant was discarded and the pellet was washed with 70 % (v/v) EtOH. After centrifugation at 4 °C, the supernatant was discarded and the pellet was resolved in ddH_2O, after evaporation of the residual alcohol.
RNA concentration was measured photometrically (NanoDrop 1000, VWR Life Science, Erlangen, Germany) and RNA quality was tested via agarose gel electrophoresis on a UV transilluminator.

2.4.3 cDNA synthesis for sqPCR and qPCR

For sqPCR, RT PCR was performed using the enzymatic workflow of Thermo Fisher Scientific (Thermo Fisher Scientific, St. Leon-Rot, Germany). Before reverse transcription, residual gDNA was wiped out by mixing 5 u DNaseI, DNaseI reaction buffer (10x), 50 u RiboLock and 10 µg RNA with RNase free water to a final volume of 50 µl. After incubation for 30 min, at 37 °C, 5 µl of 50 mM was added and the mixture was incubated for 10 min, at 65 °C. 5 µl random hexamer primer (200 ng/µl) were added to the mix, incubated for min, at 65 °C and subsequently cooled down on ice. For cDNA synthesis, to the 60 µl reaction mix, 100 u RevertAid reverse transcriptase, RevertAid reaction buffer (5x), 100 u RiboLock, 10 µl dNTP Mix (10mM, each) and RNase free water were added to a final volume of 100 µl. The PCR cycler program for reverse transcription consisted of three steps, starting with an incubation at 25 °C for 10 min followed by an incubation at 42 °C for 60 min and a final step at 70 °C for 10 min.
For qPCR, RT PCR was performed via the QuantiTect Reverse Transcription Kit and according the manufacturers manual (Qiagen, Hilden, Germany). To achieve gDNA elimination, gDNA wipeout buffer (7x), 1 µg RNA and RNase free water were mixed to 14 µl final volume which was incubated at 42 °C for 10 min (instead of 2 min as described by the manual). After cooling down on ice, the reverse transcription was performed. Therefore, to the reaction mixture 4 µl QuantiScript reverse transcriptase buffer (5x), 1 µl QuantiScript reverse transcriptase and 1 µl random hexamer primer mix was added to a final volume of 20 µl. The PCR cycler program for reverse transcription consisted of two steps, starting with an incubation at 42 °C, for 30 min (instead of 15 min as described by the manual), followed by an incubation at 95 °C, for 3 min.

2.5 Primer design and performance of sqPCR and qPCR

2.5.1 Target gene selection for qPCR

To select putative α-fucosidases and α-fucosyltransferases, active on xyloglucan in barley, the according enzymes in rice, listed by Del Bem and Vincentz via LocOs_Identifiers (Del Bem and Vincentz, 2010), were used to obtain the protein sequences, available by the 'Rice Genome Annotation Project' (http://rice.plantbiology.msu.edu; Kawahara *et al.*, 2013). These protein sequences of putative rice α-fucosidases and α-fucosyltransferases were used to check the PLEXdb database (www.plexdb.org) for related proteins in barley, via the Basic Local Alignment Search Tool (BLAST). Promising candidates were reviewed on 'Genevestigator' (https://genevestigator.com; Hruz *et al.*, 2008) for *Bgh* dependent expression patterns, using the according Barley1 22k Microarray Sequence IDs. The PLEXdb sequences of pathogen dependent expressed candidates were aligned via BLAST to the nucleotide collection (Hordeum vulgare; taxid 4513) of the National Center for Biotechnology Information (NCBI) which enabled the accession to the published protein sequences.

2.5.2 Primer design and nomenclature for sqPCR and qPCR

All primers (Supp table 1) were designed using the Primer3 software (Untergasser *et al.*, 2012), based on the cDNA/gDNA sequence and annotation data, available on the plant expression data base PLEXdb (www.plexdb.org), the NCBI nucleotide collection (*Hordeum vulgare*; taxid 4513), respectively. For database assignment and entry tracking, lab internal primer and target gene names consist of letters and numerals. The letters refer to the gene annotation, whereas the numerals point to the database accession numbers. A numerical code with five or four digits stands for the Barley1 22k Microarray Sequence ID of the PLEXdb database (ex: FUC_1402 for fucosidase; Barley1_01402 or Contig_1402_at), six digits stand for the NCBI accession number (ex: FUT_362089 for fucosyltransferase; AK362089). Primers were tested for gene or transcript specificity using BLAST and therein with nucleotide blast against the *H. vulgare* database (http://blast.ncbi.nlm.nih.gov), the PLEXdb expression database (www.plexdb.org) and amplicon size assessment in agarose gels before running qPCR. If possible, primers were designed spanning an intron sequence. For intron-exon prediction, cDNA and protein sequences from the NCBI and PLEXdb databases were aligned to gDNA sequences from NCBI or Barley Harvest database (http://harvest-web.org; Genome_0.05) using the PlantGDB GeneSeqer software

(http://www.plantgdb.org/cgi-bin/GeneSeqer/index.cgi), the rice splice site model and stringent alignment stringency level (Schlueter *et al.*, 2003).

2.5.3 Semiquantitative reverse transcription PCR (sqPCR)

For sqPCR, plant material was inoculated, harvested and treated for RNA extraction like described before (chapter 2.4). SqPCR was carried out by a standard PCR with gene specific conditions for primer annealing temperature and number PCR cycles (Supp table 1). Primer design was done as described before (chapter 2.5.2). PCR reactions were performed with 0.5 µl DNA template, 400 nM forward, reverse primer, respectively, 8 mM dNTP mix, 0.025 u Taq DNA Polymerase (SupraTherm, Ares Bioscience GmbH, Köln, Germany) and Taq Polymerase buffer (10x) in a final volume of 25 µl. The PCR cycler program consisted of an initial step at 95 °C, for 5 min, followed by a gene specific number of PCR cycles (Supp table 1), starting with 95 °C, for 30 s and gene specific annealing temperature for 30 s and elongation at 72 °C for 30 sec. Finally, an elongation step at 72 °C, for 10 min was done. For semiquantitative measurement of gene transcripts, two PCRs were carried out for each gene, addressing the *HvUBC2* gene, whose amount of PCR product was qualitatively used for normalization and the actual gene of interest (Supp table 1). The PCR product amounts were visualized via agarose gel electrophoresis on a UV transilluminator.

2.5.4 Quantitative reverse transcription PCR (qPCR)

Quantitative gene expression analysis was carried out by reverse transcription quantitative real-time PCR (qPCR) in a Mx3005P cycler (Agilent Technologies, Santa Clara, CA, USA) using the Maxima SYBR Green qPCR master mix (2×) (Thermo Fisher Scientific, St. Leon-Rot, Germany). Primer design was done as described before (chapter 2.5.2; Supp table 1). Reactions were performed in triplicates with 20 ng of cDNA and 300 nM forward and reverse primer, each in a final volume of 10 µl. Expression values of barley genes were normalized to a barley housekeeping ubiquitin (*Hv*UBC2) (Ovesná *et al.*, 2012), using primer efficiency correction as suggested by Pfaffl, 2001. The program consisted of an initial step at 90 °C, for 10 min and 95 °C, for 30 s, followed by 40 cycles at 60 °C, for 30 s and at 72 °C, for 25 s. The melting curve analysis was performed at 60–95 °C. Processing the measured fluorescence data for calculation of the melting curve and abundance of relative transcript quantities was done by the multiplex quantitative PCR software MxPro (Agilent Technologies, Santa Clara, CA, USA).

2.6 The transient induced gene silencing assay

2.6.1 Primer design and PCR of the RNAi constructs

Primer for the transient inducing gene silencing FUT_362089 RNAi constructs were designed, using the Primer3 software (Untergasser *et al.*, 2012), according the settings of Douchkov and colleagues (Douchkov *et al.*, 2005) and as described above (Supp table 1; chapter 2.5.2). The long-double stranded RNAi constructs were tested for target specificity and silencing efficiency via 'si-Fi', a software for RNAi off-target prediction launched by the IPK Gatersleben (http://labtools.ipk-gatersleben.de/). For amplification of the RNAi construct the Phusion high-fidelity DNA polymerase (Thermo Fisher Scientific, St. Leon-Rot, Germany) was used according the manufacturer's protocol. Reaction were performed with 2 µl cDNA template, 1 µl (10 µM) forward, reverse primer, respectively, 0,4 µl (10mM) dNTP mix, 1 u Phusion Polymerase, HF Polymerase buffer (5x) and 0.6 µl DMSO in a final volume of 20 µl. The PCR cycler program consisted of an initial step at 98 °C for 30 s, followed by 37 PCR cycles, starting with 95 °C for 10 s, annealing at 63 °C for 20 s and elongation at 72 °C for 20 s. At last, a final elongation step at 72 °C for 10 min was done. The PCR products were cleaned up using the NucleoSpin® Gel and PCR Clean-up (Machery-Nagel GmbH & Co. KG, Düren, Germany). Concentration and product size were evaluated photometrically and by gel-electrophoresis, like described above (chapter 2.5.3).

2.6.2 Cloning of the RNAi constructs

The RNAi PCR products were ligated in the entry vector pIPKTA38, according the protocol of Douchkov and colleagues based on the Gateway® recombinational cloning system (Douchkov *et al.*, 2005; Karimi *et al.*, 2007), using the enzymes of Thermo Fisher Scientific (St. Leon-Rot, Germany). For ligation, 4 µl PCR product, 150 ng entry vector, 2.5 u T4 DNA Ligase, 5 u SwaI restriction enzyme, (0.5 M) NaCl, PEG 50 % 4000, ligase buffer (10x) 1 µl each, were mixed in a final volume of 10 µl, incubated first at 25 °C, for 75 min and afterwards at 65 °C, for 10 min. Elimination was done by adding 2.5 u SwaI, 0.5 µl (0.5 M) NaCl, 3.5 µl ddH_2O and SwaI buffer (10x) to the ligation and incubation of the reaction mix at 25 °C for 75 min.

Transformation of competent DR5α *E .coli* cells with the entry vector was achieved by adding 10 µl of the vector to 100 µl defrosted bacteria solution, gently mixing and incubating on ice, for 20 min. Afterwards, the cells were heatshocked at 42 °C, for 42 s, before 500 µl LB medium was added. The bacteria were incubated for 1 h, at 37 °C and subsequently plated on LB medium with kanamycin

as selection additive (Douchkov *et al.*, 2005), where positively transformed bacteria propagated over night, at 37 °C.

To test for a positive transformation and correct ligation events to the pIPKTA38 vector, single and clearly separated *E. coli* colonies were harvested and directly used for a PCR based colony check. PCR reaction with the *E. coli* colony as template was performed with 2 µl (10 µM) forward, reverse primer, respectively, 2.5 µl (2 mM) dNTP mix, 1.25 u Taq Polymerase (SupraTherm, Ares Bioscience GmbH, Köln, Germany) and Taq Polymerase buffer (10x), 1.5 µl (25 mM) $MgCl_2$ and ddH_2O in a final volume of 25 µl. The PCR cycler program consisted of an initial step at 95 °C, for 5 min, followed by 37 PCR cycles, starting with 95 °C, for 1 min, annealing at 53 °C, for 2 min and elongation at 72 °C, for 2 min. At last, a final elongation step at 72 °C, for 10 min was done. Presence of correct PCR products were evaluated via gel-electrophoresis as described above (chapter 2.5.4). Positive tested colonies were further propagated in liquid LB culture and plasmids were extracted, using the NucleoSpin® Plasmid purification kit, according the low copy plasmid protocol (Machery-Nagel GmbH & Co. KG, Düren, Germany). The plasmids were sequenced (Eurofins Genomics GmbH, Ebersberg, Germany) to reveal incorrect amplifications events like base substitutions and PCR terminations.

Insertion of the RNAi constructs into the final destination vector pIPKTA30N was performed according Douchkov and colleagues (Douchkov *et al.*, 2005), by mixing 1 µl RNAi construct containing entry vector (pIPKTA38), with 1 µl pIPKTA30N, 2 µl Clonase Mix (Gateway® LR Clonase® Enzyme mix; Thermo Fisher Scientific, St. Leon-Rot, Germany) and ddH_2O to 10 µl final volume. The insertion reaction was incubated over night, at 25 °C. Transformation of competent *E. coli* cells with the LR insertion reaction mixture, propagation of the transformed cells on LB agar plates with ampicillin as selective additive, colony PCRs verifying presence and correct direction of insertions and following procedures leading to the purified plasmid, containing a functional FUT_362089 RNAi construct were, performed as described above (chapter 2.6.1) and according Douchkov and colleagues (Douchkov *et al.*, 2005).

2.6.3 TIGS via ballistic transformation

Bombardment of detached barley leaves with gold microparticles, for transient induced gene silencing (TIGS), was based on already published protocols (Douchkov *et al.*, 2005; Sivamani *et al.*, 2009). A gold stock solution was prepared by washing the gold particles (1.0 µm Gold Microcarriers; Bio-Rad; München, Germany) twice in ddH_2O and once with absolute EtOH. The EtOH was

discarded and the particles were incubated at 50 °C until complete drying. Afterwards, the gold was resuspended in 50 % (v/v) aqueous glycerol to a final concentration of 27.5 mg/ ml.

Detached barley leaves were placed in petri dishes, containing 50 % (w/v) water agar, the adaxial epidermis facing up. For plasmid coating of the gold particles, 11 µl evenly distributed gold stock solution was mixed with 1 µg pGY-1-GFP (GFP under control of CaMV 35S promoter as transformation marker), 1 µg pIPKTA30N, empty vector control, respectively, 8.3 µl CaCl (2.5M) and 2 µl of a 2 % (w/v) aqueous protamine solution, per shot. The mixture was incubated at RT, for 30 min, mixed from time to time, washed once in 70 % (v/v) and absolute EtOH and finally resuspended in 6 µl absolute EtOH, before evenly distributed on macro-carriers (Bio-Rad, München, Germany). For ballistic transformation of the barley leaves, a helium particle gun with hepta-adapter was used (PDS-1000; Bio-Rad, München, Germany), 26 Hg (quicksilver) vacuum was applied and the gas pressure was regulated by rupture discs of 900 psi (pounds per square inch; Bio-Rad München, Germany). The petri dishes were put in an environmental chamber under conditions as described above (chapter 2.1.2).

2.6.4 PE evaluation after ballistic transformation

One day after ballistic transformation, the leaves were inoculated with *Bgh* (about 100 spores/ mm^2) as described above (chapter 2.1.3). They were put back in the environmental chamber for another day, before they were stained in darkness, for several minutes, at RT, in an aqueous staining, containing 0.1 % (w/v) calcofluor white and 0.05 % (w/v) Evan's Blue (Sigma-Aldrich, St Louis, MO, USA), at pH 13. The stained fungal cell wall, together with the GFP transformation marker, allowed evaluation of the penetration efficiency, with and without transient silencing of the target gene (FUT_362089). Therefore, a Leica DM 1000 fluorescence microscope (Leica Microsystems, Heidelberg, Germany) as used.

3 Results

3.1 Defective stomata and an epidermal disarray characterize the *HvRACB* RNAi leaves

The physiological and cell biological phenotype of the *HvRACB* RNAi line was investigated. The investigations were based on already published *Hv*RACB-dependent aberrations in physiology, morphology, and development (Schultheiss *et al.*, 2005; Pathuri *et al.*, 2008, 2009; Hoefle *et al.*, 2011). It was described in previous publications that stable barley lines which express a constitutive active *Hv*RACB protein under the ectopic maize ubiquitin promotor (*HvRACB* OECA) showed several physiological and cell biological effects. It was observed that the *HvRACB* OECA plants are shorter than the control plants and the leaves exhibited a curled phenotype (Schultheiss *et al.*, 2005). On a cellular level, a misshaping of B-cells was reported as well as a defective formation of the stomata (Pathuri *et al.*, 2008, 2009). Additionally, the stable transgenic *HvRACB* knockdown lines (*HvRACB* RNAi) had an obvious reduction in growth, when compared to the control plants (Hoefle *et al.*, 2011). Hence, it seemed obvious to take a closer look at the leaves of the *HvRACB* RNAi plants to search for further physiological and cell biological phenotypes.

3.1.1 *HvRACB* RNAi promotes defective stomata formation

For examination of the cell architecture of the cells in the leaf epidermis, the leaf blades were stained via the modified pseudo Schiff propidium iodide staining method (mPS-PI) (Truernit *et al.*, 2008; Pathuri *et al.*, 2008).

Using this method, the stained cell walls clearly displayed the cell outlines under the microscope. This allowed the direct comparison of the *HvRACB* RNAi line and its wild type sister segregant (azygous) control (Figure 10). The disarray in the epidermal architecture of *HvRACB* RNAi plants, when compared to the control, was striking. It was obvious that the *HvRACB* RNAi plants developed a severe defect in formation of the subsidiary cells. However, the severity of the deformations was highly variable in the *HvRACB* RNAi plants. They comprised small aberrations such as slight variances in size and shape and extended up to massive effects or complete loss of the subsidiary cells (Figure 10B).

Additionally, a cellular disarray was observed which affected parts of the epidermis. It comprised next to the subsidiary cells, the A-cells (short epidermal cells directly adjacent to stomata) and B-cells (short epidermal cells in files not directly adjacent to stomata). However, if a subsidiary cell on the *HvRACB* RNAi plant was normally developed also the A-cell next to it did not show any atypical morphologies and so did the neighboring B-cells. These results suggest that these cell types on the barley epidermis were indirectly misshapen by the disturbed formation of the subsidiary cells but not directly affected by the *HvRACB* knockdown.

The control plants also showed deformations of the subsidiary cells to some extent, but the severity of this deformations always remained low and was restricted to slight aberrations in cell size and shape. The quantification of stomata with one or both deformed subsidiary cells revealed that the *HvRACB* RNAi plants also had significant more defective stomata than their azygous control plants (Figure 10C). In the control about 3.5 % of all counted stomata were classified as "defective", whereas in the *HvRACB* RNAi plants over 21 % showed a formation defect in one or both subsidiary cells.

Even though the mPS-PI staining gave interesting insights into the epidermal architecture and cell shaping, it was inconvenient to microscope larger areas. To gain an overview over the leaf surfaces

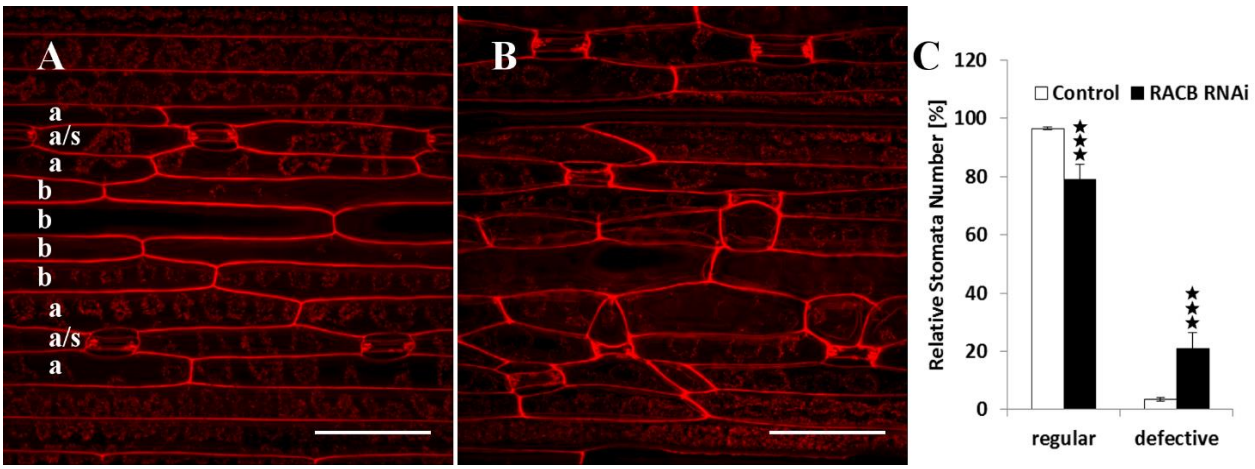

Figure 10: mPS-PI stained adaxial barley epidermis and quantification of stomata shape defects.
(A) Epidermal cell shapes of azygous control leaves and (B) *HvRACB* RNAi leaves. (C) For quantification of the stomata defect, stomata were counted and classified to "regular" if both subsidiary cells were normally shaped or "defective" if one or both subsidiary cells showed a deformed outline. Columns show the average of four leaf samples with 10171 stomata counted on the controls and 9689 Stomata counted on *HvRACB* RNAi leaves. Error bars show the standard deviation of the average. Student's t test: $p < 0.001$. Scale bar (A), (B): 100µm. Small letters in (A) indicate rows of A-cells ("a"), B-cells ("b") and A-cells alternating with stomata complexes ("a/s"). The 2nd leaves of 14 days old barley plants were used.

of the *HvRACB* RNAi plants and their azygous controls the scanning electron microscopy method (SEM) was used. It was combined with critical point drying (CPD) for sample preparation.

The adaxial surfaces of *HvRACB* RNAi leaves and their azygous controls were surveyed (Figure 11). The overview pictures showed that the subsidiary cell formation phenotype of the *HvRACB* RNAi plants were clearly visible along large epidermal areas. An additional feature of the subsidiary cell formation phenotype in the *HvRACB* RNAi plants was its unequal distribution along the leaf surface, as it can be seen on the SEM pictures (Figure 11A, B). It seemed that areas with a high number of defective stomata are alternating with areas almost not distinguishable from the azygous controls. The high variance of the deformed subsidiary cells was visualized as well as the normal shaping of all other cell types existing on the barley epidermis. Especially the guard cells as parts of the stomata complexes should be pointed out. They were always correctly formed, independently of a proper or defective subsidiary cell formation.

The stomata on barley leaf blades are formed close to the basis of the leaf, shortly after the cells left the region of the intercalary meristem and switched to the zone of elongation (Stebbins and Jain,

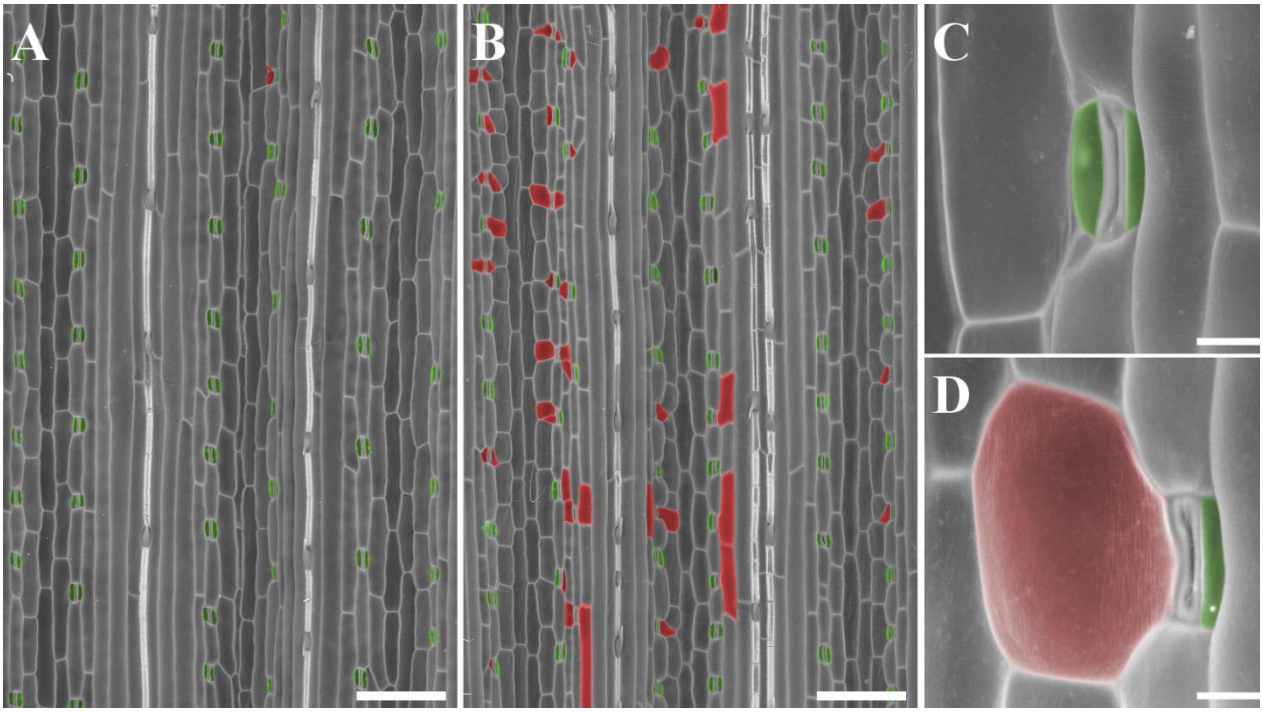

Figure 11: Adaxial leaf surfaces of *Hv*RACB RNAi barley plants and their azygous control visualized via SEM.
(A) Adaxial leaf epidermis of azygous control plants and the (B) *Hv*RACB RNAi plants. (C) Higher magnification of a regularly developed stomata of the azygous control. (D) One kind of formation defects, observable on the *Hv*RACB RNAi epidermis. The cells were colored afterwards using the software GIMP 2.8. Regular formed subsidiary cells were marked in green, while defective ones were colored in red. Scale bar (A), (B): 200µm; (C), (D): 20µm. The 2nd leaves of 14 days old plants were used.

1960; Stebbins and Shah, 1960). However, no developmental intermediates could be visualized by imaging the surface of the region of the intercalary meristem via mPS-PI or SEM (Supp Figure 1). Furthermore, the intercalary meristem turned out to be difficult to access for proper microscopy. The qPCR data of the *HvRACB* gene exhibited a higher relative transcript level in the intercalary meristem than in the leaf blade. This was the case for the control as well as for the knockdown line (Supp Figure 2). Additionally, the decrease of the *HvRACB* transcripts in the blade was about 41 %, when compared to the azygous control. In the meristematic region, the reduction reached more than 53 %. Both results confirm the presence of *Hv*RACB in the meristem and the efficient knockdown of the gene in the *HvRACB* RNAi plants.

Worth the mention is that the deformation of the subsidiary cells is also observable on the abaxial leaf epidermis which also possess stomata in barley (data not shown). Additionally, the sheath of the *HvRACB* RNAi barley plants displayed these defective stomata (data not shown). No evident indication for differences in the number of defective stomata or severity, when compared to the adaxial epidermis of the leaf blade were observed.

In summary, the images exhibited a phenotype of defect stomata complexes on the *HvRACB* RNAi plants. It consists of misshaped subsidiary cells in a high variance of deformation severity. Quantification revealed multiple more defect stomata on the *HvRACB* knockdown leaf blades, when compared to the azygous control. The qPCR data showed the availability of *HvRACB* in the intercalary meristem and an efficient knockdown in the *HvRACB* RNAi plants in this tissue.

3.1.2 *HvRACB* RNAi leaf blades reveal disturbances in the epidermal architecture

The above described defects in the formation of subsidiary cells suggested a specific affection of this cell type on the leaf epidermis of *HvRACB* RNAi plants. The residual cell types did not show any deformations. This could not be explained from the defective formation of subsidiary cells. However, the formation phenotype of the subsidiary cells could not elucidate some formerly published effects such as smaller and curlier leaves (Schultheiss *et al.*, 2005; Hoefle *et al.*, 2011). Therefore, the leaf architecture of the *HvRACB* RNAi leaf blade and their azygous control plants was analyzed. Via bright field microscopy, the number of parallel ribs, parallel B-cell rows, and number of B-cells in a longitudinal line was quantified.

The parallel ribs were counted to evaluate their impact on the reduced width of the blade of the *HvRACB* RNAi plants. However, the number of parallel ribs on the leaf blade revealed no significant

differences between *HvRACB* RNAi leaves and the azygous control. The control plants possessed averaged 14.2 ribs, whereas the number on *HvRACB* RNAi blades is slightly reduced with averaged 13.2 ribs (Figure 12A).

Additional to the ribs also the parallel-longitudinal rows of B-cells were counted (Figure 12B). In contrast to the ribs a significant reduction of parallel rows of B-cells was detected. They decreased from averaged 3.2 rows per rib in the control to about 2.4 rows per rib on the *HvRACB* RNAi leaf

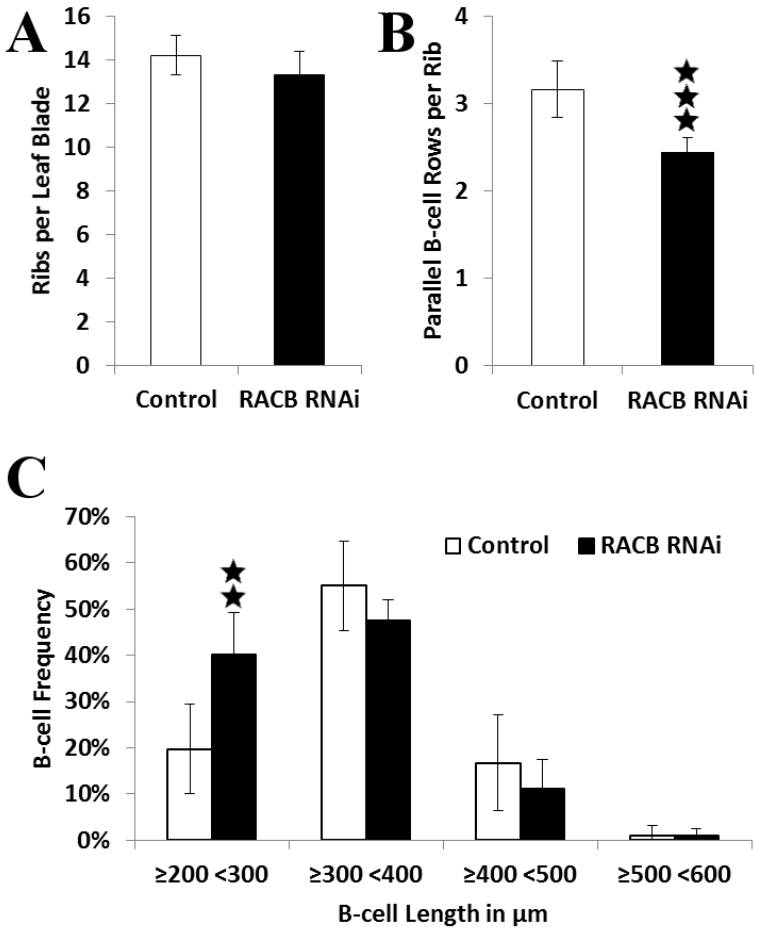

Figure 12: Quantification of the ribs, B-cell rows and B-cell length on *HvRACB* RNAi and control leaf blades.
(A) Counting of the parallel ribs on the leaf blades. For quantification six leaves of *HvRACB* RNAi and azygous control were counted for rips nine times at defined points at the longitudinal blade axis. These nine counts were averaged per leaf. The bars represent the mean of six leaves. (B) Counting of the parallel B-cell rows. The counting and calculation method was the same already described for (A). (C) Classification of the B-cells according their cell length. The B-cells were counted along a defined distance on the blade. Several rows per blade were counted and averaged per leaf. The bars represent the mean of five leaves concerning the azygous control and six leaves concerning *HvRACB* RNAi. Error bars show the confidence interval ($\alpha = 0.05$) of the mean. Student's t test: (A), $p > 0.05$; (B), $p < 0.001$; (C), $0.01 < p < 0.05$. The 2nd leaves of 14 days old plants were used.

blade. This represents a relative reduction of more than 20 %, when compared to the azygous control.

The *HvRACB* RNAi leaves were not only reduced in the width but also in the length of their blades. To evaluate whether this phenotype was due to a reduced length of the cells, the B-cells were counted along the B-cell rows in a longitudinal section of defined length (Figure 12C). The numbering of the B-cells showed that the *HvRACB* RNAi plants had in average shorter cells than their azygous control plants. After classification, it became evident that the differences were highest in the class of the shortest cell length (≥200 <300 µm). While about 20 % of all B-cells were assigned to this class of cell length in the azygous control, this happened to more than 40 % in the *HvRACB* RNAi plants. The residual three classes showed a reduced number of assigned cells concerning the *HvRACB* RNAi line, when compared to the azygous control.

Summarizing, the *HvRACB* RNAi plants possessed in average less parallel B-cell rows and the B-cells were shorter, when compared to the azygous control. Like for the defective formation of subsidiary cells (chapter 0), also for the changes of the epidermal architecture the intercalary meristem represents the probable tissue of origin. Hence, the described qPCR data also supported the *Hv*RACB dependency of the reduced B-cell size and decreased number of B-cell rows (Supp Figure 2). The data suggested to further investigate the cell sizes of the cells of the *HvRACB* RNAi leaf blade.

3.1.3 *HvRACB* RNAi leaf blade in cross-section exhibit cell size reduction

The previously described phenotypes were obtained by examination of the surface of the leaf epidermis. Thus, the consistent next step was to take a closer look inside the leaf. Therefore, cross-sections of the leaf blades were prepared and treated with Toluidine Blue, resulting in a permanent blue staining of the primary cell wall. This allowed the examination of single cell properties measurable in the leaf blade cross-section.

The quantification of the leaf height revealed a reduction of the height of the *HvRACB* RNAi leaf blade, when compared to the azygous control (Figure 13A). The leaf height of the control blade was about 158 µm, whereas the blade height in the *HvRACB* RNAi plants came up to 130 µm which represents a relative reduction of about 18%. The height reduction of the leaf blade in the *HvRACB* RNAi plants could be caused through several reasons. These may be a decreased cell size of the epidermal and mesophyll cells, a reduced number of horizontal cell layers, or a mixture of both reasons. To evaluate this, the number of the horizontal cell layers in the microtome cross-sections

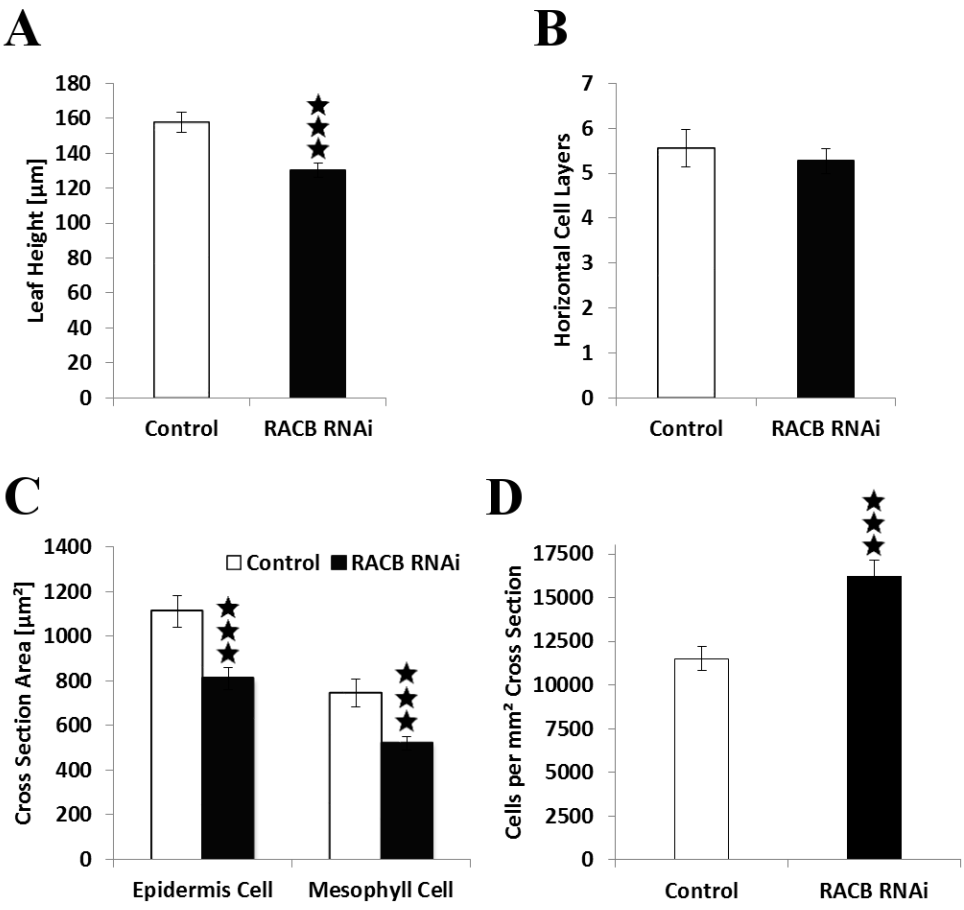

Figure 13: Measuring of leaf cell parameters in leaf blades via microtome sections
(A) Measurement of the leaf height in *HvRACB* RNAi and control blades. (B) Quantification of the horizontal cell layers (mesophyll and B-cells) in the leaf blades. (C) Measurement of the cell cross-section areas. (D) Average cell number per mm² in the measured cross-sections. All measurements (A), (B), (C) and (D) were done using microtome cross-sections of the 2nd leaf of 14 days old barley plants. As region of interests (ROI) the B-cell containing sections between two rips were used. (A) For leaf height analysis, the height was measured three to ten times in the ROI at different positions and was subsequently averaged. The bar represents the mean of 16 ROIs for the control and 26 ROIs for *HvRACB* RNAi. (B) The cell layers were counted three to four times per ROI at different positions and were averaged afterwards. The bars represent 25 ROIs for the control and 26 for the *HvRACB* RNAi plants. (C) The individual cross-section areas of all mesophyll and epidermal cells in the ROI were measured and subsequently averaged. The bars show the mean of 25 ROIs for the azygous control and 27 ROIs for the *HvRACB* RNAi line. (D) The areas containing the epidermal B-cells or mesophyll cells were measured per ROI (including intercellular space) and divided by the number of existing cells in this area. This calculation revealed the theoretical number of cells per mm². Each ROI was calculated individually. The bars represent the mean of 25 ROIs for the control and 27 ROIs for the *HvRACB* RNAi lines. The error bars (A), (B), (C) and (D) represent the confidence interval ($\alpha = 0.05$) of the means. Student's t test: (A), (C) and (D), $p < 0.001$; (B), $p > 0.05$.

were quantitated (Figure 13B). The results showed that there was no significant difference in the quantity of cell layers between the leaf blades of *HvRACB* RNAi plants and the azygous control. The average number of the cell layers which includes one layer each of the abaxial and the adaxial epidermis, was 5.6 in the control and about 5.3 in the *HvRACB* RNAi line. This left 3.6 layers over for the mesophyll cells in the azygous control and about 3.3 in the *HvRACB* RNAi plants.

These results implicated that the number of cell layers could not be the main reason for the decreased leaf height. Hence, the cross-section areas of the mesophyll cells and the epidermal B-cells was quantified (Figure 13C). Both cell types showed a significant reduction in their cross-section areas in the *HvRACB* RNAi sections, when compared to azygous control. A *HvRACB* RNAi epidermal cell had an average cross-section area of about 811 µm², contrary to 1109 µm² of a control epidermal cell. This resulted in a relative reduction of nearly 27 %. The total area of the cross-sections of an average mesophyll cell was more than 744 µm² in the control compared to about 520 µm² in the *HvRACB* RNAi leaf. Hence, the mesophyll cells showed a relative decrease in the cross-section area of over 30 %.

Finally, the number of epidermal and mesophyll cells which are available in the measured areas of the cross-sections were quantified (Figure 13D). The data revealed that in average significant more cells were existing in one mm² area in the cross-section of *HvRACB* RNAi plants, when compared to the azygous control. The resulting relative increase reached more than 41 % and exceeded the anticipation based on the reduction of the cell size (Figure 13C). This suggested a further influencing effect like a reduction of the intercellular space within the *HvRACB* RNAi blades compared to their azygous control.

Altogether, the analysis of the cross-section showed a reduced leaf height of the *HvRACB* RNAi blades, when compared to the azygous control. Furthermore, this decrease was caused by a reduction of epidermal and mesophyll cells.

3.2 *HvRACB* RNAi roots generate trichoblasts but no root hairs

Additional to the already mentioned phenotypes in the leaf epidermis formerly described in the literature (Schultheiss *et al.*, 2005; Pathuri *et al.*, 2008, 2009; Hoefle *et al.*, 2011) and the new gained insights shown in this study (chapter 3.1), also effects in *HvRACB* RNAi plants concerning the plant root were reported previously (Hoefle *et al.* 2011). Thus, it was reported that *HvRACB* RNAi seedlings had no or only stunted root hairs. However, no detailed phenotype studies were done on

the *HvRACB* RNAi root so far. To catch up on this, the *HvRACB* RNAi root and the roots of the azygous control were examined via electron scanning microscopy (SEM). To distinguish trichoblasts and atrichoblasts the cells of the root epidermis were stained with propidium iodide (PI) or the live cell dye rhodamine-123 (r123) and visualized via fluorescence microscopy.

3.2.1 Imaging the versatility of *HvRACB* RNAi root hair outgrowth defects

The visualization of the phenotype by Hoefle and colleagues (Hoefle *et al.*, 2011) was restricted to macroscopic images using the low magnification of a binocular or to restricted sections using the high magnification of a confocal fluorescence microscope. Thus, SEM images were recorded. This technique meets the requirements of an overview picture of the root and a high magnification to estimate the abundance of root hairs at a glance (Figure 14A, B). The specimens were scanned in small sections using high magnification/ high resolution settings of the SEM. Afterwards, the single pictures were combined to obtain overview pictures of high resolution of the *HvRACB* RNAi and control roots.

In contrast to the control, *HvRACB* RNAi roots generated no or only few root hairs which were additionally reduced in their size (Figure 14A, B). A simple slowed development of the root hairs seemed unlikely because there were no further initiations of root hairs along the whole examined *HvRACB* RNAi root. The few stunted hairs did not further elongate in older tissues of the root. They remained in their limited size as it was defined shortly after their outgrowth. However, if the *HvRACB* RNAi roots formed some stunted root hairs, they started a few hundred micrometers more distant to the tip of the root than in the azygous control roots. Hence, the initiation of the bulgings was suggestive of being delayed.

Like the formation defect of the subsidiary cells in the epidermis (chapter 0), also the here described root phenotype is restricted to one specific cell type, namely the root hair forming trichoblasts. Apart from that, the overall morphology of the root did not exhibit further obvious alterations, when compared to the roots of the azygous control.

Taking a closer look at the *HvRACB* RNAi roots it was observed that most of the roots did sporadically initiate root hairs. However, these root hairs remained stunted in their size (Figure 14B). To study the sporadic initiations and restricted outgrowths in more detail, the roots were stained with propidium iodide. Single cells were subsequently imaged using a confocal fluorescence microscope (Figure 14C to J). The number and morphology of these sporadic root hairs were characterized by a high versatility from plant to plant within the *HvRACB* RNAi line and even between roots of the same seedling. Thus, not all subsequently described outgrowth phenotypes of the root hairs were

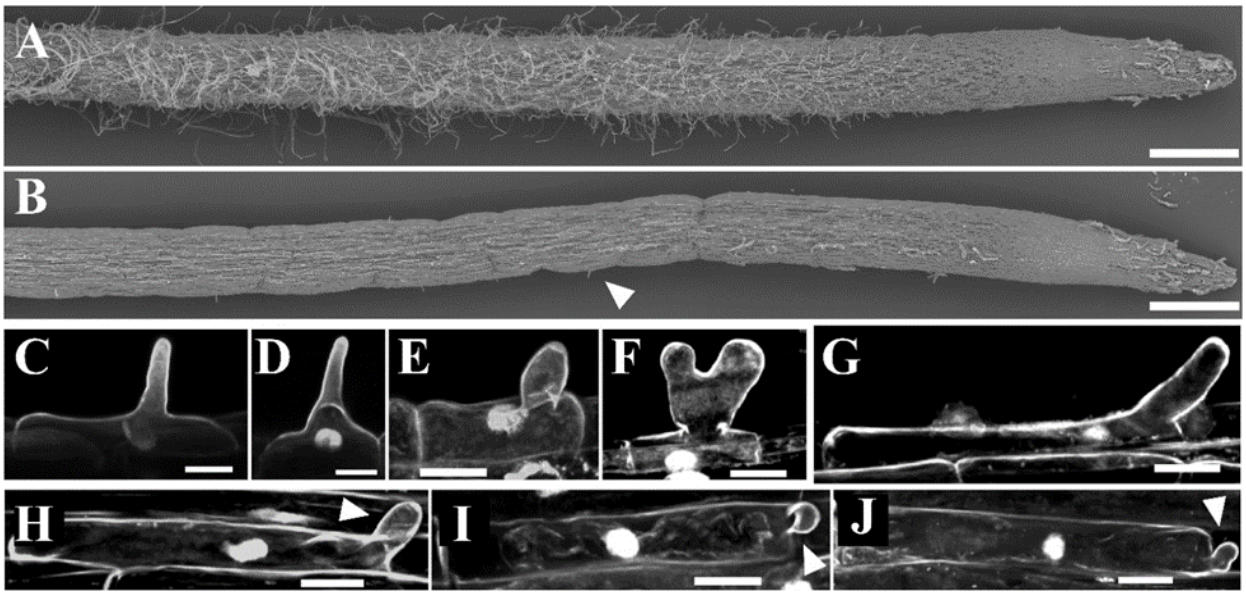

Figure 14: Overviews and single cell images of *HvRACB* RNAi roots and their azygous control.
(A) SEM image of an azygous control root and (B) of a *HvRACB* RNAi root. Single scans of smaller root sections were done, corrected in brightness and contrast and subsequently merged along the longitudinal axis. The first clear visible stunted root hair in the *HvRACB* RNAi root (B) is marked with a white arrowhead. (C) to (J) show the observable outgrowth phenotypes on the *HvRACB* RNAi roots. The outgrowths are marked with white arrowheads in (H), (I) and (J). The pictures were made after staining the roots with propidium iodide using a confocal fluorescence microscope. The outgrowth defects are quite diverse among the different *HvRACB* RNAi plants and even among the roots of the same seedling. Scale bar (A), (B): 1 mm; (C) to (D): 20 µm. As material the roots of 2 days old seedlings were used.

detectable in the same number or extent in all *HvRACB* RNAi roots. It was ensured that the mentioned deformations were not existent or only detectable in a negligible number on the azygous control roots.

The stunted root hair which was not distinguishable from a root hair of the azygous control in the same developmental stage of tip growth was the most prominent one (Figure 14C). Another type of deformation of the root hairs was a stunted root hair with a noticeable ballooned base (Figure 14D). Usually young root hairs show the largest diameter at their base and narrow along the longitudinal axis to the tip (Figure 14C). However, the stunted root hairs of the *HvRACB* RNAi plants sometimes showed an abnormal wide broadening with the largest diameter not at the base but in the middle of the longitudinal axis (Figure 14E). Another phenotype can be seen in Figure 14F which showed an initial of a root hair with two spatially restricted regions of tip growth. Additionally, the location of the initiation of the root hair was occasionally misguided (Figure 14G). In these cases, the root hair grew out at the very tipward end of the epidermal cell. Usually, root hairs are initiated at the lower third of the trichoblast cell (Figure 14C). The outgrowths exemplarily shown in Figure 14H indicate

a combination of a misguided outgrowth (Figure 14G) with an abnormal wide broadening in the middle of the longitudinal axis (Figure 14E). These misguided outgrowths were also detectable showing a total loss of any similarity to a root hair (Figure 14I, J). Here, the outgrowths remained restricted to a small evagination at the most tip oriented region of the trichoblast.

Measuring the transcript level of *HvRACB* in different regions of the azygous control roots revealed that it is most abundant in the root zone of root hair initiations. This region is characterized by visible bulgings of the trichoblasts. Furthermore, concerning the *HvRACB* RNAi plants, the expression of *HvRACB* is reduced up to 92 % in this area, when compared to the azygous control. This even outreached the knocking down effect of 90 % in the tip and of 77 % in the differentiated region (Supp Figure 3). Thus, the transcript profiling in the control roots confirmed the presence of *Hv*RACB in these regions and an efficient knockdown in the *HvRACB* RNAi plants.

To sum up, the trichoblasts in the *HvRACB* RNAi roots revealed a diverse phenotype of outgrowth. It ranged from complete missing to misguided and deformed initiations of root hairs. In the bulging region *HvRACB* transcripts were available and efficiently reduced in the RNAi line, when compared to the control. This supports a *Hv*RACB dependency of the root hair phenotype. The data encouraged further investigations of the trichoblasts in the roots of *HvRACB* RNAi plants.

3.2.2 Detection and quantification of the trichoblasts in *HvRACB* RNAi roots

As described previously, the *HvRACB* RNAi roots produced no or only stunted and scattered root hairs. Though the phenotypes of the outgrowths of epidermal cells were quite versatile, the most frequent defect was complete loss of initiation of root hairs (chapter 3.2.1 and Hoefle *et al.* 2011). This failure could be based on the inability of the root to define trichoblasts or the inability of trichoblasts to initiate the process of root hair formation (Schiefelbein, 2000). Therefore, the *HvRACB* RNAi root was examined for the existence of trichoblasts and atrichoblasts.

The roots of the azygous control and the *HvRACB* RNAi line were stained with propidium iodide or rhodamine 123 (r123). The latter is a live cell dye for staining of mitochondrial activity. The first dye utilized the different morphological, the second the physiological features of the trichoblasts and atrichoblasts to verify their identity (Marzec *et al.*, 2013).

At first the roots were stained using a newly developed protocol of propidium iodide staining. This allowed the differentiation of short trichoblasts and long atrichoblasts with root hairs in the elongation zone. The obtained pictures revealed that shortly after entering the elongation zone, longer and shorter epidermal cells can be distinguished in the azygous control plants as well as in the *HvRACB* RNAi roots (Figure 15A, B). This was a strong indication for the existence of

trichoblasts in the epidermis of *HvRACB* RNAi roots.

However, this staining technique could not give further information whether the detected longer cells are indeed defined atrichoblasts and the shorter cells defined trichoblasts. In contrast to the cell size, their physiological properties were shown to be a clear indicator for already defined trichoblasts and atrichoblasts (Marzec *et al.*, 2013). Hence, the physiological properties of the two cell types were utilized by staining the roots with r123. The pictures were made in the transition zones of the roots of the azygous control (Figure 15C) and the *HvRACB* RNAi plants (Figure 15D). This means that the atrichoblasts were in a developmental stage before entering the process of fast elongation

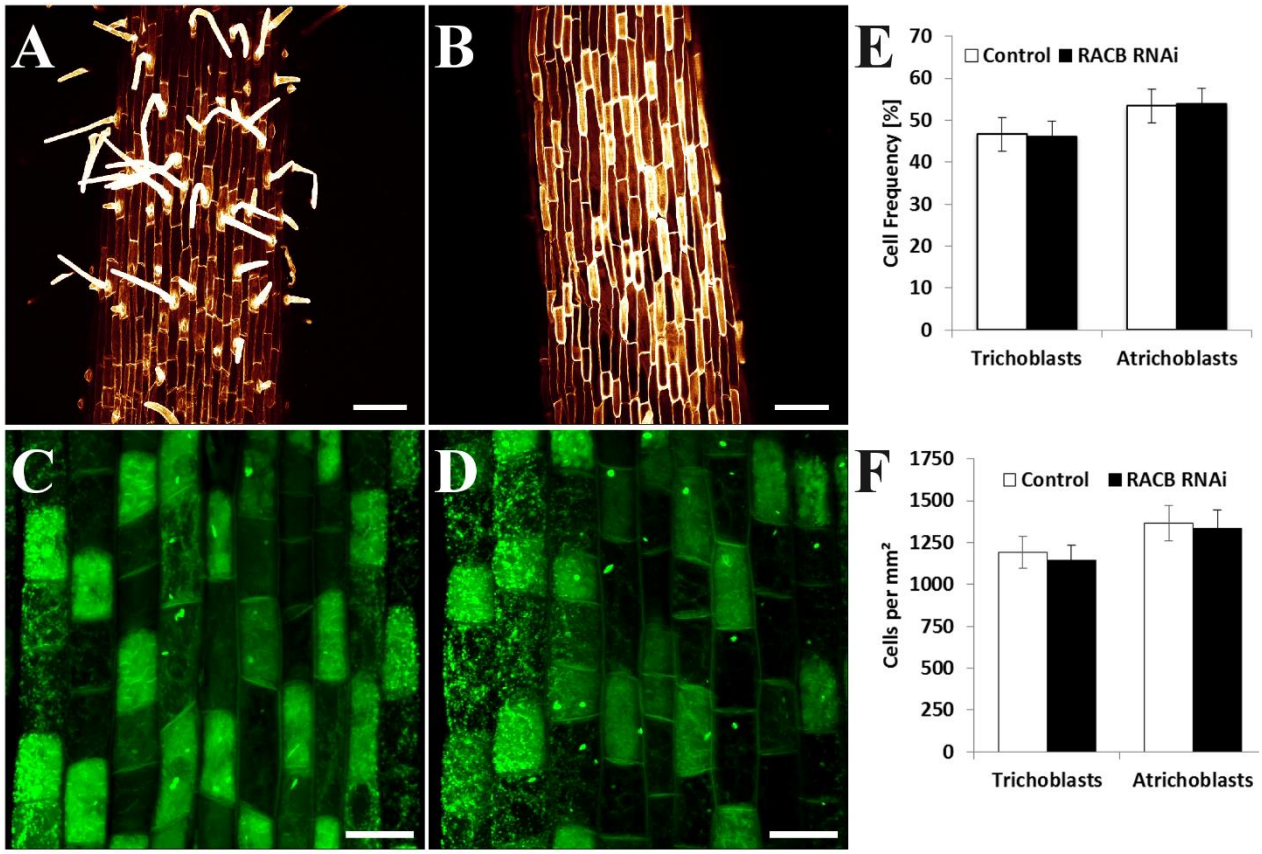

Figure 15: Characterization and quantification of the trichoblasts of *HvRACB* RNAi roots and the azygous control.
Staining of (A) azygous control and (B) *HvRACB* RNAi roots using an improved propidium iodide staining. Staining of control (C) and *HvRACB* RNAi roots (D) with rhodamine 123. The trichoblasts produced a brighter fluorescence signal than the atrichoblasts in both lines. (E) Relative frequency distribution of trichoblasts and atrichoblasts. (F) Absolute cell abundance in a defined area. All images were done using a confocal fluorescent microscope. Scale bars (A), (B) 100µm; (C), (D) 25µm. (E) Cells were counted in a 0.024 mm² restricted area and their relative distribution was calculated based on the absolute numbers. The bars show the mean of 31 independent roots, each. (F) Recalculation of the absolute cell numbers from (E) to the 0.024 mm² showed the same quantity of cells per mm² in both lines. Error bars: (E), (F) confidence interval ($\alpha = 0.05$). Student's t test: (E), (F) $p > 0.05$. As material the roots of 2 days old seedlings was used.

and the trichoblasts before the first initiation of roots. Bright stained trichoblasts could be distinguished from weaker stained atrichoblasts. No differences in fluorescence activity of *HvRACB* RNAi trichoblasts and trichoblasts of the control roots were observable. This experiment confirmed the already indicated existence of defined trichoblasts in the root epidermis of *HvRACB* RNAi plants (Figure 15A, B). In older tissues of both, *HvRACB* RNAi and azygous control plants, this staining pattern diminished again and the trichoblasts and atrichoblasts were not distinguishable by r123 staining anymore.

Additional to the verification of trichoblasts in the *HvRACB* RNAi roots, the rhodamine 123 staining also allowed the quantification of this epidermal cell type (Figure 15E). The counting showed that the relative distribution of trichoblasts and atrichoblasts was unaltered in the *HvRACB* RNAi plants, when compared to their azygous control. Furthermore, the number of the epidermal cells can be recalculated to the defined area in which they were counted. This revealed that not only the distribution is unchanged but also the absolute numbers of these cells in the measured area (Figure 15F). This suggests that the size of epidermal cells in the transition zone of the roots of *HvRACB* RNAi plants and their azygous control is the same.

Altogether, the experiments showed that *HvRACB* RNAi plants developed trichoblasts in the root in the same number and size as in the azygous control. The root hairlessness is therefore likely caused by an inability to grow out root hairs. In several cases which were described in the literature this could be attributed to a disturbed reactive oxygen species (ROS) production. The accumulation and production of ROS in the root was addressed in the following experiments.

3.3 ROS in the root give no indication for altered enzyme activity

Root hair phenotypes which are similar to the ones described in this work (chapter 3.2), were in many cases suggested to be directly or indirectly caused by disorders in the local production of ROS (Carol *et al.*, 2005; Huang *et al.*, 2013; Kwasniewski *et al.*, 2013). Hence, the abundance of ROS and indirectly the activity of peroxidases and NAD(P)H oxidases in the *HvRACB* RNAi roots were evaluated. This allowed to evaluate a potential impact of ROS on the outgrowth phenotypes of the root epidermis.

3.3.1 OH• detection indicated no differences in peroxidase activity in *HvRACB* RNAi roots

It was suggested that the activity of peroxidases is crucial in barley for the initiation of root hairs and their subsequent elongation (Kwasniewski *et al.*, 2013). Therefore, the detection and quantification of OH• (hydroxyl radical) as product of peroxidases was performed using 3'-(p-hydroxyphenyl) fluorescein (HPF) as probe. HPF turns over after reaction with OH• to a bright green fluorescent product which was visualized using a confocal fluorescence microscope (Figure 16).

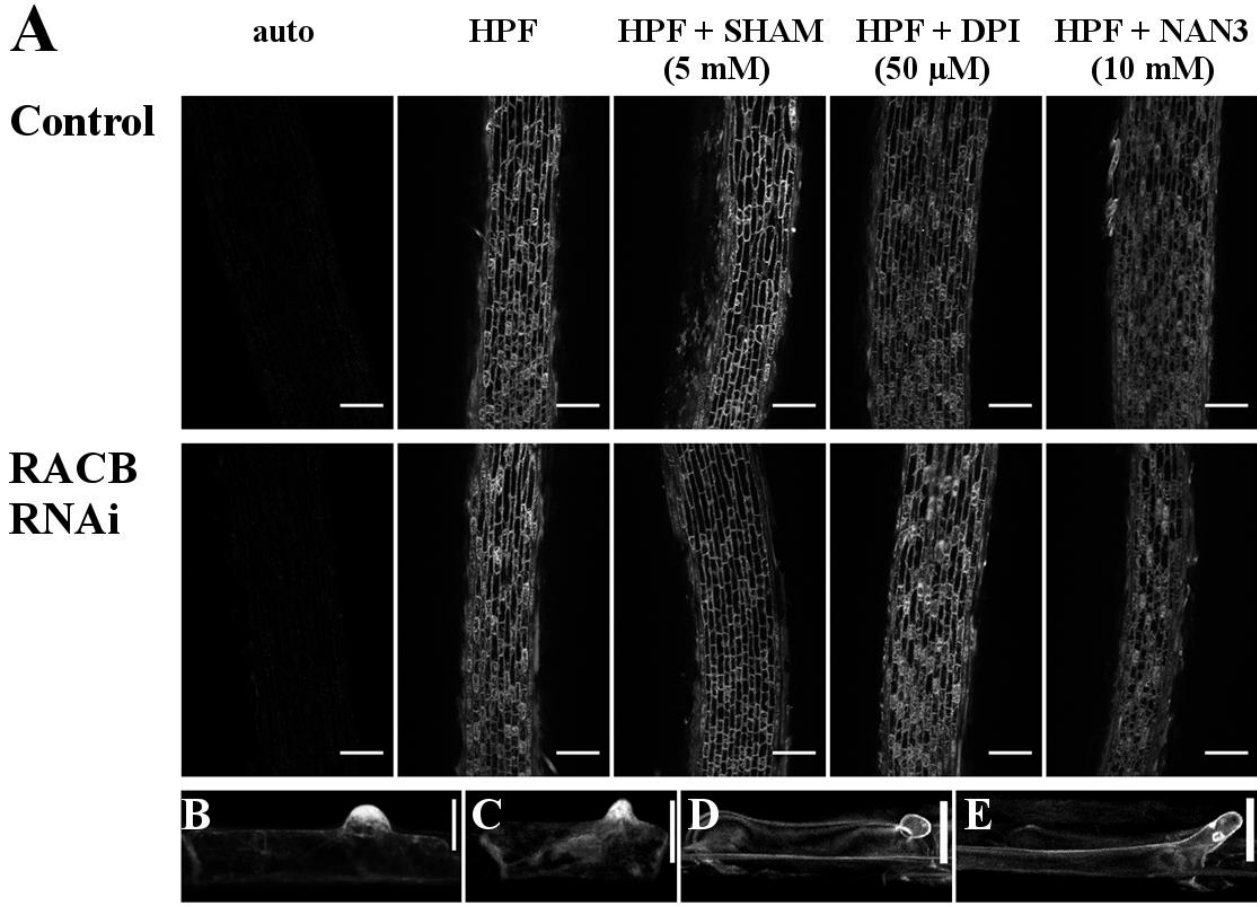

Figure 16: Detection of hydroxyl radicals in the root via HPF.
(A) Autofluorescence and HPF derived fluorescence of the *HvRACB* RNAi and control roots with and without inhibitors of ROS producing enzymes. (B) HPF fluorescence in the root hair bulging in the control, (C) in the *HvRACB* RNAi line and (D), (E) in displaced and deformed root epidermal outgrowths in *HvRACB* RNAi roots. Scale bars: (A) 100 µm; (B) to (E) 20 µm. As material the roots of 2 days old seedlings were used. The images were done using a confocal fluorescence microscope. The settings for excitation, detector sensitivity and others were the same for all pictures. auto: autofluorescence; HPF: 3'-(p-hydroxyphenyl) fluorescein (5 µM); SHAM: salicylhydroxamic acid (5 mM); DPI: diphenyleneiodonium chloride (50 µM); NaN_3: sodium azide (10 mM).

The examined root tissues comprised parts of the transition zone and the elongation zone. After treatment with HPF a clear increase in fluorescent brightness was observed in this region of the root. The untreated controls just exhibited the autofluorescence signal (Figure 16A). However, no differences were observable between the *HvRACB* RNAi plants and the azygous control.

To identify the source of the hydroxyl radicals, different classes of ROS producing enzymes such as peroxidases, NAD(P)H oxidases, and cytochrome oxidases were inhibited parallel to HPF treatment. Nevertheless, no obvious alterations were achieved inhibiting peroxidases via salicylhydroxamic acid (SHAM), or NAD(P)H oxidases using diphenyleneiodonium chloride (DPI). Only the application of sodium azide (NaN_3) as inhibitor of cytochrome oxidase and peroxidase activity (NIH, 1991) caused an apparent reduction of the fluorescent signal (Figure 16A). Furthermore, the roots of *HvRACB* RNAi and control plants reacted similarly to the addition of the different inhibitors, concerning their fluorescence derived from HPF.

Worth a mention is a subcellular specific bright fluorescence after treatment with HPF in the root hair initiation zones. This fluorescence in the bulge initiations were observable in the azygous control (Figure 16B) but also in the *HvRACB* RNAi line, if root hair initiations were available (Figure 16C). But not only the regular shaped outgrowths of the root cells showed the spatial accumulation of the fluorophore. The irregular, displaced, and deformed outgrowths and evaginations, already described in chapter 3.2.1, featured this specific bright fluorescence, too (Figure 16D, E).

Quantification of the fluorescence by measuring the pixel intensity only partly coincided with the qualitative assessments, already described above (Figure 17). The autofluorescence led to a pixel intensity of about 6.5 in the control and about 5.7 in the *HvRACB* RNAi root. After HPF treatment the pixel intensity increased to 56 in the azygous control and about 63 in the *HvRACB* RNAi root. The quantitation revealed that it was possible to reduce the fluorescence signal in the azygous control significantly using DPI or NaN_3 as an inhibitor, if comparing to the HPF treated control roots. In the *HvRACB* RNAi roots SHAM and NaN_3 treatment decreased the pixel intensity significantly, when compared to the HPF treated roots of the same line. In both lines the NaN_3 had the greatest impact. It reduced the intensity in the control by 42% and in the *HvRACB* RNAi line by 53%. However, if the pixel intensities of the different treatments in the *HvRACB* RNAi roots were compared to their corresponding azygous control in no case significant distinctions were observed.

The HPF treatment exhibited no alterations in OH• abundance in the region of root hair initiation, comparing *HvRACB* RNAi and azygous control. The inhibitor treatment triggered no differences in amount and distribution between these two lines. This indirectly suggested no distinctions in the peroxidase activity in this root zone of root hair production. Therefore, the NAD(P)H oxidase activity in the *HvRACB* RNAi and azygous control root was examined.

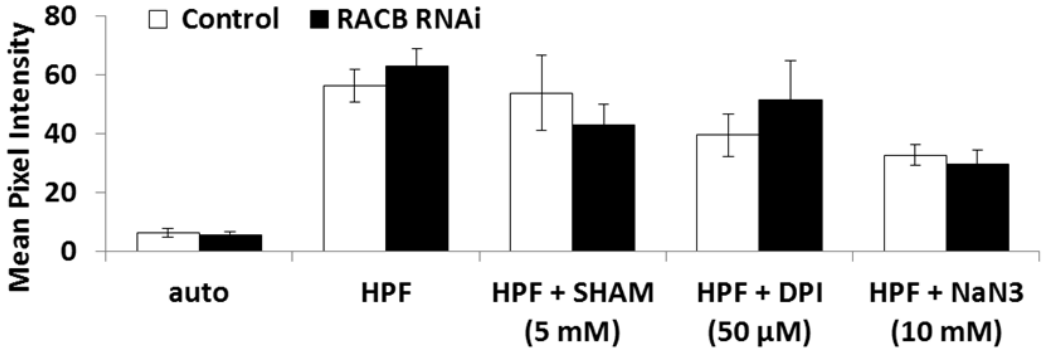

Figure 17: Quantification of HPF derived fluorescence in the root.
As ROIs the transition zones and the beginning of the elongation zones were examined. The fluorescence was measured via the mean pixel intensity after HPF treatment with and without inhibitors of ROS producing enzymes. Pixel intensity: 0 ("black") and 255 ("white"). All pixels of the root were averaged for the picture mean pixel intensity. The bars show the mean of these intensities. Control: Auto n = 15; HPF n = 42; SHAM n = 10; DPI n = 6; NaN_3 = 6. *HvRACB* RNAi: Auto n =12; HPF n = 40; SHAM n = 7; DPI n = 6; NaN_3 n = 6. Error bars: Confidence interval ($\alpha = 0.05$). Student's t test: $p > 0.05$. As material the roots of 2 days old seedlings were used. Auto: autofluorescence; HPF: 3'-(p-hydroxyphenyl) fluorescein (5 µM); SHAM: salicylhydroxamic acid (5 mM); DPI: diphenyleneiodonium chloride (50 µM); NaN_3: sodium azide (10 mM).

3.3.2 Detection of $O_2^{\bullet-}$ indicated NAD(P)H- oxidase activity in emerging root hairs

The visualization of distribution and quantification of hydroxyl radicals via HPF turnover to a detectable fluorophore revealed no differences between *HvRACB* RNAi roots and the azygous control (chapter 3.3.1).

NAD(P)H oxidases were shown to have an crucial impact on the initiation and development of root hairs (Carol *et al.*, 2005). Furthermore, *Arabidopsis thaliana* mutant lines of a NAD(P)H oxidase developed similar phenotypes in the formation of root hairs, as described previously in this work (chapter 3.2.1). Therefore, the distribution of superoxide anion radicals ($O_2^{\bullet-}$) which derive from NAD(P)H oxidases was visualized in in the roots of the *HvRACB* RNAi plants.

Therefore, Nitroblue tetrazolium (NBT) was used. It reacts with superoxide to a blue insoluble formazan dye and is detectable via bright field microscopy. Overview pictures of roots treated with

NBT (Figure 18A, B) revealed similar staining patterns in *HvRACB* RNAi roots and the azygous control. Obvious differences arose by the existence of root hairs on the control roots, which were specifically stained. The residual coloring of the roots indicated a staining of ROS species derived from mitochondria. This pattern was not distinctive between the mutant line and the azygous control and revealed no obvious subcellular patterning. The intensity of formazan diminished in older tissues and was especially intensive in the meristematic regions and in the growing

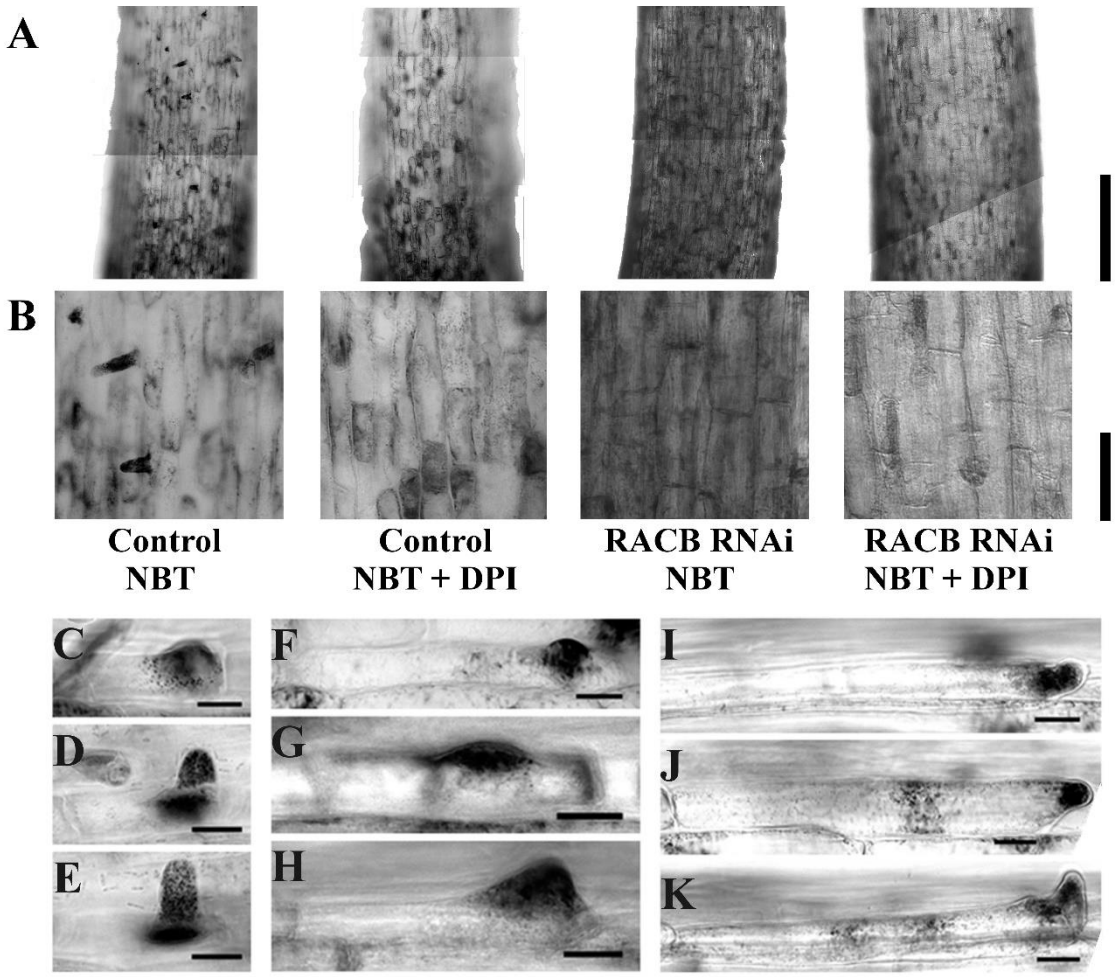

Figure 18: Detection of superoxide anion radicals in the root via NBT.
(A) Overview images of azygous control and *HvRACB* RNAi roots after NBT treatment or extra addition of the NAD(P)H oxidase inhibitor DPI (50 µM). The overviews were generated by merging several single pictures. *HvRACB* RNAi and azygous control tissues exhibited similar staining patterns, probably displaying mitochondrial activity. (B) Enlarged detail sections of (A) for better view. (C), (D), (E) display the NBT staining pattern in root hair bulgings and young root hairs in the control plants. (F), (G), (H) NBT staining in *HvRACB* RNAi root hair initiations. (I), (J), (K) show similar staining of irregular cell outgrowths in the *HvRACB* RNAi root epidermis. Scale bars: (A) 200µm; (B) 50µm; (C) to (K) 20µm. All images were transformed to grey scale for a better visualization of the dark colored formazan. As material the roots of 2 days old seedlings were used.

root hairs. Addition of the NAD(P)H oxidase inhibitor DPI eliminated root hair located NBT staining, whereas the unspecific formazan accumulation in the epidermal cells remained unaltered. In case *HvRACB* RNAi plants had initiated root hairs, DPI affected the NBT staining in *HvRACB* RNAi in the same way as in azygous control roots (Figure 18A, B).

A closer look to the stained initiations of root hairs revealed that during the bulging event the whole evagination is stained by NBT in the trichoblasts of the azygous control (Figure 18C). During later stages of the root hair development a strong accumulation of formazan can be seen at the base of the growing root hair and in the tube oriented to the apex (Figure 18D, E). Similar patterns of staining in emerging root hairs were exhibited on the *HvRACB* RNAi roots, if root hair initiations were observed (Figure 18F to H). The disoriented and deformed outgrowths of the root epidermis (chapter 3.2.1 and chapter 3.3.1) showed also a specific pattern of NBT staining (Figure 18I to K). The previously mentioned fading of the NBT staining in older root tissues without growth activities was also observable in the *HvRACB* RNAi line. This fading comprised all kind of outgrowths of epidermal cells.

To summarize, the NBT staining exhibited indirectly a specific activity of NAD(P)H oxidases in the initiation of root hairs and other kinds of outgrowths. After treatment with DPI, specific staining of the root hairs vanished and no differences were observed between the control and the *HvRACB* RNAi line. *HvRACB* RNAi lines largely lacked specific staining derived from NAD(P)H oxidases as seen in outgrowing trichoblasts of the azygous controls.

3.4 *HvRACB* RNAi nuclei are less attracted after fungal attack

Detection of ROS without a bulging event indicated no differential activity of peroxidases and NAD(P)H oxidases between the *HvRACB* RNAi line and the control (chapter 3.3). Hence, the focus turned to the event of single cell polarization. This appeared to be a common and basic principle of all developmental events which are influenced by *HvRACB* (Schultheiss *et al.*, 2005; Pathuri *et al.*, 2008, 2009; Hoefle *et al.*, 2011). Part of this cell polarization in the interaction of plants and pathogens, formation of subsidiary cells, and development of root hairs is the temporal and spatial coordinated movement of the nucleus to a specific site of the plant cell (Stebbins and Shah, 1960; Čiamporová *et al.*, 2003; Griffis *et al.*, 2014). The directed migration of the nucleus was used as an indicator for the degree of polarization of the plant cell during fungal attack. Hence, the distance of

the nucleus to the attempted site of penetration of the powdery mildew fungus was visualized and measured in fixed leaf material after staining with propidium iodide.

3.4.1 Temporal resolution in *HvRACB* RNAi cells reveals an early delay effect on the nucleus movement

HvRACB RNAi plants showed a reduced penetration efficiency of *Bgh*, when compared to the wildtype (Hoefle *et al.*, 2011). This data indicated a prepenetration effect of *HvRACB* RNAi on the accommodation of the fungus. Therefore, relevant processes causing the decreased susceptibility could be expected in the time before the formation of the haustorium.

The polarization of the attacked plant cell and therefore the migration of the nucleus is focused to the attempted site of penetration. The timing of the movement is defined by the development of the fungus. To assess suitable points in time for the inspection of the plant cell nucleus, azygous control plants were inoculated with *Bgh* and subsequently visualized. For microscopy of the fungal development the fixed material was treated with the fluorophore tetra-methyl-rhodamine (TMR) which is linked to wheat germ agglutinin (WGA). This resulted in specific staining of the fungal structures on the barley leaf (Figure 19). Already at 12 hpi haustorial initials were formed, whereas

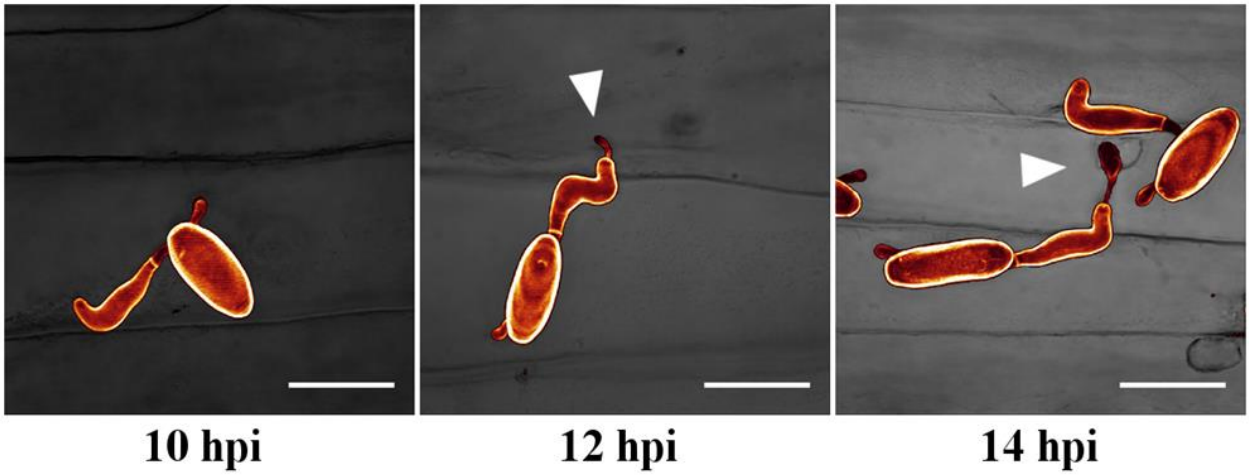

Figure 19: Visualization of *Bgh* development on the barley leaf via staining with WGA-TMR.
Ten hours after inoculation, the fungal spore already grew out the primary germ tube and formed the hook - shaped appressorium. However, no haustorial initials were visible at this point in time. After 12 hours haustorial initials were observable and after 14 hpi the haustoria expanded to a clubbed structure. Spores which didn't show any haustorial pattern at this point in time were assessed as failed for plant cell wall penetration. Haustoria are marked by white arrowheads. Scale bar 25µm. As material the harvested and fixed 2nd leaf blades of 14 days old azygous control plants were used.

10 hpi no such structures were observable. 14 hpi the spores exhibited at least a haustorial initial or already a further developed clubbed haustorium. It was assumed that appressoria without any indication of haustorial development at 14 hpi failed already to penetrate the cell wall.

Based on these results 8, 10 and 12 hours after inoculation were chosen as points in time to evaluate the migration of the plant nucleus to the attempted site of penetration. Additionally, these measurements were used to indirectly assess the degree of cell polarization. The inoculated and fixed leaf material was viewed under the microscope at the points in time. For visualization of the plant cell nucleus, the plant cell wall, and the fungal appressorium the leaf material was stained with propidium iodide. Using a confocal fluorescence microscope, z-stacks of the attacked plant cell and the appressorium were recorded. Normalizing the distance between nucleus and appressorium to the cell size generated the nucleus attraction index (NAI) as an indicator for cell polarization (see also Supp Figure 5).

Based on their NAI the cells were classified in three groups. These groups ranged from a "very close" (0 - <0.1) plant nucleus to the attempted site of penetration over "close" (0.1 < 0.3) to "distant" (0.3 < 1) (Figure 20). This classification revealed distinctions in the NAI between the *HvRACB* RNAi plants and the azygous control. Furthermore, a time dependent nucleus movement to the appressorium was observed. The NAI data revealed in the *HvRACB* RNAi plants a reduced and delayed migration of the plant cell nuclei to the attempted site of penetration, when compared to the azygous control. The differences in the frequency distribution of the NAI was most significant

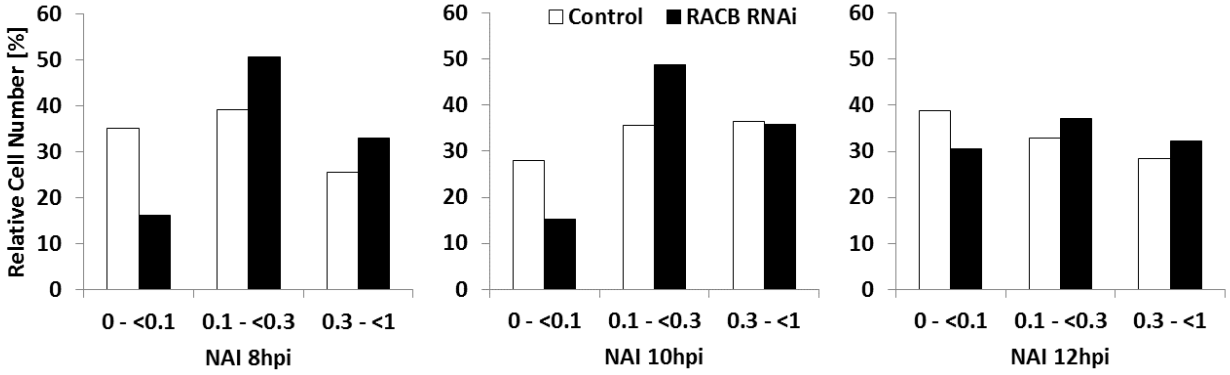

Figure 20: Evaluation of the nucleus attraction index (NAI) at different points in time after inoculation.
For each point in time and line 5 independent leaves were pooled and between 129 and 240 cells were evaluated. The cells were grouped according to their NAI, in three classes: "very close" (0 - <0.1), "close" (0.1- <0.3) and "distant" (0.3 - <1). Whether the cells of the control and the *HvRACB* RNAi plants were differently distributed was evaluated with the chi^2 test. 8 hpi: $p < 0.001$; 10 hpi: $0.001 > p < 0.01$; 12 hpi: $p > 0.05$. As material the 2nd leaves of 14 days old barley plants were used.

8 hours after inoculation. At this point in time more than 35 % of the investigated control cells were classified as "very close" but only about 16 % in the *HvRACB* RNAi line. 10 hpi the frequency distribution was still differing between the two lines but less significant. 12 hpi the control and the *HvRACB* RNAi cells showed similar NAI distributions. At this point in time almost 39 % of the nuclei were "very close" in the azygous control and about 31 % in the mutant line.

The NAI data indicated a delayed migration of the nucleus to the fungal appressorium in the less susceptible *HvRACB* RNAi line. This indirectly suggests a slowed or reduced capability for cell polarization. Furthermore, *HvRACB* RNAi and control roots are similarly colonized by a mycorrhiza fungus at a late point in time after inoculation (Supp Figure 4). This is a further indication for a delayed but not completely inhibited polarization of Hv*RACB* RNAi cells.

3.4.2 H*vRACB* knockdown, nucleus movement delay and enhanced resistance can be detected in the same tissue

A temporal resolution of the movement of the plant nucleus showed significant differences in the attraction of the nucleus to the site of attempted penetration at 8 hpi (chapter 3.4.1). This point in time was chosen for parallel evaluation of penetration efficiency, the NAI, and the expression of *HvRACB* in the same tissue. Coevaluation of *HvRACB* expression and susceptibility on the very same leaf was not performed prior to this work. The lower half of the 1st leaf was used because it revealed the most efficient knock down effect by the *HvRACB* RNAi insertion of all tested leaf

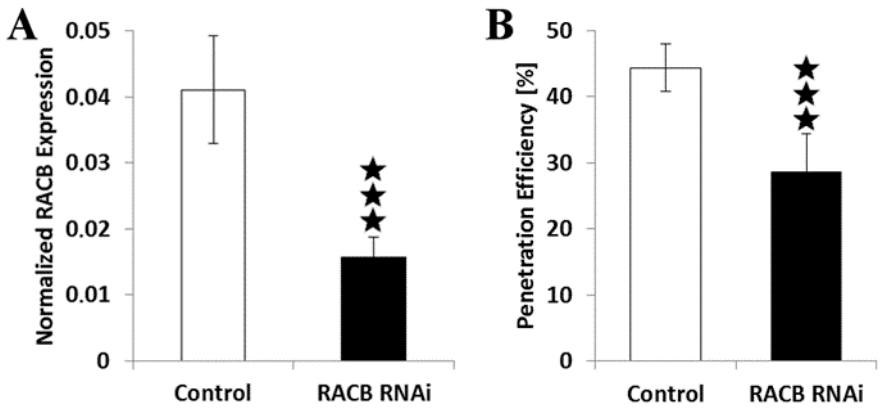

Figure 21: Coevaluation of the *HvRACB* transcript level and the penetration efficiency. (A) qPCR of *HvRACB* and (B) penetration efficiency in the very same leaf. As material the lower half of 1st leaf of 14 days old plants at 16 hpi was longitudinally split in half. One half was used for qPCR analysis, the other one for assessment of the penetration efficiency. Each leaf was evaluated independently. The bars represent the mean of 5 plants. Error bars: standard deviation. Student's t test (A), (B): $p < 0.001$.

tissues (Supp Figure 6). The gained half of the leaf blade was subsequently split in half again, but along the longitudinal axis. One half was used for the determination of the transcription level of *HvRACB* and the other half for investigation of the NAI or the penetration efficiency. It was shown that in *HvRACB* RNAi plants the reduction of *HvRACB* abundance came along with a reduction of susceptibility, when compared to the azygous control. The relative *HvRACB* transcript level was decreased about 62 % in the *HvRACB* RNAi plants. Furthermore, the penetration efficiency of the fungus dropped from over 44 % in the control to less than 29 % in the *HvRACB* RNAi line (Figure 21A, B).

Evaluating the expression of *HvRACB* and the NAI on the very same *HvRACB* RNAi leaves revealed that the *HvRACB* transcript abundance was reduced by more than 72 %, when compared to the azygous control (Figure 22A). The measurement of the NAI at 8 hpi (Figure 22B) showed that less nuclei of the *HvRACB* RNAi plants were classified as "very close" (12 %) but more as "distant" (48 %) than in the control (22 % and 27 % respectively). Testing the frequency distribution via chi^2-test exhibited a significant distinction in the distribution to the three classes between the control and the *HvRACB* RNAi line.

The NAI represents the distance from the nucleus to the appressorium normalized to the cell size. Both values are measured independently for each examined cell. Thus, it was taken care about the

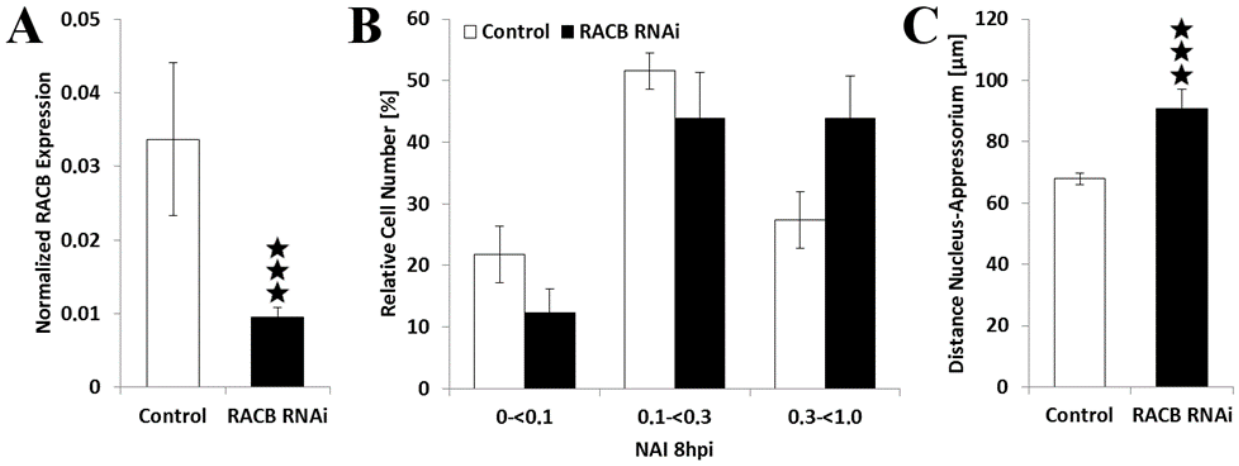

Figure 22: Coevaluation of the *HvRACB* transcript level and the nucleus attraction index (NAI).
(A) qPCR of *HvRACB* and (B) and NAI evaluation at 8 hpi. (C) Nucleus-appressorium distance without normalization to the cell size. (A), (B) and (C): all measured data represents the average of the same 6 independently examined control and 5 *HvRACB* RNAi leaves All Error bars show the STD. (B) and (C): between 86 and 135 cells per leaf were measured. (A). Student's t test: p<0.001. (B) The cells were grouped according to their NAI, in three classes: "very close" (0 - <0.1), "close" (0.1- <0.3) and "distant" (0.3 - <1). chi^2 test: 8 hpi: p < 0.001. (C) Student's t test: p<0.001.

reduced epidermal cell size of the *HvRACB* RNAi plants (chapter 3.1.2 and chapter 3.1.3). Without this normalization the nucleus would be per se closer to the appressorium in the mutant line than in the azygous control. This is due to the smaller epidermal cells of the Hv*RACB* RNAi plants, when compared to the control (chapter 3.1.2 and chapter 3.1.3). However, even without this normalization the distance was significantly longer in the Hv*RACB* RNAi plants than in the control (Figure 22C). The distance increased from average 68 µm in the control to almost 91 µm in the *HvRACB* RNAi plants. This underlined the robustness of the suggested delayed or inhibited migration of the nucleus in the *HvRACB* RNAi line after fungal attack.

The gained data showed a reduced expression of *HvRACB*, a reduced nucleus polarization, and a reduced penetration efficiency in the very same leaf material after fungal attack. This suggested a causal relationship of these three factors in the same order.

3.5 Omnidirectional approaches exhibit alterations in the *HvRACB* RNAi cell wall

Preliminary (Melanie Bischof, TU München, Germany, unpublished data) and recent microarray data (Vera Schnepf, TU München, Germany unpublished data) revealed that in the *HvRACB* OECA and *HvRACB* RNAi plants a high quantity of genes were altered at their transcriptional level, when compared to the wildtype (WT). A considerable number of these genes were assigned to cell wall related processes. Also the described *Hv*RACB dependent phenotypes in the literature (Schultheiss *et al.*, 2005; Pathuri *et al.*, 2008; Hoefle *et al.*, 2011) and in this work, gave indications for a direct or indirect involvement of *Hv*RACB in the modification of the cell wall. Based on this background it was reasonable to investigate if the cell wall of the *HvRACB* RNAi plants was altered in its chemical, mechanical and lytic features.

3.5.1 Cell wall modifier genes are differential expressed in the *HvRACB* RNAi line

To verify the microarray data semiquantitative reverse transcription PCRs (sqPCR) of selected genes were performed. Genes were selected according the available microarray data. The primer design was based on sequence and annotation data listed in the PLEXdb database (www.plexdb.org).

The abundance of the transcripts was evaluated in a time series at zero-time ("0"), 12 hpi, 32 hpi and their corresponding not inoculated controls at 12 and 32 hours after zero-time. These points in time were used because of the average development of the fungus. At 12 hpi *Bgh* is penetrating the plant cell wall or is beginning to establish a haustorium initial. At 32 hpi the haustorium developed finger-like protrusions and is still expanding but already functional. Thus, 12 hpi represents an early stage in the infection with powdery mildew on barley. At this time *Bgh* shows no or only initial establishment. 32 hpi stands for a rather late stage of development of *Bgh* with a further developed haustorium and secondary epicuticular hyphae (Figure 19; personal communication Vera Schnepf, TU München, Germany).

The visualized transcripts are shown in Figure 23 and confirmed the data of the microarray. However, some genes revealed only slight differences in their expression patterns. The auxin-binding protein 1 (ABP1_12253; Supp Figure 7) and a positive control for *Bgh* infection on barley P21_14958 did hardly show alterations between the wildtype and the *HvRACB* RNAi plants. This was also the case for some examined cell wall modifier genes such as the arabinogalactan protein 16 (AGP16_06537) and the polygalacturonase PG_08722.

Nevertheless, most of the investigated cell wall modifiers revealed moderate to strong enhancements of the transcription level in *HvRACB* RNAi lines. Among these are the expansin EXP_02877 or the alpha-L-arabinofuranosidase/beta-D-xylosidase ARA-I_07032. The data suggested that these genes are constitutively distinct in their transcription level between the wildtype and the *HvRACB* RNAi line. According to this, the knockdown of *HvRACB* showed a minor impact on fungal dependent alterations in the expression of the cell wall modifiers than the WT.

An exception was e.g. the polygalacturonase PG_12475. Transcripts of this gene were less abundant 12 hpi than in the control. Even though the shown transcript abundancies suggested an overall upregulation, several other genes such as pathogenesis related (PR) genes, were reduced in their transcript levels (Supp Figure 7). It seemed that the general transcription patterns, such as transcript enhancement after fungal attack (e.g. PR genes) was not repealed. However, it was rather shifted in the time-series of the *HvRACB* RNAi line, when compared to the WT. This could be seen for example by assessing the transcript amounts of the ascorbate oxidase gene ASO_30512 (Supp Figure 7) which was less expressed at 12 hpi than in the WT but stronger at 32 hpi.

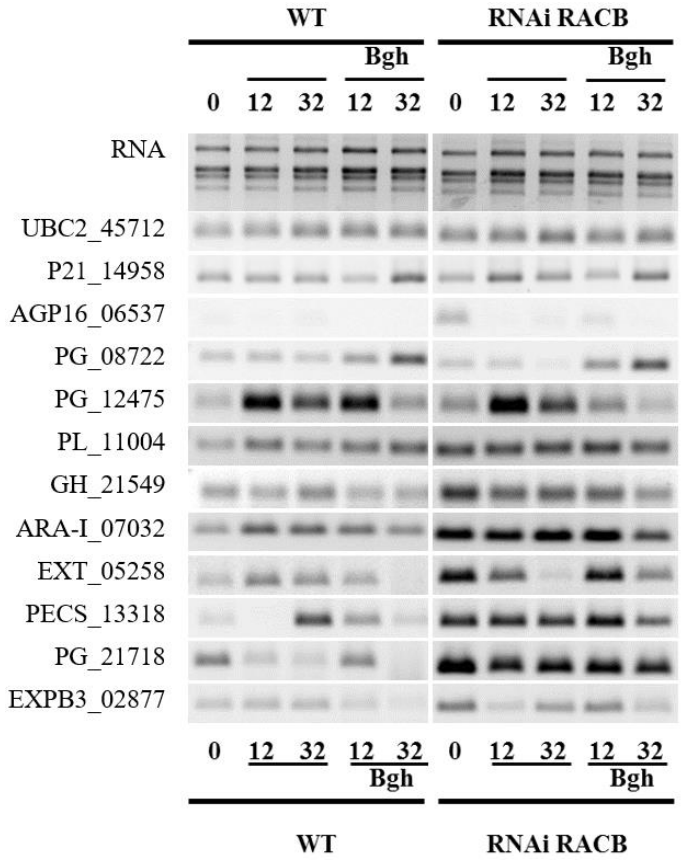

Figure 23: Expression analysis of selected genes in the WT and *HvRACB* RNAi line via sqPCR.
The transcript level was evaluated at zero-time ("0"), 12 and 32 hours after zero-time with and without inoculation with *Bgh*. The gene identifiers were composed of the gene abbreviation and a five digit code, representing the contig number in the PLEXdb database (www.plexdb.org). As control the extracted RNA was visualized on the gel as well as the transcript level of the housekeeping gene UBC2 for each treatment. The PCR conditions were adapted for each gene but were the same for all shown transcript abundancies. The same is observed for the exposure time of the agarose gel. UBC2: ubiquitin-conjugating enzyme E2; ABP1: auxin-binding protein 1. P21: p21 c-terminal-binding protein. AGP16: arabinogalactan protein 16. PG: polygalacturonase. PL: pectate lyase. GH: glycosyl hydrolase. ARA-I: alpha-L-arabinofuranosidase/beta-D-xylosidase. EXT: xyloglucan endotransglucosylase/hydrolase. PECS: pectinesterase. EXPB3: expansin-B3. As material at least 5 blades of the 2nd leaf, of 14 days old barley plants were pooled per line and each point in the time-series.

Summarized, the sqPCR of selected genes confirmed the preliminary microarray data. A set of cell wall modifier genes was differentially expressed in the *HvRACB* RNAi plants, when compared to the WT-control. Because of the differences in the transcript levels, it was logical to investigate the composition of the cell wall of Hv*RACB* RNAi plants and the control.

3.5.2 The protoplast release assay shows a higher lytic resistance of the *HvRACB* RNAi cell wall

The previous results of the sqPCR (chapter 3.5.1) suggested an examination of the cell wall itself. Therefore, it was tested if the cell wall of the *HvRACB* RNAi plants revealed distinctions in the lytic resistance to fungal cell wall degrading enzymes, when compared to the azygous control. In a protoplast release assay small leaf pieces of the same size were incubated in the enzyme mix for several hours. Released protoplasts were counted using a bright field microscope. The number of freed protoplasts indirectly showed the lytic resistance of the cell walls which was attributed to differences in the chemical composition.

The results of the protoplast release assay are shown in Figure 24. After 2 hours of incubation in a solution of the enzyme mix, significantly less protoplasts were released from the *HvRACB* RNAi leaf pieces than from the azygous control. Thus, in the control about 25 protoplasts were counted per µl solution. In the mutant line only about 12 protoplasts were available. The counting after three hours of incubation revealed that in the control 47 protoplasts were present per µl solution and in the *HvRACB* RNAi approach 33 protoplasts. The differences after 3 hours were not significant anymore. Nevertheless, they showed an existing tendency of a decreased protoplast release concerning the *HvRACB* RNAi plants, when compared to the azygous control.

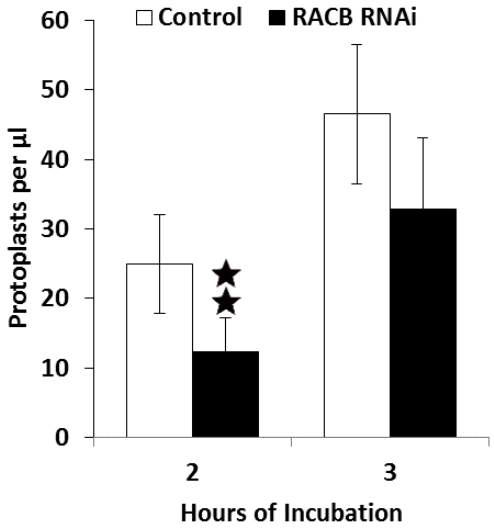

Figure 24: Evaluating the lytic resistance of the cell wall via the protoplast release assay. Small leaf pieces were incubated in a fungal cell wall digesting enzyme mix. After 2 and 3 hours of incubation the released protoplasts were counted. The bars represent the mean of three biological replicates. Error bar: confidence interval (α = 0.05). Student's t test: 2 hoi $0.05 > p < 0.001$; 3 hoi $p > 0.05$. As material leaf pieces of the 2nd leaves of the same size and comparable areas were used

The gained results of the protoplast release assay should be evaluated on the background that *HvRACB* RNAi plants have smaller cells than the control plants (chapter 3.1.2 and 3.1.3). Therefore, the commensurate leaf pieces of the *HvRACB* RNAi plants possessed more cells than the control which could be putatively released.

Together, the assay showed less freed protoplasts in the *HvRACB* RNAi line than in the control. This indicated a higher lytic resistance and differences in the chemical composition of the primary cell wall. The analysis of the composition of the cell wall was therefore the next logical step.

3.5.3 Analysis exhibit differences in the cell wall monosaccharide composition between *HvRACB* RNAi and control plants

The protoplast release assay (chapter 3.5.2) showed differences in the lytic resistance between cell walls of the azygous control and the Hv*RACB* RNAi line. Thus, it was suggested that the differences in the expression of the cell wall modifiers (chapter 3.5.1) also influenced the actual chemical composition of the cell wall. To examine the chemical composition of the primary cell wall a high-performance anion-exchange chromatography with pulsed amperometric detection (HPAEC-PAD) was performed in collaboration with Timo Engelsdorf and Lars Voll (University of Erlangen, Germany). This method allowed the elucidation of the absolute and relative monosaccharide amount of the cell walls of the Hv*RACB* RNAi plants and the control.

At first the total amount of monosaccharides was quantified (Supp Figure 8). This revealed that the RNAi plants had significant more primary cell wall monosaccharides per gram fresh weight than the azygous control plants. In the control about 15.9 nmol per gram fresh weight were measured. The Hv*RACB* RNAi material possessed 18.5 nmol per gram fresh weight. This is an enhancement of more than 16 % of total amount of monosaccharides in the Hv*RACB* RNAi line, when compared to the control. This possibly reflects smaller volumes of the *HvRACB* RNAi cells. Next, the relative amounts of the seven measurable monosugars were compared between the azygous control and the *HvRACB* RNAi line (Figure 25). This showed significant differences in the relative amount for the monosaccharides fucose, galactose, and xylose. The rhamnose, glucuronic acid, galacturonic acid, and arabinose were not significantly altered. The highest relative difference was observed for the fucose. It was decreased by almost 28 %, when compared to the control. Galactose was decreased by more than 11 % and xylose significantly was enhanced by more than 2 %. Even though fucose represented the major relative reduction in the *HvRACB* RNAi plants, it should be kept in mind that this monosaccharide only stands for about a quarter-percent of the relative monosugar amount

(0.28 %) in the control. The relative reductions of the galactose and the xylose were smaller. However, they represented about 8.3 % and 64.1 % of the relative monosaccharide amount in the control leaves.

Finally, the monosugar analysis revealed aberrations in the relative content of xylose, galactose and fucose. This made it possible to focus in further studies on enzymes acting on these monosaccharides in the cell wall.

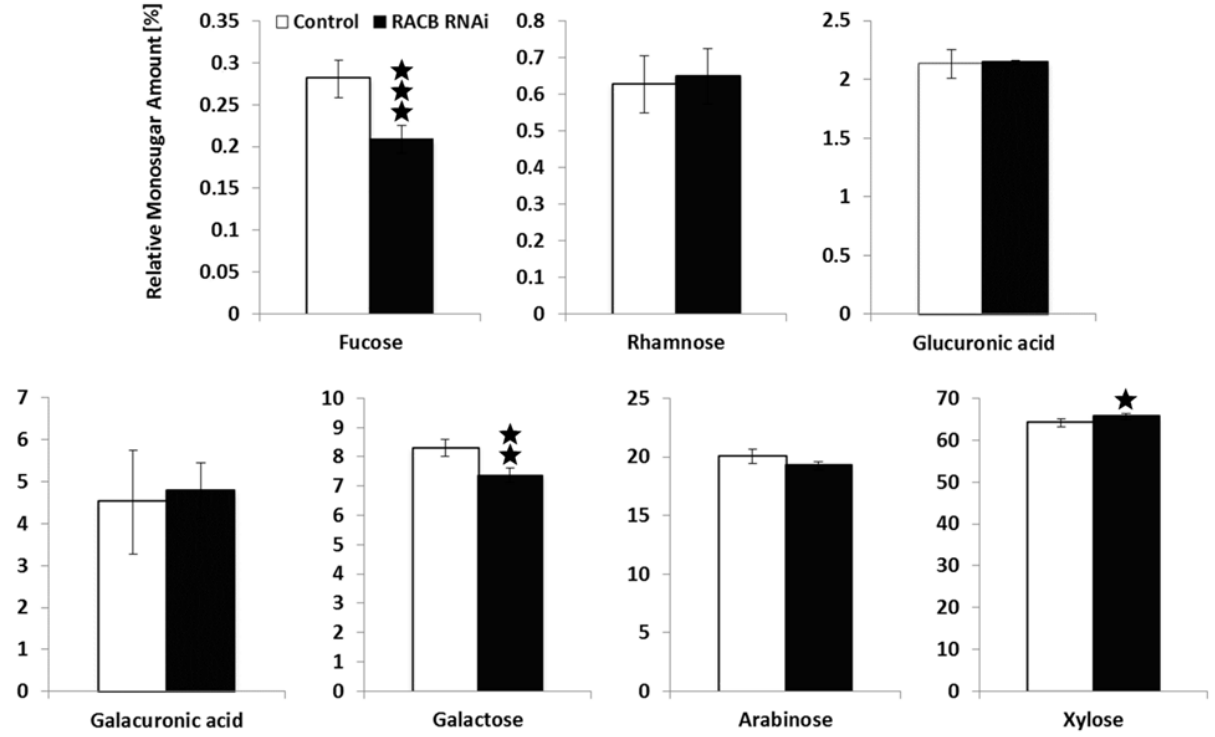

Figure 25: Analysis of the relative monosaccharide distribution of the primary cell wall via HPAEC-PAD.
The relative proportions of the seven monosugars fucose, rhamnose, glucuronic acid, galacuronic acid, galactose, arabinose and xylose were measured in the azygous control and the *HvRACB* RNAi leaf blades. The monosaccharides were listed accordingly to their relative amount. The bars represent the means of 5 biological replicates. Error bars: confidence interval ($\alpha = 0.05$), Student's t test: fucose $p < 0{,}001$; galactose $0.01 > p > 0.001$; xylose $0.05 > p > 0.01$. All other monosugars $p > 0.05$. As material the 2nd leaf of 14 days old barley plants were used. Each replicate was a pool of 5 independent leaves.

3.6 Directional investigations in barley reveal several enzymes active on xyloglucan

The monosaccharide analysis of the primary cell wall of the *HvRACB* RNAi line and the azygous control revealed distinctions in the relative monosugar composition between the *HvRACB* RNAi plants and their azygous controls (chapter 3.5.3). Most prominent was the reduction of the relative

share of the monosaccharide fucose. In the primary cell wall of monocotyledons, fucose is only available in the hemicellulose xyloglucan (Vogel, 2008). Therefore, the data pointed to this component of the primary cell wall and shifted the investigative focus on it.

3.6.1 Identification of *Bgh* dependent expressed xyloglucan modifiers

As a first step, genes were identified which were putatively involved in modifying the monosugar composition of xyloglucan via their enzymatic activity. As a starting point, published sequences of xyloglucan related genes in monocots were used for BLAST search (Del Bem and Vincentz, 2010). As reference sequences the Barley1 22k Microarray (www.plexdb.org) and the nucleotide collection of Hordeum vulgare (taxid: 4513) of the National Center for Biotechnology Information (http://www.ncbi.nlm.nih.gov) were used.

In a second step, all found genes were filtered for an additional altered expression after inoculation with Bgh. This was based on publicly available data in the expression database of Genevestigator® (www.genevestigator.com).

As last step, 27 genes were selected hitting these criteria (Table 2). The genes were unevenly divided on the following 8 different enzyme groups: α-Fucosyltransferases (4 genes), β-Galactosyltransferases (5 genes), α-Xylosyltransferases (2 genes), Xyloglucan Transglycosilases/Hydrolases (7 genes), α-Fucosidases (4 genes), β-Galactosidases (1 gene), α-Xylosidases (1 gene), and β-Glucosidases (3 genes).

Table 2: Genes coding for putative xyloglucan modifiers in barley

α-Fucosyltransferases	β-Galactosyltransferases	α-Xylosyltransferases	Xyloglucan Transglycosilases/ Hydrolases
FUT_355743	Contig3965_at	Contig6858_at	Contig1616_at
FUT_362089	Contig3966_at	Contig15389_at	Contig2669_at
FUT_362802	Contig5919_at		Contig2670_x_at
FUT_375786	Contig5920_at		Contig2672_at
	Contig11321_at		Contig2673_at
			Contig5258_at
			*HV*SMEb0004L16r2_at

α-Fucosidases	β-Galactosidases	α-Xylosidases	β-Glucosidases
FUC_1402	Contig4930_at	Contig9432_at	Contig4970_at
FUC_3023			Contig8591_at
FUC_4897			Contig13674_at
FUC_20663			

3.6.2 Expression analysis of fucosidases and fucosyltransferases for candidate selection

In the previous chapter, several genes were identified which are putatively involved in the modification of xyloglucan and were additionally expressed during interaction with *Bgh*. The reduction of the relative content of fucose was the highest relative effect comparing the azygous control and *HvRACB* RNAi cell wall composition (chapter 3.5.3). Hence, the pattern of fucosylation became especially interesting. Furthermore, click-chemistry experiments revealed, that labeled fucose can be tracked to the bulgings of root hairs in barley seedling roots (Supp Figure 9).

Based on these outcomes, for further expression analysis the four identified putative α-fucosidases and four α-fucosyltransferases were chosen (chapter 3.6.1). Fucosidases remove the fucosyl residue

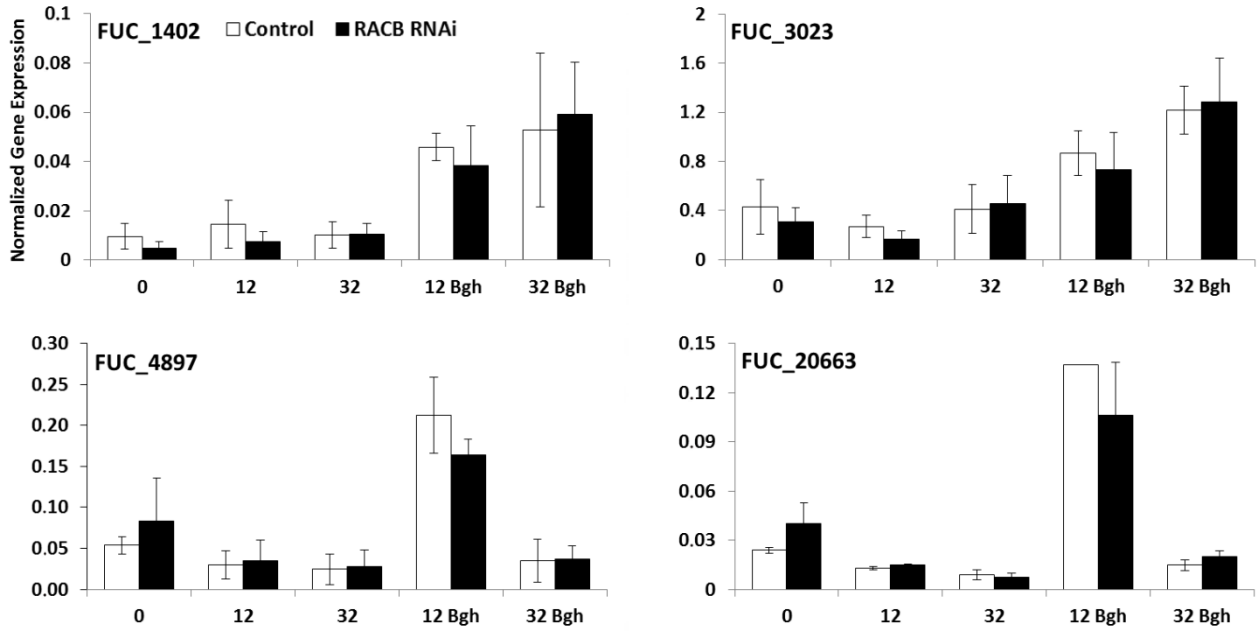

Figure 26: Expression analysis of putative xyloglucan α-fucosidases via qPCR.
The transcript abundancies of the four putative α-fucosidases identified by BLAST search (Table 2) were examined via qPCR. The amounts of the transcripts were evaluated in a time series at zero-time ("0"), 12 hpi, 32 hpi and their corresponding not inoculated controls at 12 and 32 hours after zero-time. The *Bgh* dependency of the expression was confirmed for all fucosidases. FUC_1402 and FUC_3023 had an increased transcript amount 12 hpi and 32 hpi. FUC_4897 and FUC_20663 showed a specific transcript increase 12 hpi, whereas 32 hpi transcription was similar to the not inoculated control again. No significant differences in the expression levels, independent of fungal presence, were observed between the *HvRACB* RNAi line and their azygous control. The bars represent the mean of three biological replicates. Each point in time consists of a pool of at least 5 independent leaves. Error bars: standard deviation. As material the inoculated or not inoculated 2nd leaves of 14 days old plants were used. The transcript level was normalized on the housekeeping gene UBC2.

from the xyloglucan, whereas the fucosyltransferases add a fucose monosaccharide to the backbone (Del Bem and Vincentz, 2010). The α-fucosidases and α-fucosyltransferases were tested for their transcript abundancies. The transcripts were quantitatively measured via qPCR. The abundances of the transcripts were evaluated in a time series at zero-time ("0"), 12 hpi, 32 hpi and their corresponding not inoculated controls at 12 and 32 hours after zero-time.

The tested putative α-fucosidases were *Bgh* dependently regulated in their transcript abundancies (Figure 26). FUC_1402 and FUC_3023 showed their highest transcript amount 32 hpi, when compared to

the not inoculated samples. However, already at 12 hpi a clear enhancement of the relative transcript abundancy was observed. FUC_4897 and FUC_20663 revealed a specific increase of their transcripts 12 hpi. At 32 hpi the expression level was similar to the not inoculated control. Even though the fucosidases genes were *Bgh* dependently expressed, no significant differences were seen comparing the azygous control and the *HvRACB* RNAi line.

The same expression analysis was done using the α-fucosyltransferases (Figure 27) listed in Table 2. The relative transcript level was lower in average than the levels of the investigated α-fucosidases

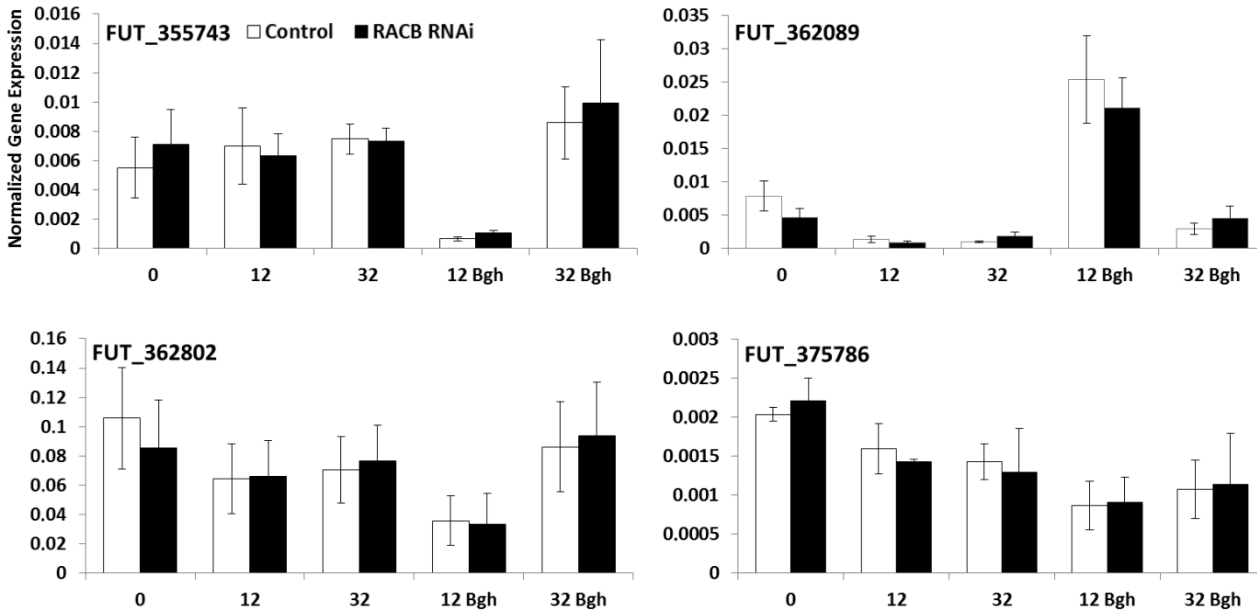

Figure 27: Expression analysis of putative xyloglucan α-fucosyltransferses via qPCR.
The transcript abundancies of the four putative α-fucosyltransferases identified by BLAST search (Table 2) were examined via qPCR. The transcripts were evaluated in a time series at zero-time ("0"), 12 hpi, 32 hpi and their corresponding not inoculated controls at 12 and 32 hours after zero-time. The bars represent the mean of three biological replicates. Each point in time consists of a pool of at least 5 independent leaves. Error bars: standard deviation. As material the inoculated or not inoculated 2nd leaves of 14 days old plants were used. The transcript level was normalized on the housekeeping gene UBC2.

(Figure 26). The *Bgh* dependent expression which was evaluated in Genevestigator®, was confirmed for the fucosyltransferases. FUT_355743, FUT_362802 and FUT_375786 were reduced in their transcription 12 hpi. At 32 hpi no clear alteration to the not inoculated controls was observed. FUT_362089 was strongly enhanced in its transcript abundance, when compared to the not inoculated control. Thus, in the azygous control the transcript level was about 13 times higher than the level in the not inoculated sample. In the *HvRACB* RNAi plants the enhancement was even stronger by 23 times. However, no significant differences were observed between the azygous control and the *HvRACB* RNAi line comparing the relative transcript abundancies.

Next to the expression analysis after *Bgh* attack, the transcript abundancies were also evaluated in the intercalary meristem and in the zone of root bulging, for the putative α-fucosidases (Supp Figure 10) and the putative α-fucosyltransferases (Supp Figure 11). The data revealed that FUC_3023 was the prominent transcribed α-fucosidase in the intercalary meristem and that the transcripts were reduced in the *HvRACB* RNAi line, when compared to the azygous control. The other fucosidases did not show this *Hv*RACB dependent expression in the meristem. However, in the bulging zone of the root FUC_4897 was the fucosidase with the highest relative transcript level and not FUC_3023. Additionally, no FUC exhibited an obvious alteration in its expression in the *HvRACB* RNAi root, when compared to the azygous control.

Concerning the α-fucosyltransferases, the FUT_362089 was the most prominent expressed FUT-gene in the intercalary meristem and in the zone of root bulging. This was the case for the *HvRACB* RNAi line and the azygous control. Furthermore, FUT_362089 was the only gene among the investigated FUTs which was clearly decreased in its transcripts in the *HvRACB* RNAi line, when compared to the azygous control. The other α-fucosyltransferases did not exhibit clear alterations in their transcript levels between the control and the knockdown line.

Summing up, all FUCs and FUTs were confirmed in their *Bgh* dependent expression as seen in the Genevestigator® database. FUT_362089 was the only fucosyltransferase with a higher transcript abundance after fungal attack. This coincided with the reduced relative fucose amount in the cell wall. It was the predominantly fungal expressed FUT in the intercalary meristem and the bulging region. In the *HvRACB* RNAi line its transcripts were reduced in these tissues, when compared to the control.

3.7 FUT_362089 a putative α-fucosyltransferase shows no impact on *Bgh* penetration success

Several genes were identified which were annotated as putative xyloglucan α-fucosidases or xyloglucan α-fucosyltransferases. Additionally, they were altered in their transcription after *Bgh* attack (chapter 3.6.2). Expression analysis of these modifiers of xyloglucan fucosylation revealed that the α-fucosyltransferase FUT_362089 was the only gene in line with all set criteria. It was significantly enhanced in its expression at 12 hpi which is the critical point in time for determination of the interaction of *Bgh* and barley (chapter 3.4.1). Furthermore, FUT_362089 was the prominent fucosyltransferase in the intercalary meristem and the zone of root bulging. In the Hv*RACB* RNAi line, the gene exhibited an obvious reduction in its transcripts in the meristem and the root, when compared to the azygous control (chapter 3.6.2). This may explain the reduction of fucose in the cell wall (chapter 3.5.3). Therefore, the α-fucosyltransferase FUT_362089 was chosen for further investigations.

3.7.1 FUT_362089 is a putative xyloglucan α-1,2-fucosyltransferase

The best characterized xyloglucan α-1,2-fucosyltransferase in plants is AtFUT1 which is a member of the AtFUT family. It is in addition the only member with a proofed activity as a fucosyltransferase on xyloglucan in *Arabidopsis thaliana* (Sarria *et al.*, 2001).

Therefore, AtFUT1 represented the best candidate available to evaluate FUT_362089 on a bioinformatics level for its α-fucosyltransferase character. AtFUT1 and FUT_362089 were aligned using the alignment tool Clustal Omega (Sievers *et al.*, 2011). The amino acid identity was 45.5 %. Three motifs were published to be present in the protein sequence of the AtFUT family (Sarria *et al.*, 2001). The motifs comprised a region of high conversation, a motif for binding of the GDP-fucose, and a motif necessary for the transferase activity. All motifs were found in the FUT_362089 protein sequence. Furthermore, all amino acids supposed to be essential for the motif activity were either conserved or at least preserved as a conservative mutation in the FUT_362089 motifs.

The sequence alignment and motif conversation compared to AtFUT1 confirmed the results of the BLAST search. This bioinformatically confirmed FUT_362089 as a putative xyloglucan α-1,2-fucosyltransferase. Hence, Fut_362089 was chosen for the transient induced gene silencing assay (TIGS) to evaluate its impact on the establishment of *Bgh* on barley.

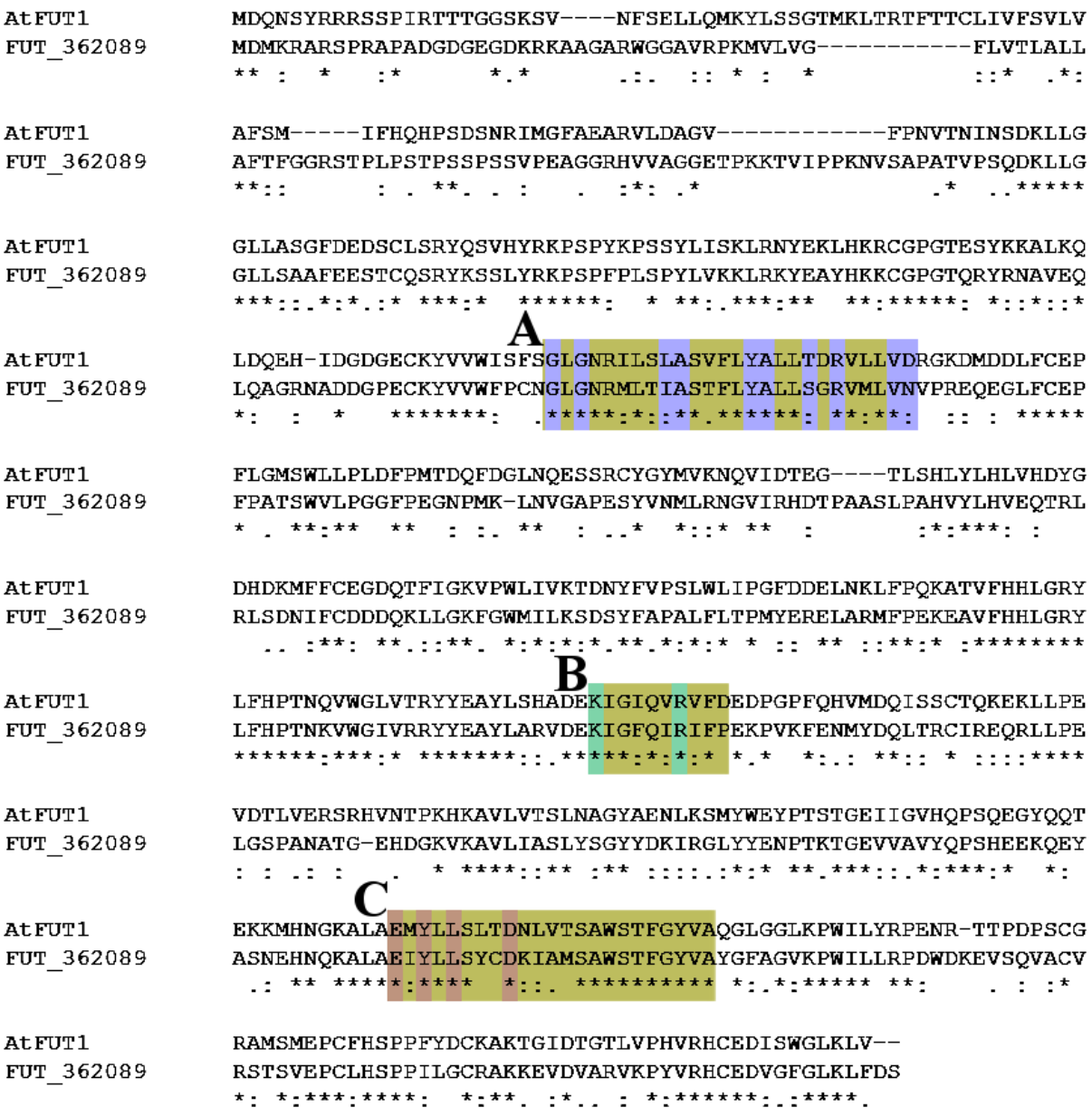

Figure 28: Sequence alignment and motif identification of AtFUT1 and FUT_362089. **FUT_362089 was aligned to the protein AtFUT1 of *Arabidopsis thaliana*. Three hypothetical motifs were identified in the AtFUT family which are highlighted in the alignment. The especially underlined amino acids in blue (A), green (B) and red (C) are supposed to be essential for the motifs. (A) Region of high conservation in the AtFUT family. (B) Motif necessary for GDP-Fucose binding. (C) Motif necessary for the transferase activity. All motifs are highly conserved between AtFUT1 and FUT_362089. GenBank accession number AtFUT1: AEC05676 (558 aa); FUT_362089: BAJ93293 (574 aa). The aa identity between AtFUT1 and FUT_362089 was 45.5 %. The alignment was done using Clustal Omega (Sievers *et al.*, 2011).**

3.7.2 Transient induced gene silencing of FUT_362089 did not alter the susceptibility

The gene FUT_362089 was confirmed on the protein sequence level to be a α-fucosyltransferase. It contained all motifs and amino acids to be necessary for the functionality (chapter 3.7.1). Hence, the impact of FUT_362089 on the outcome of the interaction between *Hordeum vulgare* and its powdery mildew fungus *Bgh* was tested.

The penetration efficiency was investigated after silencing FUT_362089 in single epidermal cells using the TIGS assay (Figure 29). One day after inoculation the penetration efficiency was measured by evaluation of transiently transformed cells in the epidermis which were also attacked by an appressorium. As control the same transformation procedure was done using the "empty" plasmid without the FUT_362089 RNAi construct as transformation vector ("empty vector control"). The evaluation of the penetration efficiency revealed a reduction from about 45 % in the empty vector control to 39 % in the FUT_362089 silenced cells. This represented a relative decrease of about 12 %. However, the reduction was not significant.

In summary, the TIGS assay exhibited that the specific knockdown of FUT_362089 has no sufficient impact to reduce the penetration efficiency of *Bgh* on barley significantly.

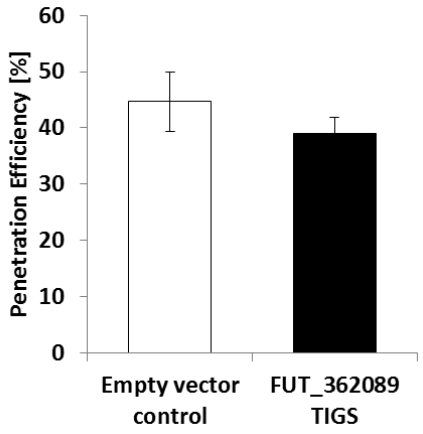

Figure 29: Penetration efficiency after transient silencing of FUT_362089.
As control the vector without the FUT_362089 RNAi construct was used for transient transformation. A vector expressing GFP was co-bombarded and displayed the successful transient transformation process by a bright green fluorescence. The penetration efficiency was measured 24 hpi and hence, 48 hours after particle bombardment. The bars represent the mean of 7 independent TIGS experiments. In the experiments 4 to 6 leaves were examined under the microscope for RNAi and control, each. Error bars: confidence interval (0.05). Student's t test: $p > 0.05$. For the assay 7 days old, detached primary leaves were used.

4 Discussion

4.1 *Hv*RACB regulates plant growth and development

4.1.1 *Hv*RACB participates in the asymmetric cell division of the subsidiary mother cell

In a previous study, Pathuri and colleagues (Pathuri *et al.*, 2009) detected, that stable *HvRACB* OECA plants possess less functional stomata, compared to the azygous control. To determine a potential influence of *Hv*RACB on stomata development, the leaf epidermis of *HvRACB* RNAi plants was investigated microscopically. This revealed an increase of stomata, which show a defect in the formation of one or both subsidiary cells. The relative number of 'defective' stomata raised from 3.5 % in the azygous control to 21 % in the *HvRACB* RNAi plants (Figure 10).

The development and structure of the stomatal complexes in maize are similar to barley (Stebbins and Shah, 1960; Facette and Smith, 2012). Additionally, the knock out of the maize type I ROPs *Zm*ROP2 and *Zm*ROP9 as well as the receptor-like pseudokinase gene *ZmPAN1* resulted in a comparable defect in the formation of subsidiary cells (Humphries *et al.*, 2011; Facette and Smith, 2012). *Zm*PAN1 directly binds to *Zm*ROP2, while *Zm*ROP2 is assumed to recruit the ROP proteins to the SMC/GMC contact site. This leads to the local accumulation of the ROPs, which may promote polarized actin dynamics and polar exocytosis (Humphries *et al.*, 2011; Facette and Smith, 2012).

Both, the *HvRACB* OECA and *HvRACB* RNAi plants exhibit a reduced number of correctly formed stomata, when compared to their respective control plants. However, the characteristics seen in the defective stomata of each line are different. In *HvRACB* OECA plants the alternating sequence of A-cells and GMCs is disturbed. This becomes apparent by multiple successive A-cells in the stomata row. The A-cells between two stomata were absent. Additionally, so called 'blank cells' occur, which are single cells approximately the size of a stoma but without GCs and SCs (Pathuri *et al.*, 2009). In *HvRACB* RNAi plants, the developmental failure of the stomata complexes is restricted to the formation of SCs. Thus, it is comparable to the phenotype described by Humphries and colleagues in the maize type I ROP mutants (Humphries *et al.*, 2011). Stebbins and colleagues described the morphology of the stomatal formation in barley (Stebbins and Jain, 1960; Stebbins and Shah, 1960; chapter 1.1.3). Based on these studies, it can be concluded, that the overexpression of a constitutively activated *Hv*RACB results in an increased failure rate of the asymmetric cell

division of the PSMC to an A-cell and a GC. On the other hand, the knockdown of *HvRACB* would affect the asymmetric division of SMCs to an A-cell and a SC. A loss of complete stomata rows was not observed in *HvRACB* RNAi or *HvRACB* OECA plants, a loss of complete stomata rows could be observed. This supports the assumption, that *Hv*RACB is not involved in the definition of the identity of stomata row files. The same conclusion can be drawn according the symmetric division of the GMC, resulting in two GCs. The obtained data is in accordance with the 'rop2/rop2; rop9/+' ROP double mutants and 'pan1/pan1; rop2/rop2;rop9/+' triple mutants in maize, where no stomatal row and GC phenotypes were reported as well (Humphries *et al.*, 2011). Based on these observations, I hypothesize, that the type I ROP protein *Hv*RACB may fulfill similar activities in premitotic polarization of SMCs as has been proposed for the role of type I proteins in maize. The proposed affected processes include the positioning of the nucleus, the polar exocytosis and the regulation of actin dynamics (Humphries *et al.*, 2011). Furthermore, stomata are formed near the intercalary meristem at the base of the leaf blade and the leaf sheath (Stebbins and Shah, 1960; Supp Figure 1). The transcripts of *HvRACB* are enhanced in the meristematic region of the leaf, when compared to the leaf blade. This further supports a function of *Hv*RACB in this part of the organ (Supp Figure 2). Stomata on the blade and the sheath are generated by two different meristems (Stebbins and Shah, 1960; Ariyanayagam and Stebbins, 1962). Hence, the occurrence of 'defective' stomata complexes in both tissues indicates a general role of *Hv*RACB in the formation of SCs.

4.1.2 *Hv*RACB influences diffuse cell expansion in the leaf

In stable *HvRACB* OECA mutant plants, Pathuri and colleagues (Pathuri *et al.*, 2008) reported an enhanced length of epidermal B-cells, when compared to the control. Hence, the epidermis and cross-sections of the leaves were investigated microscopically. This allowed the evaluation of potential differences in the cell size of stable *HvRACB* RNAi and control plants. The studies revealed a disturbed architecture of the epidermis, an average reduction in the length of B-cells, a decreased area of the cross-sections of B-cells and mesophyll cells and a reduced number of parallel rows of B-cells in the leaf epidermis (Figure 12 and Figure 13).

Besides the increased length of epidermal B-cells in barley *HvRACB* OECA plants, a cell shape effect of the B-cells was observed. This effect was characterized by less regularity of the pavement cells (PCs) in the leaf epidermis, than the strictly arrayed and brick-shaped B-cells of the control plants (Pathuri *et al.*, 2008; chapter 1.1.2). The PCs of WT *Arabidopsis* show a highly regulated jigsaw pattern. This interdigitation of the PCs represents a form of anisotropic diffuse growth, which was shown to be highly ROP-regulated. Hence, the irregularity of the pavement architecture of the

leaf epidermis was more pronounced in *Arabidopsis thaliana* mutant plants, expressing either *At*ROP2 OECA or *At*ROP2 DN (chapter 1.4.3; Kropf *et al.*, 1998; Qin and Dong, 2015). *At*ROP2 OECA plants exhibited enlarged pavement cells and mesophyll cells. Additionally, they almost completely lost the interdigitation of their PCs, which resulted in cylindrical shapes. This was assumed to be caused by an abnormal promotion of the lobe expansion (Li *et al.*, 2001; Fu *et al.*, 2002). The *At*ROP2 DN mutants showed a reduced size of PCs and mesophyll cells and a reduced interdigitation of the PCs. It was suggested that, in contrast to the *At*ROP2 OECA plants, this was caused by an inhibition of the lobe expansions (Li *et al.*, 2001; Fu *et al.*, 2002). A similar loss of the jigsaw pattern of the PCs was observed in *At*ROP6 OECA and *At*ROP6 DN mutant plants. *At*ROP6 OECA PCs were cylindrical shaped. This is supposedly due to a decreased expansion of the lobes and indentations. On the other hand, the expression of *At*ROP6 DN results in more rectangular PCs with fewer and flattened lobes (Fu *et al.*, 2009; Poraty-Gavra *et al.*, 2013). Taken together, the authors concluded an involvement of ROPs in radial and lateral cell expansion of different cell types in the plant. This includes the anisotropic diffuse growth of interdigitating PCs via the regulation of the cytoskeleton (Fu *et al.*, 2002, 2009; Poraty-Gavra *et al.*, 2013; Qin and Dong, 2015; chapter 1.4.3).

Similar to these findings in *Arabidopsis*, *HvRACB* RNAi plants display the reduced length of epidermal B-cells and the decreased cross-section areas of the B-cells and mesophyll cells (Figure 12 and Figure 13). This is in line with the enhanced length of epidermal B-cells in *HvRACB* OECA plants (Pathuri *et al.*, 2008). Thus, I conclude, that *Hv*RACB plays a role as positive regulator of diffuse radial and lateral cell expansion. This can be postulated for the mesophyll cells and the epidermal B-cells of the barley leaf. However, the observed irregularities of the epidermal architecture of *HvRACB* RNAi plants were not observed next to correctly formed stomata complexes. Therefore, these irregularities, comprising the A-cells and B-cells of the epidermis (chapter 1.1.2 and chapter 3.1.2), likely represent an indirect effect of the misshapen or lacking SCs. Thus, I could not observe a generally disturbed regularity of the epidermal B-cells in *HvRACB* RNAi plants, as described for the *HvRACB* OECA plants (Pathuri *et al.*, 2008). This finding corresponds to the 'rop2/rop2; rop9/+' ROP double mutants and 'pan1/pan1; rop2/rop2; rop9/+' triple mutants in maize (Humphries *et al.*, 2011). They also, do not exhibit irregularities in the architecture of the epidermis, besides the described disturbed formation of the SCs. Furthermore, it should be considered, that no anisotropic diffuse growth occurs in the barley epidermis, which would be comparable to the complex jigsaw pattern of A*rabidopsis* PCs. Additionally, the A-cells, B-cells and C-cells in barley are cylindrical and possess brick-like shapes (Stebbins and Jain, 1960; Stebbins and Shah, 1960; Koga *et al.*, 1990; chapter 1.1.2).

Parallel rows of B-cells were counted in Hv*RACB* RNAi plants and the azygous control. This revealed a fewer number of rows in the mutant than in the control (Figure 12). However, the number of leaf ribs remained unaffected (Figure 12). Each rib consists of several parallel C-cells (Figure 1). The same was observed for the number of horizontal leaf cell layers (Figure 13). The number comprises the abaxial epidermal layer of B-cells, three to four layers of mesophyll cells and the adaxial layer of B-cells (Figure 1). The architecture of the grass epidermis mainly contains cylindrical cells in a parallel alignment (Stebbins and Jain, 1960; Cerioli *et al.*, 1994). Dicotyledonous plants lack this row and rib based arrangement of the epidermis. Therefore, a comparison with Dicotyledons, like *Arabidopsis thaliana*, is not feasible. In monocotyledons, I could not find any study, dealing with ROP proteins, which could confirm or deny such a phenotype. Expansion of the grass leaf via cell division and cell expansion occurs in the growth zone. It is located at the base of the leaf blade and can be further subdivided in the proximal division zone and the more distal elongation-only zone (Kavanova *et al.*, 2006). Therefore, I postulate, that the occurrence of the reduced cell expansion and the decreased number of parallel B-cell rows of the *HvRACB* RNAi plants, originates in the growth zone. This is supported by the higher expression of *HvRACB* in the meristem and the basal area of the leaf, compared to older leaf tissue (Supp Figure 2 and Supp Figure 6). Furthermore, both phenotypes may partially account for the reduced length, width and height of the *HvRACB* RNAi leaves, compared to the control. Thus, the *HvRACB* RNAi leaves exhibited a 20 % reduction of the leaf height without a changed number of horizontal cell layers (Figure 13; Hoefle *et al.*, 2011). *HvRACB* OECA plants were shown to develop enlarged B-cells. Interestingly, the size of these plants was reduced, but the reduction was not as severe as in the RNAi plants (Schultheiss *et al.*, 2005; Pathuri *et al.*, 2008; Hoefle *et al.*, 2011). This situation, concerning cell expansion effects and overall plant sizes, coincides with the *At*ROP2 OECA and *At*ROP2 DN mutants in *Arabidopsis thaliana* (Li *et al.*, 2001; Fu *et al.*, 2002).

When the cytoskeleton is disturbed it affects the growth and the organogenesis of the plant. Thus, I suggest a similar function of *Hv*RACB and *At*ROP2, such as the regulation of the cytoskeleton dynamics.

4.1.3 *Hv*RACB promotes initiation of the root hair and polar tip growth

Hoefle and colleagues (Hoefle *et al.*, 2011) observed a lack of root hairs in stable *HvRACB* RNAi plants. This was further addressed in this work via extensive microscopic examinations. Detailed information about the morphogenesis of the root hairs as well as spatial distribution of ROS was obtained through these examinations. The latter was reported to be a ROP-dependently organized

factor in the growth of root hairs (chapter 1.4.2; Foreman *et al.*, 2003; Jones *et al.*, 2007; Grierson *et al.*, 2014). *HvRACB* RNAi strongly affected outgrowth and elongation of root hairs. The formation of trichoblasts remained unaffected and the accumulation of ROS correlated with the absence or presence of the outgrowths of the epidermis.

Seedling roots of *HvRACB* RNAi plants were shown to produce no or only few and stunted root hairs, when compared to their azygous controls. Additionally, *HvRACB* OECA resulted in shortened root hairs and loss of polar tip growth leading to ballooned tips (Pathuri *et al.*, 2008; Hoefle *et al.*, 2011). In *Arabidopsis thaliana At*ROP2, *At*ROP4 and *At*ROP6 were described to influence the formation of root hairs (chapter 1.4.2; Li *et al.*, 2001; Molendijk *et al.*, 2001; Jones *et al.*, 2002, 2007). In *At*ROP4 OECA and *At*ROP6 OECA plants, root hairs were stunted and their tips were ballooned (Molendijk *et al.*, 2001). Overexpression of the native *At*ROP2 led to the lengthening and branching of root hairs, as well as their increased initiations per trichoblast.

On the other hand, *Arabidopsis* plants expressing a constitutively activated form of *At*ROP2 exhibited dramatically stunted and ballooned root hairs if grown in contact with air (Jones *et al.*, 2002). Expression of dominant negative forms surprisingly had minimal effects on root hair development, if any were seen at all. No effects were observed in *At*ROP4 DN and *At*ROP6 DN plants. Mild effects, such as a decreased number and shortened root hairs, were observed in *At*ROP2 DN plants (Molendijk *et al.*, 2001; Jones *et al.*, 2002). A recently published *rop6* T-DNA insertion line, also displayed no alteration in the formation of root hairs (Lin *et al.*, 2012). On the other hand, roots of *Nicotiana tabacum Nt*Rac1 RNAi were hairless, which is similar to *HvRACB* RNAi plants (Tao *et al.*, 2002). Furthermore, *Arabidopsis thaliana* plants expressing a bacterial (*Clostridium difficile*) transgene coding for the *At*ROP4 inhibiting toxin B are root hairless (Singh *et al.*, 2013). However, the specificity of the effects of the transgene *in vivo* was objected to require further confirmation (Burkart *et al.*, 2015).

Altogether, interfering with the activity of ROPs results in heterogeneous phenotypes of root hair formation. This may plausibly be explained by the redundant, overlapping, distinct or diverse functionality of ROP proteins in the cell. Additionally, different techniques to reduce ROP activity in the plant, such as the expression of ROP DN forms, ROP RNAi constructs, T-DNA insertion lines or ROP inactivation via bacterial toxins could also account for that (chapter 1.4.1; Molendijk *et al.*, 2001; Jones *et al.*, 2002; Tao *et al.*, 2002; Hoefle *et al.*, 2011; Lin *et al.*, 2012; Singh *et al.*, 2013; Burkart *et al.*, 2015). *HvRACB* expression was reduced up to 92 % in the bulging area of the root of the *HvRACB* RNAi plants (chapter 1.1.4; Supp Figure 3). Hence, the high efficacy of the RNAi construct used in the examined *HvRACB* RNAi line may cause the severe failure of the formation of the root hairs. This is supported by another *HvRACB* RNAi mutant line which exhibited less

efficient silencing of *HvRACB.* These plants formed stunted root hairs which is a less pronounced failure of root hair formation (Hoefle *et al.*, 2011). Furthermore, the number of ROP proteins encoded in the genome (Christensen *et al.*, 2003), is lower in barley (6 ROPs) or tobacco (6 ROPs) than in Arabidopsis thaliana (11 ROPs). It would be interesting to know whether the lower number of ROP proteins correlates with a minor functional redundancy in the formation of root hairs. This would support stronger effects of single ROP protein knockdowns or knockouts. However, the ROP protein *Hv*RACD is most similar to *Hv*RACB in barley and *At*ROP6 in *Arabidopsis thaliana* (Schultheiss *et al.*, 2003). Expression data shows that it is partially co-silenced by the *HvRACB* RNAi construct (Hoefle *et al.*, 2011). Hence, an additional effect on the formation of root hairs by the reduction of *Hv*RACD transcripts on the formation of root hairs cannot be excluded.

In the examined *HvRACB* RNAi line, the root epidermis was root hairless. This phenotype was occasionally interrupted by occurrences of stunted root hairs (Figure 14). However, a potential inability of *HvRACB* RNAi plants to develop trichoblast (chapter 1.1.4) could be excluded. The majority of short epidermal cells of the *HvRACB* RNAi roots were hairless (Figure 15). However, they showed distinct characteristics of barley trichoblasts (chapter 1.1.4; Marzec *et al.*, 2013). They also occurred in the same frequency, when compared to the control. In context to the reduction of diffuse cell expansion in the leaf epidermis of *HvRACB* RNAi plants, an interesting detail (chapter 4.1.2) should be mentioned: The size of the cells of the root epidermis in the transition zone was unaltered, when compared to the control (Figure 15). This additionally excluded a general effect on the cell expansion of the *HvRACB* knockdown, before entering the elongation zone of the root.

Concerning these data, I support the idea, that *Hv*RACB participates in the initiation of root hairs as well as in further elongation. This function of *Hv*RACB would be similar to *At*ROP2 (Jones *et al.*, 2002) and was already proposed (Pathuri *et al.*, 2008; Hoefle *et al.*, 2011).

Furthermore, root hairs were observed which were mispositioned on the trichoblast, branched at the tip, or deformed and exhibiting enlargements at their bases or tips (Figure 14). In the literature, no studies were found that describe such phenotypes in ROP deficient mutants. Instead, the most similar phenotypes were found in the *At*RhoGDI1 (*At*SCN1) loss of function mutant *scn1* (Carol *et al.*, 2005) and the *At*RopGEF4 OE, *At*GEF10 OE mutants, respectively (Huang *et al.*, 2013). *At*RopGEF4, *At*RopGEF10, and *At*RhoGDI1 were suggested to participate in the amount and spatial restriction of ROS production. Regulation of ROS is essential for the correct positioning and outgrowth of root hairs (Foreman *et al.*, 2003; Carol *et al.*, 2005; Jones *et al.*, 2007; Huang *et al.*, 2013). Thus, *At*RhoGDI1 was proposed to regulate the activity of the ROS-producing NAD(P)H oxidase *At*RHD2 (*At*rbohC; Carol *et al.*, 2005).

The barley mutants root hairless 1.a (*rhl1.a)* and root hair primordia 1.b (*rhp1.b*) are disturbed in the formation of root hairs. The first one produces neither root hairs nor root hair bulgings. The latter only induced bulges without further elongation. Unfortunately, no information is available about the *rhl1.a* and *rhp1.b* mutations on the genomic level (Szarejko *et al.*, 2005). In a microarray approach the root transcriptome of the mutant lines was addressed. It became evident, that the expression of the peroxidase gene *HvPRX45* was reduced more than 120,000-fold in *rhl1.a*, compared to the WT. Additionally, the expression of a putative *At*RopGDI1 ortholog was considerably decreased (Kwasniewski *et al.*, 2010). In a later study, the ROS production and spatial accumulation of ROS in *rhl1.a* and *rhp1.b* plants were addressed. The authors reported a reduced quantity of peroxidase-dependent hydroxyl radicals (OH•) in the *rhl1.a* roots compared to the WT. Superoxide anion radicals ($O_2^{\bullet-}$), derived from NAD(P)H oxidases, were visualized via NBT. This resulted in blue staining of young root hairs. Staining occurred mainly at the base and the tip of the root hairs in the WT and the *rhp1.b* plants. An additional irregular staining of epidermal cells occurred in both mutant lines and the WT (Kwasniewski *et al.*, 2013).

Visualization and quantification of ROS was performed in *HvRACB* RNAi roots, according Kwasniewski and colleagues (Kwasniewski *et al.*, 2013). However, the examination was done in the transition zone and the adjacent area of bulging trichoblasts. This allowed the evaluation of differences in the accumulation of OH• and $O_2^{\bullet-}$ before and during the initiation of root hairs (chapter 1.1.4; chapter 3.3). In contrast to the *rhl1.a* mutant, no differences in qualitative and quantitative appearance of OH• and $O_2^{\bullet-}$ were observed before root hair initiation (Figure 16: Detection of hydroxyl radicals in the root via HPF.; Figure 17 and Figure 18). Subcellular localization of OH• and $O_2^{\bullet-}$ in the root epidermis and bulgings of the trichoblasts appeared similar to the pattern described before (Kwasniewski *et al.*, 2013). Interestingly, the misplaced and deformed root hairs and the outgrowths of the trichoblasts (chapter 3.2.1; Figure 16; Figure 18) also exhibited specific distributions of OH• and $O_2^{\bullet-}$. This was comparable to the initial root hairs in the azygous control. Based on these results, the presence of ROS at any outgrowth at the root epidermis was confirmed (Carol *et al.*, 2005). On the other hand, there was no indication for a spatially restricted accumulation of ROS prior to visible outgrowths at the epidermis. Because root hairs rarely grew out in *HvRACB* RNAi roots, it was difficult to interpret the lack of accumulation of ROS in the mutant. Furthermore, a direct involvement of *Hv*RACB in the regulation of ROS accumulation can be neither postulated nor excluded. In this regard, it is worth mentioning that neither *HvRACB* RNAi nor *HvRACB* OECA exhibited an influence on the ROS burst. The ROS burst occurs as an early defense response of the plant and is dependent on the activity of NAD(P)H oxidases (chapter 1.4.5; Scheler *et al.*, 2016).

However, *At*ROP2 accumulates early at the future bulging site (Molendijk *et al.*, 2001). Furthermore, it mediates the activation of *At*RHD2 in the root hairs of *Arabidopsis thaliana* (Foreman *et al.*, 2003; Jones *et al.*, 2007). Hence, *Hv*RACB may act upstream of ROS generating enzymes, in specific growth processes of the plant, such as polar tip growth. This would explain the absence of spatial restricted ROS at the growth apex since ROP-dependent polarization or activation of NAD(P)H oxidases had previously failed. Misguided or lacking polarization of ROPs due to *HvRACB* knockdown could then cause misplaced, deformed and stopped outgrowths of the root epidermis.

4.2 *Hv*RACB functions in cell polarization after *Bgh* attack

To examine a possible role of *Hv*RACB on cell polarization (Schultheiss *et al.*, 2005; Pathuri *et al.*, 2008; Hoefle *et al.*, 2011; this work), the attraction of the nucleus of the attacked B-cell to the attempted penetration site of *Bgh* was quantified (chapter 3.4). The measurements revealed that nuclei of *Bgh*-challenged *HvRACB* RNAi cells were further away from the attack site at an early point in time before penetration than in the azygous control. The distance lessened at later points in time before penetration.

After attack of the fungus, the plant cell polarizes towards the contact site of the plant and the pathogen. The polarization includes cytoplasmic translocation and rearrangement of the cytoskeleton and the endomembrane system. These processes are necessary for efficient transport of defense molecules, vesicles, and organelles. Therefore, they are essential for a successful defense of the plant (chapter 1.3.4; Schmelzer, 2002; Hückelhoven, 2007; Hématy *et al.*, 2009). The directed movement of the nucleus to the attempted penetration site of a fungal pathogen is known in plants for a long time (Pappelis *et al.*, 1974). However, the role of the migration in the interaction of the plant and the pathogen remains unknown (Griffis *et al.*, 2014).

Heath and colleagues (Heath *et al.*, 1997) examined migration patterns of the nucleus during incompatible and compatible interactions of resistant and susceptible cowpea cultivars with the obligate biotrophic rust fungus *Uromyces vignae*. In all cultivars, the plant nucleus migrated to the site of attempted pathogen penetration. In the case of unsuccessful attempts of penetration, it remained at the attack site at least during the formation of the papillae. During successful penetrations no effective papilla was formed in the susceptible or resistant cultivar. In these cases, the nuclei left the site before the fungus detectably entered the cell. In most incompatible

interactions, the nucleus did not return to the developing fungus and the infection was stopped via HR. However, in compatible interactions, the plant nucleus returned to the site when the infection hyphae of the fungus initiated tip growth. This led to a close association between hypha and nucleus which persisted for a longer period during tip growth of the hypha (Skalamera and Heath, 1998). Interestingly, treatment of the plants with the actin polymerization inhibitor cytochalasin E significantly reduced the number of close associations between the nucleus and the hypha. Additionally, the average length of the hypha in compatible interactions was reduced after treatment with cytochalasin E (Skalamera and Heath, 1998). The attraction of the nucleus towards the site of attempted penetration was also observed in other plant-fungus pathosystems like *Arabidopsis thaliana -Erysiphe cichoracearum* (Koh *et al.*, 2005) and barley- *Blumeria graminis* (Kita *et al.*, 1981; Opalski *et al.*, 2005).

Eight hours after inoculation and before penetration (Figure 19), the nucleus of B-cells of *HvRACB* RNAi plants is less attracted towards the contact site of barley and *Bgh* than in the control (Figure 20). Migration of the nucleus always occurs in concert with polarization of the cell (Schmelzer, 2002; Griffis *et al.*, 2014). Hence, it can be concluded that at this point in time, the attacked *HvRACB* RNAi cells exhibit a lower grade of polarization than control cells. This effect weakened at later points in time. Hence, a delayed polarization of the cell, instead of a generally reduced ability of polarization could be assumed. However, an overlap with a possible effect of nuclei leaving the contact site again, as described by Heath and colleagues (Heath *et al.*, 1997), cannot be excluded. It is possible that this effect impacts the NAI at later stages of the interaction of barley and *Bgh*. Interestingly, polarization of the plant cell and the attraction of the nucleus was shown to be more frequent and persistent in incompatible interactions than in compatible ones (Schmelzer, 2002). This seems contradictory to the reduced penetration efficiency of *Bgh* on *HvRACB* RNAi plants which correlates with the enhanced distance of the nucleus to the contact site. However, as observed in compatible interactions of cowpea and the cowpea rust fungus, the nucleus migrated closely to and associated with the tip growing hypha. Largely, this did not occur in resistant plants (Heath *et al.*, 1997; Skalamera and Heath, 1998). Furthermore, during the interaction of plant roots with symbiotic arbuscular mycorrhizal fungi (AMF), an oriented migration of the nucleus towards the site of attempted penetration can be observed (Genre *et al.*, 2005). In both cases, the function of the targeted migration of the nucleus for the establishment of the fungus remains unclear. An obstacle for current studies is the inability to exclusively inhibit nuclear motion without global disturbance of the cytoskeleton (Griffis *et al.*, 2014). Nevertheless, it seems possible that in the interaction of barley

and *Bgh*, the positioning of the nucleus is potentially necessary for a successful accommodation of the fungus.

An efficient knockdown of *HvRACB*, a reduced penetration efficiency and a further distance of the nucleus were evaluated in parallel in the same tissue (Figure 21 and Figure 22). Thus, the penetration efficiency and the migration of the nucleus might be dependent on *Hv*RACB. This would also involve polarization of the cell, as has been previously suggested (Schultheiss *et al.*, 2002; Opalski *et al.*, 2005; Hoefle *et al.*, 2011).

The participation of ROP proteins in the colonization of the root by symbiotic AMF seems likely. However, the knowledge about ROPs in this mutualistic interaction is scarce. This is probably due to the fact that the model organism *Arabidopsis thaliana* is an AMF non-host plant (Veiga *et al.*, 2013). Kiirika and colleagues (Kiirika *et al.*, 2012) examined transgenic *Medicago truncatula* plants. These mutant plants are characterized by a drastic, RNAi mediated knockdown of the ROP gene *Mt*ROP9. This resulted in pleiotropic effects, such as overall reduction of the plant size and different shapes of the leaf, when compared to the control. However, no alterations in the formation of root hairs were observed. Compared to the control, the suppression of *Mt*ROP9 stimulated the pathogenic colonization with the oomycete root pathogen *Aphanomyces euteiches*. Interestingly, it also promoted the mutualistic colonization with the AMF *Glomus intraradices* (Kiirika *et al.*, 2012). Both effects were detectable at early stages of the interaction. At later stages, this effect vanished and the control plants exhibited comparable colonization intensities.

In *HvRACB* RNAi roots no differences in AFM colonization at a late stage of the interaction could be observed, compared to the control (Supp Figure 4). Based on the available data obtained from the *Mt*ROP9 RNAi plants, I speculate, that a possible colonization effect caused by *HvRACB* RNAi would only be detectable at early points in time after inoculation. This could be due to a potentially delayed response of the plant cell to the fungus, as mentioned above. Alternatively, *Hv*RACB could also be functionless in the establishment of the symbiosis of arbuscular mycorrhiza. Redundant functionality of other ROP proteins in barley (chapter 1.4.1) could also explain the missing effect of *HvRACB* RNAi on the colonization of the root.

4.3 *HvRACB* RNAi dependent resistance is probably not caused by Induced Resistance

Induced resistance is known to affect the outcome of the interaction of plants and the attacking pathogen (Kogel and Langen, 2005). To evaluate whether *HvRACB* RNAi mediates induced

resistance, the expression of defense-related genes was examined via sqPCR. The examined pathogenesis-related (PR) genes and jasmonate induced proteins (JIPs) exhibited no considerable enhancements of their transcript abundancies. Compared to the control however, two checked barley leaf thionins and one oxalate oxidase-like protein (Supp Figure 7) showed an increase in transcript amounts.

Induced resistance describes, as a broad term, the prior activation of defense pathways in the plant. This leads to an enhanced resistance towards attacking pests and pathogens and includes the defense priming effect. The latter comprises the phenomenon of a defense system, that is alerted prior to the actual pathogen threat. This results in a faster and stronger expression of defense responses at lower stimuli level than in non-primed cells (Kogel and Langen, 2005; Conrath, 2011). Priming can be achieved via chemical pretreatments (e.g. phytohormones) and biological pretreatments with microorganisms (Schweitzer *et al.*, 1999; Beßer *et al.*, 2000; Kogel and Langen, 2005). Furthermore, constitutively primed mutant lines exist. The *enhanced disease resistance 1* (*edr1*) mutant of *Arabidopsis*, does not need biological or chemical pretreatments (van Hulten *et al.*, 2006). The *edr1* mutant plants exhibit a reduced susceptibility to different bacterial and fungal pathogens. When compared to the control, the *At*PR1 gene of *edr1* is expressed faster and stronger during pathogen attack rather than being expressed constitutively (Frye and Innes, 1998; Frye *et al.*, 2001). However, expression of PR-genes is not generally reliable as indicator for priming in crops. Furthermore, the group of plant defense-related genes, which is differentially expressed due to Induced Resistance, appears to be quite heterologous among the plant species (Molina *et al.*, 1999; Maleck *et al.*, 2000; Schaffrath *et al.*, 2000; Kogel and Langen, 2005). In *Arabidopsis*, *At*ROP6 DN mutants are less susceptible to the powdery mildew fungus *Golovinomyces orontii*. Furthermore, the mutant exhibits a constitutively enhanced expression of *At*PR1 and *At*PR5 (Poraty-Gavra *et al.*, 2013). However, it was shown that this SA-dependent expression of PR-genes in the *At*ROP6 DN mutants can be uncoupled from the enhanced resistance against *G. orontii* and the observed morphological and developmental phenotypes. Hence, in order to evaluate a possible Induced Resistance, mediated by *HvRACB* RNAi, a whole set of genes was examined via sqPCR. The evaluated genes are known to be differentially regulated under biotic or abiotic stress in barley. Among these are several PR genes (Vallélian-Bindschedler *et al.*, 1998), JIPs (Kogel *et al.*, 1995), thionins (Bohlmann *et al.*, 1988; Andresen *et al.*, 1992; Ma *et al.*, 2010) and oxalate-oxidase like proteins (Dumas *et al.*, 1995; Zhang *et al.*, 1995; Wei *et al.*, 1998).

Concerning the JIPs, no noteworthy alterations were found compared to the control. The PR-genes appeared to be expressed less strongly and were induced later after fungal attack, compared to the control (Supp Figure 7; Scheler *et al.*, 2016). These results coincide with other published data which

revealed no effect of *HvRACB* RNAi on the ROS burst and the activation of mitogen-activated protein kinases (MAPKs). Both processes are known as quick and early responses of plant defense (Scheler *et al.*, 2016). However, the thionins Thio_01576 and Thio_01580 exhibited a moderate enhanced and *Bgh*-independent expression in the *HvRACB* RNAi plants. The expression of both thionins was also shown to be enhanced after treatment with physicon. This anthraquinone analogue is a commercially offered bioactive agent against *Bgh*. Physicon is assumed to be a chemical trigger for Induced Resistance (Ma *et al.*, 2010). The impact of these thionins in *HvRACB* RNAi plants remains unclear. Suppression of *HvRACB* resulted in a reduced penetration efficiency (Hoefle *et al.*, 2011; chapter 3.4.2). However, physicon treatment resulted in an almost complete inability of conidia germination (Yang *et al.*, 2008; Ma *et al.*, 2010). There was no indication that *Bgh* conidia exhibited a reduced ability to germinate on *HvRACB* RNAi leaves, compared to the azygous control. Nevertheless, the antifungal activity of the leaf thionins of barley was reported earlier (Bohlmann *et al.*, 1988; Andresen *et al.*, 1992; Nawrot *et al.*, 2014). Therefore, an impact on the reduced susceptibility of the *HvRACB* RNAi plants to *Bgh* cannot be excluded.

Similar to the thionins, the oxalate oxidase-like protein OxOxl_03155 showed a moderately enhanced constitutive expression in the *HvRACB* RNAi plants, when compared to the control (Supp Figure 7). Oxalate oxidases, also called germin oxalate oxidases or simply germins, were shown to be involved in defense responses of cereals against the invasion of fungal pathogens. Their antifungal activity is presumably carried out via their catalyzed reaction of H_2O_2 production which was postulated to promote papilla formation (Dumas *et al.*, 1995; Hurkman and Tanaka, 1996; Zhou *et al.*, 1998; Lane, 2002). sqPCR data of OxOxl_03155 was also available for *HvRACB* OECA plants. Interestingly, the gene exhibits a moderately enhanced constitutive expression, compared to the control (data not shown). This is similar to the *HvRACB* RNAi plants. However, in contrast to the *HvRACB* RNAi plants, *Bgh* exhibits enhanced penetration success on *HvRACB* OECA plants, when compared to the control. (Pathuri *et al.*, 2008; Hoefle *et al.*, 2011). Thus, it is questionable whether OxOxl_03155 significantly influences the penetration efficiency of *Bgh* on the *HvRACB* RNAi and *HvRACB* OECA mutants. Furthermore, since germins do not occur in dicotyledons (Lane, 2002), they could not explain the altered susceptibility in Arabidopsis *At*ROP6 DN mutants (Poraty-Gavra *et al.*, 2013). Therefore, it remains unclear to what extent OxOxl_03155 contributes to the enhanced resistance of *HvRACB* RNAi plants against *Bgh*.

Most of the genes related to the plant defense were not differentially or less strongly expressed in the *HvRACB* RNAi plants, when compared to the control (Supp Figure 7; Supp Figure 6; Scheler *et al.*, 2016). The exceptions, two thionins and a germin, showed a moderate enhanced expression in the Hv*RACB* RNAi plants. However, a significant impact on the penetration efficiency of *Bgh* due

to the thionins and the germin, appears questionable. Hence, I postulate that Induced Resistance is unlikely the major reason of *Bgh* resistance in Hv*RACB* RNAi plants. This is further supported by similarities in the ROS burst and MAPKs signaling of *HvRACB* RNAi and *HvRACB* OECA plants, and the control plants (Scheler *et al.*, 2016).

4.4 *Hv*RACB affects barley primary cell wall characteristics

4.4.1 *Hv*RACB influences the cell wall composition and its lytic resistance

Unpublished microarray data suggested a differential expression of cell wall modifying genes in *HvRACB* RNAi and *HvRACB* OECA plants (Ralph Hückelhoven, Vera Schnepf, TU München, personal communication). Taken together with the described phenotypes in growth and cell expansion (Schultheiss *et al.*, 2005; Pathuri *et al.*, 2008; Hoefle *et al.*, 2011), it raised the question of a potential impact of *Hv*RACB on the composition of the cell wall. In this thesis, the differential expression of selected genes which are predicted to function in pathways of cell wall modification was confirmed (chapter 3.5.1). Furthermore, it was shown that the primary cell walls of *HvRACB* RNAi plants possess an increased lytic resistance against fungal cell wall degrading enzymes (chapter 3.5.2) and an altered monosugar composition (chapter 3.5.3).

Unfortunately, information about transcriptomic patterns, which are functionally evaluated in the interaction of plants and pathogens, are scarce in *Triticeae* plants (Bischof *et al.*, 2010). The type II cell wall class of grasses is a complex topic and only a small number of research groups have focused on it. Hence, it should be considered that the cell wall pathways and the involved cell wall modifying enzymes in grasses are rarely understood (chapter 1.1.5). This especially concerns the functionality of the enzymes in the cell wall and their impact on the interactions of plants and pathogens (Vogel, 2008; Santiago *et al.*, 2013; Franková and Fry, 2013). However, Douchkov and colleagues (Douchkov *et al.*, 2016) have recently reported about the cellulose synthase-like D2 (*Hv*CslD2) in the interaction of barley and powdery mildew. They generated *Hv*CslD2 RNAi plants, which showed a suppressed expression of the cellulose synthase but no growth defects. Compared to the control, the cell walls had lower contents of cellulose as well as a lower lytic resistance against fungal cell wall degrading enzymes was observed. When attacked by adapted or non-adapted isolates of the powdery mildew fungus *Blumeria graminis*, the epidermal cell wall and the papillae were more

often successfully penetrated. These results suggest an important impact of the composition of the cell wall on the outcome of barley-*Bgh* interaction.

Furthermore, unpublished microarray data in barley revealed a significantly different cell wall pathway regulation between *Bgh* and untreated WT barley plants. Furthermore, *HvRACB* RNAi and *HvRACB* OECA significantly influenced the expression of cell wall-related genes in the transgenic plants. It was shown that in Hv*RACB* OECA plants many genes involved in the biosynthesis, expansion, and softening of the cell wall generally were not or only slightly downregulated, when compared to the WT. Consequently, their expression levels were higher under the attack of *Bgh* than in the control. Eventually, the transcriptomic studies suggested a possible impact of cell wall modifiers on the outcome of the interaction of barley and *Bgh.* Differentially expressed genes related to the biosynthesis or softening of the cell wall could support the super-susceptibility mediated by *HvRACB* OECA. On the other hand, genes related to the rigidity of the cell wall could support the resistance mediated by *HvRACB* RNAi. In *Arabidopsis thaliana*, Vogel and colleagues (Vogel and Somerville, 2000; Vogel *et al.*, 2002, 2004) isolated and characterized several powdery mildew resistant (PMR) mutant lines. The reduced susceptibility of these lines is most likely not caused by constitutive activation of the salicylic acid or ethylene- and jasmonic acid-dependent defense pathways. The *pmr5* and *pmr6* knockout plants exhibited dwarfed growth, reduced cell size, and altered compositions of their primary cell walls. *AtPMR5* encodes for a protein of unknown function (Vogel *et al.*, 2004). *AtPMR6* encodes for a pectate lyase (Vogel *et al.*, 2002), an enzyme group known to be involved in degradation of pectin. The authors suggested different explanations for the powdery mildew resistance via constitutively altered cell wall compositions (Vogel and Somerville, 2000; Vogel *et al.*, 2002, 2004). They proposed a reduced hospitality due to a compositionally changed extrahaustorial matrix (chapter 1.2.2), an increased number of DAMPs derived from the cell wall that trigger PTI (chapter 1.3.3), and an enhanced lytic resistance to digestion attempts of the fungus. The latter may be particularly important. Biotrophic fungi such as *Bgh* parasitize the host cells without causing host cell death. This requires a spatial restricted and precise breaching of the plant cell wall (Zhang *et al.*, 2005; chapter 1.2.2). For the penetration of the cell wall, biotrophic fungi use mechanical pressure of the penetration peg (Pryce-Jones *et al.*, 1999; Wilson and Talbot, 2009) and the synergistic action of a large number of cell wall degrading enzymes (CWDEs). These enzymes are secreted in small amounts to induce a local softening and loosening of the cell wall (Pryce-Jones *et al.*, 1999; Zhao *et al.*, 2013; Bellincampi *et al.*, 2014). The importance of this process can be seen in mutant plants that express transgene CWDE inhibitors. This results in a reduced susceptibility to various fungal pathogens (Lionetti *et al.*, 2007, 2014; Volpi *et al.*, 2011; Ferrari *et al.*, 2012; Moscetti *et al.*, 2013; Bellincampi *et al.*, 2014).

The altered expression of genes related to the cell wall was confirmed via sqPCR in the stable *HvRACB* RNAi line, when compared to the control (Figure 23). This supported a possible influence of *Hv*RACB on properties of the cell wall and consequently on the penetration efficiency of *Bgh*. Interestingly, in most cases the transcript abundancy of the cell wall modifiers was constitutively enhanced independently of *Bgh*. This might indicate a constitutively altered cell wall composition. However, constitutively altered properties of the cell wall could barely explain the reduced penetration efficiency of *Bgh* in *HvRACB* TIGS assays (Schultheiss *et al.*, 2002, 2003). Furthermore, several genes examined via sqPCR belong to enzyme families which are known to be involved in processes related to the softening and degradation of the cell wall (Walton, 1994; Aro *et al.*, 2005; Cosgrove, 2005). Among these are expansins (EXPB3_02877), pectate lyases (PL_11004) and polygalacturonases (PG_21718). This seems to contradict the assumed enhanced rigidity of the cell wall of *HvRACB* RNAi plants. However, even if the expression of a cell wall modifier gene is enhanced, it does not self-evidently result in an increased activity of the enzyme in the cell wall. Possible reasons for that could be unavailable ('masked') substrates, lacking colocalization of enzyme and substrate, non-optimal pH, absence of cofactors and activators or presence of inhibitors (Marcus *et al.*, 2010; Franková and Fry, 2013). Enhanced rigidity of the *HvRACB* RNAi cell wall is further supported by the protoplast release assay (Figure 24). It revealed an increased lytic resistance to a fungal cell wall degrading enzyme mix, when compared to the control. This could indicate that *HvRACB* RNAi results in a more resilient cell wall of barley towards wall loosening enzymes and therefore towards penetration attempts of *Bgh*. Similar results, concerning the connection of lytic resistance and penetration efficiency, were obtained in the *Hv*CslD2 RNAi plants, as mentioned above (Douchkov *et al.*, 2016).

Any kind of expansion of the plant cell depends on the careful control and selective loosening of the cell wall (Cosgrove, 2005; Marga *et al.*, 2005). Thus, I further speculate that the less digestible cell wall of *HvRACB* RNAi plants is at least partially responsible for the reduced cell size and impaired formation of root hairs (chapter 3.1.3 and chapter 3.2.1). Additionally, extensibility of the cell wall is determined by the composition of the cell wall as well as the structure and crosslinking of its components (Cosgrove, 2005). This coincided with the changes in the relative amount of the monosugars xylose (plus 2 %), galactose (minus 11 %) and fucose (minus 28 %) in the *HvRACB* RNAi plants, compared to the control (Figure 25). Furthermore, this data supports the suggested alterations in the composition of the cell wall of *HvRACB* RNAi plants. Interestingly, the hemicellulose xyloglucan was mentioned as an exclusive component of the grass type II cell walls, containing fucosyl residues (Vogel, 2008). When compared to the control, *HvRACB* RNAi plants possess a higher total amount of monosugars per gram fresh weight (Supp Figure 8). This is likely

explained by the enhanced number of cells per gram fresh weight, due to the reduced cell size, as was described above (chapter 3.1.3 and chapter 4.1.2).

4.4.2 The α-fucosyltransferase FUT_362089 may not impact the outcome of the barley-*Bgh* interaction

Hv*RACB* RNAi plants possess less fucose in their primary cell wall. Therefore, the expression of putative xyloglucan-active α-fucosidases and α-fucosyltransferases was examined. It was evaluated whether an association between the observed phenotypes and the enhanced resistance against *Bgh* can be concluded.

The tested genes were expressed in a *Bgh*- but not *Hv*RACB dependent manner in the leaf. Only the putative α-fucosyltransferase FUT_362089 matched the set criteria and was chosen as a candidate gene. However, transient silencing of FUT_362089 did not significantly alter the susceptibility to *Bgh*. The hemicellulose xyloglucan consists of a β (1,4) linked glucose backbone. It can be substituted with xylose or side chains of two (xylose followed by galactose) or three (xylose, followed by galactose and fucose) monosugar residues. (Vogel, 2008; Pauly *et al.*, 2013). Besides pectins and cellulose, xyloglucan represents one of the primary components in the type I cell walls of dicotyledons such as *Arabidopsis thaliana*. In dicotyledons it is highly fucosylated at the end of its side chains. Therefore, it is also called 'fucogalactoxyloglucan' (Vogel, 2008; Pauly *et al.*, 2013). The transfer of the fucose to the xyloglucan side chains is performed by the activity of α-fucosyltransferases (FUTs). On the other hand, α-fucosidases (FUCs) release the fucosyl residue (Del Bem and Vincentz, 2010). In *Arabidopsis*, the *mur2* mutant was characterized. It was shown to be mutated in the gene *At*FUT1, encoding for an α-fucosyltransferase. This mutation resulted in an almost complete loss of fucosylation specific to xyloglucan (Reiter *et al.*, 1997; Vanzin *et al.*, 2002). The amount of fucogalactoxyloglucan decreased in the *mur2* mutant more than 98 %, compared to the WT. Thus, it was suggested that *At*FUT1 is fully responsible for transferring the fucose to the xyloglucan side chains (Vanzin *et al.*, 2002). Interestingly, the *mur2* mutant exhibited no visible phenotype except for a minor defect in trichome papilla formation (Vanzin *et al.*, 2002). Additionally, the tensile strength of the cell wall was unaffected (Vanzin *et al.*, 2002). Therefore, it was concluded that fucosylation of xyloglucan is not necessary for proper growth and development under laboratory conditions (Vanzin *et al.*, 2002; Perrin *et al.*, 2003). To date, the role of this cell wall modification remains unclear. In type II cell walls of grasses, xyloglucan appears only in minor amounts. Furthermore, although fucosylation of xyloglucan was considered to be possible (Vogel,

2008), for a long time no indications of fucosylated side chains were evident (Carpita, 1996; Hsieh and Harris, 2009; Brennan and Harris, 2011). On the other hand, it was shown that suspension cell cultures of the *Poaceae Oryza sativa* (rice) and *Festuca arundinacea* (tall fescue) incorporated fucose in low amounts into their xyloglucan. This required the corresponding enzymatic activity *in vivo* (Kato and Matsuda, 1985; McDougall and Fry, 1994). Recently, Liu and colleagues (Liu *et al.*, 2015) were able to detect fucosylated xyloglucan in young root tissue of rice. It predominantly accumulated in the outer layer of epidermal cells and in the root hairs. Furthermore, the transgene α-fucosyltransferase *Os*MUR2 was verified to be active *in vivo* in *Arabidopsis*. This suggested *Os*MUR2 as a true functional equivalent of *At*MUR2 (*At*FUT1). However, the transcript abundance of *Os*MUR2 appeared to be too low for reliable quantification in the rice root (Liu *et al.*, 2015). Therefore, the authors assumed that the expression of *Os*MUR2 is restricted to specific cells such as the epidermal cell layer of young root tissue (Liu *et al.*, 2015).

According to the amino acid sequence and the occurrence of published motifs necessary for α-fucosyltransferase activity (Sarria *et al.*, 2001), FUT_362089 appears to be a FUT on the bioinformatics level (chapter 3.7.1). However, in Arabidopsis, besides *At*FUT1 (*At*MUR2), nine additional genes, were assumed to encode for putative *At*FUTs (*At*FUT2 to *At*FUT10). This was based on their high amino acid identity to *At*FUT1 which ranged from 47 % to 62 %. Additionally, the hypothetical motifs assumed to be necessary for α-fucosyltransferase activity, were conserved (Sarria *et al.*, 2001). However, none of them were be proven to exhibit a xyloglucan fucosylation activity in vivo (Sarria *et al.*, 2001). Hence, even though all sequence requirements are fulfilled, FUT_362089 cannot be confirmed to exhibit α-fucosyltransferase activity on the substrate xyloglucan *in vivo* without further experiments.

The expression of FUT_362089 was generally low, when compared to the housekeeping gene *Hv*UBC2. It was the lowest in the leaf blade and considerably higher in the meristematic leaf region and the root bulging area (chapter 3.6.2; Supp Figure 10; Supp Figure 11). This coincided with the quite low expression level of *Os*MUR2 (Liu *et al.*, 2015). Furthermore, *At*FUT1 was expressed in low levels in *Arabidopsis*. Expression was the highest in growing and lower in mature tissues (Perrin *et al.*, 2003). However, higher amounts of fucosylated xyloglucan were not necessarily associated with higher *At*FUT1 expression and vice versa. Therefore, it was suggested that already a low basic enzymatic activity would be sufficient for complete xyloglucan fucosylation (Perrin *et al.*, 2003). Additionally, Arabidopsis plants ectopically overexpressing *At*FUT1 did not possess more fucosylated xyloglucan (Perrin *et al.*, 2003). Furthermore, Perrin and colleagues (Perrin *et al.*, 2003) suggested a positive correlation between the expression of *At*FUT1 and the current intensity of cell wall deposition. Hence, it seems possible that the increased transcript amount of FUT_362089 at

12 hpi correlates with the formation of the papilla (chapter 1.3.4). According to this, the relatively high expression in the meristematic region and the bulging zone of the root may be correlated to cell wall depositions during diffuse cell growth, cell divisions, and polar growth of the root hairs. This would also coincide with the accumulation of labeled fucose to the initiations of root hairs in the bulging zone of the root (Supp Figure 9). Furthermore, Liu and colleagues (Liu *et al.*, 2015) observed that the fucosylated xyloglucan mainly occurs in the epidermis of young rice roots. Therefore, they suggested a possible role of fucosylated xyloglucan at the interface of root and the environment. Interestingly, some oligosaccharides derived from the plant cell wall are suggested to play signaling roles in the plant during the expansion of cells (Franková and Fry, 2013). In pea, nanomolar concentrations of a fucosylated oligosaccharide derived from xyloglucan was shown to antagonize the cell expansion induced by auxin (McDougall and Fry, 1989*a*). Further experiments confirmed that the fucose residue is essential for the antagonistic effect on the cell expansion (McDougall and Fry, 1989*b*, 1990). Based on this data, it seems possible that fucosylated xyloglucan oligosaccharides could also be utilized in barley to influence deposition and growth processes of the cell wall.

The role of FUT_362089 and putative fucosylation of xyloglucan during the interaction of barley and *Bgh* remains unclear. The expression of FUT_362089 is increased after fungal attack in control and *HvRACB* RNAi plants (Figure 27). However, suppression of FUT_362089 via RNAi revealed no significant alteration in the susceptibility to *Bgh* (Figure 29). This coincides with recent findings in *Arabidopsis*. Additionally, in *mur2* mutant plants, no differences in the susceptibility to adapted or non-adapted strains of the bacterial pathogen *Pseudomonas syringae* could be observed (Djonović *et al.*, 2013).

4.5 Proposed *Bgh*-*Hv*RACB co-option model via hypothesized actin-dependent and actin-independent processes

This work builds upon previous research in describing several phenotypes in growth and development of *HvRACB* OECA and *HvRACB* RNAi plants. Among these are altered susceptibility to *Bgh*, altered cell expansion, impaired initiation of root hairs, disturbed formation of subsidiary cells, polar tip growth, and nucleus migration. All processes mentioned are associated with cell polarization and altered cytoskeleton dynamics (this work; Schultheiss *et al.*, 2002, 2005; Opalski

et al., 2005; Pathuri *et al.*, 2008; Hoefle *et al.*, 2011). This is strongly supported by the scientific consensus that ROP proteins in animals and plants are essential regulators for cell polarization. Amongst other mechanisms, this is orchestrated via cytoskeleton dynamics. It was shown that the regulation of the cytoskeleton represents a conserved universal target for the signaling of small monomeric G-Proteins. It was shown that the regulation of the cytoskeleton represents a conserved universal target for the signaling of small monomeric G-Proteins (Brembu *et al.*, 2006; Craddock *et al.*, 2012; Burkart *et al.*, 2015). Additionally, manifold studies evidenced fundamental cytoskeleton dynamics in the processes listed above (Bo, 2011; chapter 1.4).

Opalski and colleagues (Opalski *et al.*, 2005) reported that super-susceptible *HvRACB* OECA plants exhibited a reduced actin filament (AF) polarization towards the contact site of barley and *Bgh*. This suggested a direct role of *Hv*RACB in actin dynamics. In *Bgh*-resistant *mlo*-barley epidermal cells, the expression of *HvRACB* OECA also partially inhibited AF polarization. However, it did not affect the resistance against *Bgh* (Schultheiss *et al.*, 2003; Opalski *et al.*, 2005). This showed that AF depolarization is not sufficient to break *mlo5*-mediated resistance. Furthermore, the influence of *HvRACB* OECA on AF polarization can be uncoupled from the susceptibility-inducing effect (Opalski *et al.*, 2005). Even the infiltration of cytochalasin A, an inhibitor of actin polymerization, resulted in a rather weak effect on *mlo5*-mediated resistance against *Bgh.* Interestingly, site-selection as well as the actual bulging of the trichoblasts also occurred in roots treated with the AF-disrupting drugs oryzalin or cytochalasin D. The bulging includes loosening of the cell wall and prior activation and accumulation of expansins (chapter 1.1.4). Therefore, these processes appear to be independent of the actin cytoskeleton. On the other hand, AF-disrupting drugs inevitably led to the termination of the polar tip growth at later stages of the formation of the root hair. (Miller *et al.*, 1999; Baluska *et al.*, 2000). Furthermore, the addition of cytochalasin D or latrunculin B did not inhibit the bulge preceding, the early polarization of *At*ROP1 to the future outgrowth site (Molendijk *et al.*, 2001). This corresponds to the observed impaired root hair formation in *HvRACB* RNAi plants (chapter 3.2). The roots mostly possess trichoblasts which lack any bulging or growing but generated stunted root hairs due to the termination of the tip growth. Additionally, Humphries and colleagues (Humphries *et al.*, 2011) suggested actin-dependent and actin-independent mechanisms of the *Zm*ROP proteins for SMC polarization during the stomata formation in maize.

Hence, I hypothesize that *Hv*RACB also functions via an actin-independent and an actin-dependent mechanism during the development of barley. Both mechanisms promote polar growth processes of the plant cell.

The actin-independent mechanism would not rely on a complex reorganization of the cytoskeleton and polar targeting of vesicles and organelles. It uses fast protein-protein interactions and rapid

diffusion of molecules which are already located at the cell wall. Therefore, it is established faster than the actin-dependent mechanism. The function of *Hv*RACB would be comparable to *At*ROP2 during initiation of the root hair in *Arabidopsis* (chapter 1.4.2; Molendijk *et al.*, 2001; Grierson *et al.*, 2014). Hence, *Hv*RACB might be a mediator of the site selection and the bulging via spatially restricted activation of enzymes. It may initiate a pH-change at the future site of the outgrowth and therefore induce processes of cell wall loosening (Bibikova *et al.*, 1998; Baluska *et al.*, 2000). The locally weakened cell wall is pressed outward due to the turgor pressure of the plant (Čiamporová *et al.*, 2003). However, the actin-independent mechanism could not promote further polar tip growth of the root hair which depends on the biosynthesis and deposition of new cell wall material (Ketelaar *et al.*, 2008).

The actin-dependent mechanism of *Hv*RACB could now function to promote the outgrowth of the initially established polar bulging. It relies on the nucleation and polymerization of actin for AF polarization and polar targeting of vesicles and organelles towards the site of growth (Ketelaar *et al.*, 2008; Pei *et al.*, 2012). Therefore, the actin-dependent mechanism would be established slower than the actin-independent one. However, the actin-dependent mechanism is needed for complex biosynthesis and remodeling processes of the cell wall. This could include polar exocytosis during polar tip growth of the root hair, formation of the cell plate during asymmetric division of the SMC, diffuse cell expansion of the leaf cells, and nucleus migration.

Next to its physiological function during the plant development of barley, *Hv*RACB was shown to function as a susceptibility factor for the obligate biotrophic fungus *Bgh*. In the interaction with *Bgh*, *Hv*RACB is necessary rather for the accommodation of the pathogen than for the control of plant defense responses (chapter 1.3.5; chapter 1.5; Schultheiss *et al.*, 2003, 2005; Opalski *et al.*, 2005; Pathuri *et al.*, 2008; Hoefle *et al.*, 2011). The haustorial accommodation of *Bgh* is based on the rapid synthesis of the extrahaustorial membrane and the extrahaustorial matrix by the plant (chapter 1.2.2). Hence, Schultheiss and colleagues (Schultheiss *et al.*, 2003) compared the accommodation with an inverted tip growth. Furthermore, it was suggested that *Bgh* could hijack barley ROP protein signaling. Thus, the fungus could force the plant to follow a tip growth-mimicking program (Schultheiss *et al.*, 2003, 2008). This strongly resembles the principle of co-option, which is, in the natural sciences, defined as the capacity of intracellular parasites to use host-cell proteins to complete their vital cycle (König *et al.*, 2010). However, literature that report about such co-options as a strategy of plant pathogens remain restricted (Frey and Robatzek, 2009; Lozano-Duran and Bejarano, 2011; Hoefle *et al.*, 2011). Interestingly, *Bgh* which penetrated *HvRACB* RNAi plants successfully showed a reduction of haustoria size (Hoefle *et al.*, 2011). This indicated that *Hv*RACB influenced pre-penetrational as well as post-penetrational accommodation of the fungus.

Hence, it appears possible that *Bgh* co-opts both the actin-independent and the actin-dependent functional mechanisms of *Hv*RACB (Figure 30). The co-option of the actin-independent functional mechanisms of *Hv*RACB could lead to the initiation of polar growth processes of the plant cell. These processes result in spatially restricted loosening of the cell wall under the appressorium. A weakened cell boundary would consequently enhance the penetration efficiency of *Bgh*. On the other hand, co-opting the actin-dependent functional mechanisms could be supportive of proper post-penetrational haustorial growth and development. Hijacked *Hv*RACB would promote AF polarization and polar targeting of vesicles and organelles. These processes are necessary for the persistent formation of the extrahaustorial membrane and the extrahaustorial matrix in a manner of polar tip growth.

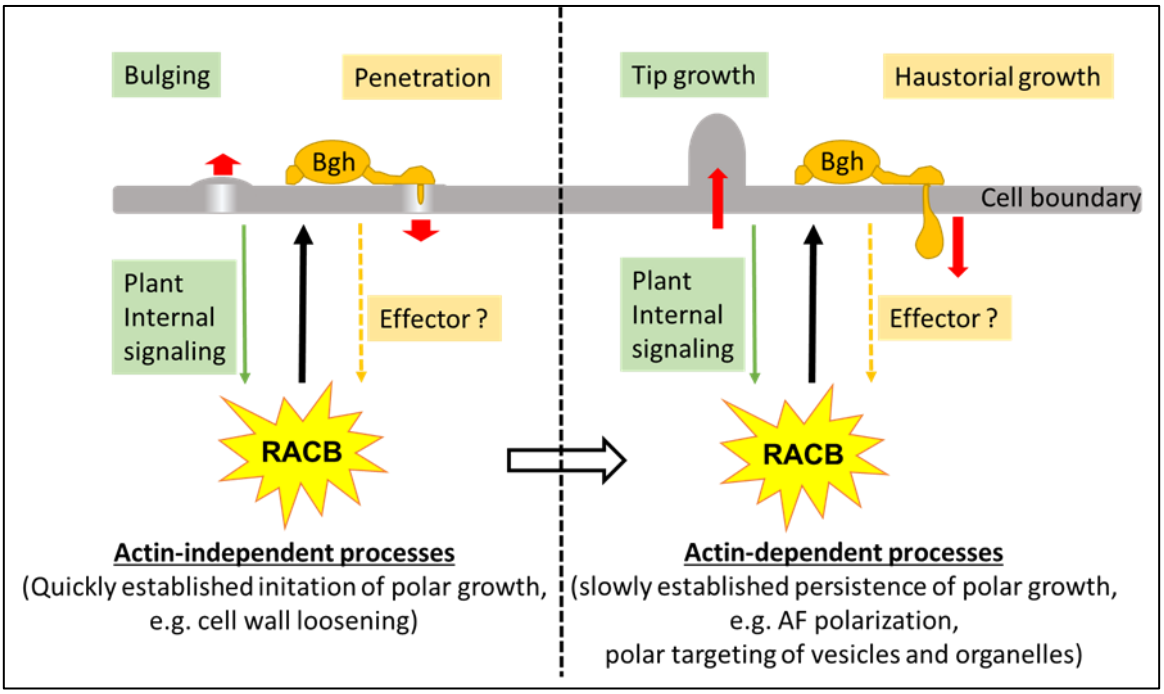

Figure 30: Proposed model of *Bgh*-*Hv*RACB co-option using the formation of root hairs as example.
***Hv*RACB-regulated actin-independent processes are established quickly. They initiate polar growth of the root hair via local loosening of the cell wall. This consequently results in bulging of the trichoblast. *Hv*RACB-regulated actin-dependent processes are established slower. They are necessary for persistent polar tip growth. *Bgh* activates *Hv*RACB via an unknown mechanism in order to initiate cell wall loosening under the appressorium to facilitate cell wall penetration. Post-penetrational, actin-dependent processes are co-opted by *Bgh* to support the haustorial establishment and growth. AF: actin filament**

This co-option model would also explain the paradox that *HvRACB* RNAi plants are less susceptible to *Bgh* even though they are impaired in cell polarization (chapter 3.4) which is an essential part of the plant defense response (chapter 1.3.4). However, the *HvRACB* RNAi plants might pay for the

enhanced resistance against *Bgh* with several pleiotropic effects in plant development, such as root hairlessness, reduced cell expansion, and impaired stomata formation.

References

Agrawal GK, Iwahashi H, Rakwal R. 2003. Small GTPase 'Rop': molecular switch for plant defense responses. FEBS Letters **546**, 173–180.

Ahmed AA, Pedersen C, Schultz-Larsen T, Kwaaitaal M, Jørgensen HJL, Thordal-Christensen H. 2015. The Barley Powdery Mildew Candidate Secreted Effector Protein CSEP0105 Inhibits the Chaperone Activity of a Small Heat Shock Protein. Plant Physiology **168**, 321–33.

Ahuja I, Kissen R, Bones AM. 2012. Phytoalexins in defense against pathogens. Trends in Plant Science **17**, 73–90.

Akamatsu A, Wong HL, Fujiwara M, *et al.* 2013. An OsCEBiP/OsCERK1-OsRacGEF1-OsRac1 Module Is an Essential Early Component of Chitin-Induced Rice Immunity. Cell Host & Microbe **13**, 465–476.

Allard RW. 1999. History of plant population genetics. Annual Review of Genetics **33**, 1–27.

Amselem J, Vigouroux M, Oberhaensli S, Brown JKM, Bindschedler L V, Skamnioti P, Wicker T, Spanu PD, Quesneville H, Sacristán S. 2015. Evolution of the EKA family of powdery mildew avirulence-effector genes from the ORF 1 of a LINE retrotransposon. BMC Genomics **16**, 917.

Anderson PM, Oelke EA, Simmons SR. 2013. Growth and development guide for spring barley. University of Minnesota.

Anderson CT, Wallace IS, Somerville CR. 2012. Metabolic click-labeling with a fucose analog reveals pectin delivery, architecture, and dynamics in Arabidopsis cell walls. Proceedings of the National Academy of Sciences **109**, 1329–34.

Andresen I, Becker W, Burges J. 1992. The identification of leaf thionin as one of the main jasmonate-induced proteins of barley (Hordeum vulgare). Plant Molecular Biology **19**, 193–204.

Ariyanayagam D V, Stebbins GL. 1962. Developmental studies of cell differentiation in the epidermis of monocotyledons. Developmental Biology **4**, 117–133.

Aro N, Pakula T, Penttilä M. 2005. Transcriptional regulation of plant cell wall degradation by filamentous fungi. FEMS Microbiology Reviews **29**, 719–739.

Assaad FF, Qiu J-L, Youngs H, *et al.* 2004. The PEN1 Syntaxin Defines a Novel Cellular Compartment upon Fungal Attack and Is Required for the Timely Assembly of Papillae. Molecular Biology of the Cell **15**, 5118–5129.

Atienza SG, Jafary H, Niks RE. 2004. Accumulation of genes for susceptibility to rust fungi for which barley is nearly a nonhost results in two barley lines with extreme multiple susceptibility.

Planta **220**, 71–79.

Baker A, Ceasar SA, Palmer AJ, Paterson JB, Qi W, Muench SP, Baldwin SA. 2015. Replace, reuse, recycle: improving the sustainable use of phosphorus by plants. Journal of Experimental Botany.

Baluška F, Mancuso S. 2013. Root apex transition zone as oscillatory zone. Frontiers in Plant Science **4**, 354.

Baluska F, Salaj J, Mathur J, Braun M, Jasper F, Samaj J, Chua NH, Barlow PW, Volkmann D. 2000. Root hair formation: F-actin-dependent tip growth is initiated by local assembly of profilin-supported F-actin meshworks accumulated within expansin-enriched bulges. Developmental Biology **227**, 618–32.

Bardin M, Ajouz S, Comby M, Lopez-Ferber M, Graillot B, Siegwart M, Nicot PC. 2015. Is the efficacy of biological control against plant diseases likely to be more durable than that of chemical pesticides? Frontiers in Plant Science **6**, 1–14.

Bellincampi D, Cervone F, Lionetti V. 2014. Plant cell wall dynamics and wall-related susceptibility in plant-pathogen interactions. Frontiers in Plant Science **5**, 228.

Del Bem LE V, Vincentz MGA. 2010. Evolution of xyloglucan-related genes in green plants. BMC Evolutionary Biology **10**, 341.

Bennett MD, Leitch IJ. 1995. Nuclear DNA amounts in Angiosperms. Annals of Botany, 113–176.

Berken A. 2006. ROPs in the spotlight of plant signal transduction. Cellular and Molecular Life Sciences **63**, 2446–59.

Berken A, Thomas C, Wittinghofer A. 2005. A new family of RhoGEFs activates the Rop molecular switch in plants. Nature **436**, 1176–80.

Berken A, Wittinghofer A. 2008. Structure and function of Rho-type molecular switches in plants. Plant Physiology and Biochemistry **46**, 380–93.

Beßer K, Jarosch B, Langen G, Kogel K-H. 2000. Expression analysis of genes induced in barley after chemical activation reveals distinct disease resistance pathways. Molecular Plant Pathology **1**, 277–286.

Bibikova T, Gilroy S. 2003. Root Hair Development. Journal of Plant Growth Regulation **21**, 383–415.

Bibikova TN, Jacob T, Dahse I, Gilroy S. 1998. Localized changes in apoplastic and cytoplasmic pH are associated with root hair development in Arabidopsis thaliana. Development **125**, 2925–34.

Bischof M, Eichmann R, Hückelhoven R. 2010. Pathogenesis-associated transcriptional patterns in Triticeae. Journal of Plant Physiology **168**, 9–19.

Bo L. 2011. *The Plant Cytoskeleton* (L Bo, Ed.). New York: Springer-Verlag.

Boerjan W, Ralph J, Baucher M. 2003. Lignin biosynthesis. Annual Review of Plant Biology **54**, 519–46.

Böhlenius H, Mørch SM, Godfrey D, Nielsen ME, Thordal-Christensen H. 2010. The multivesicular body-localized GTPase ARFA1b/1c is important for callose deposition and ROR2 syntaxin-dependent preinvasive basal defense in barley. The Plant Cell **22**, 3831–3844.

Bohlmann H, Clausen S, Behnke S, Giese H, Hiller C, Reimann-Philipp U, Schrader G, Barkholt V, Apel K. 1988. Leaf-specific thionins of barley-a novel class of cell wall proteins toxic to plant-pathogenic fungi and possibly involved in the defence mechanism of plants. The EMBO Journal **7**, 1559–65.

Brembu T, Winge P, Bones AM, Yang Z. 2006. A RHOse by any other name: a comparative analysis of animal and plant Rho GTPases. Cell Research **16**, 435–445.

Brennan M, Harris PJ. 2011. Distribution of fucosylated xyloglucans among the walls of different cell types in monocotyledons determined by immunofluorescence microscopy. Molecular Plant **4**, 144–56.

Brutus A, Sicilia F, Macone A, Cervone F, De Lorenzo G. 2010. A domain swap approach reveals a role of the plant wall-associated kinase 1 (WAK1) as a receptor of oligogalacturonides. Proceedings of the National Academy of Sciences **107**, 9452–9457.

Burkart GM, Baskin TI, Bezanilla M. 2015. A family of ROP proteins that suppresses actin dynamics, and is essential for polarized growth and cell adhesion. Journal of Cell Science **128**, 2553–2564.

Buschges R, Hollricher K, Panstruga R, *et al.* 1997. The barley Mlo gene: a novel control element of plant pathogen resistance. Cell **88**, 695–705.

Caldwell DG, McCallum N, Shaw P, Muehlbauer GJ, Marshall DF, Waugh R. 2004. A structured mutant population for forward and reverse genetics in Barley (Hordeum vulgare L.). The Plant Journal **40**, 143–150.

Cano-Delgado A, Penfield S, Smith C, Catley M, Bevan M. 2003. Reduced cellulose synthesis invokes lignincation and defense responses in Arabidopsis thaliana. The Plant Journal **34**, 351–362.

Carol RJ, Dolan L. 2002. Building a hair: tip growth in Arabidopsis thaliana root hairs. Philosophical transactions of the Royal Society of London. Series B, Biological sciences **357**, 815–21.

Carol RJ, Takeda S, Linstead P, Durrant MC, Kakesova H, Derbyshire P, Drea S, Zarsky V, Dolan L. 2005. A RhoGDP dissociation inhibitor spatially regulates growth in root hair cells. Nature **438**, 1013–6.

Carpita NC. 1996. Structure and Biogenesis of the Cell Walls of Grasses. Annual Review of Plant

Physiology and Plant Molecular Biology **47**, 445–476.

Carpita NC, Gibeaut DM. 1993. Structural models of primary cell walls in flowering plants: consistency of molecular structure with the physical properties of the walls during growth. The Plant Journal **3**, 1–30.

Cartwright HN, Humphries JA, Smith LG. 2009. PAN1: a receptor-like protein that promotes polarization of an asymmetric cell division in maize. Science **323**, 649–651.

Cerioli S, Marocco A, Maddaloni M, Motto M, Salamini F. 1994. Early Event in Maize Leaf Epidermis Formation as Revealed by Cell Lineage Studies. Development **120**, 2113–2120.

Césari S, Kanzaki H, Fujiwara T, Bernoux M, Chalvon V, Kawano Y, Shimamoto K, Dodds P, Terauchi R, Kroj T. 2014. The NB-LRR proteins RGA4 and RGA5 interact functionally and physically to confer disease resistance. EMBO Journal **33**, 1941–1959.

Cesari S, Thilliez G, Ribot C, *et al.* 2013. The rice resistance protein pair RGA4/RGA5 recognizes the Magnaporthe oryzae effectors AVR-Pia and AVR1-CO39 by direct binding. The Plant Cell **25**, 1463–1481.

Chai S, Ge F-R, Feng Q-N, Li S, Zhang Y. 2016. PLURIPETALA mediates ROP2 localization and stability in parallel to SCN1 but synergistically with TIP1 in root hairs. Plant Journal **86**, 413–425.

Chang F, Gu Y, Ma H, Yang Z. 2013. AtPRK2 promotes ROP1 activation via RopGEFs in the control of polarized pollen tube growth. Molecular Plant **6**, 1187–1201.

Chen L, Shiotani K, Togashi T, Miki D, Aoyama M, Wong HL, Kawasaki T, Shimamoto K. 2010. Analysis of the Rac/Rop small GTPase family in rice: expression, subcellular localization and role in disease resistance. Plant & Cell Physiology **51**, 585–95.

Cheung AY, Wu H-M. 2011. THESEUS 1, FERONIA and relatives: a family of cell wall-sensing receptor kinases? Current opinion in plant biology, 1–10.

Chowdhury J, Henderson M, Schweitzer P, Burton RA, Fincher GB, Little A. 2014. Differential accumulation of callose, arabinoxylan and cellulose in nonpenetrated versus penetrated papillae on leaves of barley infected with Blumeria graminis f. sp. New Phytologist **204**, 650–660.

Christensen TM, Vejlupkova Z, Sharma YK, Arthur KM, Spatafora JW, Albright CA, Meeley RB, Duvick JP, Quatrano RS, Fowler JE. 2003. Conserved subgroups and developmental regulation in the monocot rop gene family. Plant Physiology **133**, 1791–1808.

Čiamporová M, Dekánková K, Hanáčková Z, Peters P, Ovečka M, Baluška F. 2003. Structural aspects of bulge formation during root hair initiation. Plant and Soil **255**, 1–7.

Cole RA, Fowler JE. 2006. Polarized growth: maintaining focus on the tip. Current Opinion in Plant Biology **9**, 579–588.

Collins NC, Thordal-Christensen H, Lipka V, *et al.* 2003. SNARE-protein-mediated disease resistance at the plant cell wall. Nature **425**, 973–977.

Conrath U. 2011. Molecular aspects of defence priming. Trends in Plant Science **16**, 524–531.

Cosgrove DJ. 2005. Growth of the plant cell wall. Nature Reviews. Molecular Cell Biology **6**, 850–861.

Craddock C, Lavagi I, Yang Z. 2012. New insights into Rho signaling from plant ROP/Rac GTPases. Trends in Cell Biology **22**, 1–10.

da Cunha L, McFall AJ, Mackey D. 2006. Innate immunity in plants: a continuum of layered defenses. Microbes and Infection **8**, 1372–1381.

D'Ovidio R, Mattei B, Roberti S, Bellincampi D. 2004. Polygalacturonases, polygalacturonase-inhibiting proteins and pectic oligomers in plant-pathogen interactions. Biochimica et Biophysica Acta - Proteins and Proteomics **1696**, 237–244.

Dangl JL, Jones JD. 2001. Plant pathogens and integrated defence responses to infection. Nature **411**, 826–833.

Dash S, Van Hemert J, Hong L, Wise RP, Dickerson JA. 2012. PLEXdb: Gene expression resources for plants and plant pathogens. Nucleic Acids Research **40**, 1194–1201.

Dean R, Van Kan JAL, Pretorius ZA, *et al.* 2012. The Top 10 fungal pathogens in molecular plant pathology. Molecular Plant Pathology **13**, 414–430.

DerMardirossian C, Bokoch GM. 2005. GDIs: Central regulatory molecules in Rho GTPase activation. Trends in Cell Biology **15**, 356–363.

Djonović S, Urbach JM, Drenkard E, *et al.* 2013. Trehalose Biosynthesis Promotes Pseudomonas aeruginosa Pathogenicity in Plants. PLoS Pathogens **9**.

Douchkov D, Lueck S, Hensel G, *et al.* 2016. The barley (Hordeum vulgare) cellulose synthase-like D2 gene (HvCslD2) mediates penetration resistance to host-adapted and nonhost isolates of the powdery mildew fungus. New Phytologist **212**, 421–433.

Douchkov D, Nowara D, Zierold U, Schweizer P. 2005. A high-throughput gene-silencing system for the functional assessment of defense-related genes in barley epidermal cells. Molecular Plant-Microbe Interactions **18**, 755–761.

Dumas B, Freyssinet G, Pallett KE. 1995. Tissue-Specific Expression of Germin-Like Oxalate Oxidase during Development and Fungal Infection of Barley Seedlings. Plant Physiology **107**, 1091–1096.

Edwards HH. 2002. Development of primary germ tubes by conidia of Blumeria graminis f.sp. hordei on leaf epidermal cells of Hordeum vulgare. Can. J. Botany **80**, 1121–1125.

Edwards HH, Allen PJ. 1970. A fine structure study of the primary infection process during

infection of Barley by Erysiphe graminis f.sp. hordei. Phytopathology **60**, 1504–1509.

Eichmann R, Bischof M, Weis C, Shaw J, Lacomme C, Schweizer P, Duchkov D, Hensel G, Kumlehn J, Hückelhoven R. 2010. BAX INHIBITOR-1 is required for full susceptibility of barley to powdery mildew. Molecular Plant-Microbe Interactions **23**, 1217–27.

Eichmann R, Hückelhoven R. 2008. Accommodation of powdery mildew fungi in intact plant cells. Journal of Plant Physiology **165**, 5–18.

Ellis C, Turner JG. 2001. The Arabidopsis mutant cev1 has constitutively active jasmonate and ethylene signal pathways and enhanced resistance to pathogens. The Plant Cell **13**, 1025–1033.

Facette MR, Smith LG. 2012. Division polarity in developing stomata. Current Opinion in Plant Biology **15**, 1–8.

Fehér A, Lajkó DB. 2015. Signals fly when kinases meet Rho-of-plants (ROP) small G-proteins. Plant Science **237**, 93–107.

Ferrari S, Sella L, Janni M, De Lorenzo G, Favaron F, D'Ovidio R. 2012. Transgenic expression of polygalacturonase-inhibiting proteins in Arabidopsis and wheat increases resistance to the flower pathogen Fusarium graminearum. Plant Biology **14**, 31–38.

Fincher GB. 2009. Revolutionary times in our understanding of cell wall biosynthesis and remodeling in the grasses. Plant Physiology **149**, 27–37.

Fodor-Dunai C, Fricke I, Potocký M, Dorjgotov D, Domoki M, Jurca ME, Ötvös K, Zárský V, Berken A, Fehér A. 2011. The phosphomimetic mutation of an evolutionarily conserved serine residue affects the signaling properties of Rho of plants (ROPs). Plant Journal **66**, 669–679.

Foreman J, Demidchik V, Bothwell JHF, *et al.* 2003. Reactive oxygen species produced by NADPH oxidase regulate plant cell growth. Nature **422**, 442–6.

Franková L, Fry SC. 2013. Biochemistry and physiological roles of enzymes that 'cut and paste' plant cell-wall polysaccharides. Journal of Experimental Botany **64**, 3519–50.

Frey NFD, Robatzek S. 2009. Trafficking vesicles: pro or contra pathogens? Current Opinion in Plant Biology **12**, 437–443.

Fry SC. 2004. Primary cell wall metabolism: tracking the careers of wall polymers in living plant cells. New Phytologist **161**, 641–675.

Frye CA, Innes RW. 1998. An Arabidopsis Mutant with Enhanced Resistance to Powdery Mildew. The Plant Cell **10**, 947–956.

Frye CA, Tang D, Innes RW. 2001. Negative regulation of defense responses in plants by a conserved MAPKK kinase. Proceedings of the National Academy of Sciences of the United States of America **98**, 373–378.

Fu Y, Gu Y, Zheng Z, Wasteneys G, Yang Z. 2005. Arabidopsis interdigitating cell growth

requires two antagonistic pathways with opposing action on cell morphogenesis. Cell **120**, 687–700.

Fu Y, Li H, Yang Z. 2002. The ROP2 GTPase Controls the Formation of Cortical Fine F-Actin and the Early Phase of Directional Cell Expansion during Arabidopsis Organogenesis. The Plant Cell **14**, 777–794.

Fu Y, Wu G, Yang Z. 2001. Rop GTPase-dependent dynamics of tip-localized F-actin controls tip growth in pollen tubes. Journal of Cell Biology **152**, 1019–1032.

Fu Y, Xu T, Zhu L, Wen M, Yang Z. 2009. A ROP GTPase signaling pathway controls cortical microtubule ordering and cell expansion in Arabidopsis. Current Biology **19**, 1827–32.

Gabriel DW, Rolfe BG. 1990. Working Models of Specific Recognition in Plant-Microbe Interactions. Annual Review of Phytopathology **28**, 365–391.

Genre A, Chabaud M, Timmers T, Bonfante P, Barker DG. 2005. Arbuscular Mycorrhizal Fungi Elicit a Novel Intracellular Apparatus in Medicago truncatula Root Epidermal Cells before Infection. The Plant Cell **17**, 3489–3499.

Gibeaut DM, Pauly M, Bacic A, Fincher GB. 2005. Changes in cell wall polysaccharides in developing barley (Hordeum vulgare) coleoptiles. Planta **221**, 729–38.

Gilroy S, Jones DL. 2000. Through form to function: Root hair development and nutrient uptake. Trends in Plant Science **5**, 56–60.

Gjetting T, Carver TLW, Skøt L, Lyngkjaer MF. 2004. Differential gene expression in individual papilla-resistant and powdery mildew-infected barley epidermal cells. Molecular Plant-Microbe Interactions **17**, 729–38.

Glawe DA. 2008. The Powdery Mildews: A Review of the World's Most Familiar (Yet Poorly Known) Plant Pathogens. Annual Review of Phytopathology **46**, 27–51.

Gómez-Gómez L, Boller T. 2000. FLS2: an LRR receptor-like kinase involved in the perception of the bacterial elicitor flagellin in Arabidopsis. Molecular Cell **5**, 1003–1011.

Gómez-Gómez L, Boller T. 2002. Flagellin perception: A paradigm for innate immunity. Trends in Plant Science **7**, 251–256.

Grebe M, Xu J, Scheres B. 2001. Cell axiality and polarity in plants-adding pieces to the puzzle. Current Opinion in Plant Biology **4**, 520–526.

Greenberg JT. 1997. Programmed Cell Death in Plant-Pathogen Interactions. Annual Review of Plant Physiology and Plant Molecular Biology **48**, 525–545.

Grierson C, Nielsen E, Ketelaar T, Schiefelbein J. 2014. Root Hairs. The Arabidopsis Book, 1–22.

Griffis AHN, Groves NR, Zhou X, Meier I. 2014. Nuclei in motion: movement and positioning of plant nuclei in development, signaling, symbiosis, and disease. Frontiers in Plant Science **5**, 129.

Gu Y, Fu Y, Dowd P, Li S, Vernoud V, Gilroy S, Yang Z. 2005. A Rho family GTPase controls actin dynamics and tip growth via two counteracting downstream pathways in pollen tubes. Journal of Cell Biology **169**, 127–138.

Gu Y, Li S, Lord EM, Yang Z. 2006. Members of a Novel Class of Arabidopsis Rho Guanine Nucleotide Exchange Factors Control Rho GTPase-Dependent Polar Growth. The Plant Cell **18**, 366–381.

Gu F, Nielsen E. 2013. Targeting and regulation of cell wall synthesis during tip growth in plants. Journal of Integrative Plant Biology **55**, 835–846.

Gutjahr C, Banba M, Croset V, An K, Miyao A, An G, Hirochika H, Imaizumi-Anraku H, Paszkowski U. 2008. Arbuscular Mycorrhiza-Specific Signaling in Rice Transcends the Common Symbiosis Signaling Pathway. The Plant Cell **20**, 2989–3005.

Hadwiger LA, Culley DE. 1993. Nonhost resistance genes and race-specific resistance. Trends in Microbiology **1**, 136–141.

Hall A. 1998. Rho GTPases and the Actin Cytoskeleton. Science **279**, 509–514.

Halterman DA, Wise RP. 2004. A single-amino acid substitution in the sixth leucine-rich repeat of barley MLA6 and MLA13 alleviates dependence on RAR1 for disease resistance signaling. Plant Journal **38**, 215–226.

Halterman D, Zhou F, Wei F, Wise RP, Schulze-Lefert P. 2001. The MLA6 coiled-coil, NBS-LRR protein confers AvrMla6-dependent resistance specificity to Blumeria graminis f. sp. hordei in barley and wheat. Plant Journal **25**, 335–348.

Ham JH, Kim MG, Lee SY, Mackey D. 2007. Layered basal defenses underlie non-host resistance of Arabidopsis to Pseudomonas syringae pv. phaseolicola. Plant Journal **51**, 604–616.

Harlan JR, Zohary D. 1966. Distribution of wild wheats and barley. Science **153**, 1074–80.

Heath MC. 1997. *Evolution of plant resistance and susceptibility to fungal parasites* (GC Carroll and P Tudzynski, Eds.). Heidelberg: Springer Berlin Heidelberg.

Heath MC, Nimchuk ZL, Xu H. 1997. Plant nuclear migrations as indicators of critical interactions between resistant or susceptible cowpea epidermal cells and invasion hyphae of the cowpea rust fungus. New Phytologist **135**, 689–700.

Heil M. 2012. Damaged-self recognition as a general strategy for injury detection. Plant Signaling & Behavior **7**, 576–580.

Hématy K, Cherk C, Somerville S. 2009. Host-pathogen warfare at the plant cell wall. Current Opinion in Plant Biology **12**, 406–13.

Henry G, Thonart P, Ongena M. 2012. PAMPs, MAMPs, DAMPs and others: an update on the diversity of plant immunity elicitors. Biotechnology, Agronomy, Society and Environment **16**, 12.

Hoefle C, Hückelhoven R. 2014. A barley Engulfment and Motility domain containing protein modulates Rho GTPase activating protein HvMAGAP1 function in the barley powdery mildew interaction. Plant Molecular Biology **84**, 469–478.

Hoefle C, Huesmann C, Schultheiss H, Börnke F, Hensel G, Kumlehn J, Hückelhoven R. 2011. A Barley ROP GTPase ACTIVATING PROTEIN Associates with Microtubules and Regulates Entry of the Barley Powdery Mildew Fungus into Leaf Epidermal Cells. The Plant Cell **23**, 2422–2439.

van der Hoorn RAL, Kamoun S. 2008. From Guard to Decoy: a new model for perception of plant pathogen effectors. The Plant Cell **20**, 2009–2017.

Hruz T, Laule O, Szabo G, Wessendorp F, Bleuler S, Oertle L, Widmayer P, Gruissem W, Zimmermann P. 2008. Genevestigator V3: A Reference Expression Database for the Meta-Analysis of Transcriptomes. Advances in Bioinformatics **2008**, 1–5.

Hsieh YSY, Harris PJ. 2009. Xyloglucans of monocotyledons have diverse structures. Molecular Plantlant **2**, 943–65.

Huang GQ, Li E, Ge FR, Li S, Wang Q, Zhang CQ, Zhang Y. 2013. Arabidopsis RopGEF4 and RopGEF10 are important for FERONIA-mediated developmental but not environmental regulation of root hair growth. New Phytologist **200**, 1089–1101.

Hückelhoven R. 2005. Powdery mildew susceptibility and biotrophic infection strategies. FEMS Microbiology Letters **245**, 9–17.

Hückelhoven R. 2007. Cell wall-associated mechanisms of disease resistance and susceptibility. Annual Review of Phytopathology **45**, 101–27.

Hückelhoven R. 2014. The effective papilla hypothesis. New Phytologist **204**, 438–440.

Hückelhoven R, Eichmann R, Weis C, Hoefle C, Proels RK. 2013. Genetic loss of susceptibility: A costly route to disease resistance? Plant Pathology **62**, 56–62.

Hückelhoven R, Kogel K. 1998. Tissue-specific superoxide generation at interaction sites in resistant and susceptible near-isogenic barley lines attacked by the powdery mildew fungus (Erysiphe graminis f. sp. hordei). Molecular Plant-Microbe Interactions **11**, 292–300.

Huesmann C, Reiner T, Hoefle C, Preuss J, Jurca ME, Domoki M, Fehér A, Hückelhoven R. 2012. Barley ROP binding kinase1 is involved in microtubule organization and in basal penetration resistance to the barley powdery mildew fungus. Plant Physiology **159**, 311–20.

van Hulten M, Pelser M, van Loon LC, Pieterse CMJ, Ton J. 2006. Costs and benefits of priming for defense in Arabidopsis. Proceedings of the National Academy of Sciences **103**, 5602–5607.

Humphrey T V, Bonetta DT, Goring DR. 2007. Sentinels at the wall: cell wall receptors and sensors. The New Phytologist **176**, 7–21.

Humphries JA, Vejlupkova Z, Luo A, Meeley RB, Sylvester AW, Fowler JE, Smith LG. 2011. ROP GTPases act with the receptor-like protein PAN1 to polarize asymmetric cell division in maize. The Plant Cell **23**, 2273–84.

Humphry M, Bednarek P, Kemmerling B, *et al.* 2010. A regulon conserved in monocot and dicot plants defines a functional module in antifungal plant immunity. Proceedings of the National Academy of Sciences **107**, 21896–21901.

Hurkman WJ, Tanaka CK. 1996. Germin Gene Expression Is Induced in Wheat Leaves by Powdery Mildew Infection. Plant Physiology **111**, 735–739.

Hwang JU, Vernoud V, Szumlanski A, Nielsen E, Yang Z. 2008. A Tip-Localized RhoGAP Controls Cell Polarity by Globally Inhibiting Rho GTPase at the Cell Apex. Current Biology **18**, 1907–1916.

Hwang J-U, Wu G, Yan A, Lee Y-J, Grierson CS, Yang Z. 2010. Pollen-tube tip growth requires a balance of lateral propagation and global inhibition of Rho-family GTPase activity. Journal of Cell Science **123**, 340–350.

Iriti M, Faoro F. 2007. Review of innate and specific immunity in plants and animals. Mycopathologia **164**, 57–64.

Jaggard KW, Qi A, Ober ES. 2010. Possible changes to arable crop yields by 2050. Philosophical Transactions of the Royal Society **365**, 2835–2851.

Jones JDG, Dangl JL. 2006. The plant immune system. Nature **444**, 323–9.

Jones MA, Raymond MJ, Yang Z, Smirnoff N. 2007. NADPH oxidase-dependent reactive oxygen species formation required for root hair growth depends on ROP GTPase. Journal of Experimental Botany **58**, 1261–1270.

Jones MA, Shen J, Fu Y, Li H, Yang Z, Grierson CS. 2002. The Arabidopsis Rop2 GTPase Is a Positive Regulator of Both Root Hair Initiation and Tip Growth. The Plant Cell **14**, 763–776.

Jorgensen JH. 1994. Genetics of powdery mildew resistance in Barley. Critical Reviews in Plant Sciences **13**, 97–119.

Jung Y-H, Agrawal GK, Rakwal R, *et al.* 2006. Functional characterization of OsRacB GTPase - a potentially negative regulator of basal disease resistance in rice. Plant Physiology and Biochemistry **44**, 68–77.

Kaku H, Nishizawa Y, Ishii-Minami N, Akimoto-Tomiyama C, Dohmae N, Takio K, Minami E, Shibuya N. 2006. Plant cells recognize chitin fragments for defense signaling through a plasma membrane receptor. Proceedings of the National Academy of Sciences **103**, 11086–11091.

Karimi M, Depicker A, Hilson P. 2007. Recombinational cloning with plant gateway vectors. Plant Physiology **145**, 1144–1154.

Kato Y, Matsuda K. 1985. Xyloglucan in the Cell Walls of Suspension-Cultured Rice Cells. Plant Cell Physiology **26**, 437–445.

Kavanova M, Lattanzi FA, Grimoldi AA, Schnyder H. 2006. Phosphorus Deficiency Decreases Cell Division and Elongation in Grass Leaves. Plant Physiology **141**, 766–775.

Kawahara Y, de la Bastide M, Hamilton JP, *et al.* 2013. Improvement of the Oryza sativa Nipponbare reference genome using next generation sequence and optical map data. Rice **6**, 4.

Kawano Y, Akamatsu A, Hayashi K, *et al.* 2010. Activation of a Rac GTPase by the NLR family disease resistance protein Pit plays a critical role in rice innate immunity. Cell host & Microbe **7**, 362–75.

Kawano Y, Kaneko-Kawano T, Shimamoto K. 2014. Rho family GTPase-dependent immunity in plants and animals. Frontiers in Plant Science **5**, 1–12.

Kawasaki T, Henmi K, Ono E, Hatakeyama S, Iwano M, Satoh H, Shimamoto K. 1999. The small GTP-binding protein rac is a regulator of cell death in plants. Proceedings of the National Academy of Sciences **96**, 10922–6.

Kawasaki T, Koita H, Nakatsubo T, Hasegawa K, Wakabayashi K, Takahashi H, Umemura K, Umezawa T, Shimamoto K. 2006. Cinnamoyl-CoA reductase, a key enzyme in lignin biosynthesis, is an effector of small GTPase Rac in defense signaling in rice. Proceedings of the National Academy of Sciences **103**, 230–5.

Ketelaar T, Faivre-Moskalenko C, Esseling JJ, de Ruijter NCA, Grierson CS, Dogterom M, Emons AMC. 2002. Positioning of nuclei in Arabidopsis root hairs: an actin-regulated process of tip growth. The Plant Cell **14**, 2941–2955.

Ketelaar T, Galway ME, Mulder BM, Emons AMC. 2008. Rates of exocytosis and endocytosis in Arabidopsis root hairs and pollen tubes. Journal of Microscopy **231**, 265–273.

Kiirika LM, Bergmann HF, Schikowsky C, Wimmer D, Korte J, Schmitz U, Niehaus K, Colditz F. 2012. Silencing of the Rac1 GTPase MtROP9 in Medicago truncatula Stimulates Early Mycorrhizal and Oomycete Root Colonizations But Negatively Affects Rhizobial Infection. Plant Physiology **159**, 501–516.

Kim MC, Lee SH, Kim JK, *et al.* 2002*a*. Mlo, a modulator of plant defense and cell death, is a novel calmodulin-binding protein. Isolation and characterization of a rice Mlo homologue. Journal of Biological Chemistry **277**, 19304–19314.

Kim S-H, Oikawa T, Kyozuka J, Wong HL, Umemura K, Kishi-Kaboshi M, Takahashi A, Kawano Y, Kawasaki T, Shimamoto K. 2012. The bHLH Rac Immunity1 (RAI1) Is Activated by OsRac1 via OsMAPK3 and OsMAPK6 in Rice Immunity. Plant & Cell Physiology **53**, 740–54.

Kim MC, Panstruga R, Elliott C, Müller J, Devoto A, Yoon HW, Park HC, Cho MJ, Schulze-

Lefert P. 2002*b*. Calmodulin interacts with MLO protein to regulate defence against mildew in barley. Nature **416**, 447–451.

Kita N, Toyoda H, Shishiyma J. 1981. Chronological analysis of cytological responses in powdery-mildewed barley leaves. Canadian Journal of Botany **59**, 1761–1768.

Kobayashi Y, Kobayashi I, Funaki Y, Fujimoto S, Takemoto T, Kunoh H. 1997. Dynamic reorganization of microfilaments and microtubules is necessary for the expression of non-host resistance in barley coleoptile cells. The Plant Journal **11**, 525–537.

Koeck M, Hardham AR, Dodds PN. 2011. The role of effectors of biotrophic and hemibiotrophic fungi in infection. Cellular Microbiology **13**, 1849–1857.

Koga H, Bushnell WR, Zeyen RJ. 1990. Specificity of cell type and timing of events associated with papilla formation and the hypersensitive reaction in leaves of Hordeum vulgare attacked by Erysiphe graminis f.sp. hordei. Canadian Journal of Botany **68**, 2344–2352.

Kogel K-H, Langen G. 2005. Induced disease resistance and gene expression in cereals. Cellular Microbiology **7**, 1555–1564.

Kogel K, Ortel B, Jarosch B, Atzorn R, Schiffer R, Wasternack C. 1995. Resistance in barley against the powdery mildew fungus (Erysiphe graminis f . sp . hordei) is not associated with enhanced levels of endogenous jasmonates. European Journal of Plant Pathology **101**, 319–332.

Koh S, André A, Edwards H, Ehrhardt D, Somerville S. 2005. Arabidopsis thaliana subcellular responses to compatible Erysiphe cichoracearum infections. Plant Journal **44**, 516–529.

König R, Stertz S, Zhou Y, *et al.* 2010. Human host factors required for influenza virus replication. Nature **463**, 813–817.

Kosami K-I, Ohki I, Nagano M, *et al.* 2014. The Crystal Structure of the Plant Small GTPase OsRac1 Reveals Its Mode of Binding to NADPH Oxidase. The Journal of Biological Chemistry **289**, 28569–78.

Kost B. 2008. Spatial control of Rho (Rac-Rop) signaling in tip-growing plant cells. Trends In Cell Biology **18**, 119–27.

Kropf DL, Bisgrove SR, Hable WE. 1998. Cytoskeletal control of polar growth in plant cells. Current Opinion in Cell Biology **10**, 117–122.

Kwasniewski M, Chwialkowska K, Kwasniewska J, Kusak J, Siwinski K, Szarejko I. 2013. Accumulation of peroxidase-related reactive oxygen species in trichoblasts correlates with root hair initiation in barley. Journal of Plant Physiology **170**, 185–95.

Kwasniewski M, Janiak A, Mueller-Roeber B, Szarejko I. 2010. Global analysis of the root hair morphogenesis transcriptome reveals new candidate genes involved in root hair formation in barley. Journal of Plant Physiology **167**, 1076–83.

Lane BG. 2002. Oxalate , Germins , and Higher-Plant Pathogens. Life **53**, 67–75.

Lavy M, Bloch D, Hazak O, Gutman I, Poraty L, Sorek N, Sternberg H, Yalovsky S. 2007. A Novel ROP/RAC Effector Links Cell Polarity, Root-Meristem Maintenance, and Vesicle Trafficking. Current Biology **17**, 947–952.

Lavy M, Bracha-Drori K, Sternberg H, Yalovsky S. 2002. A cell-specific, prenylation-independent mechanism regulates targeting of type II RACs. The Plant Cell **14**, 2431–2450.

Lavy M, Yalovsky S. 2006. Association of Arabidopsis type-II ROPs with the plasma membrane requires a conserved C-terminal sequence motif and a proximal polybasic domain. Plant Journal **46**, 934–947.

Li S, Gu Y, Yan A, Lord E, Yang ZB. 2008. RIP1 (ROP Interactive Partner 1)/ICR1 marks pollen germination sites and may act in the ROP1 pathway in the control of polarized pollen growth. Molecular Plant **1**, 1021–1035.

Li H, Shen JJ, Zheng ZL, Lin Y, Yang Z. 2001. The Rop GTPase switch controls multiple developmental processes in Arabidopsis. Plant Physiology **126**, 670–684.

Lin D, Cao L, Zhou Z, Zhu L, Ehrhardt D, Yang Z, Fu Y. 2013. Rho GTPase Signaling Activates Microtubule Severing to Promote Microtubule Ordering in Arabidopsis. Current Biology **23**, 290–297.

Lin M-R, Edwards HH. 1974. Primary Penetration Process in Powdery Mildewed Barley Related To Host Cell Age, Cell Type, and Occurrence of Basic Staining Material. New Phytologist **73**, 131–137.

Lin Q, Fuji RN, Yang W, Cerione RA. 2003. RhoGDI Is Required for Cdc42-Mediated Cellular Transformation. Current Biology **13**, 1469–1479.

Lin D, Nagawa S, Chen J, *et al.* 2012. A ROP GTPase-Dependent Auxin Signaling Pathway Regulates the Subcellular Distribution of PIN2 in Arabidopsis Roots. Current Biology **22**, 1319–1325.

Lionetti V, Raiola A, Camardella L, Giovane A, Obel N, Pauly M, Favaron F, Cervone F, Bellincampi D. 2007. Overexpression of pectin methylesterase inhibitors in Arabidopsis restricts fungal infection by Botrytis cinerea. Plant Physiology **143**, 1871–1880.

Lionetti V, Raiola A, Cervone F, Bellincampi D. 2014. Transgenic expression of pectin methylesterase inhibitors limits tobamovirus spread in tobacco and arabidopsis. Molecular Plant Pathology **15**, 265–274.

Liu L, Paulitz J, Pauly M. 2015. The Presence of Fucogalactoxyloglucan and Its Synthesis in Rice Indicates Conserved Functional Importance in Plants. Plant Physiology **168**, 549–560.

Lozano-Duran R, Bejarano ER. 2011. Geminivirus C2 protein might be the key player for

geminiviral co-option of SCF-mediated ubiquitination. Plant Signaling & Behavior **6**, 999–1001.

Ma X, Yang X, Zeng F, Yang L, Yu D, Ni H. 2010. Physcion, a natural anthraquinone derivative, enhances the gene expression of leaf-specific thionin of barley against Blumeria graminis. Pest Management Science **66**, 718–24.

Macara IG, Lounsbury KM, Richards SA, McKiernan C, Bar-Sagi D. 1996. The Ras superfamily of GTPases. FASEB journal : official publication of the Federation of American Societies for Experimental Biology **10**, 625–30.

Maimbo M, Ohnishi K, Hikichi Y, Yoshioka H, Kiba A. 2007. Induction of a small heat shock protein and its functional roles in Nicotiana plants in the defense response against Ralstonia solanacearum. Plant Physiology **145**, 1588–1599.

Maleck K, Levine A, Eulgem T, Morgan A, Schmid J, Lawton KA, Dangl JL, Dietrich RA. 2000. The transcriptome of Arabidopsis thaliana during systemic acquired resistance. Nature Genetics **26**, 403–410.

Marcus SE, Blake AW, Benians TAS, *et al.* 2010. Restricted access of proteins to mannan polysaccharides in intact plant cell walls. Plant Journal **64**, 191–203.

Marga F, Grandbois M, Cosgrove DJ, Baskin TI. 2005. Cell wall extension results in the coordinate separation of parallel microfibrils: Evidence from scanning electron microscopy and atomic force microscopy. Plant Journal **43**, 181–190.

Marzec M, Melzer M, Szarejko I. 2013. Asymmetric growth of root epidermal cells is related to the differentiation of root hair cells in Hordeum vulgare (L.). Journal of Experimental Botany **64**, 5145–55.

Marzec M, Melzer M, Szarejko I. 2014. The evolutionary context of root epidermis cell patterning in grasses (Poaceae). Plant Signaling & Behavior **9**, 1–5.

Mayer KFX, Waugh R, Langridge P, *et al.* 2012. A physical, genetic and functional sequence assembly of the barley genome. Nature **491**, 711–716.

McDougall GJ, Fry SC. 1989*a*. Anti-auxin activity of xyloglucan oligosaccharides: The role of groups other than the terminal alpha-l-fucose residue. Journal of Experimental Botany **40**, 233–238.

McDougall GJ, Fry SC. 1989*b*. Structure-Activity Relationships for Xyloglucan Oligosaccharides with Antiauxin Activity. Plant Physiology **89**, 883–887.

McDougall GJ, Fry SC. 1990. Xyloglucan Oligosaccharide Promote Growth an Cellulase : Evidence for a Role fo Cellulasse Cell Expansion. Plant Physiology **93**, 1042–1048.

McDougall GJ, Fry SC. 1994. Fucosylated Xyloglucan in Suspension-Cultured Cells of the Graminaceous Monocotyledon, Festuca arundinacea. Journal of Plant Physiology **143**, 591–595.

Meng Y, Wise RP. 2012. HvWRKY10, HvWRKY19, and HvWRKY28 Regulate Mla-Triggered

Immunity and Basal Defense to Barley Powdery Mildew. Molecular Plant-Microbe Interactions **25**, 1492–1505.

Miki D, Itoh R, Shimamoto K. 2005. RNA silencing of single and multiple members in a gene family of rice. Plant Physiology **138**, 1903–13.

Miller DD, De Ruijter NCA, Bisseling T, Emons AMC. 1999. The role of actin in root hair morphogenesis: Studies with lipochito-oligosaccharide as a growth stimulator and cytochalasin as an actin perturbing drug. Plant Journal **17**, 141–154.

Miya A, Albert P, Shinya T, Desaki Y, Ichimura K, Shirasu K, Narusaka Y, Kawakami N, Kaku H, Shibuya N. 2007. CERK1, a LysM receptor kinase, is essential for chitin elicitor signaling in Arabidopsis. Proceedings of the National Academy of Sciences **104**, 19613–8.

Miyawaki KN, Yang Z. 2014. Extracellular signals and receptor-like kinases regulating ROP GTPases in plants. Frontiers in Plant Science **5**, 449.

Molendijk AJ, Bischoff F, Rajendrakumar CS, Friml J, Braun M, Gilroy S, Palme K. 2001. Arabidopsis thaliana Rop GTPases are localized to tips of root hairs and control polar growth. The EMBO Journal **20**, 2779–88.

Molendijk AJ, Ruperti B, Palme K. 2004. Small GTPases in vesicle trafficking. Current Opinion in Plant Biology **7**, 694–700.

Molina A, Görlach J, Volrath S, Ryals J. 1999. Wheat genes encoding two types of PR-1 proteins are pathogen inducible, but do not respond to activators of systemic acquired resistance. Molecular Plant-Microbe Interactions **12**, 53–58.

Monaghan J, Zipfel C. 2012. Plant pattern recognition receptor complexes at the plasma membrane. Current Opinion in Plant Biology **15**, 349–357.

Montesano M, Brader G, Palva ET. 2003. Pathogen derived elicitors: Searching for receptors in plants. Molecular Plant Pathology **4**, 73–79.

Moscetti I, Tundo S, Janni M, Sella L, Gazzetti K, Tauzin A, Giardina T, Masci S, Favaron F, D'Ovidio R. 2013. Constitutive expression of the xylanase inhibitor TAXI-III delays Fusarium head blight symptoms in durum wheat transgenic plants. Molecular Plant-Microbe Interactions **26**, 1464–72.

Mysore KS, Ryu CM. 2004. Nonhost resistance: How much do we know? Trends in Plant Science **9**, 97–104.

Nagawa S, Xu T, Lin D, Dhonukshe P, Zhang X, Friml J, Scheres B, Fu Y, Yang Z. 2012. ROP GTPase-dependent actin microfilaments promote PIN1 polarization by localized inhibition of clathrin-dependent endocytosis. PLoS Biology **10**, e1001299.

Nawrot R, Barylski J, Nowicki G, Broniarczyk J, Buchwald W, Goździcka-Józefiak A. 2014.

Plant antimicrobial peptides. Folia Microbiologica **59**, 181–196.

NFS. 1953. *The Third Annual Report of the NATIONAL SCIENCE FOUNDATION*.

Nibau C, Wu H, Cheung AY. 2006. RAC/ROP GTPases: 'hubs' for signal integration and diversification in plants. Trends in Plant Science **11**, 309–15.

Nicaise V, Roux M, Zipfel C. 2009. Recent advances in PAMP-triggered immunity against bacteria: pattern recognition receptors watch over and raise the alarm. Plant Physiology **150**, 1638–1647.

Nielsen KA, Nicholson RL, Carver TLW, Kunoh H, Oliver RP. 2000. First touch: An immediate response to surface recognition in conidia of Blumeria graminis. Physiological and Molecular Plant Pathology **56**, 63–70.

NIH. 1991. Toxicology and Carcinogenesis Studies of Sodium Azide in F344/N Rats. NATIONAL TOXICOLOGY PROGRAM Technical Report Series **389**, 1–171.

Niks RE, Marcel TC. 2009. Nonhost and basal resistance: How to explain specificity? New Phytologist **182**, 817–828.

Nuernberger T, Lipka V. 2005. Non-host resistance in plants: new insights into an old phenomenon. Molecular Plant Pathology **6**, 335–345.

O'Connell RJ, Panstruga R. 2006. Tete a tete inside a plant cell: Establishing compatibility between plants and biotrophic fungi and oomycetes. New Phytologist **171**, 699–718.

Oerke E-C, Dehne H-W. 2004. Safeguarding production—losses in major crops and the role of crop protection. Crop Protection **23**, 275–285.

Okuyama Y, Kanzaki H, Abe A, *et al.* 2011. A multifaceted genomics approach allows the isolation of the rice Pia-blast resistance gene consisting of two adjacent NBS-LRR protein genes. Plant Journal **66**, 467–479.

Ono E, Wong HL, Kawasaki T, Hasegawa M, Kodama O, Shimamoto K. 2001. Essential role of the small GTPase Rac in disease resistance of rice. Proceedings of the National Academy of Sciences **98**, 759–764.

Van Ooijen G, Lukasik E, Van Den Burg HA, Vossen JH, Cornelissen BJC, Takken FLW. 2010. The small heat shock protein 20 RSI2 interacts with and is required for stability and function of tomato resistance protein I-2. Plant Journal **63**, 563–572.

Opalski KS, Schultheiss H, Kogel K-H, Hückelhoven R. 2005. The receptor-like MLO protein and the RAC/ROP family G-protein RACB modulate actin reorganization in barley attacked by the biotrophic powdery mildew fungus Blumeria graminis f.sp. hordei. The Plant Journal **41**, 291–303.

Ovesná J, Kučera L, Vaculová K, Štrymplová K, Svobodová I, Milella L. 2012. Validation of the β-amy1 transcription profiling assay and selection of reference genes suited for a RT-qPCR assay

in developing barley caryopsis. PLoS ONE **7**.

Panteris E, Apostolakos P, Galatis B. 2006. Cytoskeletal asymmetry in Zea mays subsidiary cell mother cells: a monopolar prophase microtubule half-spindle anchors the nucleus to its polar position. Cell Motility and the Cytoskeleton **63**, 696–709.

Panteris E, Galatis B, Quader H, Apostolakos P. 2007. Cortical actin filament organization in developing and functioning stomatal complexes of Zea mays and Triticum turgidum. Cell Motility and the Cytoskeleton **64**, 531–48.

Pappelis AJ, Pappeli GA, Kulfinski FB. 1974. Nuclear Orientation in Onion Epidermal Cells in Relation to Wounding and Infection. Phytopathology **64**, 1010–1012.

Parlevliet JE. 1978. Race-specific aspects of polygenic resistance of barley to leaf rust, Puccinia hordei. Netherlands Journal of Plant Pathology **84**, 121–126.

Parry MAJ, Hawkesford MJ. 2010. Food security: increasing yield and improving resource use efficiency. Proceedings of the Nutrition Society **69**, 592–600.

Paszkowski U, Jakovleva L, Boller T. 2006. Maize mutants affected at distinct stages of the arbuscular mycorrhizal symbiosis. Plant Journal **47**, 165–173.

Pathuri IP, Eichmann R, Hückelhoven R. 2009. Plant small monomeric G-proteins (RAC/ROPs) of barley are common elements of susceptibility to fungal leaf pathogens, cell expansion and stomata development. Plant Signaling & Behavior **4**, 109–110.

Pathuri IP, Reitberger IE, Hückelhoven R, Proels RK. 2011. Alcohol dehydrogenase 1 of barley modulates susceptibility to the parasitic fungus Blumeria graminis f.sp. hordei. Journal of Experimental Botany **62**, 3449–3457.

Pathuri IP, Zellerhoff N, Schaffrath U, Hensel G, Kumlehn J, Kogel K-H, Eichmann R, Hückelhoven R. 2008. Constitutively activated barley ROPs modulate epidermal cell size, defense reactions and interactions with fungal leaf pathogens. Plant Cell Reports **27**, 1877–87.

Pauly M, Gille S, Liu L, Mansoori N, de Souza A, Schultink A, Xiong G. 2013. Hemicellulose biosynthesis. Planta **238**, 627–42.

Pavan S, Jacobsen E, Visser RGF, Bai Y. 2010. Loss of susceptibility as a novel breeding strategy for durable and broad-spectrum resistance. Molecular Breeding **25**, 1–12.

Payne RJH, Grierson CS. 2009. A theoretical model for ROP localisation by auxin in Arabidopsis root hair cells. PloS ONE **4**, e8337.

Pedersen C, Ver Loren van Themaat E, McGuffin LJ, *et al.* 2012. Structure and evolution of barley powdery mildew effector candidates. BMC Genomics **13**, 694.

Pei W, Du F, Zhang Y, He T, Ren H. 2012. Control of the actin cytoskeleton in root hair development. Plant Science **187**, 10–8.

Pennington HG, Gheorghe DM, Damerum A, Pliego C, Spanu PD, Cramer R, Bindschedler L V. 2016. Interactions between the Powdery Mildew Effector BEC1054 and Barley Proteins Identify Candidate Host Targets. Journal of Proteome Research **15**, 826–839.

Perrin RM, Jia Z, Wagner TA, O'Neill MA, Sarria R, York WS, Raikhel N V, Keegstra K. 2003. Analysis of xyloglucan fucosylation in Arabidopsis. Plant Physiology **132**, 768–778.

Pfaffl MW. 2001. A new mathematical model for relative quantification in real-time RT-PCR. Nucleic Acids Research **29**, 16–21.

Pogorelko G, Lionetti V, Bellincampi D, Zabotina O. 2013. Cell wall integrity: Targeted post-synthetic modifications to reveal its role in plant growth and defense against pathogens. Plant Signaling & Behaviour **8**, 1–8.

Poraty-Gavra L, Zimmermann P, Haigis S, Bednarek P, Hazak O, Stelmakh OR, Sadot E, Schulze-Lefert P, Gruissem W, Yalovsky S. 2013. The Arabidopsis Rho of Plants GTPase AtROP6 Functions in Developmental and Pathogen Response Pathways. Plant Physiology **161**, 1172–88.

Pozo MJ, Cordier C, Dumas-Gaudot E, Gianinazzi S, Barea JM, Azcón-Aguilar C. 2002. Localized versus systemic effect of arbuscular mycorrhizal fungi on defence responses to Phytophthora infection in tomato plants. Journal of Experimental Botany **53**, 525–34.

Prell HH, Day P. 2001. *Plant Fungal Interaction: a Classical and a Molecular View*. Berlin: Springer Science & Business Media.

Proels RK, Westermeier W, Hückelhoven R. 2011. Infection of barley with the parasitic fungus Blumeria graminis f.sp. hordei results in the induction of HvADH1 and HvADH2. Plant Signaling & Behavior **6**, 1584–1587.

Pryce-Jones E, Carver T, Gurr SJ. 1999. The roles of cellulase enzymes and mechanical force in host penetration by Erysiphe graminis f.sp.hordei. Physiological and Molecular Plant Pathology **55**, 175–182.

Qin Y, Dong J. 2015. Focusing on the focus: What else beyond the master switches for polar cell growth? Molecular Plant **8**, 582–594.

Ray DK, Mueller ND, West PC, Foley JA. 2013. Yield Trends Are Insufficient to Double Global Crop Production by 2050. PloS ONE **8**, e66428.

Rayapuram C, Jensen MK, Maiser F, Shanir JV, Hornshøj H, Rung JH, Gregersen PL, Schweizer P, Collinge DB, Lyngkj??r MF. 2012. Regulation of basal resistance by a powdery mildew-induced cysteine-rich receptor-like protein kinase in barley. Molecular Plant Pathology **13**, 135–147.

Reiter WD, Chapple C, Somerville CR. 1997. Mutants of Arabidopsis thaliana with altered cell

wall polysaccharide composition. The Plant Journal **12**, 335–45.

Reymond P, Grünberger S, Paul K, Müller M, Farmer EE. 1995. Oligogalacturonide defense signals in plants: large fragments interact with the plasma membrane in vitro. Proceedings of the National Academy of Sciences **92**, 4145–4149.

Ridout CJ, Skamnioti P, Porritt O, Sacristan S, Jones JDG, Brown JKM. 2006. Multiple avirulence paralogues in cereal powdery mildew fungi may contribute to parasite fitness and defeat of plant resistance. The Plant Cell **18**, 2402–14.

Sammons RD, Gaines TA. 2014. Glyphosate resistance: State of knowledge. Pest Management Science **70**, 1367–1377.

Santiago R, Barros-Rios J, Malvar RA. 2013. Impact of cell wall composition on maize resistance to pests and diseases. International Journal of Molecular Sciences **14**, 6960–6980.

Sarria R, Wagner T, O'Neill M. 2001. Characterization of a family of Arabidopsis genes related to xyloglucan fucosyltransferase1. Plant Physiology **127**, 1595–1606.

Sauer M, Friml J. 2010. *Plant Developmental Biology: Methods in Molecular Biology* (L Hennig and C Köhler, Eds.). Humana Press.

Schaffrath U, Zabbai F, Dudler R. 2000. Characterization of RCI-1 , a chloroplastic rice lipoxygenase whose synthesis is induced by chemical plant resistance activators. European Journal of Plant Pathology **267**, 5935–5942.

Scheler B, Schnepf V, Galgenmüller C, Ranf S, Hückelhoven R. 2016. Barley disease susceptibility factor RACB acts in epidermal cell polarity and positioning of the nucleus. Journal of Experimental Botany **67**, 3263–3275.

Schiefelbein JW. 2000. Constructing a plant cell. The genetic control of root hair development. Plant Physiology **124**, 1525–1531.

Schlueter SD, Dong Q, Brendel V. 2003. GeneSeqer@PlantGDB: Gene structure prediction in plant genomes. Nucleic Acids Research **31**, 3597–3600.

Schmelzer E. 2002. Cell polarization, a crucial process in fungal defence. Trends in Plant Science **7**, 411–415.

Schmidt SM, Kuhn H, Micali C, Liller C, Kwaaitaal M, Panstruga R. 2014. Interaction of a Blumeria graminis f. sp. hordei effector candidate with a barley ARF-GAP suggests that host vesicle trafficking is a fungal pathogenicity target. Molecular Plant Pathology **15**, 535–549.

Schneider CA, Rasband WS, Eliceiri KW. 2012. NIH Image to ImageJ: 25 years of image analysis. Nature Methods **9**, 671–675.

Schröder JJ, Smit AL, Cordell D, Rosemarin A. 2011. Improved phosphorus use efficiency in agriculture: A key requirement for its sustainable use. Chemosphere **84**, 822–831.

Schultheiss H, Dechert C, Kogel K. 2002. A small GTP-binding host protein is required for entry of powdery mildew fungus into epidermal cells of barley. Plant Physiology **128**, 1447–1454.

Schultheiss H, Dechert C, Kogel K-H, Hückelhoven R. 2003. Functional analysis of barley RAC/ROP G-protein family members in susceptibility to the powdery mildew fungus. The Plant Journal **36**, 589–601.

Schultheiss H, Hensel G, Imani J. 2005. Ectopic expression of constitutively activated RACB in barley enhances susceptibility to powdery mildew and abiotic stress. Plant Physiology **139**, 353–362.

Schultheiss H, Preuss J, Pircher T, Eichmann R, Hückelhoven R. 2008. Barley RIC171 interacts with RACB in planta and supports entry of the powdery mildew fungus. Cellular Microbiology **10**, 1815–26.

Schweitzer P, Schlagenhauf E, Schaffrath U, Dudler R. 1999. Different patterns of host genes are induced in rice by Pseudomonas syringae, a biologicak inducer of resistance, and the chemical inducer benzothiadiazole (BTH). European Journal of Plant Pathology **105**, 659–665.

Serrano M, Coluccia F, Torres M, L'Haridon F, Métraux J-P. 2014. The cuticle and plant defense to pathogens. Frontiers in Plant Science **5**, 274.

Shen Q-H. 2003. Recognition Specificity and RAR1/SGT1 Dependence in Barley Mla Disease Resistance Genes to the Powdery Mildew Fungus. The Plant Cell **15**, 732–744.

Shen Q-H, Saijo Y, Mauch S, Biskup C, Bieri S, Keller B, Seki H, Ulker B, Somssich IE, Schulze-Lefert P. 2007. Nuclear activity of MLA immune receptors links isolate-specific and basal disease-resistance responses. Science **315**, 1098–103.

Shimizu T, Nakano T, Takamizawa D, *et al.* 2010. Two LysM receptor molecules, CEBiP and OsCERK1, cooperatively regulate chitin elicitor signaling in rice. Plant Journal **64**, 204–214.

Shiu SH, Bleecker AB. 2001. Receptor-like kinases from Arabidopsis form a monophyletic gene family related to animal receptor kinases. Proceedings of the National Academy of Sciences **98**, 10763–10768.

Shiu S, Karlowski W, Pan R. 2004. Comparative analysis of the receptor-like kinase family in Arabidopsis and rice. The Plant Cell **16**, 1220–1234.

Sievers F, Wilm A, Dineen D, *et al.* 2011. Fast, scalable generation of high-quality protein multiple sequence alignments using Clustal Omega. Molecular Systems Biology **7**.

Singh MK, Ren F, Giesemann T, *et al.* 2013. Modification of plant Rac/Rop GTPase signalling using bacterial toxin transgenes. Plant Journal **73**, 314–324.

Sivamani E, Delong RK, Qu R. 2009. Protamine-mediated DNA coating remarkably improves bombardment transformation efficiency in plant cells. Plant Cell Reports **28**, 213–221.

Skalamera D, Heath MC. 1998. Changes in the Cytoskeleton Accompanying Infection-Induced Nuclear-Movements and the Hypersensitive Response in Plant- Cells Invaded by Rust Fungi. Plant Journal **Vol 16**, 191–200.

Sorek N, Poraty L, Sternberg H, Bar E, Lewinsohn E, Yalovsky S. 2007. Activation status-coupled transient S acylation determines membrane partitioning of a plant Rho-related GTPase. Molecular and Cellular Biology **27**, 2144–2154.

Sorek N, Segev O, Gutman O, *et al.* 2010. An S-acylation switch of conserved G domain cysteines is required for polarity signaling by ROP GTPases. Current Biology **20**, 914–20.

Spanu PD, Abbott JC, Amselem J, *et al.* 2010. Genome Expansion and Gene Loss in Powdery Mildew Fungi Reveal Tradeoffs in Extreme Parasitism. Science **330**, 1543–1546.

Stebbins GL, Jain SK. 1960. Developmental studies of cell differentiation in the epidermis of Monocotyledons. Developmental Biology **2**, 409–425.

Stebbins GL, Shah SS. 1960. Developmental Studies of Cell Differentiation in the Epidermis of Monocotyledons. Developmental Biology **2**, 477–500.

Stergiopoulos I, de Wit PJGM. 2009. Fungal effector proteins. Annual Review of Phytopathology **47**, 233–63.

Suzuki S, Komiya Y, Mitsui T, Tsuyumu S, Kunoh H, Carver TLW, Nicholson RL. 1998. Release of Cell Wall Degrading Enzymes from Conidia of Blumeria graminis on Artificial Substrata. Japanese Journal of Phytopathology **64**, 160–167.

Sylvester AW, Smith L, Freeling M. 1996. Acquisition of identity in the developing leaf. Annual Review of Cell and Developmental Biology **12**, 257–304.

Szarejko I, Janiak A, Chmielewska B, Nawrot M. 2005. Genetic analysis of several root hair mutants of barley. Barley Genetics Newsletter **35**, 36–38.

Takai Y, Sasaki T, Matozaki T. 2001. Small GTP-Binding Proteins. Physiological Reviews **81**, 153–208.

Takken FLW, Tameling WIL. 2009. To nibble at plant resistance proteins. Science **324**, 744–746.

Tao LZ, Cheung AY, Wu HM. 2002. Plant Rac-like GTPases are activated by auxin and mediate auxin-responsive gene expression. Plant Cell **14**, 2745–2760.

Thordal-Christensen H. 2003. Fresh insights into processes of nonhost resistance. Current Opinion in Plant Biology **6**, 351–357.

Tratwal A, Weber Z. 2006. Virulence Frequency of Blumeria Graminis F. Sp. Hordei and the Occurrence of Powdery Mildew on Four Winter Barley Cultivars. Journal of Plant Protection Research **46**, 221–230.

Truernit E, Bauby H, Dubreucq B, Grandjean O, Runions J, Barthélémy J, Palauqui J-C.

2008. High-resolution whole-mount imaging of three-dimensional tissue organization and gene expression enables the study of Phloem development and structure in Arabidopsis. The Plant Cell **20**, 1494–503.

Underwood W, Somerville SC. 2008. Focal accumulation of defences at sites of fungal pathogen attack. Journal of Experimental Botany **59**, 3501–8.

Untergasser A, Cutcutache I, Koressaar T, Ye J, Faircloth BC, Remm M, Rozen SG. 2012. Primer3-new capabilities and interfaces. Nucleic Acids Research **40**.

Vallélian-Bindschedler, Métraux J, Schweizer P. 1998. Salicylic Acid Accumulation in Barley Is Pathogen Specific but Not Required for Defense-Gene Activation. Molecular Plant-Microbe Interactions **11**, 702–705.

Vanzin GF, Madson M, Carpita NC, Raikhel N V, Keegstra K, Reiter W-D. 2002. The mur2 mutant of Arabidopsis thaliana lacks fucosylated xyloglucan because of a lesion in fucosyltransferase AtFUT1. Proceedings of the National Academy of Sciences **99**, 3340–5.

Veiga RSL, Faccio A, Genre A, Pieterse CMJ, Bonfante P, van der Heijden MGA. 2013. Arbuscular mycorrhizal fungi reduce growth and infect roots of the non-host plant Arabidopsis thaliana. Plant, Cell & Environment **36**, 1926–37.

Verbelen J-P, De Cnodder T, Le J, Vissenberg K, Baluška F. 2006. The Root Apex of Arabidopsis thaliana Consists of Four Distinct Zones of Growth Activities. Plant Signaling & Behaviour **1**, 296–304.

Vernoud V, Horton AC, Yang Z, Nielsen E. 2003. Analysis of the small GTPase gene superfamily of Arabidopsis. Plant Physiology **131**, 1191–1208.

Vetter IR, Wittinghofer A. 2001. The guanine nucleotide-binding switch in three dimensions. Science **294**, 1299–1304.

Vogel J. 2008. Unique aspects of the grass cell wall. Current Opinion in Plant Biology **11**, 301–7.

Vogel JP, Raab TK, Schiff C, Somerville SC. 2002. PMR6 , a Pectate Lyase – Like Gene Required for Powdery Mildew Susceptibility in Arabidopsis. The Plant Cell **14**, 2095–2106.

Vogel JP, Raab TK, Somerville CR, Somerville SC. 2004. Mutations in PMR5 result in powdery mildew resistance and altered cell wall composition. The Plant Journal **40**, 968–78.

Vogel J, Somerville S. 2000. Isolation and characterization of powdery mildew-resistant Arabidopsis mutants. Proceedings of the National Academy of Sciences **97**, 1897–1902.

Volpi C, Janni M, Lionetti V, Bellincampi D, Favaron F, D'Ovidio R. 2011. The ectopic expression of a pectin methyl esterase inhibitor increases pectin methyl esterification and limits fungal diseases in wheat. Molecular Plant-Microbe Interactions **24**, 1012–1019.

Vorwerk S, Somerville S, Somerville C. 2004. The role of plant cell wall polysaccharide

composition in disease resistance. Trends in Plant Science **9**, 203–209.

Walton JD. 1994. Deconstructing the Cell Wall. Plant Physiology **104**, 1113–1118.

Wamaitha MJ, Yamamoto R, Wong HL, Kawasaki T, Kawano Y, Shimamoto K. 2012. OsRap2.6 transcription factor contributes to rice innate immunity through its interaction with Receptor for Activated Kinase-C 1 (RACK1). Rice **5**, 35.

Wei Y, Zhang Z, Andersen CH, Schmelzer E, Gregersen PL, Collinge DB, Smedegaard-Petersen V, Thordal-Christensen H. 1998. An epidermis/papilla-specific oxalate oxidase-like protein in the defence response of barley attacked by the powdery mildew fungus. Plant Molecular Biology **36**, 101–12.

Weiss E, Wetterstrom W, Nadel D, Bar-Yosef O. 2004. The broad spectrum revisited: evidence from plant remains. Proceedings of the National Academy of Sciences **101**, 9551–9555.

Whigham E, Qi S, Mistry D, *et al.* 2015. Broadly conserved fungal effector BEC1019 suppresses host cell death and enhances pathogen virulence in powdery mildew of barley (Hordeum vulgare L.). Molecular Plant-Microbe Interactions **28**, 968–983.

Wilson RA, Talbot NJ. 2009. Under pressure: investigating the biology of plant infection by Magnaporthe oryzae. Nature Reviews. Microbiology **7**, 185–195.

Winge P, Brembu T, Bones AM. 1997. Cloning and characterization of rac-like cDNAs from Arabidopsis thaliana. Plant Molecular Biology **35**, 483–495.

Wolf S, Mravec J, Greiner S, Mouille G, Höfte H. 2012. Plant cell wall homeostasis is mediated by brassinosteroid feedback signaling. Current biology : CB **22**, 1732–7.

Wong HL, Sakamoto T, Kawasaki T, Umemura K, Shimamoto K. 2004. Down-regulation of metallothionein, a reactive oxygen scavenger, by the small GTPase OsRac1 in rice. Plant Physiology **135**, 1447–1456.

Wright AJ, Thomas BJ, Kunoh H, Nicholson RL, Carver TL. 2002. Influences of substrata and interface geometry on the release of extracellular material by Blumeria graminis conidia. Physiological and Molecular Plant Pathology **61**, 163–178.

Wu FS. 1987. Localization of mitochondria in plant cells by vital staining with rhodamine 123. Planta **171**, 346–357.

Wu G, Gu Y, Li S, Yang Z. 2001. A genome-wide analysis of Arabidopsis Rop-interactive CRIB motif-containing proteins that act as Rop GTPase targets. The Plant Cell **13**, 2841–56.

Wu G, Hai L, Yang Z. 2000. Arabidopsis RopGAPs Are a Novel Family of Rho GTPase-Activating Proteins that Require the Cdc42/Rac-Interactive Binding Motif for Rop-Specific GTPase Stimulation. Plant Physiology **124**, 1625–1636.

Wu H, Hazak O, Cheung AY, Yalovsky S. 2011. RAC/ROP GTPases and auxin signaling. The

Plant Cell **23**, 1208–18.

Xu T, Wen M, Nagawa S, Fu Y, Chen J-G, Wu M-J, Perrot-Rechenmann C, Friml J, Jones AM, Yang Z. 2010. Cell surface- and rho GTPase-based auxin signaling controls cellular interdigitation in Arabidopsis. Cell **143**, 99–110.

Yamaguchi K, Yamada K, Kawasaki T. 2013. Receptor-like cytoplasmic kinases are pivotal components in pattern recognition receptor-mediated signaling in plant immunity. Plant Signaling & Behavior **8**, e25662.

Yan A, Xu G, Yang Z-B. 2009. Calcium participates in feedback regulation of the oscillating ROP1 Rho GTPase in pollen tubes. Proceedings of the National Academy of Sciences **106**, 22002–22007.

Yang Z. 2002. Small GTPases: versatile signaling switches in plants. The Plant Cell **14**, 375–389.

Yang Z, Lavagi I. 2012. Spatial control of plasma membrane domains: ROP GTPase-based symmetry breaking. Current Opinion in Plant Biology **15**, 601–607.

Yang X, Yang L, Yu D, Ni H. 2008. Effects of physcion, a natural anthraquinone derivative, on the infection process of Blumeria graminis on wheat. Canadian Journal of Plant Pathology **30**, 391–396.

Yu F, Qian L, Nibau C, *et al.* 2012. FERONIA receptor kinase pathway suppresses abscisic acid signaling in Arabidopsis by activating ABI2 phosphatase. Proceedings of the National Academy of Sciences **109**, 14693–14698.

Zhang Z, Collinge DB, Thordal-Christensen H. 1995. Germin-like oxalate oxidase, a H2O2-producing enzyme, accumulates in barley attacked by the powdery mildew fungus. The Plant Journal **8**, 139–145.

Zhang X, Facette M, Humphries JA, Shen Z, Park Y, Sutimantanapi D, Sylvester AW, Briggs SP, Smith LG. 2012*a*. Identification of PAN2 by quantitative proteomics as a leucine-rich repeat-receptor-like kinase acting upstream of PAN1 to polarize cell division in maize. The Plant cell **24**, 4577–89.

Zhang Z, Henderson C, Perfect E, Carver TLW, Thomas BJ, Skamnioti P, Gurr SJ. 2005. Of genes and genomes , needles and haystacks : Blumeria graminis. Molecular Plant Pathology **6**, 561–575.

Zhang Y, McCormick S. 2007. A distinct mechanism regulating a pollen-specific guanine nucleotide exchange factor for the small GTPase Rop in Arabidopsis thaliana. Proceedings of the National Academy of Sciences **104**, 18830–18835.

Zhang WJ, Pedersen C, Kwaaitaal M, Gregersen PL, Mørch SM, Hanisch S, Kristensen A, Fuglsang AT, Collinge DB, Thordal-Christensen H. 2012*b*. Interaction of barley powdery mildew effector candidate CSEP0055 with the defence protein PR17c. Molecular Plant Pathology **13**, 1110–1119.

Zhao Z, Liu H, Wang C, Xu J. 2013. Comparative analysis of fungal genomes reveals different plant cell wall degrading capacity in fungi. BMC Genomics **15**, 6.

Zhou F, Zhang Z, Gregersen PL, Mikkelsen JD, de Neergaard E, Collinge DB, Thordal-Christensen H. 1998. Molecular characterization of the oxalate oxidase involved in the response of barley to the powdery mildew fungus. Plant Physiology **117**, 33–41.

Zipfel C. 2009. Early molecular events in PAMP-triggered immunity. Current Opinion in Plant Biology **12**, 414–420.

Zipfel C, Kunze G, Chinchilla D, Caniard A, Jones JDG, Boller T, Felix G. 2006. Perception of the Bacterial PAMP EF-Tu by the Receptor EFR Restricts Agrobacterium-Mediated Transformation. Cell **125**, 749–760.

Zipfel C, Robatzek S, Navarro L, Oakeley EJ, Jones JDG, Felix G, Boller T. 2004. Bacterial disease resistance in Arabidopsis through flagellin perception. Nature **428**, 764–767.

Supplements

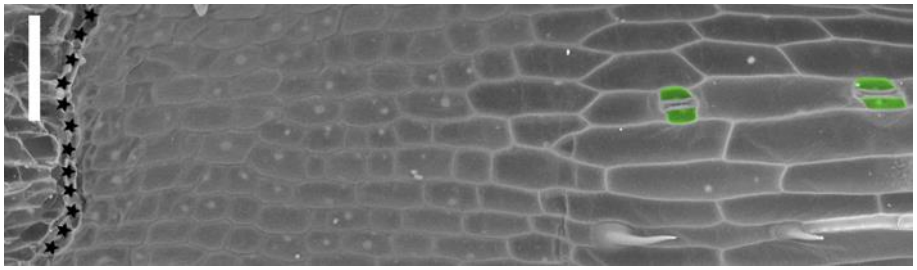

Supp Figure 1: SEM imaging of the barley intercalary meristem region.
The transition from the sheath (left side) to the intercalary meristem of the blade (right side) is marked with black stars. For a better visualization, the subsidiary cells were colored afterwards in green using the software GIMP 2.8. Scale bar 100µm. As material the intercalary region of the 2nd leaves of 14 days old azygous control plants were used.

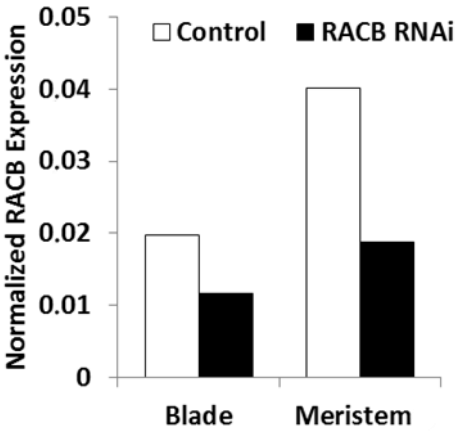

Supp Figure 2: Expression of *HvRACB* in the leaf blade and the intercalary meristem.
Measurement of the transcript abundance in the *HvRACB* RNAi plants and their azygous controls via qPCR. The bars represent the transcript level of *HvRACB* normalized to the housekeeping gene ubc2, measured in one biological replicate. As material blade sections and the intercalary meristems of several dozen 14 days old plants were pooled.

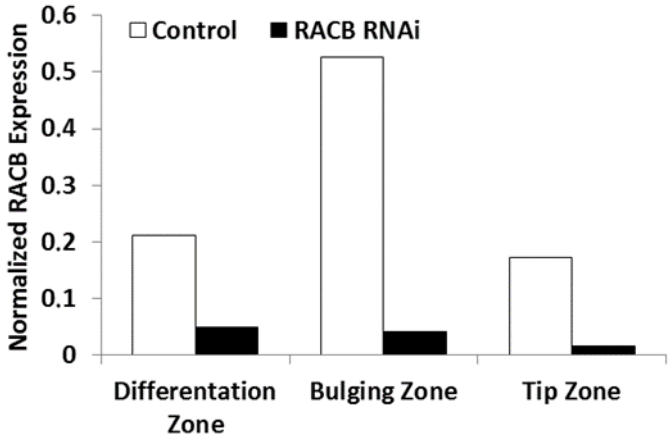

Supp Figure 3: Expression of *HvRACB* in different root zones.
Measurement of the transcript abundance in the *HvRACB* RNAi plants and their azygous controls via qPCR. The bars represent the transcript level of *HvRACB* normalized to the housekeeping gene ubc2, measured in one biological replicate. As material root tissue sections of hundreds of independent two days old seedling roots were pooled.

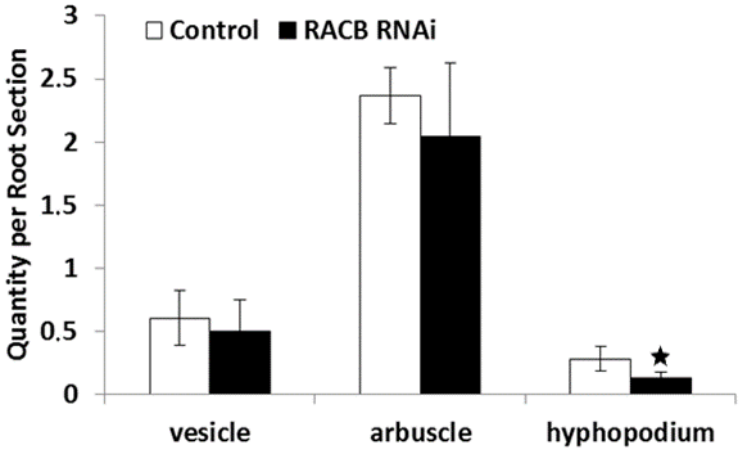

Supp Figure 4: Quantification of mycorrhizal structures in infected barley roots.
Mycorrhiza fungal structures were counted in defined areas of infected barley roots, 42 days after inoculation. For quantitation vesicles, arbuscles and hyphopodia were counted in defined root areas. For each plant between 15 and 27 of these areas were examined and the gained numbers were averaged per plant. The bars represent the mean of 6 plants in the azygous control and 8 for the *HvRACB* RNAi line. Error bars: standard deviation. Student's t test: vesicle, arbuscle $p > 0.05$; hyphopodium $0.01 > p < 0.05$. For measurement 44 days old barley plants were used.

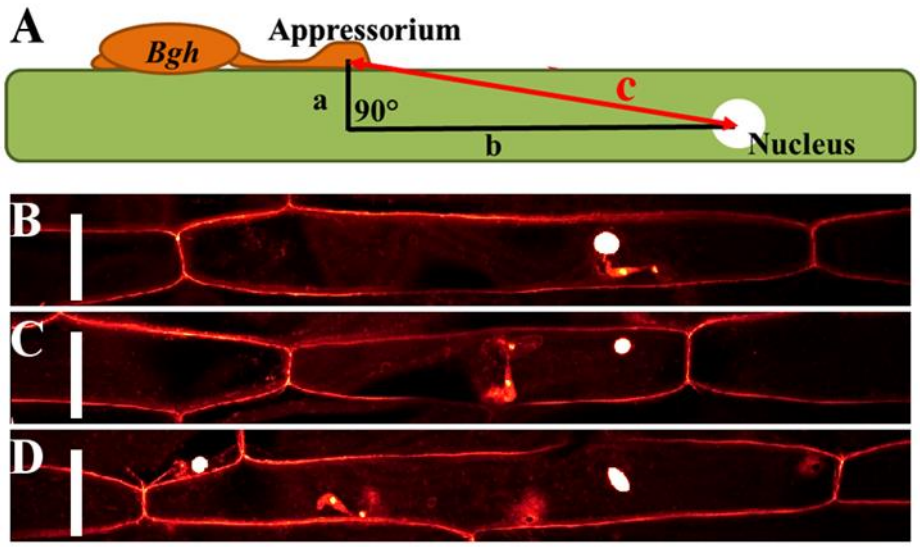

Supp Figure 5: Quantification of the nucleus attraction.
(A) Comic illustration of the distance measurement. The distance between the nucleus and the appressorium was calculated using the Pythagoras's Theorem. The legs of the triangle "a" and "b" were measured by recording z-stacks from the appressorium to the plant nucleus using a confocal fluorescence microscope. (B), (C), (D) example z-stacks of fixed and PI stained leaf material showing different distances between the hooked appressorium and the bright fluorescing nucleus. Additionally, the distance was divided by the diagonal of the plant cell (not drawn), generating the cell size normalized appressorium – nucleus distance (NAI). The smaller the NAI the nearer the nucleus at the attempted penetration site. In (B) the NAI was 0.035, in (C) 0.31 and in (D) 0.43. Scale bar (B), (C), (D) 50 µm. Adaxial epidermal B-cells on the 2nd leaf of 14 days old plants were examined under the microscope.

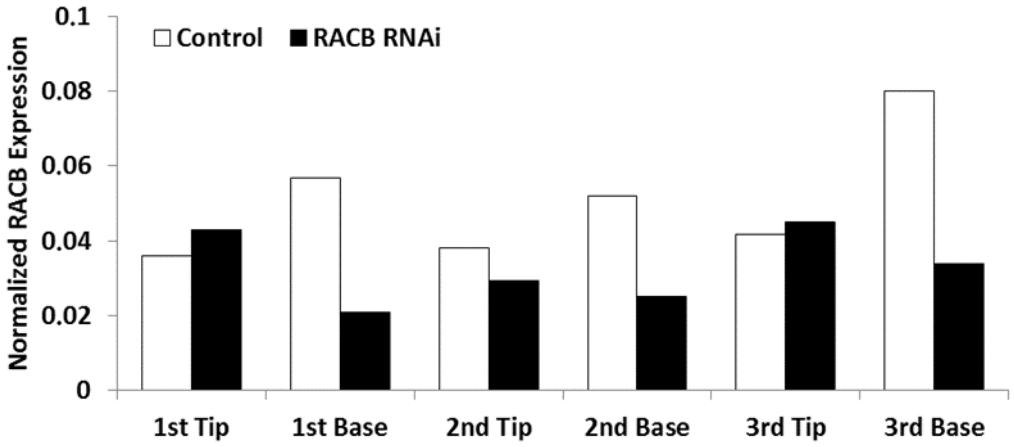

Supp Figure 6: Expression of *HvRACB* in different old leaves and leaf tissues.
For qPCR the first (1st), second (2nd) and third (3rd) leaf of *HvRACB* RNAi and azygous control barley plants were harvested and split in half. Therefore. a tip region (Tip), comprising older leaf tissues and a basic region (Base), including younger tissues were gained. As material 14 days old plants were used. The bars represent the transcript level of *HvRACB* normalized to the housekeeping gene ubc2, measured in one biological replicate. For each leaf and tissue region, the material of 20 plants was pooled.

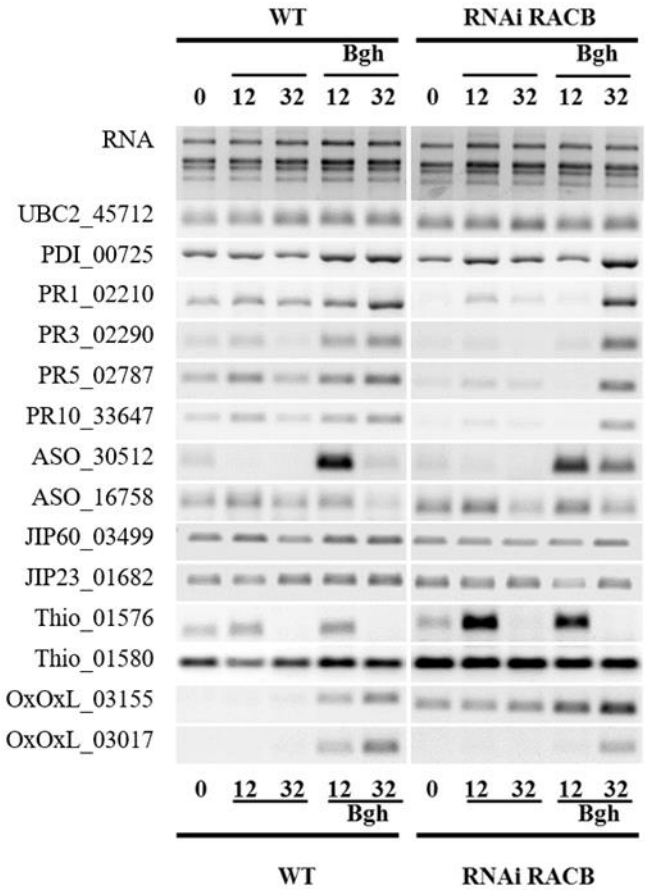

Supp Figure 7: Expression analysis of selected genes in the WT and the *HvRACB* RNAi line. The transcript levels of a gene selection were examined and compared between the WT and the *HvRACB* RNAi line via sqPCR. The time series comprised the zero-time ("0"), 12 and 32 hours after zero-time with and without inoculation with *Bgh*. The gene identifiers were composed of the gene abbreviation and a five digit code, representing the contig number in the PLEXdb database (www.plexdb.org). For a further control, the extracted RNA was visualized on the gel as well as the transcript level of the housekeeping gene UBC2 for each treatment. The PCR conditions were adapted for each gene but the same for all shown transcript abundancies. The same is true for the exposure time of the agarose gel. UBC2: ubiquitin-conjugating enzyme E2; PDI: protein disulfide-isomerase; PR1: pathogenesis-related protein 1; PR3: pathogenesis-related protein 3; PR5: pathogenesis-related protein 5; PR10: pathogenesis-related protein 10; ASO: L-ascorbate oxidase; JIP60: 60 kDa jasmonate-induced protein; JIP23: 23 kDa jasmonate-induced protein; Thio: thionin; OxOxL: oxalate oxidase-like protein. As material at least 5 blades of the 2nd leaf, of 14 days old barley plants were pooled per line and each point in the time-series.

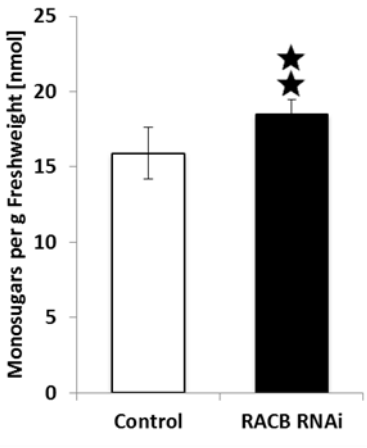

Supp Figure 8: Total amount of monosaccharides measured via HPAEC-PAD.
The total amount comprised the seven measured monosaccharides fucose, galactose, xylose, rhamnose, glucuronic acid, galacturonic acid and arabinose. The bars represent the mean of 5 biological replicates. Error bar: confidence interval (α = 0.05). Student's t test: 0.05 > p > 0.001. As material the 2nd leaf of 14 days old barley plants were used. Each replicate was a pool of 5 independent leaves.

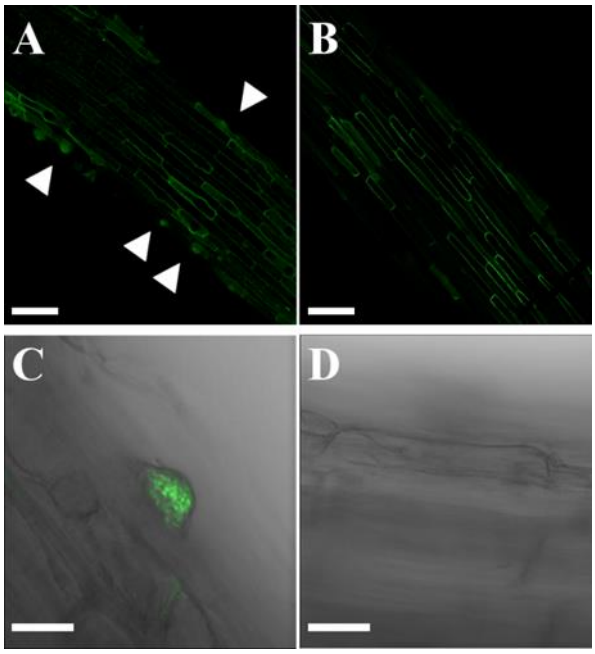

Supp Figure 9: Tracking the incorporation of labeled fucose into root hair bulgings.
Using the technique of click-chemistry it was able to indirectly detect alkynylated fucose via a bio-orthogonal, copper-catalyzed cycloaddition with an azidylated Alexa488 fluorophore (green fluorescence). (A) Root of an azygous control seedling. The root hair bulgings are indicated by white arrowheads. (B) Root of an *HvRACB* RNAi seedling. (C) Close-up of a bulging event in the azygous control. (D) Equivalent root region of the *HvRACB* RNAi plant. Scale bars: (A), (B) 100 µm; (C), (D): 20 µm. As material the roots of 2 days old barley seedlings were used. For microscopy the root bulging area was examined. (C) and (D) show an overlay of the fluorescence and the bright field image

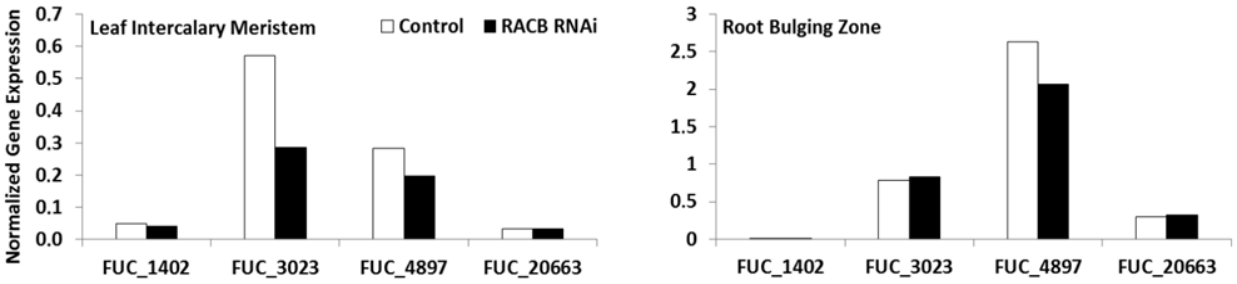

Supp Figure 10: Expression of putative α-fucosidases in the intercalary meristem and root bulging zone.
The transcript abundancies of the four putative α-fucosidases identified by BLAST search (Table 2) were examined via qPCR. The bars represent the transcript levels normalized to the housekeeping gene ubc2, measured in one biological replicate. As material intercalary meristems of several dozen 14 days old plants or root tissue sections of hundreds of independent two days old seedling roots were pooled.

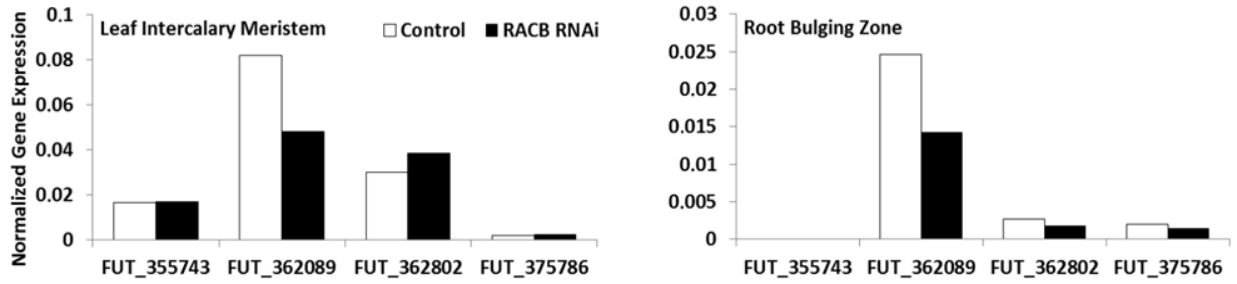

Supp Figure 11: Expression of putative α-fucosyltransferses in the intercalary meristem and root bulging zone.
The transcript abundancies of the four putative α-fucosyltransferases identified by BLAST search (Table 2) were examined via qPCR. The bars represent the transcript levels normalized to the housekeeping gene ubc2, measured in one biological replicate. As material intercalary meristems of several dozen 14 days old plants or root tissue sections of hundreds of independent two days old seedling roots were pooled.

Supp table 1: List of all primers used.
The gene UBC2_45712 and its transcripts was used as control and normalizer in different experiments, which required annealing temperatures between 58 and 64 °C.

Target gene	Primer ID	Lab code	Direction	Sequence (5'-3')	Product size (bp)	Annealing temp (°C)	usage	PCR cycles
UBC2_45712	HvUBC2_fwd	#1255	fwd	ACCCTCGCCGACTACAACAT	263	58-64	qPCR/ sqPCR	30-40
	HvUBC2_rev	#1256	rev	CAGTAGTGGCGGTCGAAGTG				
RACB RNAi	Ubi-Prom-5'UTR_2	#158	fwd	GTCGGCACCTCCGCTTC	629	60	transgenity check	36
	RacBTestBW_for	#534	rev	GGCTTGCTCCATCTTGTGATC				
AGP16_06537	AGB16_2_06537_F	#2279	fwd	AAATGGCGGCGTGGACCT	160	64	sqPCR	46
	AGB16_2_06537_R	#2280	rev	GCCACCAGCATCAGCACGTA				
ARA-I_07032	ARA-I_2_07032_F	#2271	fwd	CATCGTGCTCCTCAAGAACAG	181	60	sqPCR	33
	ARA-I_2_07032_R	#2272	rev	CTGGTACACGGTGTTGACCTT				
ASO_16758	ASO_16758_F	#2312	fwd	CGTCGAAGGGGTAGACAAGAT	171	63	sqPCR	40
	ASO_16758_R	#2313	rev	GCGAGGAGCTTATCCATGAGT				
ASO_30512	ASO_30512_F	#2312	fwd	ATGAAAGACGCGTACGAACAG	179	63	sqPCR	40
	ASO_30512_R	#2313	rev	GTCTCGCTCTTGTTGTTGAGC				
EXPB3_02877	EXPB3_02877_F	#2191	fwd	AACGAGCCCATCTTCAAGG	144	64	sqPCR	33
	EXPB3_02877_R	#2192	rev	GTCGAAGTGGTACTTGGCAAC				
EXT_05258	U35_15359fwd	#1795	fwd	ACAGACCGCGAACGATACG	205	60	sqPCR	37
	U35_15359rev	#1796	rev	AAGCACGCATGAGCATACAG				
GH_21549	U35_26812fwd	#1797	fwd	GGAAGACCCTTGGTTATTGAGC	71	61	sqPCR	40
	U35_26812rev	#1798	rev	TCCAGGCAACCAAGCAAC				
JIP23_01682	JIP23_01682_F	#2353	fwd	TGTTGCAGACTATGCCATGAA	168	63	sqPCR	34
	JIP23_01682_R	#2354	rev	TGCCAATCGTTGTACTTAGCC				
JIP60_03499	JIP60_03499_F	#2355	fwd	TTCTTCTTCCGGGCTGTAAAT	151	63	sqPCR	34
	JIP60_03499_R	#2356	rev	GTACGCTGAGCTACCCAGACA				
P21_14958	p21b_BRCA2ia_fwd	#2048	fwd	CCCGGGTCATGCCTTCTCTTCCAGCAG	421	64	sqPCR	36
	p21b_BRCA2ia_rev	#2049	rev	CCCGGGCGCGACAAGGACACCAAGA				
PDI_00725	I-14:3fwd3'frag	#327	fwd	GAGCCAAGGGGCTTTCCAGT	598	60	sqPCR	30
	I-14:3Pstlrev	#329	rev	CTGCAGTGCTCAGAGCTCATCCTTCA				
PECS_13318	PECS_13318_F	#2197	fwd	TGGGGAAGAACCACAAGAAC	145	64	sqPCR	37
	PECS_13318_R	#2198	rev	TCGCGGGCTAGAAAGTTG				
PG_12475	U35_3466fwd	#1779	fwd	GCCTGAACTGCCCAAATG	186	64	sqPCR	40
	U35_3466rev	#1780	rev	TGGGAGTCATTTCATTGCAC				
PG_21718	PG_3_21718_F	#2277	fwd	CCAACGTCCACATCAAGGAT	186	60	sqPCR	43
	PG_3_21718_R	#2278	rev	TGAACATGGTGTCCGTCTTG				
PL_11004	PL_11004_F	#2199	fwd	CTTCCATGTGGTGAACAATGAC	179	60	sqPCR	37
	PL_11004_R	#2200	rev	ATCTCCAGTTCCAGGCCTTC				
PR1_02210	T-PR1b/3´-3	#98	fwd	TTACTCGCTCGGTCCCTCT	622	57	sqPCR	37
	HvPR1b	#560	rev	TGGTATAGAGCAGGCCCATAGAA				
PR3_02290	PR3_02990_F	#2322	fwd	CTACACGTACGACGCCTTCAT	187	63	sqPCR	25
	PR3_02990_R	#2323	rev	GTGGCCTTGCTTATCTCTTCC				
PR5_02787	PR5_02787_F	#2316	fwd	CACGGACATCACCAAGGATT	153	62	sqPCR	28
	PR5_02787_R	#2317	rev	TTGCCCTTGAAGAACATTGAG				
PR10_33647	PR10_33647_F	#2326	fwd	AAGCTCCGGGTAGAGTACGAG	182	62	sqPCR	30
	PR10_33647_R	#2327	rev	TTCAAACGAAGGGAGAGTTGA				
Thio_01576	ThioPrec_01576_F	#2347	fwd	CTTCTCCCTGAATCCGGTAAG	159	56	sqPCR	37
	ThioPrec_01576_R	#2348	rev	ACAGAATTCCTGCATCCAATG				
Thio_01580	ThioPrec_01580_F	#2349	fwd	AAGTCATGCTTCCAATTGTGC	165	56	sqPCR	37
	ThioPrec_01580_R	#2350	rev	AAGCTGAATCTTGTCCGTGAA				
OxOxl_03017	OxOxL_03017_F	#2351	fwd	AAGACGGAAGCCTACATGGTT	180	60	sqPCR	28
	OxOxL_03017_R	#2352	rev	GGGCTCATGGAAGTTAAGACC				
OxOxl_03155	OxOxL_03155_F	#2301	fwd	ACCCTAGCCCACTCCAAGAC	153	60	sqPCR	28
	OxOxL_03155_R	#2302	rev	AGCCAACCTTGTTTGTCACC				

Continued on next page

Supp table 1: continued

FUC_1402	FUC1_1402_1_fwd	#3268	fwd	CATCTTCAACCTCGGTGACTC	121	60	qPCR	40
	FUC1_1402_1_rev	#3269	rev	GCTCCCCAGAGAATCCAGATA				
FUC_3023	FUC1_3023_1_fwd	#3276	fwd	TCCGACAAGATCTGGAACAAC	129	60	qPCR	40
	FUC1_3023_1_rev	#3277	rev	GAACTCCCCGAAGATGAAGAG				
FUC_4897	FUC1_4897_1_fwd	#3274	fwd	CTGTTCAACTTCGGGGACTC	218	60	qPCR	40
	FUC1_4897_1_rev	#3275	rev	TACCTGAAGTCGGAGTGGTTG				
FUC_20663	FUC1_20663_3_fwd	#3272	fwd	TCGTCTACTTCAAGCGCAGAT	104	60	qPCR	40
	FUC1_20663_3_rev	#3273	rev	GCCGATGTCCATCATGTAGAG				
FUT_355743	FUT_AK355743_F1	#3417	fwd	GTGCTTGCAGTTGTCTCCTTC	94	60	qPCR	40
	FUT_AK355743_R1	#3418	rev	TGCGTTCTTCTTCTTCTCGTG				
FUT_362089	FUT_AK362089_F4	#3419	fwd	ACGAGGCGTACCACAAGAAG	114	60	qPCR	40
	FUT_AK362089_R4	#3420	rev	ACACCACGTACTTGCACTCG				
FUT_362802	FUT_AK362802_F1	#3421	fwd	TGAGATCACTTCAGCGTTCCT	174	60	qPCR	40
	FUT_AK362802_R1	#3422	rev	TAGCTCTCCGGACTATGCTCA				
FUT_375786	FUT_AK375786_F3	#3423	fwd	GTGCGCAATAAGCAGATTTTC	100	60	qPCR	40
	FUT_AK375786_R3	#3424	rev	TAGCTAGTACCTGCGGCAAAA				
RACB_5202	RK172	#556	fwd	TGCACCAGGTGTGCCTATTATC	309	60	qPCR	40
	RacBRT3'rev	#1436	rev	CTTCGCCCTTGTTCTTTGTC				
pIPKTA38	pIPKTA38fwd	#402	fwd	AGCAGGCTTTAAAGGAACC		53	colony PCR	36
	pIPKTA38rev	#403	rev	TGTACAAGAAAGCTGGGTCT				
pIPKTA30N Intron II	TA30Intr-II	#468	fwd	ATAGCCCTCATAGATAGAGTACTAACTAA		52	colony PCR	36
	35S-Term-R	#471	rev	ATGAGCGAAACCCTATAAGAACCCTA				
pIPKTA30N IntronI	TA30N-Intr-I	#469	fwd	TCAAATTAAACAAATGCAGTATGAAGA		49	colony PCR	36
	35S-Prom-F	#470	rev	GATGACGCACAATCCCACTATCCT				
FUT_362089 RNAi	FUT_362089_si1F	#3815	fwd	AAAACCGTAATCCCTCCGAAGA	551	63	TIGS	37
	FUT_362089_si7R	#3827	rev	GTGTCGTGCCGGATCACGCCGT				

Danksagung

Eine Doktorarbeit in den Naturwissenschaften ist ohne die Unterstützung und Hilfsbereitschaft vieler Menschen nicht vorzustellen. Daher möchte ich die Gelegenheit nutzen, mich bei all denen herzlich zu bedanken, mit deren Hilfe diese Dissertation erst ermöglicht wurde und die mir immer unterstützend zur Seite standen.

Großer Dank gebührt Prof. Dr. Ralph Hückelhoven, für die Bereitstellung des Themas, für die Möglichkeit meine Dissertation an seinem Lehrstuhl anfertigen zu dürfen, für seine außerordentliche wissenschaftliche Expertise und für seine tragende Rolle bei der Publikation der Daten im Journal of Experimental Botany.

Vielen Dank an Prof. Dr. Erwin Grill für die Übernahme des Vorsitzes der Prüfungskommission, sowie an Prof. Dr. Kay Schneitz für seine Tätigkeit als zweiter Prüfer.

In Memoriam, möchte ich mich herzlich bedanken bei Prof. Dr. Dieter Treutter für die Möglichkeit wichtige Experimente an seinem Lehrstuhl durchführen zu dürfen, sowie bei Ina Tittel, für die herzliche und kompetente Betreuung. Selber Dank geht an Dr. Lars Voll und Timo Engelsdorf von der Universität Erlangen-Nürnberg.

Herzlicher Dank geht an Dr. Stefanie Ranf, Vera Schnepf und Carolina Galgenmüller für ihre unersetzliche Mitarbeit an der Publikation.

Ich möchte mich auch bei allen Mitarbeitern, Kollegen und Freunden am Lehrstuhl für Phytopathologie, am Wissenschaftszentrum Weihenstephan an der TU München und im SFB924 bedanken für die herzliche Aufnahme in die Laborgemeinschaft, die freundliche und kompetente Hilfe bei allen Problemen und Fragen und für das Gefühl, dass Arbeitszeit auch Lebenszeit bedeutet.

Danke an meine Eltern für ihre ungebrochene Unterstützung seit meinem ersten Tag des Studiums bis heute.

Mein größter Dank gilt meiner Frau Claudia, für ihre bedingungslose Liebe und Unterstützung in guten und wie in schlechten Zeiten.